NOTICE

The quality of this microform is heavily dependent upon the quality of the original thesis submitted for microfilming. Every effort has been made to ensure the highest quality of reproduction possible.

If pages are missing, contact the university which granted the degree.

Some pages may have indistinct print especially if the original pages were typed with a poor typewriter ribbon or if the university sent us an inferior photocopy.

Reproduction in full or in part of this microform is governed by the Canadian Copyright Act, R.S.C. 1970, c. C-30, and subsequent amendments.

AVIS

La qualité de cette microforme dépend grandement de la qualité de la thèse soumise au microfilmage. Nous avons tout fait pour assurer une qualité supérieure de reproduction.

S'il manque des pages, veuillez communiquer avec l'université qui a conféré le grade.

La qualité d'impression de certaines pages peut laisser à désirer, surtout si les pages originales ont été dactylographiées à l'aide d'un ruban usé ou si l'université nous a fait parvenir une photocopie de qualité inférieure.

La reproduction, même partielle, de cette microforme est soumise à la Loi canadienne sur le droit d'auteur, SRC 1970, c. C-30, et ses amendements subséquents.

Canada

Non-Uniform-Band Digital filter Banks: Design and Performance Analysis

By
Genzao Zhang

A Thesis Submitted to
the School of Graduate Studies and Research
in Partial Fulfillment of the Requirements
for the Degree of
Doctor of Philosophy

Ottawa-Carleton Institute for Electrical Engineering

Department of Electrical Engineering
Faculty of Engineering
University of Ottawa

ISBN 0-612-00562-3

UNIVERSITÉ D'OTTAWA
UNIVERSITY OF OTTAWA

ABSTRACT

New design techniques of digital filter banks are presented in this thesis. The research has been focused on systematic design methods for computationally efficient filter banks with arbitrary center frequencies, which could be easily implemented and are useful in acoustic, speech signal processing, and communication systems. Frequency interpolation filter banks (FIFB) are first derived based on an adaptive filtering structure. FIFB banks show good frequency responses, interesting sensitivities and negligible parameter quantization effects and roundoff noise when they are implemented using modern DSP processors with fixed-point arithmetic. For maximally flat FIFB filter banks, the adjusted pole selection strategy by an optimization procedure is applied. Then, the resonator-based arbitrarily spaced center frequency filter banks (RFB) are proposed. They show better behaviour than general FIFB banks from the point of view of frequency responses and the implementation. In order to suppress the non-negligible sidelobes and further improve the passband performance of the non-uniform band filter banks, frequency domain windowing techniques are studied and linear programming is used to produce optimal windows for different banks. Thus the design methods of non-uniform band filter banks with windowing processing are presented and significant improvements are obtained on the filter bank performance. Finally, the FIFB filter bank techniques are successfully extended to the field of allpass and perfect reconstruction analysis/synthesis systems. This widens the application area of the FIFB filter banks. In an allpass system, a synthesis FIFB filter bank is derived based on a general analysis FIFB bank and the allpass requirement. In the perfect reconstruction system, multirate techniques are applied and the efficient general FIR synthesis filter bank and IIR FIFB filter bank are designed to construct the system.

ACKNOWLEDGEMENTS

I would like to repress my most sincere appreciation and gratitude to my supervisor, Dr. William McGee for his academic guidance, encouragement, and spiritual and financial support during the course of my Ph.D. thesis research. Furthermore, I would like to thank him for directing me how, and how important it is, to be a practical researcher.

I am very grateful to all members of my supervisory committee, Dr. Willem Steenaart, Dr. L. Robert Morris of Carleton University and Dr. Tyseer Aboulnasr for their valuable technical advice. In addition, I feel deeply indebted to Drs. W. Steenaart and T. Aboulnasr for their support and all kinds of help and encouragement during the course of my Ph.D. program.

Financial support obtained for this research work from Bell-Northern Research (BNR) and the Natural Sciences and Engineering Research Council of Canada (NSERC) under the Industrial Chair Program, and the University of Ottawa is gratefully acknowledged.

Many thanks to all professors, colleagues and friends at the Department of Electrical Engineering, University of Ottawa, for their help and encouragement during the period of my studies.

I also wish to deeply thank my wife Lin Luo for her constant encouragement and support throughout my studies.

Finally, I would like to express my appreciation to my mother school, Northwestern Polytechnical University in Xian, for giving me the opportunity to come to study for the Ph.D in the field of digital signal processing at the University of Ottawa.

TABLE OF CONTENTS

LIST OF FIGURES

LIST OF TABLES

I INTRODUCTION

1.1 Introduction

Digital filter banks arise in many areas of science and engineering[1-18]. They are extremely important in systems for speech analysis[1,5], bandwidth compression[8,11], radar and sonar processing, spectral parameterization of signals[9,19,18] and anywhere that signals need to be decomposed into subbands in frequency, or where a new signal is reconstructed from the elementary signal components.

What is a filter bank? From the structural point of view, a filter bank is a simple collection of filters which cover the different frequency bands based on the application. There are two basic types of filter banks. Those are the analysis filter bank and the synthesis filter bank. Fig.1.1 illustrates the basic structure for both N-channel analysis and synthesis filter banks. An N-channel analysis filter bank is the bank which splits a signal $x(n)$ into N subband signals $y_i(n)$, $1 \leq i \leq N$. An N-channel synthesis filter bank is the bank which reconstructs a new signal $y(n)$ from N input elementary signals $x_i(n)$, $1 \leq i \leq N$. Except for the basic forms in Fig.1.1, there exist other different ways in which filter banks are used. Fig.1.2 simply illustrates some of these possible system structures which will be discussed in detail in the next section from the application point of view.

What are the important issues for the design and realization of the filter banks? The problem may be considered from different levels. For example, in the system of Fig.1.2(c), the issues related to the individual filters, the filter bank, and the bank-based analysis/synthesis system should be discussed, individually. The filter design problem exhibits all of the constraints and tradeoffs of the general filter design problem. In analysis filter banks, the stopband, passband, and transition band characteristics of the individual

filters must be constrained to control magnitude, phase, and aliasing distortion in the channel signals. In the synthesis bank, in addition to the reconstruction issues exactly the same properties must be addressed so as to control the effects of the processing distortion in the reconstructed signal. Of course, the type and order of the filter and the numerical sensitivity of the filter and implementation structure must also be considered in the design process.

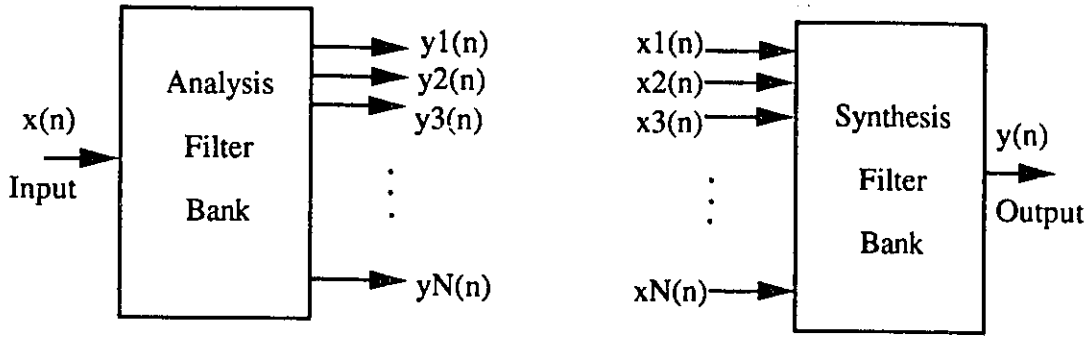

(a) N-channel analysis filter bank

(b) N-channel synthesis filter bank

Figure 1.1 Two basic framework for filter banks.

On the filter bank level, first, the quality of the frequency coverage of the analysis filter bank is important since the total set of the channel signals constitutes a time-frequency representation. Secondly, the efficiency of the whole filter bank realization is an issue since it may be possible to implement the entire filter bank with fewer operations than the sum of the operation in the individual filters. Finally, the fact that the synthesis filter bank is to be used to reconstruct from the distorted channel signals imposes constraints on the passband, stopband and aliasing rejection properties of the individual synthesis filters. In Fig.1.2(c), the goal of the entire analysis/synthesis system (without any channel processing) is to split and then to recreate the input signal at the output. Thus, the distortions introduced at the analysis/synthesis level can be characterized in term of the

spectral magnitude and phase distortions and the aliasing. The requirements imposed by the minimization of analysis/synthesis distortions are quite severe, and make the filter and filter bank design problem considerably more difficult.

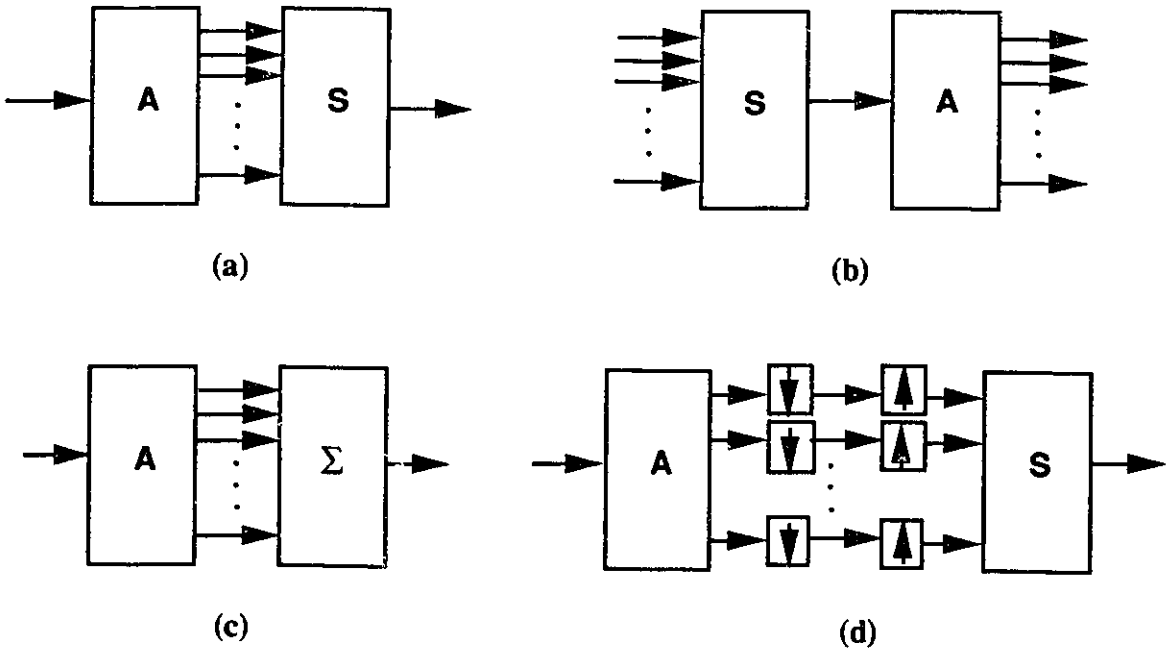

Figure 1.2 Some of possible structures of filter bank systems.
A: Analysis bank; S: Synthesis bank; Σ: Summation.

The discussion on the issues above is based on the filter bank-based analysis/synthesis subband coding system in Fig.1.2(c). However, for a filter bank-based spectrum analyzer and a cochlear modeling system(see Fig.1.1(a)), since there is no synthesis filter bank in the system at all, the issues on the reconstruction system level do not exist. But the requirements on the resolution of the analyzer and the nonlinear frequency sensitivity of the human auditory system impose new problems on the filter and filter bank design. For example, the shapes of the filter frequency responses and the center frequency spacing of the filter banks are two important issues. Before viewing the area of the filter bank

applications in the next section, we first describe some important characteristics classifying the filter banks.

There are several important characteristics that distinguish different classes of filter banks. One of them is the manner in which the spacing and widths of the frequency bands are chosen. Generally speaking, there are two types of bandwidths or center frequency spacing filter banks, the uniform filter banks and nonuniform filter banks. Uniform filter banks in which all the channels have the same bandwidths, are often very appealing in practice because they can be realized with the aid of fast transform algorithms such as the FFT (fast Fourier transform). Another significant merit of uniform filter banks is that it is possible for them to be designed to construct exact pure delay analysis-synthesis systems. This is important since in practical systems, it is desired to have an analysis-synthesis system such that if the output of the analysis filter bank is applied directly (i.e., without any processing) to the input of the synthesis filter bank, the output of the synthesis filter bank should be an exact replica of original input of the analysis filter bank. Different filter bank structures and design techniques have been proposed and developed for this[20-27]. Among them polyphase structure DFT(discrete fourier transform) filter banks and tree structure quadrature mirror filter banks (QMF) are most dominant two ones.

Nonuniform filter banks are defined in innumerable ways depending on the channel stacking arrangements. Different nonlinearly-spaced filter banks have been studied because of their special functions and practical requirements. One important class of nonuniform filter banks is the octave-spaced filter banks[17,28]. Fig.1.3 illustrates an example of 6-band octave-spaced stacking arrangement in which each band is twice the width of preceding band. Because it was shown by researchers that one stage of the human auditory system is similar, in function, to a filter bank whose center frequencies are nonlinearly spaced, the nonuniform filter banks play an important role in acoustics

analysis and speech processing. However, the efficient techniques for designing and implementing this class of filter banks are not obvious, specially when the center frequencies are spaced arbitrarily. Later on, it will be clear that the main works of this dissertation are related to these nonuniform-band filter banks: logarithmic filter banks, where the center frequencies of the bank are spaced logarithmically.

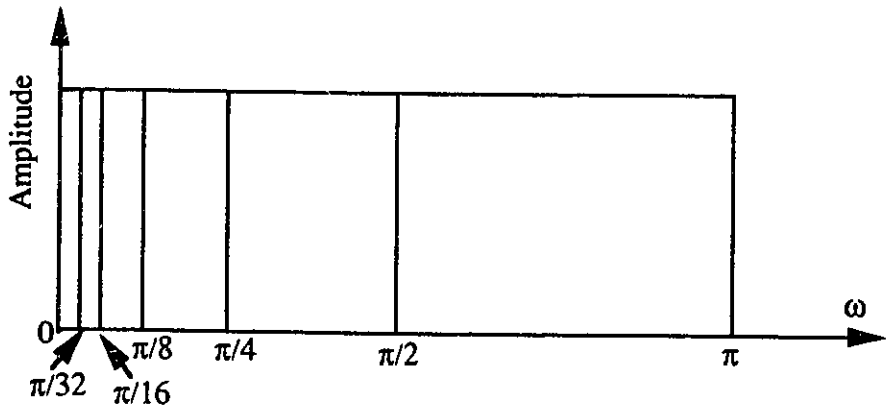

Figure 1.3 Octave-band stacting arrangement for filter bank channels (N = 6).

Another major difference in filter bank systems results from the manner in which the filters are designed for the channels. There are three different kinds of filter designs which result in nonoverlapping, slight overlapping, and substantial overlapping of the bands of the filter bank (see Fig.1.4). Nonoverlapping designs are of interest, for example, in time division to frequency division (TDM/FDM) transmultiplexers for communication systems[2,3,15]. In this case the crosstalk problem due to finite stopband attenuation must be overcome. Slightly overlapping filter bank designs are sometimes desired in systems, such as bandwidth compression systems, where an input signal is analyzed in terms of its spectral components for encoding into a compressed digital form[1,6,7]. In reconstruction, the spectral components are decoded and used to synthesize an output signal which is intended to be a replica of the original input signal. Many contributions

have been made in the area of design and realization of perfect reconstruction filter bank based systems[20-22].

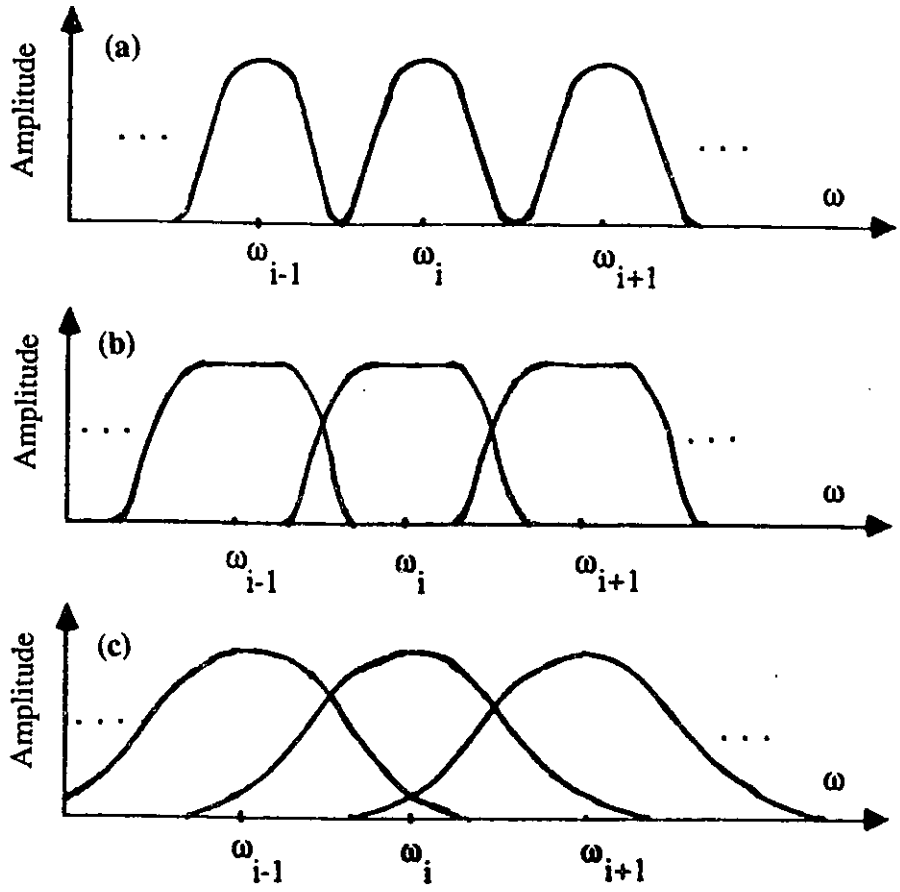

Figure 1.4 Different covering of filter bank designs,
(a) Nonoverlapping;
(b) Slight amount of overlapping;
(c) Substantial amount of overlapping.

Heavily overlapped filter bank designs are of interest in systems such as spectrum analyzers[8-11], where a high-resolution analysis and a smooth or well-interpolated spectral model may be desired. In this case each filter bank channel conveys information about the amount of spectral energy in input signal near the center frequency of the band. The spectral leakage for this class of banks is to be avoided to model the true spectrum. So the

filter banks with the sidelobes as small as possible are desired. A typical filter response is drawn in Fig.1.5 with the illustration of sidelobes.

There are other important characteristics that distinguishe different classes of filter banks. For examples, for analysis/synthesis bank systems, two of them are, the manner in which the channel signals are modulated, and the rate at which the channel signals are sampled. Two modulation methods are the complex modulation or quadrature modulation and the single-sideband (SSB) modulation. In the case of complex modulation, the channel signals are complex-valued signals, whereas for single-sideband modulation they are real valued. Complex modulation is generally preferred in systems such as spectrum analyzers[4,8,9], whereas single-sideband modulation is generally preferred in systems such as communication systems[2,3,6] and coding systems[11-13].

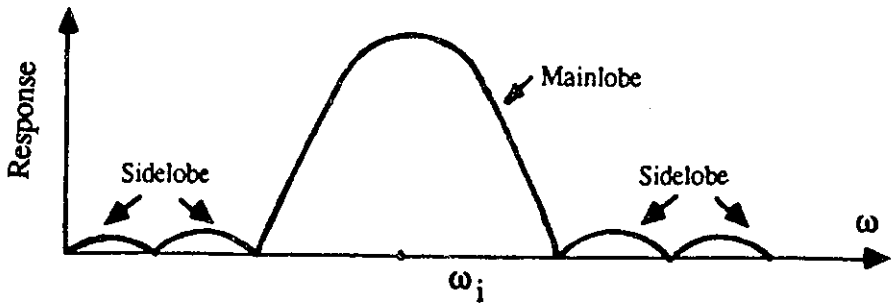

Figure 1.5 Typical filter response with illustration of sidelobes which are crosstalk in nonoverlapping filter banks(TDM/FDM) and spectral leakage in overlapping filter banks for spectrum analysis.

Theoretically, for the N-band uniform bank system, the sampling rate of each of the channel signals can be reduced by a factor N [29]. If it is so, the filter banks are referred to as critically-sampled filter banks, and otherwise they are referred to as oversampled filter banks. In order to make the channel signals work at lower sampling frequency, the channel signals first are decimated after the analysis filter bank, then are interpolated

before the synthesis bank. Decimation can cause aliasing and interpolation can cause imaging[28,30]. The aliasing and imaging make the design and realization of exactly reconstructing analysis-synthesis bank systems challenging. However, several successful techniques have been developed to solve the problems based on the fact that information about the aliased signals in one channel is available in the other channel signals[20,27,25].

From the point of view of the design of digital filter banks, there appear to be many different techniques available in common use. For examples, FIR and IIR filter banks, DFT filter banks[28], quadrature mirror filter (QMF) banks[31], all-pass filter banks and adaptive spectrum analyzer-based filter banks[32,33]. For some of design methods, there are several different realization structures. More details about those will be briefly reviewed based on the literatures in section **1.3**.

1.2 Some Applications of Filter Banks

As we mentioned earlier, filter banks have wide application areas, including frequency division multiplexing (FDM) transmission system, the conversion between time division multiplexing (TDM) and frequency division multiplexing (FDM), subband coding system and vocoders, spectrum analyzer, modeling of the human auditory system, analog voice privacy system and so on. We shall now review a number of important applications of filter banks, with pointers to the literature for details, examples, and demonstrations. The applications in the modeling of the human auditory system and related speech processing are outlined in section **1.4** with the emphasis that the efficiency design and implementation of the nonuniform-band filter banks are still open questions.

In an FDM communication system, N signals from N lines are to be transferred along one single transmission channel by dividing the available bandwidth of the transmission channel into N narrower bands. In the transmitter, the modulator, in fact, is an N chan-

nel synthesis filter bank and in receiver the demodulator is an N channel analysis filter bank(see Fig.1.6[35]). These filter banks are equidistantly spaced identical passbands. Similar to in FDM system, the filter banks play the key role in FDM/TDM conversion and vice versa, which are widely applied in telecommunication network. The TDM/FDM conversion needs a synthesis filter bank while the FDM/TDM needs an analysis filter bank. Different transmultiplexing algorithms have been derived and developed such as, bandpass filter bank technique[36-38], lowpass filter bank technique[39,40], and Weaver structure[41,42]. Note that the filter banks used in FDM system or in FDM/TDM conversions, are nonoverlapping filter banks. The frequency band gaps between the passbands are left to reduce the crosstalk over channels.

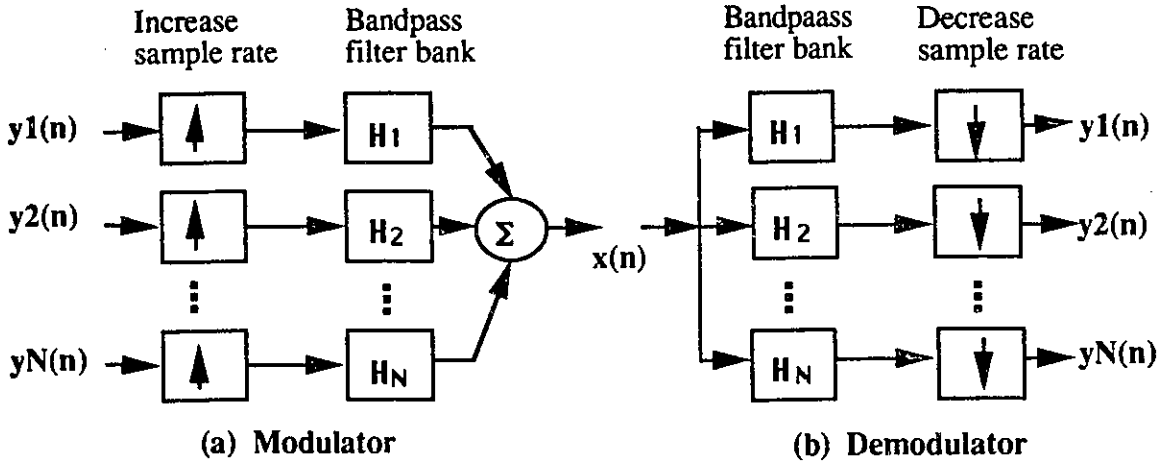

Figure 1.6 Block diagram of filter banks for modulator and demodulator in TDM/FDM translation.

Now we are going to see the role of filter banks in the subband coding systems. In practice, one often encounters signals with energy concentrated in a particular region of frequency. An extreme example was shown in Fig.1.7(a), where all the energy is in

$0 \leq |\omega| \leq \pi L/M$ (where L and M are integers and $M > L$). In this case it is possible to compress the signal simply by decimating it by a factor M/L.

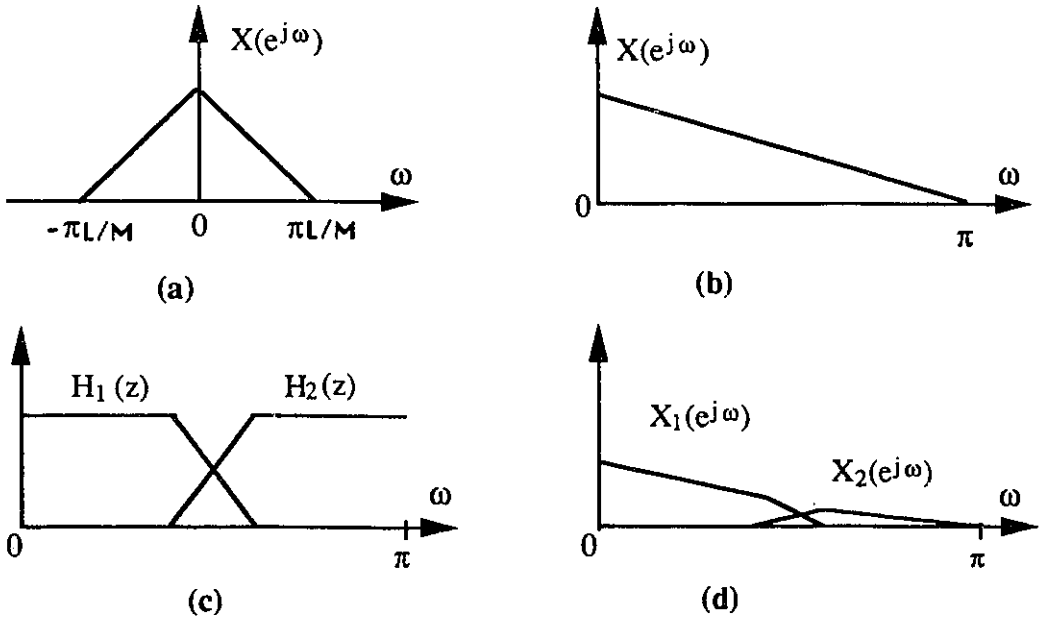

Figure 1.7 Splitting a signal into subband signals.
(a) $X(e^{j\omega})$, transform of a signal x(n) which may be compressed simply by decimating it by a factor M/L.
(b) Transform of orignal signal x(n) which can't be decimated without cousing aliasing.
(c) Splitting the signal in (b) by using analysis filter bank with M=2 (Fig.1.1(a)).
(d) Transform of the subband signals.

It is more common, however, to encounter signals that are not bandlimited but still have dominant frequency bands. An example is shown in Fig.1.7(b). The information in $|\omega| > \pi/2$ of the transform $X(e^{j\omega})$ of original signal $x(n)$ is not small enough to be discarded. And thus we cannot decimate $x(n)$ without causing aliasing either. But there is a way to overcome this difficulty. The signals can be split into two frequency bands by an analysis filter bank (Fig.1.1(a) with N=2), with responses as in Fig.1.7(c). The subband signal $x_2(n)$ has less energy than $x_1(n)$, and so can be encoded with fewer bits than $x_1(n)$. As an example, let $x(n)$ be a 10 kHz signal normally requiring 8 bits per

sample so that the data rate is 80 $k$bits/s. If the subband signals $x_1(n)$ and $x_2(n)$ can be represented with 8 bits and 4 bits per sample, respectively, the data rate now works out to be $40 + 20 = 60k$bits/s after being decimated by two, which is a compression by 4/3. This is the basic principle of subband coding: split the signal to N subbands by an analysis filter bank, decimate each subband signal, and allocate bits for samples in each subband depending on the energy content. In speech coding practice, further use of the perceptive properties in each subband is exploited before quantization[43,44]. The reconstruction of the full band signal is done using the interpolators and synthesis filter bank. The block diagram of the whole system is shown in Fig.1.2(b), and when $N = 2$, the detail illustration is drawn in Fig.1.8.

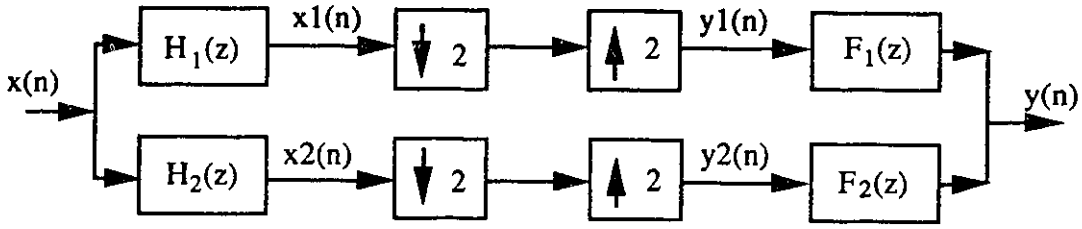

Figure 1.8 Analysis /synthesis system for subband coding (i.e.: two-band QMF bank).

Another application field of filter banks is analog voice privacy systems[30,45]. The systems are intended to communicate speech over standard analog telephone links, while at the same time ensuring voice privacy. The main idea is to split a signal $x(n)$ into N subband signals $x_i(n)$ and then permute each subband signal into segments in the time domain. These segments of subband signals are then permuted and recombined into a single encrypted signal $y(n)$, which can then be transmitted. For example, if there are eight subbands and ten time segments in each subband, then there are eighty possible permutations, and unless somebody has the key for decryption, he will be unable to get the

original voice information in the signals. The aims of the designer of such a privacy system are: the encrypted message should be very difficult to understand, and the decrypted signal should be of good quality retaining naturalness and voice characteristics. At the receiver end, $y(n)$ is again split into subbands, and the time segments of the subbands unshuffled to get $x_i(n)$, which can then be interpolated and recombined through the synthesis filters. The block diagram of the voice privacy system is given in Fig.1.9, where the filter banks are the important fundamental units. Filter banks in this system may be uniform band or nonuniform band, but heavily overlapped design should be applied since no frequency element of the voice signals should be lost due to the system itself.

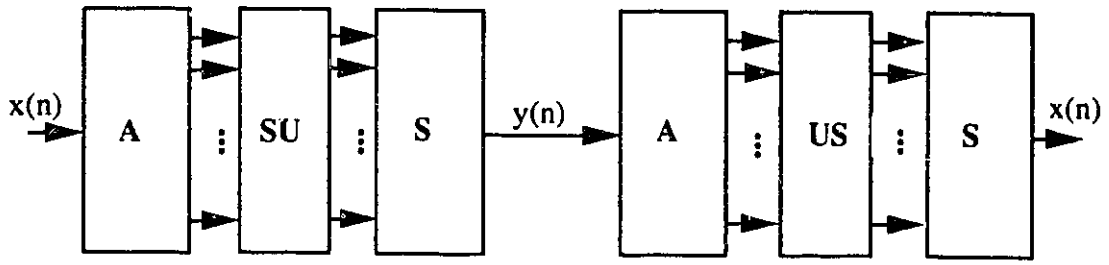

Figure 1.9 The block diagram of a voice privacy system.
A: Analysis filter bank; SU: Shuffling;
S: Synthesis filter bank; US: Unshuffling.

Signal analysis and detection (spectrum analyzer) is another of those most basic and important applications of filter banks. In a filter-bank-based spectrum analyzer, the bank are used to measure the energy distribution of signals in various bands. The filter-bank-based spectrum analyzers are widely applied in speech and music processing and signal transmission. For examples, in the channel vocoder(see Fig.1.10) [46,47], a filter bank is used to provide an approximation to the spectrum envelope of the speech. This slower varying envelope is sampled and then transmitted together with the side information

(F_0: fundmental frequency and V/UV: voice or unvoice decision). In the receiver, the spectrum signals modulated by the pulse generator based on the side information are excited to the inputs of a match synthesis filter bank. The bank thus attempts to recreate the transmitted voice. In [48], a filter-bank-based real-time phase vocoder was derived and developed, where the center frequencies of the filter bank are logarithmically spaced (twelfth-octave) and correspond to the frequencies of the equally tempered piano. In [49], a third-octave filter bank with the center frequencies spaced logarithmically is designed and implemented in TMS DSP processor. This filter bank is used as a spectrum analyzer in the first stage of the neural network for speech recognition.

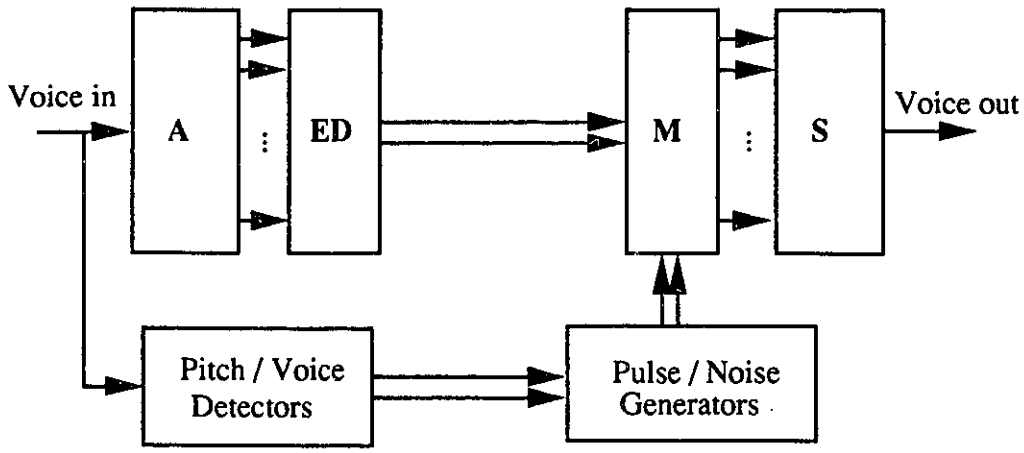

Figure 1.10 A channel vocoder. The amplitude spectrum of the voice signal is analyzed by analysis filter bank and the channel amplitude are used to control the matching synthesis filter bank at receiver. ED: Envelope Detectors; M: Modulators.

In [34], adaptive applications of the resonator-based filter-bank are presented, which include: spectral line enhancement, tracking of periodic signals, and frequency-domain noise-cancellation and equalization. More about the resonator-based filter-bank proposed

in [34] will be reviewed and referred in following chapters since this is the topic very closely to what we are working on in this thesis.

1.3 Reviews of Digital Filter Banks

Filter banks composed of FIR (finite impulse response) digital filters, are applied conventionally in systems where filter banks with specified composite response (usually flat, or having bandpass characteristics) are required. For example, filter banks are used in analyzing speech signals for speech recognition applications[50]. There are many techniques for designing FIR filter banks[29]. For example, each filter in the filter banks can be designed independently by either the *Remez* exchange method in optimal min-max sense[51], or the statistical approach for the optimal *Wiener* FIR filters[52], or the popular window method for simplicity. From the point of view of implementation, people prefer to make the filter banks by the method of frequency translated versions of a prototype for efficiency. More new techniques given in[53,54] are WMMSE(weighted minimum mean square error) and optimal uniform filter banks for specified composite response.

The use of FIR filters for filter banks is attractive for the usual reasons, no stability problems, possibilities for linear phase, simple realization. However, the number of coefficients per filter is too large for some requirements. For example, consider the implementation of a spectrum analyzer for music signals in the range covered by the fundamental frequency of the piano keys, that is, from 27.5 Hz to 4186 Hz, covering 88 frequencies and 88/12=7+ octaves. The frequencies are related to each other by twelfth roots of 2, about 6 percent and in particular note that the filter bandwidth is 1.5 Hz at lowest frequency and 225 Hz at the highest. If the sampling frequency is chosen as *Nyquist* frequency, the lowest band filter requires many coefficients (the orders of the filters are so high up to several thousands when the Park and McClellan method is applied with ripples 0.05-0.1 and transition bands about 0.4-0.75 times of the passband). Furthermore, each filter

requires at least $(N-1)$ zeros to satisfy the interpolation property.

IIR (infinite impulse response) filters have the desired bandwidth and center frequency properties, and are efficient. But the phase is not linear. Many techniques have been developed, such as well-known impulse invariance and bilinear transformation of classical analog *Elliptic* and *Butterworth* filters[29].

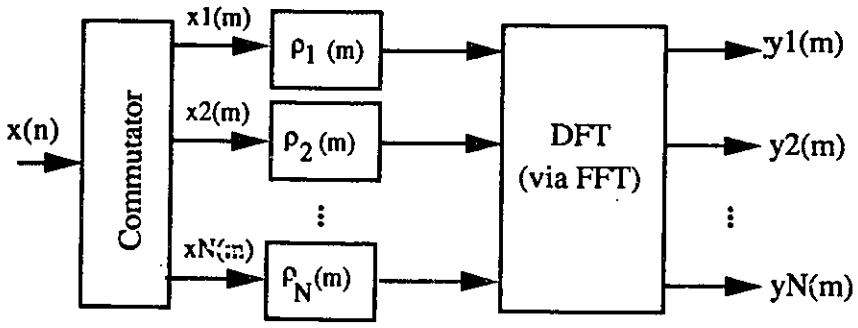

Figure 1.11 Polyphase DFT filter bank structure.

The DFT(discrete Fourier transform) filter bank is one of the most important filter banks. The concepts of DFT filter banks evolved primarily through the need to do spectral analysis and synthesis of quasi-stationary signals such as speech [1,3,4]. In a DFT filter bank, a block of N successive samples of an input signal is applied to a DFT structure to yield a computationally efficient frequency interpolation filter bank in which the center frequencies are uniformly spaced. Conceptually, it is possible to consider the DFT filter banks as a non-block filter with the structure of a DFT preceded by a block that may be viewed as a commutator or as delayed versions of the input being applied as successive inputs[28,33]. This is the so-called polyphase realization of the DFT filter banks from the point of view of structure [11,19] (see Fig.1.11).

Another efficient structure to realize the DFT filter bank, is the weighted overlap-add

structure [55]. This is somewhat more general than that of polyphase structure in that it can be more easily applied to cases where the channel decimation/interpolation ratio (in the analysis/synthesis filter bank systems), is unrelated to the number of frequency channels. Generally speaking, there is a windowing block before the DFT structure for analysis bank (after the DFT for synthesis bank). This is for reducing the large sidelobes of the filter responses and the aliasing distortion which is usually followed the decimation for the rate reduction (or the imaging distortion followed the interpolation for rate increasing).

The DFT filter bank is equivalent to a bank of FIR filters realized in a particularly efficient manner based on the high speed algorithms such as FFT(fast *Fourier* transform). Therefore there have been some approaches using the FFT-based filter bank for nonlinearly spaced frequencies in the literature. The digital frequency warping technique was proposed in [56,57], in which the sampled input is fed to a chain of networks, the outputs of each being *Fourier* analyzed using FFT. The limitation of this technique is it appears suitable for small size banks (only two to three octaves). The common approach of performing a higher order FFT and then reorganizing the many frequencies corresponding to one frequency band for higher frequencies is presented in [58], where the problem of calculating *Fourier* components at arbitrary frequencies was considered.

When the two-band filter bank with aliasing cancellation was introduced by Croisier et in[59], the very active research topic of the design and application of this class of filter bank, started. The filter bank is the QMF(quadrature mirror filter) filter bank (see Fig.1.8). These two-band systems consisting of a lowpass and a highpass filter followed by a 2-to-1 downsampler could be cascaded in a tree structure to form a variety of different spectral decompositions. These filters also have the advantage that they could achieve similar frequency decompositions but with much less computation. Furthermore and perhaps most important, QMF has the advantage of using the mutual information between

the channel signals to cancel aliasing and imaging distortion. For this reason, quadrature mirror filters were a major advance and their use in octave-band structures for subband coders substantively improved the speech quality. In addition, the QMF filter banks can be realized in the tree structures or the polyphase networks[60]. In Fig.1.12, two tree structures based on the QMF filters are given to implement the uniform-band(in Fig.1.12(a)) and octave-band(in Fig.1.12(b)) filter banks. Fig.1.13 shows the polyphase structure of basic QMF filter. Identical to that in FFT filter bank above, the polyphase implementation is efficient because multiplies and adds may be shared between the lowpass and highpass filters.

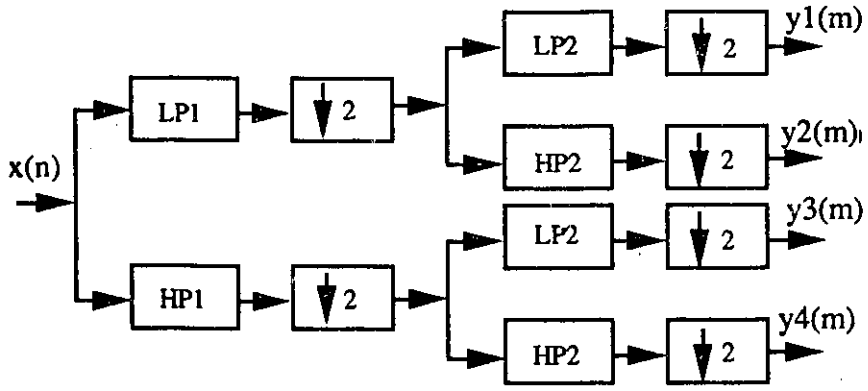

Figure 1.12 Tree structure QMF filter banks:
(a) Two stage tree structure for a four band uniform SSB filter bank;

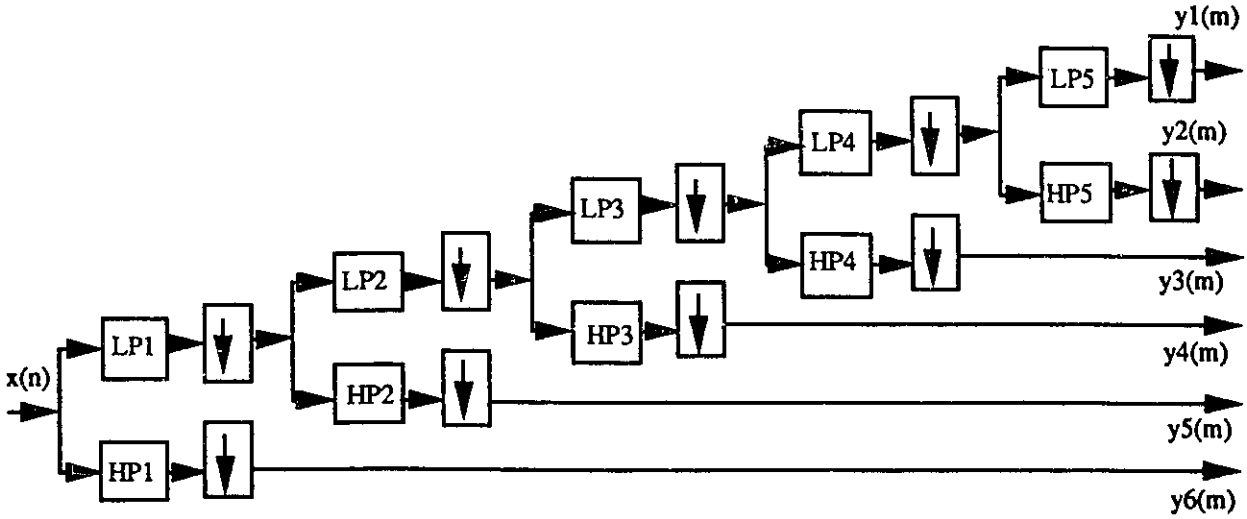

Figure 1.12 Tree structure QMF filter banks. (b) Five stage tree structure for a six-band-octave spaced SSB filter bank. LP: low pass filter, HP: high pass filter.

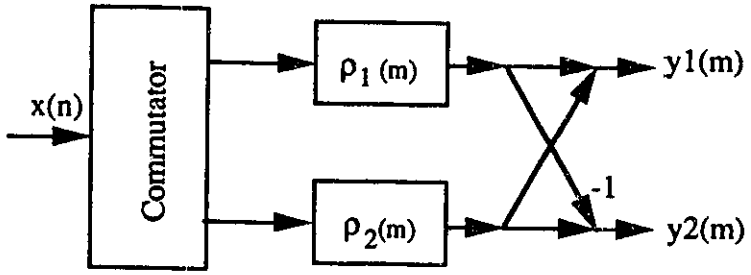

Figure 1.13 Polyphase structure of elementary QMF filters.

Many reports in the literature have addressed the problem of the QMF filter bank design, which includes symmetric FIR filters [12,61], IIR filters[62,63], and variations of half-band filters[64]. Although all the categories of filter design above lead to appropriate methods of QMF filter bank design, a particularly useful class of designs are those based on symmetric FIR filters. They have the advantage of linear phase response (flat group delay), which allows the two-band design to be conveniently cascaded in the tree structures without the necessity for phase compensation. Perhaps the most well-known design method is the method based on computer-aided optimization techniques[65,31], which produced the QMF filters with better characteristics and smaller reconstruction errors for a given filter length. The problem can be formulated in the framework of a non-linear optimization problem by defining a real-valued error function[31]. The QMF filters designed by these methods have been widely used as the standard sets. Computational efficiency and good filter quality were recognized as important issues in the design of QMF filters and related filter banks. For uniform multiband systems it was shown that good reconstruction quality can be achieved by only canceling the major aliasing components in the reconstructed signals[66,67,68].

Recursive filter banks can also achieve computational gains over FIR banks but without the constraint of a uniform multiband structure. IIR filter bank designs has been considered previously by a number of researchers for application in subband speech coding[69,70,71]. Many of these approaches employed the *Remez Exchange* algorithm in a way that forced the denominator polynomial of the filter to be a function of z^{-2}. This constraint on the denominator enables the filters to be realized with an efficient polyphase implementation. It was later discovered that a specialized class of filters which include optimal equiripple filters satisfies this design constraint and has a higher degree of numerical efficiency[72,73].

Along with the development of the QMF filter banks, the focal point of research on analysis/synthesis filter bank design shifted to the design of systems with exact reconstruction properties several years ago[20,22,74,21,25]. A major advancement in this area was the introduction of N-band exact reconstruction solution[25,27,23]. It was shown that exact reconstruction could be achieved for arbitrary uniform N-band systems as well as two-band systems. This formulation is based on the circuit theory concept of losslessness. When the analysis/synthesis systems are constrained to be lossless a convenient lattice structure emerges which can be used for design and implementation. These FIR lattices have the property that they preserve their exact reconstruction property even when the lattice coefficients are quantized.

Two-band systems, which form the basic building block for tree structure have also undergone examination and hence are now better understood. For example, a linear phase constraint can be imposed on the analysis-synthesis filters without loss of the exact reconstruction property. However the price paid for this is a relative loss in the quality of the magnitude response[23] for a given order. Nonetheless by using efficient implementation structures these filters are competitive with the rest in terms of computational complexity. Interesting solutions have also been discovered as an outgrowth of narrowband systems which involve block transforms[75-77]. If the window of a block transform is permitted to exceed the number of transformed output samples and thus results in overlapping windows, the new system is equivalent to a conventional filter bank. Several solutions have been reported which are primarily narrowband filter banks and result in exact reconstruction. Among solutions are the perfect reconstruction filter in [21], the lapped orthogonal transform in [75,76], and the TDAC(time domain aliasing cancellation) system in [77].

In the area of QMF filters, filter banks and related analysis-synthesis systems, there was the development of the systematic theory of the design problems in terms of matrices

and vectors[78,25,79,22]. By imposing constraints on these matrices, different aspects of the overall system can be addressed such as phase distortion, magnitude distortion, aliasing, filter structure and so on.

Besides the filter banks and related systems reviewed above, there are also some other types of filter banks. For example, filter bank designed using all-pass structures appear to have the possibility of a variety of bandwidths[80]. Matched filters are used to make the filter banks which are useful in modern telephone network[81]. The filter banks based on the design and realization of LMS adaptive filtering systems, are the good model of a spectrum analyzer. This bank with linearly spaced frequencies, by a certain choice of LMS gains, is the same as the DFT filter bank in the outputs[63,82].

1.4 Motivation and Organization of the Dissertation

The reviews in the previous section show that the techniques of design and implementation of digital filter banks in which the center frequencies are spaced linearly (or with uniform bandwidth), have been established and reached a certain level of maturity, even though there remain some open questions and research problems of considerable interest, such as refining the perfect reconstruction of QMF filter bank based analysis/synthesis systems, the control over system delay and computational complexity, and the progress in two-dimension area. The FFT-based polyphase filter has emerged as an efficient structure and the QMF filter banks have been widely applied in sub-coding system of speech communications. However, a big gap left is the systematic and computational efficient method of design and implementation of the digital filter bank in which the center frequencies of the filters are not linearly spaced and the bandwidth of the filters is not constant.

Because of the nonlinear selectivity of basilar membrane of human auditory system in the displacement with the frequency of sound wave, the cochlear of human ear was

interpreted as a special spectrum analyzer, i.e., a special filter bank[46,47], which has partly linearly spaced frequencies(0 to 1 kHz) and partly nonliearly spaced frequencies, or approximately logarithmically spaced frequencies(above 1 kHz). Different types of the models of basilar membrane have been reported to simulate human cochlear or whole auditory system[83-86]. All these models or systems base on the filter bank expression of the basilar membrane. These filter banks may be constant-Q, varying-Q, or with adaptive Q circuit. In Fig.1.14, the block diagram of modeling system is shown.

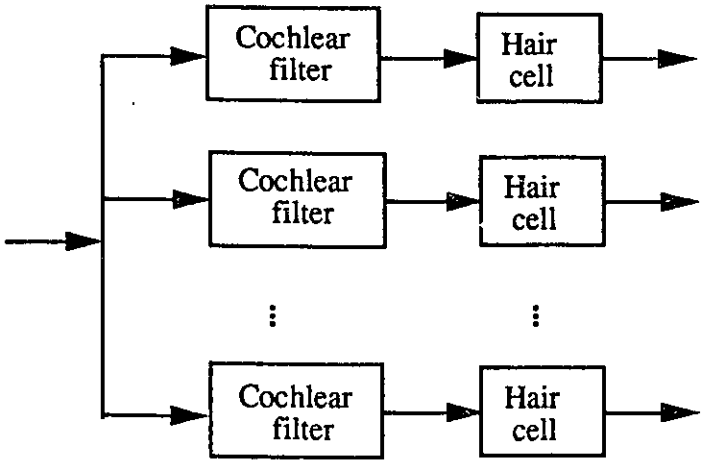

Figure 1.14 The block diagram of the model of human auditory system.

For the same reasons as above, the nonuniform-band filter banks are widely used in the speech enhancement, power spectrum analysis of speech signals, pitch and format estimation, and speech recognition. In particular, it is due to the nonlinear frequency sensitivity of human auditory system that the uniform band subcoding systems may be nonuniform to achieve higher transmission efficiency and improve the speech quality. We know that the headway is just beginning in the study of fractional nonuniform band analysis/synthesis and other non-traditional decomposition based on the QMF techniques[87,30]. However,

for the design and implementation of the nonlinearly-spaced-frequency filter banks with constant-Q or non-constant-Q, there are not obvious choices. The DFT filter banks or polyphase-structure-based filter banks produce inherently linearly-spaced center frequencies. The problem of calculating *Fourier* components at arbitrary frequencies was considered in[57,58], but it does not seem to lend itself to a decomposition of a signal into constituent elements. For QMF filter banks, the limitation is on the arbitrarity of filter bandwidth structure due to the symmetric QMF filters. The tree-structure implementation means that the octave-spaced filter bank can be realized. However, it seems to be very hard to get elegant solutions to sampling rate conversion when the frequency spacing is nonlinear.

The topics of this dissertation are mainly focused on the design, implementation, and performance analysis of digital filter banks, in which the center frequencies may be spaced arbitrarily and the filter bandwidth in the structure may be uniform or nonuniform. We start the study of the systematic design of computationally-efficient filter banks by introducing the Frequency Interpolation Filter Banks (FIFB) based on an adaptive filter structure. A different type of FIFB filter banks is proposed based on the resonator filters with better behaviour, which are called resonator-based FIFB filter banks. In order to suppress the appreciable sidelobes of the filters designed by both approaches above and improve their passband performance, new design methods are proposed with the application of equivalent frequency domain windowing techniques. Furthermore, the techniques are extended to the FIFB filter bank-based allpass and perfect reconstruction analysis/synthesis systems. This widens the application area of the FIFB digital filter banks and completes the structure of the FIFB filter banks.

The organization of this thesis is as follows. In chapter II, the adaptive structure-based FIFB filter bank is generally introduced with the discussions on the principle of

FIFB filter banks, design method, and performance analysis. In addition, the relationship to adaptive algorithm and the implementation structure of FIFB banks will be described. The pole optimization design approach for maximally-flat FIFB filter banks is derived. The nonlinear optimization equation sets are formulated and numerical methods are applied to achieve the optimal pole sets for the design examples. The sensitivity of the FIFB filter banks and parameter quantization effects on the filter frequency responses and pole positions are studied. The filter bank output noise powers caused by fixed-point arithmetic rounding are considered.

In chapter III, the resonator-based frequency interpolation filter banks(RFB) are proposed. Based on the presentation of the general theory of resonator filters concentrating on the Foster property of the resonators, the resonator-based digital filter bank structure and the approximation problem for logarithmic filter banks are presented. Four different pole-zero structures for designing the banks are explored and the sensitivity and the implementation structure are derived. The banks with large number of filters or infinite filters are also studied from theoretical point of view.

In chapter IV, windowing techniques for improvement of the filter bank stopband and passband performance are described. The filter bank design procedure with windows consists of two steps: The design of mother filter banks and the frequency windowing processing for the final filter banks. The weighted outputs of the mother filter banks are summed to produce the final banks with significantly improved responses. Linear programming is applied to find the optimal weighting coefficients and the experiments for a variety of windows are made with a discussion of the results and a comprehensive consideration to the type of windows, the performance of the filter banks and the implementation complexity.

In chapter V, the design technique of the FIFB filter bank-based allpass analy-

sis/synthesis system is proposed. The system consists of an analysis filter bank and a synthesis filter bank, where the analysis filter bank is a general FIFB bank with an arbitrary spacing of the filter frequencies and bandwidths, and then the synthesis filter bank is derived based on the analysis bank and the requirement of the allpass system property. The design examples are presented and the design technique is evaluated by performance analysis and computer calculation of imaging rejection.

In chapter VI, the FIFB filter bank techniques are extended to the multirate FIFB filter bank analysis/synthesis systems. The matrix theory of multirate filter banks and the conditions for perfect reconstruction with the decimation and interpolation are introduced. The general FIR synthesis filter banks are derived out based on the IIR FIFB filter banks for perfect reconstruction systems. The examples with uniformly and logarithmically spaced channels are designed and the computation results are discussed.

Finally, in the chapter VII, we summarize the contributions of this research work and present a number of suggestions and ideas for future research.

II FREQUENCY INTERPOLATION FILTER BANKS WITH ARBITRARY CENTER FREQUENCIES

2.1 Introduction

In this chapter, the frequency interpolation filter banks(FIFB) are introduced based on an adaptive filter structure originally described in [32] for signal spectrum analysis. The FIFB filter bank can have the filter-center-frequencies arbitrarily set, and gets its name due to the frequency interpolation property: i^{th} filter has exactly unity response at i^{th} center frequency and zero responses at all other center frequencies. Since the structure of the filter banks consists of, in fact, a set of resonators with common feedback around all of them, sometimes these filter banks are called resonator-based filter banks[88,89,34] or resonator-based filters[90-92]. The same structure of the filter banks(with slight variations) is independently arrived at by using different approaches. Besides the approach[93,88,89] to be presented in this and the next chapters, the approach described in [90,91] is based on the work in [94] and uses observer theory to estimate the states of a hypothetical system of resonators that models the input signal. The approach described in [34] is based on a modification of the lossless discrete integrator(LDI) simulation of a singly terminated ladder filter, with the emphasis on the case where LDI-based biquads are used as the digital resonators, and adaptive applications of these filter banks.

We first present the principle of FIFB filter banks in section 2.2, where the contents are described in the subsections: An adaptive filtering structure for identifying the frequencies of speech or music signals; The equivalent FIFB filter banks of the adaptive spectrum analyzer; The design of the FIFB filter banks and a discussion of the performance; And the consideration of the filter bank implementation. Then in order to obtain maximally flat filter bank responses, the pole optimization of FIFB is studied in section

2.3, where the nonlinear optimization equations are derived and the *Newton's* method and *Steepest Descent* method are applied to give the numerical solutions of optimal pole sets. Filter bank examples with the applications of optimal pole sets are designed, typical frequency responses are presented, and performance analysis is discussed. Finally in section 2.4, based on the implementation structure given in section 2.2, the finite word length effects of FIFB filter banks are considered. The filter transfer function sensitivities with respect to coefficients, zeros, and poles are derived and discussed. The parameter quantization effects on filter frequency responses and pole positions are calculated. Furthermore filter bank output noise powers caused by fixed-point arithmetic rounding are calculated by the conventional white noise model and numerical integration techniques.

2.2 Principle of FIFB Filter Banks[33,93]

2.2.1 Adaptive structure for identifying signal frequency components

The block diagram of this adaptive filtering structure is shown in Fig.2.1, where oscillators have their fixed resonating frequencies which can be selected arbitrarily for any specific purposes. The outputs of the oscillators are modulated adaptively to match an incoming signal. The difference of the incoming signal (or the input signal) and the summed weighted outputs of the oscillators is the error signal. The different adaptive algorithms may be applied to update the oscillator weights based on different error criterion such as least mean squares (LMS) and recursive least squares (RLS) [95].

We consider the discrete time implementation, i.e., all signals in the system are sampled. If the sampling period is normalized (i.e. sampling period T=1) and time index is n, we may define the oscillator vector $\mathbf{X}_n$ with its elements, $X_{n,i}$, the output of the i^{th} oscillator at time n, $1 \leq i \leq N$, as

$$\mathbf{X}_n^T = [X_{n,1},\ X_{n,2},\ ...,\ X_{n,N}], \tag{2.1}$$

where the i^{th} element of the vector is

$$X_{n,i} = e^{j\omega_i n}, \tag{2.2}$$

and the superscript T indicates vector transpose. The weight vector $\mathbf{C}_n$ has the complex weight elements $C_{n,i}$, $1 \leq i \leq N$, as

$$\mathbf{C}_n^T = [C_{n,1}, C_{n,2}, ..., C_{n,N}]. \tag{2.3}$$

The inner product of the oscillator vector $\mathbf{X}_n$ and weight vector $\mathbf{C}_n$

$$\mathbf{C}_n^T \mathbf{X}_n, \tag{2.4}$$

gives an estimate of the input signal, which is the sum of the product of the oscillator output and the corresponding weight. The input signal is d_n and the error signal $e_{(n/r)}$ is defined as

$$e_{(n/r)} = d_r - \mathbf{C}_n^T \mathbf{X}_r. \tag{2.5}$$

Note that there are two kinds of the errors, the a posteriori error $e_{(n/n)}$, (or sometime ε_n), and the a priori error $e_{(n-1/n)}$, (or sometimes α_n). The updating equation of the weight vector $\mathbf{C}_n$ is

$$\mathbf{C}_n = \mathbf{C}_{n-1} + e_{(n-1/n)} \mathbf{U}_n. \tag{2.6}$$

The i^{th} element of the vector $\mathbf{U}_n$ is

$$U_{n,i} = K_i X_{n,i}^*, \tag{2.7}$$

where the asterisk denotes complex conjugation. Physically $C_{n,i}$ represents the amplitude and phase modulation of a carrier at frequency ω_i. For the input speech signals, generally speaking, $C_{n,i}$ tends to vary rather slowly. The magnitudes of the weight vector are, in fact, the time-frequency representation of the input signal. For the purpose of tracking

the input, it is equivalent to taking the modulated carriers as the system outputs, which may be represented by the vector $\mathbf{G}_n$ with its elements

$$G_{n,i} = C_{n,i}\, e^{j\omega_i n}. \tag{2.8}$$

The only thing remaining to realize this adaptive system is to determine the complex number K_i in equation (2.7). The K_i's are called the Kalman gains because they occur in the Kalman filter solution to the problem of mean-square estimation for a process in which the state vector is the oscillator vector and with no process noise. In the next section, the Kalman gains will be decided as the filter coefficients of the equivalent filter banks using a variety of techniques.

2.2.2 Equivalent FIFB filter banks

If the modulated oscillator outputs are taken as the output signals, then these N signals, $(C_{n,i}\, e^{j\omega_i n})$, $1 \leq i \leq N$, are simply filtered versions of the input signal d_n. In other words, the adaptive system may be described with N transfer functions, which is an equivalent digital filter bank. If H_i represents the transfer function from the input to the i^{th} weighted oscillator output, the block diagram of the equivalent filter bank can be drawn in Fig.2.2. We will now study the system from the equivalent filter bank point of view.

When this structure is analyzed in the sinusoidal steady state, i.e., when the input signal $d_n = e^{j\omega n}$ and ω a constant frequency, the elements of the output vector $\mathbf{G}_n$ will have the same sinusoidal variation, and the elements of the weight vector $\mathbf{C}_n$ are down-converted by the frequency ω_i (for $i = 1, 2, ..., N$). The equations above may be solved for $C_{n,i}$ with the assumption

$$C_{n,i} = H_i\, e^{(j\omega n - j\omega_i n)}, \tag{2.9}$$

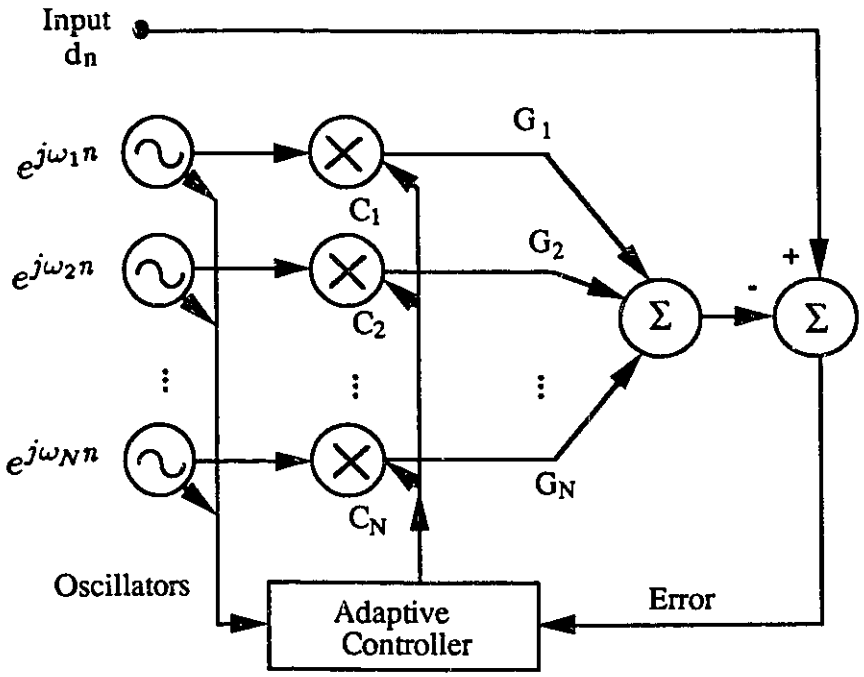

Figure 2.1 The block diagram of the adaptive structure to realize a general filter bank.

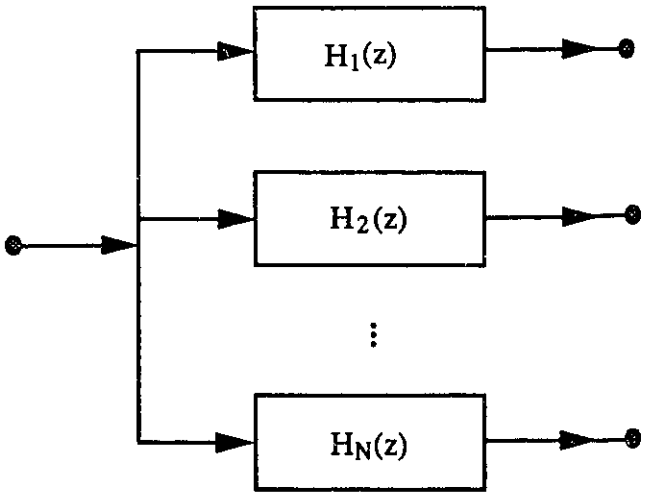

Figure 2.2 The block diagram of the equivalent filter bank in Figure 2.1.

where H_i is a constant and does not depend on the sampling instant index n.

Since the weighted oscillator output $(C_{n,i}\ X_{n,i})$ is equal to $H_i\ e^{j\omega n}$, the transfer function of the i^{th} filter in the equivalent filter bank above may be considered consequently as H_i. The transfer function is given by

$$H_i(e^{j\omega}) = \frac{\frac{K_i}{e^{(j\omega - j\omega_i)}-1}}{1 + \sum_{j=1}^{N} \frac{K_j}{e^{(j\omega - j\omega_j)}-1}} = \frac{N_i(e^{j\omega})}{D(e^{j\omega})}. \tag{2.10}$$

The z-domain form of the transfer function, replacing $e^{j\omega}$ with z, is

$$H_i(z) = \frac{K_i \frac{z_i z^{-1}}{1 - z_i z^{-1}}}{1 + \sum_{j=1}^{N} K_j \frac{z_j z^{-1}}{1 - z_j z^{-1}}} = \frac{N_i(z)}{D(z)}, \tag{2.11}$$

where $z_i = e^{j\omega_i}$ and $z_j = e^{j\omega_j}$. The derivations of (2.10-2.11) are given in subsection 2.2.4.

As a filter bank, all the filters in the bank have the same poles, and the zeros of the i^{th} filter occur at those other oscillator frequencies not equal to ω_i. Furthermore the i^{th} filter has its unity response at ω_i, the i^{th} center frequency of the bank. Thus the outputs of the filter bank obey the frequency interpolation property.

The design of the filter banks is to arrange the center frequencies and to calculate the filter coefficients. The center frequencies are the oscillator frequencies or the poles of numerator $N_i(z)$, and the filter coefficients are the Kalman gains K_i. Based on the theory of adaptive filters[95], several approaches for choosing the Kalman gains have been explored. Of course, this corresponds different ways to choose the center frequencies and system poles. The following conclusion is based on references[33,93].

General Normalized LMS algorithm with linearly spaced frequencies, results in all equal gains, and the gain coefficient is $1/N$ if all the poles are located at the origin, where N is the number of oscillators.

For nonlinearly spaced zeros, when the sum of the Kalman gains is unity, there is a zero in the denominator polynomial $D(z)$ at the origin, in this case, the transfer function

has a pole in the origin. However, the other pole locations are not obvious; in general they fall between the zeros, sometimes close to the unit circle. In unequal weighted LMS algorithm[33], it is supposed that the changes should occur faster for high frequencies. This leads to unequal but real gain coefficients.

Application of the powerful recursive least squares(RLS) theory results in the Kalman gains which makes the filter bank have poles with the same phase angle as the zeros and on a circle of radius λ, where the λ is the exponential forgetting factor[95]. For the problem of 12 frequencies per octave, this approach yields poor gain coefficients for more than 4 octaves[33].

From the simulation results, we find that a good way is to put the poles with the same angles as those of the corresponding zeros but closer to the unit circle for lower frequencies. The different pole magnitude functions may be tested. This will produce more constant-Q filters and appears to provide useful filter banks. We have done many designs with this approach[33,93,96]. The straightforward procedure to calculate the Kalman coefficients is as follows: First choose N oscillator frequencies, i.e., filter center frequencies ω_j in the bank, and choose N poles according to $\Gamma(\phi_j)$, where the $\Gamma(\phi_j)$ is the pole function(see the next page) and here we have $\phi_j = \omega_j$ for $j = 1, 2, ..., N$. Then the denominator $D(e^{j\omega})$ in equation (2.10) can be expressed (perform a partial fraction expansion) as

$$\begin{aligned} D(e^{j\omega}) &= 1 + \sum_{j=1}^{N} N_j(e^{j\omega}) \\ &= 1 + \sum_{j=1}^{N} \frac{K_j}{e^{(j\omega - j\omega_j)} - 1} \\ &= \frac{\prod_{j=1}^{N}[\, e^{j\omega} - \Gamma(\phi_j)\,]}{\prod_{j=1}^{N}(e^{j\omega} - e^{j\omega_j})}. \end{aligned} \tag{2.12}$$

This is the definition of $D(e^{j\omega})$ and from (2.12) the K_i can be easily derived as

$$K_i = \frac{\prod_{j=1}^{N}[\, e^{j\omega_i} - \Gamma(\phi_j)\,]}{e^{j\omega_i}\prod_{j=1,j\neq i}^{N}(e^{j\omega_i} - e^{j\omega_j})}. \tag{2.13}$$

Considering the simulation problem of fundamental frequency of the piano keys (see chapter I in page 14) again, instead of several thousandth order FIR filters or FFT, an 85th order FIFB filter bank may be applied to solve the problem. Thus we may say that the FIFB filter banks are computationally very efficient.

2.2.3 Filter bank design examples

In this subsection, we show some numerical examples with different selections for the forgetting factor λ and different filter-bank center-frequency spacing. Figure 2.3 illustrates the frequency responses of four filter banks. First the curves in Fig.2.3(a) correspond to a bank with $N = 33$, $\lambda = 0.85$, and linear center frequency spacing. In Fig.2.3(b), (c), and (d), the frequency responses are for the three banks which were designed based on the procedure discussed above, i.e., to put the poles with the same angles to the corresponding zeros but closer to the unit circle for lower frequencies. All the three banks are sixth-octave bank with logarithmic center frequencies. The filter bank in Fig.2.3(b) is with the forgetting factor $\lambda = 0.85$, and the bank in Fig.2.3(c) with $\lambda = 0.90$, where the Kalman gains are calculated according to formulation (2.13) and the pole functions are as

$$\Gamma(\phi_i) = \lambda^{\frac{\phi_i}{\pi}} e^{j\phi_i}. \tag{2.14a}$$

The filter bank in Fig.2.3(d) is similar to the bank in Fig.2.3(b) but with the pole function as

$$\Gamma(\phi_i) = \lambda^{\frac{2.0\phi_i}{\pi}} e^{j\phi_i}. \tag{2.14b}$$

From the figures we can see that the selection of the forgetting factor and the pole function affect the filter responses. The larger λ value make the filter response with smaller

sidelobes while the smaller λ leads to the flatter passband but larger sidelobes. Notice the high sidelobes which may be suppressed by a windowing process (similar to that in FFT) which will be studied in Chapter IV.

2.2.4 Implementation considerations

Considering the implementation of the filter banks, we will first consider the structure in Fig.2.1 and the adaptive algorithm equations in section 2.2.1. To implement the filter bank we could use the updating equations (2.5-2.7) with the oscillation generators (2.2) which can be realized by table look-up or sinewave generation methods. The implementation of the filter banks in this way is called the C-formulation implementation since it mainly bases on the definition of the vector $\mathbf{C}_n$. The three equations related are rewritten with slightly different forms.

$$C_{n,i} = C_{n-1,i} + K_i \, e_{(n-1/n)} \, X^*_{n,i}. \tag{2.15}$$

$$e_{(n-1/n)} = d_n - \sum_{j=1}^{N} C_{n-1,j} \, X_{n,j}. \tag{2.16}$$

$$X_{n,i} = e^{j\omega_i n}. \tag{2.17}$$

The C-formulation implementation is attractive because the variables $C_{n,i}$ in the updating equation do not change much from iteration to iteration. However, the computation cost is relatively high.

A second possibility for implementation of the filter banks is to consider an update to the modulated oscillator output variables $G_{n,i}$, and therefore the following formulation is named G-formulation implementation. From the $G_{n,i}$ definition in (2.8), it is easy to get

$$e^{j\omega_i} \, G_{n-1,i} = C_{n-1,i} \, e^{j\omega_i n}. \tag{2.18}$$

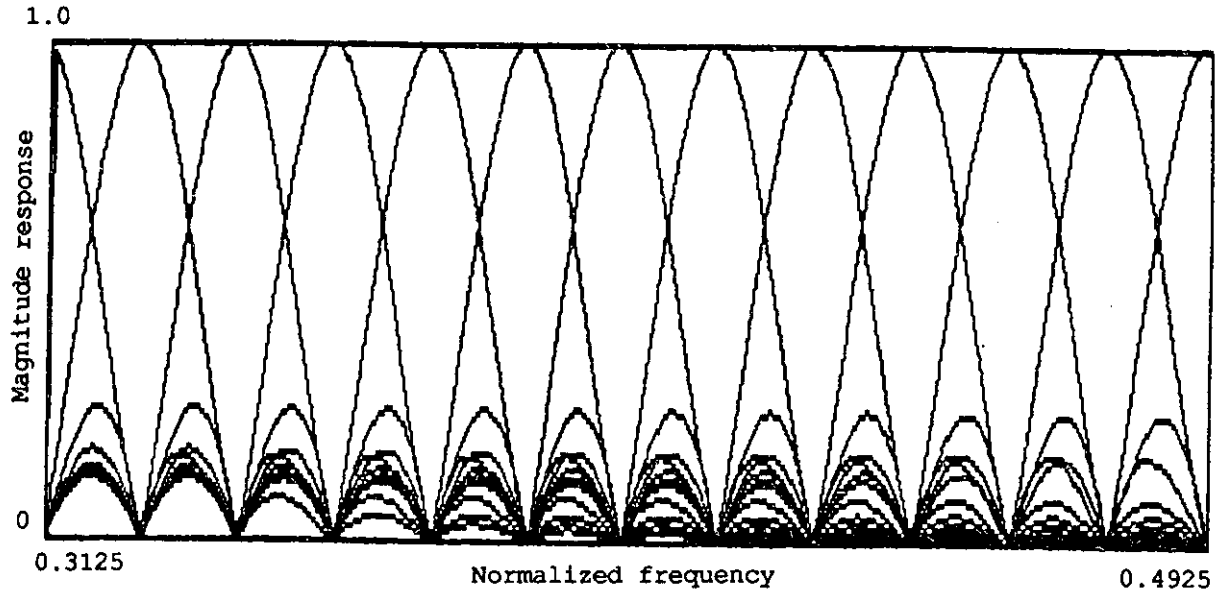

(a) Linear center frequency spacing;

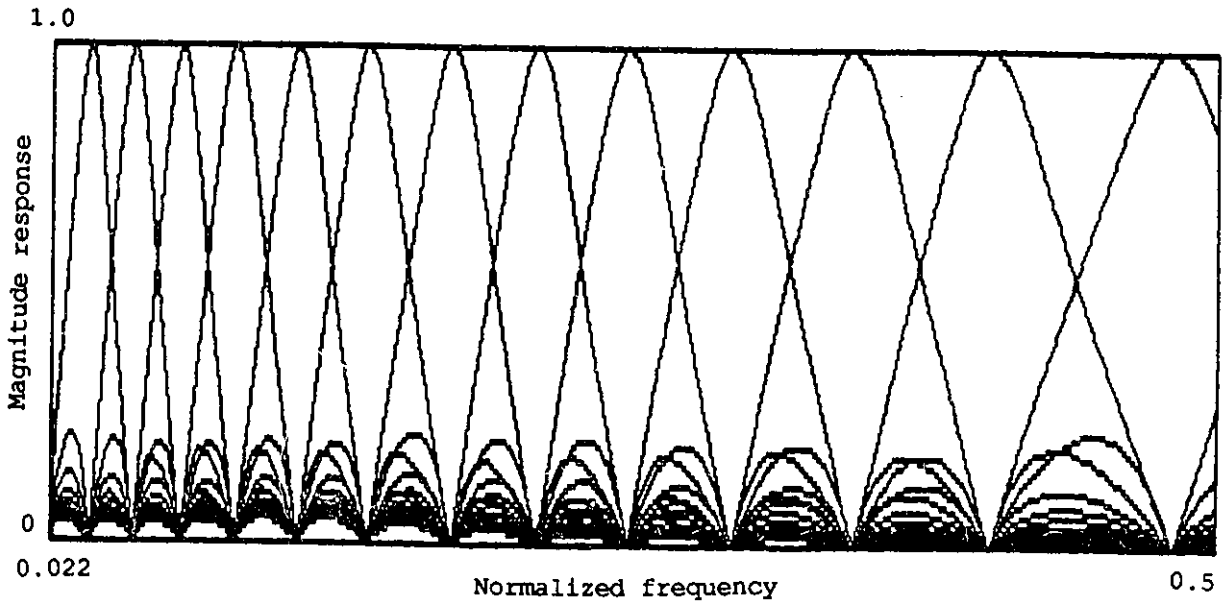

(b) Sixth-octave filter bank with λ =0.85;

Figure 2.3 The frequency responses of FIFB filter banks.

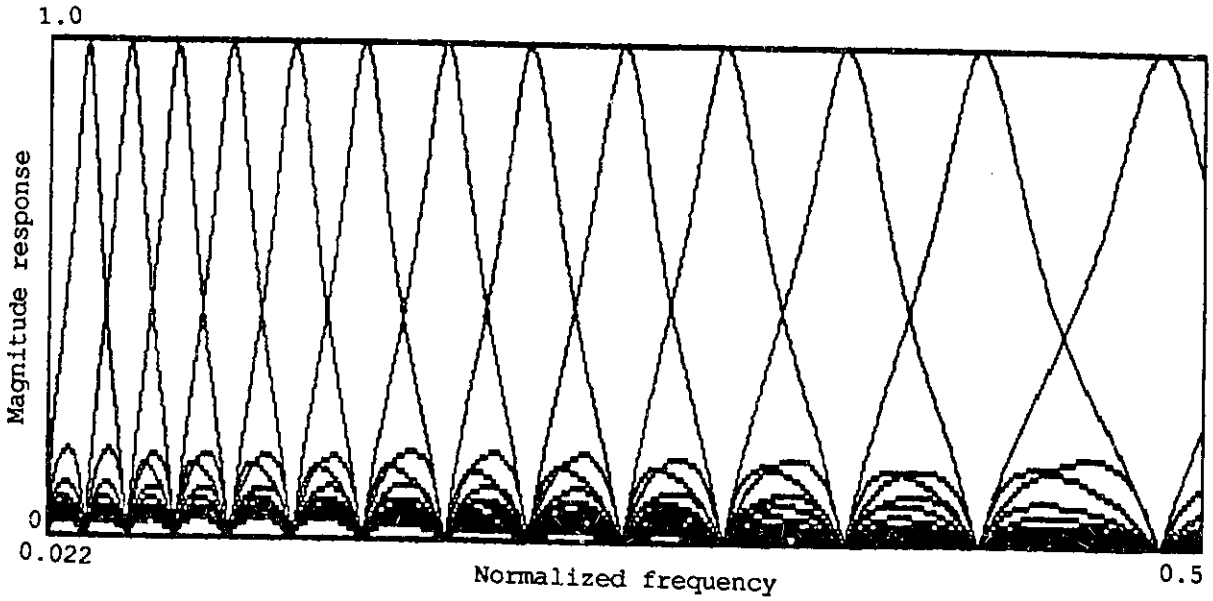

(c) Sixth octave filter bank λ=0.90;

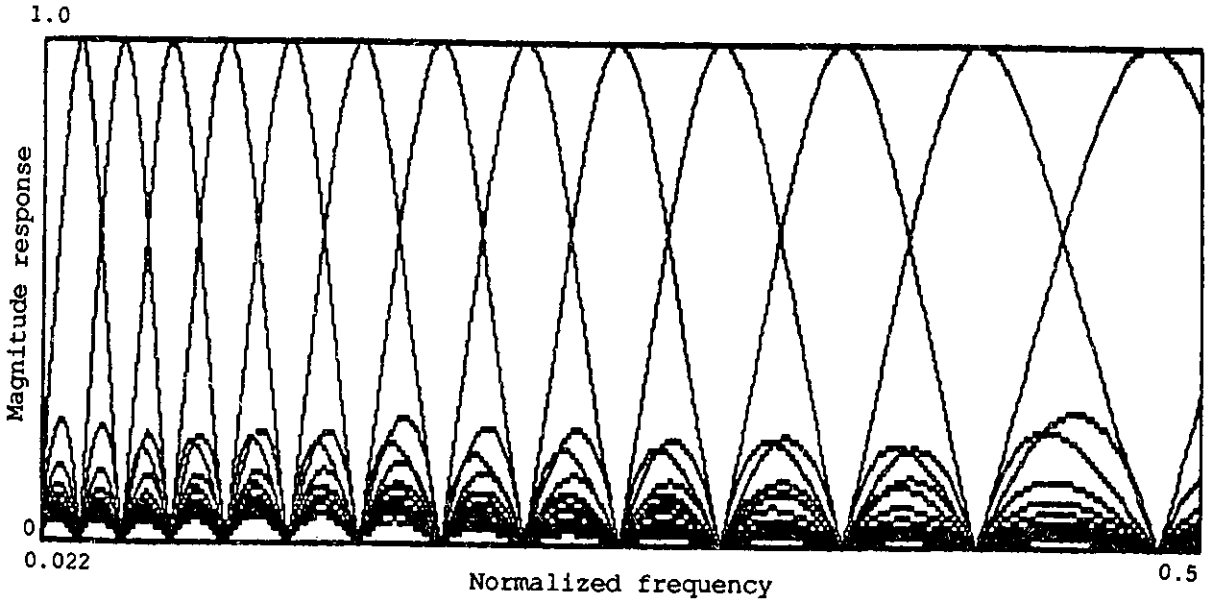

(d) Sixth octave filter bank λ=0.85 with different pole function.

Figure 2.3 The frequency responses of FIFB filter banks.

Thus, multiplying two sides of equation (2.15) by $e^{j\omega_i n}$ and considering (2.18) relation in (2.15-2.16), the G-formulation is derived as

$$G_{n,i} = e^{j\omega_i} G_{n-1,i} + e_{(n-1/n)} K_i, \tag{2.19}$$

and

$$e_{(n-1/n)} = d_n - \sum_{j=1}^{N} G_{n-1,j} e^{j\omega_j}. \tag{2.20}$$

This formulation is interesting since it directly represents the actual equivalent-filter-bank outputs. However, the calculations involve two complex multiplications per filter per sample.

The last implementation approach is to use the H-formulation. The derivation from the G-formulation to the H-formulation is similar to the procedure from the C-formulation to the G-formulation. We define the new updating variables $H_{n,i}$ by

$$H_{n,i} = G_{n,i} e^{j\omega_i}, \tag{2.21}$$

which indicates that $H_{n,i}$ variables have a phase shift from the variables $G_{n,i}$ and produce the predicted outputs at the next sample time. Considering the relation

$$e^{j\omega_i} H_{n-1,i} = G_{n-1,i} e^{j2\omega_i}, \tag{2.22}$$

and multiplying two sides of (2.19) by $e^{j\omega_i}$, we will have the resulting equations

$$H_{n,i} = e^{j\omega_i} H_{n-1,i} + e_{(n-1/n)} e^{j\omega_i} K_i, \tag{2.23}$$

and

$$e_{(n-1/n)} = d_n - \sum_{j=1}^{N} H_{n-1,j}. \tag{2.24}$$

In the H-formulation, there are no multiplications for the determination of the error, and the expression $e^{j\omega_i} K_i$ in (2.23) may be pre-computed. Another advantage of this

implementation method is its lower rounding-noise effects. Note that when the input is a real signal, the feedback error is real since $\sum_{j=1}^{N} H_{n-1,j} = 2\sum_{j=1}^{N/2} Re[H_{n-1,j}]$ is real. Thus, equation (2.23) can be performed by only 6 real multiplications and not eight like the G-formulation and the C-formulation. This means that the rounding noise sources are only six and the filter output-noise-power is reduced. This will be discussed in detail in section 2.4.

When the filter banks are implemented in some specific digital signal processors, such as TMS320C25 and DSP56000, one of the important things is to reduce the number of instruction cycles per filter per sample as much as possible, since we get the tradeoff between the number of the filters in the bank and the maximum sampling frequency. If the number of instruction cycles per filter per sample is L, the number of filters is N(complex filters), the number of additional instruction cycles per sample is S, the DSP processing speed is f_P (cycles per second), and the sampling frequency is f_S, then the basic condition to be met by the implementation is

$$(N * L + S) < \frac{f_P}{f_S} . \tag{2.25}$$

Comparing the number of multiplications and additions for the three formulations above, we find that the minimum L and S are obtained in H-formulation. Thus, the H-formulation is applied in our implementations[49].

It is easy to obtain the filter transfer function (2.11) in the equivalent filter bank from the H-formulation. Taking z-transform of equations (2.23-2.24), we have

$$\bar{H}_i(z) = e^{j\omega_i} \bar{H}_i(z)z^{-1} + E(z)\, e^{j\omega_i} K_i \tag{2.26}$$

and

$$E(z) = d(z) - \sum_{j=1}^{N} \bar{H}_j(z)z^{-1}, \tag{2.27}$$

where $\bar{H}_i(z)$, $E(z)$ and $d(z)$ are the z-transforms of $H_{n,i}$, $e_{(n-1/n)}$ and d_n, respectively. With the input $X(z)$ as $d(z)$ and the i^{th} output $Y_i(z)$ as $\bar{H}_i(z)z^{-1}$, the signal flow graph of the system is drawn in Fig.2.4. From the signal flow graph, the *Mason's Rule* directly results in the transfer function of the i^{th} filter in the bank as

$$H_i(z) = \frac{Y_i(z)}{X(z)} = \frac{K_i \frac{e^{j\omega_i z^{-1}}}{1-e^{j\omega_i z^{-1}}}}{1 + \sum_{j=1}^{N} K_j \frac{e^{j\omega_j z^{-1}}}{1-e^{j\omega_j z^{-1}}}}. \tag{2.28}$$

Note that if the $\bar{H}_i(z)e^{-j\omega_i}$ is considered as the i^{th} filter output (but not $\bar{H}_i(z)z^{-1}$) expressed as $\hat{Y}_i(z)$, the transfer function will be a different form as

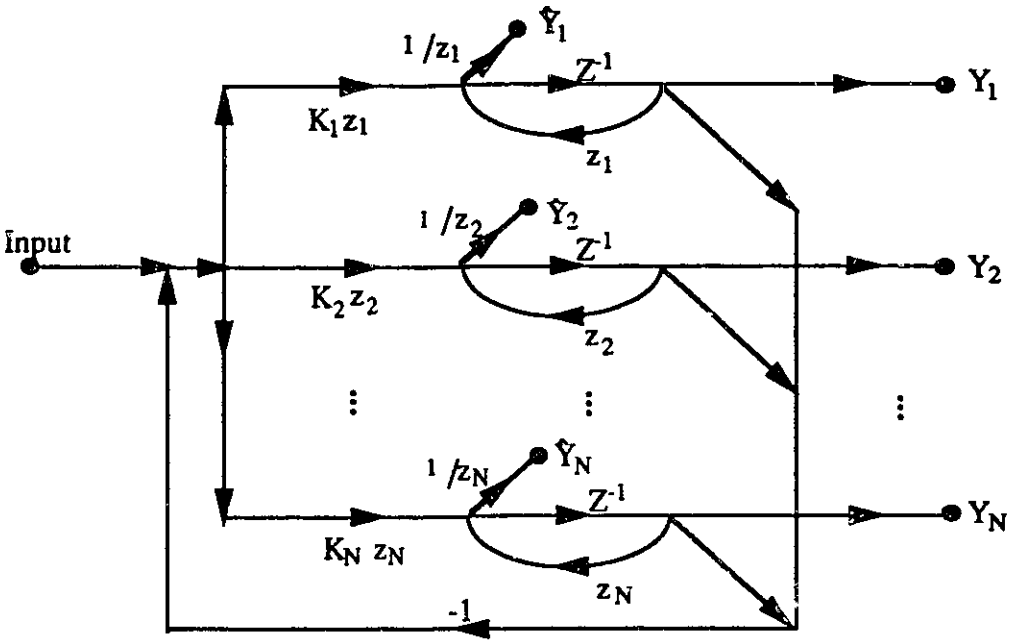

Figure 2.4 The signal flow graph of the H-formulation implementation of FIFB filter banks, where $z_1 = e^{j\omega_1}$

$$\hat{H}_i(z) = \frac{\frac{K_i}{1-e^{j\omega_i z^{-1}}}}{1 + \sum_{j=1}^{N} \frac{K_j e^{j\omega_j z^{-1}}}{1-e^{j\omega_j z^{-1}}}}. \tag{2.29}$$

This type of filters form an allpass filter bank (see Chapter V in details).

2.3 Design of Maximally Flat FIFB Filter Banks

2.3.1 The problem

In the last section, the design of FIFB filter banks was presented and the procedure was given for designing a constant-Q filter bank, that is, the poles are chosen with the same phase angles as the zero's, i.e., $\phi_j = \omega_j$, where the ϕ_j and ω_j are the phase angles of the j^{th} pole and j^{th} zero of the filter bank. But the magnitudes of the poles are made closer to unity for low frequencies. Usually, the pole location is specified by the function $\Gamma(\phi_j)$ as

$$\Gamma(\phi_j) = \lambda^{\frac{\phi_j}{\pi}} e^{j\phi_j} \tag{2.14a}$$

where λ, the same as before and called forgetting factor, is a positive constant less than 1, and ϕ_j is the phase angle of j^{th} pole. From the viewpoint of the filter design, λ is a parameter adjustable for better frequency responses.

The problem with the procedure above is that the frequency response of the bank is not flat, i.e., some peaks of the filter response magnitudes are larger than unity, even though unity response is obtained at $\omega = \omega_i$. Fig.2.5 shows part of the frequency response of a third-octave filter bank designed by using above method to choose poles and calculate Kalman gain coefficients. It can be seen that the peaks of the responses of some filters in the bank are over unity. Recently, G. Peceli proposed[90] the same structure for designing a single filter, and gave the condition which guarantees that the magnitudes of the filter transfer functions are less than or equal to unity. However, that is only for the single filter with a windowing procedure and therefore is not suitable for our case. M. Padmanahan and K. Martin[34] have noted the unflat filter response problem in the LDI-based-biquad resonator-based filter banks.

In this section we present an approach to solve the problem by finding the optimal pole

positions in the sense that they guarantee that the magnitudes of the frequency responses of all the filters in a bank are less than or equal to one, the peaks of the response curves occur at $\omega = \omega_j$ $(j = 1, 2, ..., N)$, and the passband properties are improved.

2.3.2 The pole optimization equations

In this subsection, we derive the equations for finding the optimal pole positions(phase angles). As mentioned above, according to the specification of the filter bank, N center frequencies are preassigned as f_j $(j = 1, 2, ..., N)$. Therefore, from Fig.2.5 and equation (2.10), we know that N zeros on the unit circle of Z-plane are decided as $e^{j\omega_j}(j = 1, 2, ..., N)$, where ω_j is the phase angle of j^{th} zero of the bank system, and

$$\omega_j = 2\pi \frac{f_j}{f_s} \tag{2.30}$$

The pole function is chosen as $\Gamma(\phi_j)$ in (2.14a). The relationship between all the poles and the transfer functions of the filters is not difficult to find if we recall equations (2.10), (2.12) and (2.13) in the last section. The new version of $H_i(j\omega)$ is obtained as[96]

$$H_i(e^{j\omega}) = \frac{\prod_{j=1, j\neq i}^{N}(e^{j\omega} - e^{j\omega_j})}{\prod_{j=1}^{N}[e^{j\omega} - \Gamma(\phi_j)\ ]} \frac{\prod_{j=1}^{N}[e^{j\omega_i} - \Gamma(\phi_j)\ ]}{\prod_{j=1, j\neq i}^{N}(e^{j\omega_i} - e^{j\omega_j})} \tag{2.31}$$

Let

$$M_i(e^{j\omega}) = |H_i(e^{j\omega})| \tag{2.32}$$

Then, taking natural logarithm of both sides of (2.32) gives:

$$\begin{aligned} & ln\ M_i(e^{j\omega}) \\ & = ln|\prod_{j=1, j\neq i}^{N}(e^{j\omega} - e^{j\omega_j})| - ln|\prod_{j=1}^{N}[e^{j\omega} - \Gamma(\phi_j)\ ]| \\ & + ln|\prod_{j=1}^{N}[e^{j\omega_i} - \Gamma(\phi_j)\ ]| - ln|\prod_{j=1, j\neq i}^{N}(e^{j\omega_i} - e^{j\omega_j})| \end{aligned} \tag{2.33}$$

This is only done to simplify the procedure of taking derivative but has no effect on the optimal pole positions since the local maximums of the functions are not changed. Taking the partial derivative with respect to the phase frequency ω gives

$$\begin{aligned}\frac{\partial}{\partial\omega}\ ln\ M_i = &\sum_{j=1,j\neq i}^{N}\frac{\partial}{\partial\omega}ln|(e^{j\omega}-e^{j\omega_j})| \\ &-\sum_{j=1}^{N}\frac{\partial}{\partial\omega}ln|[e^{j\omega}-\Gamma(\phi_j)\ ]|\end{aligned} \tag{2.34}$$

Note that the order of summation, taking logarithm and absolute value have been changed. By using the relations:

$$|(e^{j\omega}-e^{j\omega_j})| = [2-2cos(\omega-\omega_j)\ ]^{\frac{1}{2}} \tag{2.35}$$

and

$$|[e^{j\omega}-\Gamma(\phi_j)\ ]| = [1-2\lambda^{\frac{\phi_j}{\pi}}cos(\omega-\omega_j)+\lambda^{\frac{2\phi_j}{\pi}}]^{\frac{1}{2}} \tag{2.36}$$

which can be easily derived, we have

$$\begin{aligned}\frac{\partial}{\partial\omega}ln|(e^{j\omega}-e^{j\omega_j})| &= \frac{\partial}{\partial\omega}ln[2-2cos(\omega-\omega_j)\ ]^{\frac{1}{2}} \\ &= \frac{sin(\omega-\omega_j)}{2-2cos(\omega-\omega_j)}\end{aligned} \tag{2.37}$$

and

$$\begin{aligned}&\frac{\partial}{\partial\omega}ln|[e^{j\omega}-\Gamma(j\phi_j)\ ]| \\ &= \frac{\partial}{\partial\omega}ln[1-2\lambda^{\frac{\phi_j}{\pi}}cos(\omega-\omega_j)+\lambda^{\frac{2\phi_j}{\pi}}]^{\frac{1}{2}} \\ &= \frac{-\lambda^{\frac{\phi_j}{\pi}}sin(\phi_j-\omega)}{1-2\lambda^{\frac{\phi_j}{\pi}}cos(\phi_j-\omega)+\lambda^{\frac{2\phi_j}{\pi}}}.\end{aligned} \tag{2.38}$$

Substituting (2.37) and (2.38) into (2.34), the partial derivative of $ln\ M_i$ is given by

$$\begin{aligned}\frac{\partial}{\partial\omega}\ lnM_i = &\sum_{j=1,j\neq i}^{N}\frac{sin(\omega-\omega_j)}{1-cos(\omega-\omega_j)} \\ &+\sum_{j=1}^{N}\frac{\lambda^{\frac{\phi_j}{\pi}}sin(\phi_j-\omega)}{1-2\lambda^{\frac{\phi_j}{\pi}}cos(\phi_j-\omega)+\lambda^{\frac{2\phi_j}{\pi}}}.\end{aligned} \tag{2.39}$$

Now let

$$\frac{\partial}{\partial \omega} ln\ M_i\ |_{\omega=\omega_i} = 0 \tag{2.40}$$

i.e.,

$$\sum_{j=1,j\neq i}^{N} \frac{sin(\omega_i - \omega_j)}{1 - cos(\omega_i - \omega_j)} + \sum_{j=1}^{N} \frac{\lambda^{\frac{\phi_j}{\pi}} sin(\phi_j - \omega_i)}{1 - 2\lambda^{\frac{\phi_j}{\pi}} cos(\phi_j - \omega_i) + \lambda^{\frac{2\phi_j}{\pi}}} = 0. \tag{2.41}$$

This is the i^{th} optimization equation. For whole bank, we have N similar equations like (2.41) as (taking i from 1 to N in (2.41))

$$\begin{cases} \sum_{j=2}^{N} \frac{sin(\omega_1 - \omega_j)}{1 - cos(\omega_1 - \omega_j)} + \sum_{j=1}^{N} \frac{\lambda^{\frac{\phi_j}{\pi}} sin(\phi_j - \omega_1)}{1 - 2\lambda^{\frac{\phi_j}{\pi}} cos(\phi_j - \omega_1) + \lambda^{\frac{2\phi_j}{\pi}}} = 0 \\ \sum_{j=1,j\neq 2}^{N} \frac{sin(\omega_2 - \omega_j)}{1 - cos(\omega_2 - \omega_j)} + \sum_{j=1}^{N} \frac{\lambda^{\frac{\phi_j}{\pi}} sin(\phi_j - \omega_2)}{1 - 2\lambda^{\frac{\phi_j}{\pi}} cos(\phi_j - \omega_2) + \lambda^{\frac{2\phi_j}{\pi}}} = 0 \\ \vdots \\ \sum_{j=1}^{N-1} \frac{sin(\omega_N - \omega_j)}{1 - cos(\omega_N - \omega_j)} + \sum_{j=1}^{N} \frac{\lambda^{\frac{\phi_j}{\pi}} sin(\phi_j - \omega_N)}{1 - 2\lambda^{\frac{\phi_j}{\pi}} cos(\phi_j - \omega_N) + \lambda^{\frac{2\phi_j}{\pi}}} = 0 \end{cases} \tag{2.42}$$

Note that each equation in the set is a nonlinear equation with N local maximums. So in order to search out the phases ϕ_j $(j = 1, 2, ..., N)$ making $|H_i(j\omega)|$ get the maximum at the frequency $\omega = \omega_i$, care must be given to the selection of the initial value ϕ_j^0 of ϕ_j $(j = 1, 2, ..., N)$. As a matter of fact, an obvious choice is to let $\phi_j^0 = \omega_j$ for $j = 1, 2, ..., N$.

2.3.3 Solving the optimization equations

In this subsection we will concentrate on the solving of the set of the nonlinear equations and the discussion of the optimal pole solutions.

There exist many methods[96] to be used to solve the nonlinear optimization equations. A typical one is *Newton's* method. The only condition of *Newton's* method is

the existence of *Jacobian* matrix. *Newton's* method applied to the pole optimization of third-octave filter bank with low order works fine. However, with the increase of the size of the bank, the computation will increase dramatically since in each recursive step N^2 terms of the second order partial derivative need to be calculated for an N-filter bank, and the inversion of a NxN matrix is required. For example, the order of a typical twelfth-octave filter bank is 85, and because a special pole with the corresponding zero to be on the minus real axis sometimes, we have to separate each pair of the complex conjugate poles into two single poles to look for the optimal angles of the poles. In this way the number of the terms of the second order derivative is 169^2, and the order of the matrix is 169 by 169.

Considering the computational complexity, the convergence speed and the available computational power, we prefer to apply the method of *Steepest Descent*[97] for larger size banks. In *Steepest Descent* we have no matrix inversion problem and the terms of second order derivatives will be reduced greatly. The general form of the second order partial derivative derived is (the long derivation is omitted)

$$\frac{\partial}{\partial\phi_j}\left(\frac{\partial}{\partial\omega}\, ln\, M_j\,|_{\omega=\omega_j}\right)$$
$$= \frac{-4\lambda^{\frac{2\phi_j}{\pi}} + 2\lambda^{\frac{\phi_j}{\pi}}\left[\,(1+\lambda^{\frac{2\phi_j}{\pi}})cos(\phi_j-\omega_j) + \frac{1}{\pi}(1-\lambda^{\frac{2\phi_j}{\pi}})ln(\lambda)\ sin(\phi_j-\omega_j)\,\right]}{[1-2\lambda^{\frac{\phi_j}{\pi}}cos(\phi_j-\omega_j)+\lambda^{\frac{2\phi_j}{\pi}}]^2} \tag{2.43}$$

where j takes the integer value between 1 and N.

If we let

$$\begin{cases} C_j(\Phi) = \dfrac{\partial}{\partial\omega}\, lnM_j\,|_{\omega=\omega_j} \\ A_j(\Phi) = \dfrac{\partial}{\partial\phi_j}\,[\,C_j(\Phi)\,] \end{cases} \tag{2.44}$$

where Φ is a vector containing the elements $\phi_1, \phi_2, ..., \phi_N$. Then, the *Steepest Descent* procedure for our problems can be described as follows:

(1) Preassign the phase angles of the zeros: ω_j $(j = 1, 2, ...N)$.

(2) Choose the initial values of the phase angles of the poles: ϕ_j^0 $(j = 1, 2, ..., N)$.

(3) Choose the small positive number ε for the convergence criterion and let $k = 0$.

(4) Compute $C_j(\mathbf{\Phi}^k)$, $j = 1, 2, ...N$.

(5) Compute $A_j(\mathbf{\Phi}^k)$, $j = 1, 2, ...N$.

(6) Let

$$B_j^{(k)} = C_j(\mathbf{\Phi}^k) \tag{2.45}$$

and for any j among $1, 2, ..., N$ if

$$|B_j^{(k)}| \leq \varepsilon \tag{2.46}$$

then finish computation and $\mathbf{\Phi}^k$ is what we want. Otherwise go on to the next step.

(7) For any j among $1, 2, ..., N$, let

$$\phi_j^{k+1} = \phi_j^k + \mu B_j^{(k)} \tag{2.47}$$

where μ is a small real negative number chosen experientially. Then let $k := k + 1$ and go to step **(4)**.

It is worth noting that the optimal phase angles of the poles change in a definite way when the forgetting factor λ changes. Following is a brief summary of the optimal pole moving with λ when $N = 2$.

(1) For different forgetting factor λ, different optimal phase angles of the poles and different radii are obtained. When λ is reduced from 0.99, the optimal poles moves from the same phase angles as the corresponding zero's $\phi_1(\lambda_{start}) = \omega_1$, and $\phi_2(\lambda_{start}) = \omega_2$ to the one same point. At this point the phase angle $\phi(\lambda_{last})$ is the arithmetic average of the phase angles of the starting points:

$$\phi(\lambda_{last}) = \frac{\phi_1(\lambda_{start}) + \phi_2(\lambda_{start})}{2}. \tag{2.48}$$

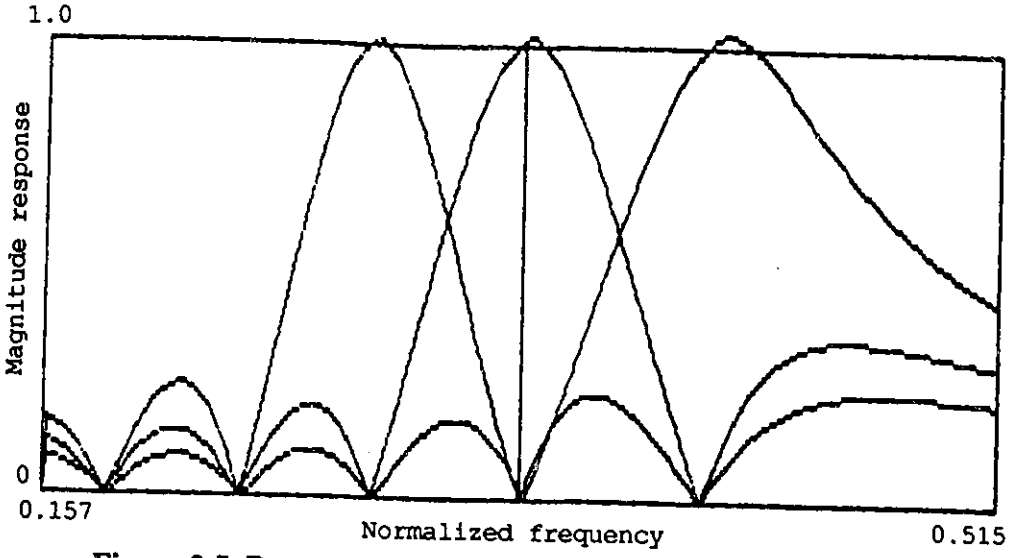

Figure 2.5 Part of the frequency respons of a FIFB filter bank with general poles, N=33 and λ=0.80. Note that the peaks of the response curves are larger than unity.

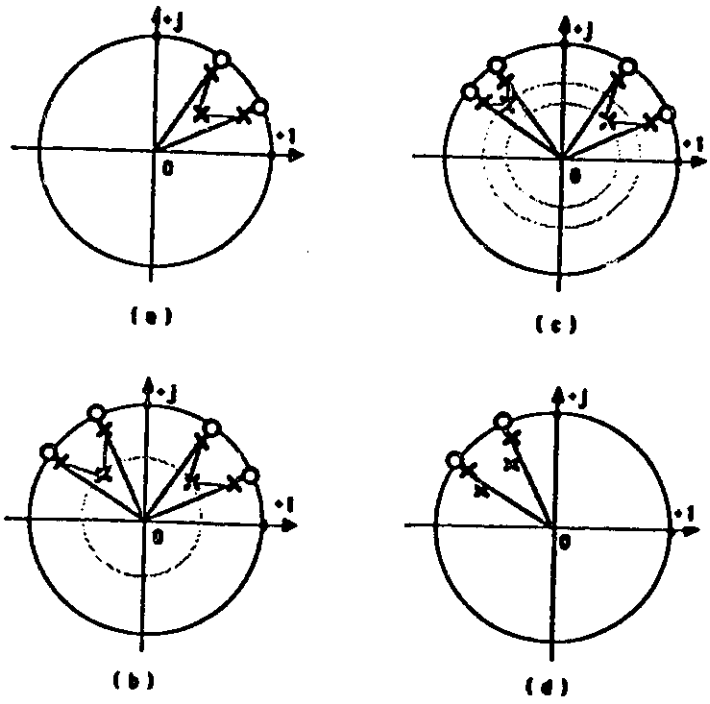

Figure 2.6 The pole-position-change plot in the pole-optimization

✖ -- pole, o -- zero.

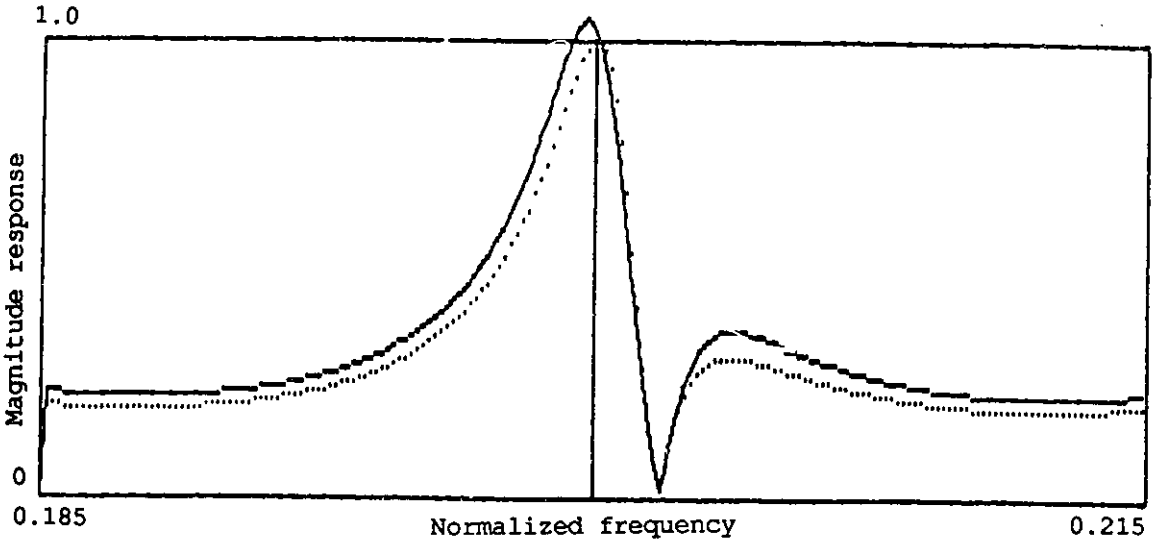

Figure 2.7 (a) Frequency responses with normal-optimal poles(N=2), i.e., the poles obtained after optimization with larger-angle-poles reducing their angles while smaller-angle-poles increasing their angles. Normal-potimal poles move the peak of curve to the center frequency and make the sidelobe smaller.

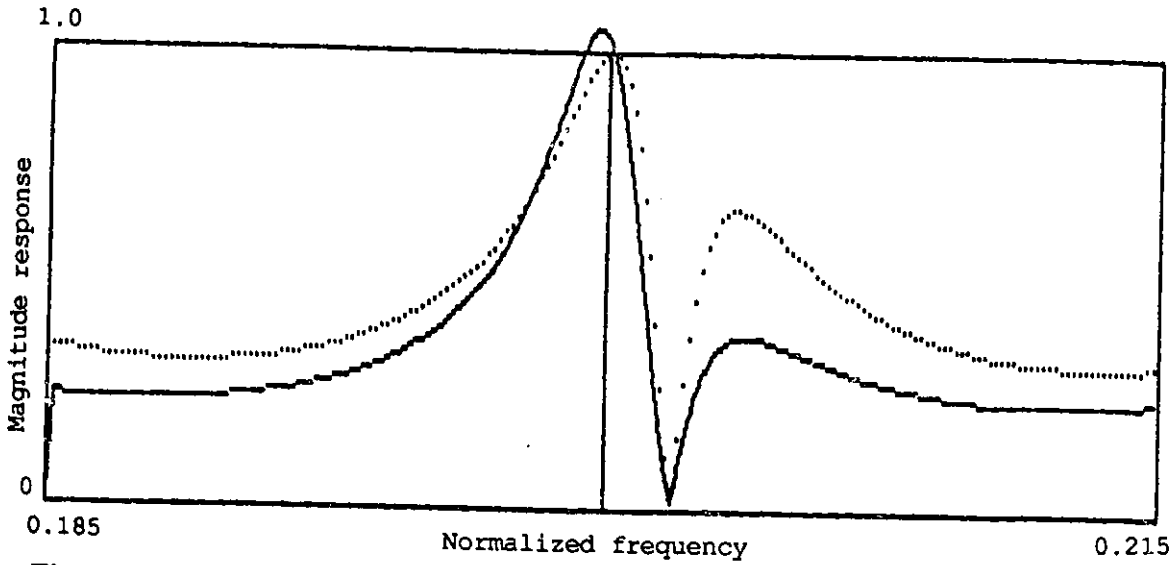

Figure 2.7 (a) Frequency responses with abnormal-optimal poles(N=2), i.e., the poles obtained after optimization with larger-angle-poles increasing their angles. Abnormal-potimal poles do move the peak of curve to the center frequency but make the filter behaviour worse.

The minimum radius is

$$r_{min} = \lambda^{\frac{\phi(\lambda_{start})}{\pi}} \tag{2.49}$$

Fig.2.6 (a) shows the complete pole trajectory situation.

(2) For the same difference of the phase angles at the starting points, $\Delta\phi$ ($\phi_2(\lambda_{start}) - \phi_1(\lambda_{start})$), the same minimum radius r_{min} is obtained, no matter where these two poles are started (see Fig.2.6 (b)).

(3) The larger the $\Delta\phi$ is, the smaller the minimum radius (see Fig.2.6 (c)).

(4) Sometimes, for the same starting phase angles $\phi_1(\lambda_{start})$, and $\phi_2(\lambda_{start})$, we get optimal angles ϕ_1 and ϕ_2 which show a difference from above rule (1), since the pole with larger angle moves with an increasing angle (see Fig.2.6 (d)). We call this special kind of solution the abnormal solution. This is because they make the sidelobe behaviour worse, even though the peaks of the response curves move to the center frequency points. Fig.2.7 (a) and (b) give the response curves of the filter bank with $N = 2$, where the curves in Fig.2.7 (a) is plotted by applying the good optimal poles, while Fig.2.7 (b) is plotted by applying the abnormal poles. The partial results of the optimal pole angles for the filter bank with N as 2, 3, 4, and 33, are given in Appendix-A.

From the simulation results with the different order logarithmic filter banks, we find that first, when the forgetting factor λ is reduced, the optimal poles move to the center of the frequency band. That is, the poles in a high frequency band reduce their angles while the poles in the low frequency band increase their angles. This behaviour changes when λ is near to or smaller than 0.8. Some of the pole angles in high band may increase, and some of the pole angles in low band may decrease. And in center band, some poles increase their angles, while some decrease. However, the case of the pole change in large size bank always can be separated into some small groups in which the poles move like the cases of small N banks. Secondly, the different forgetting factor λ gives different optimal poles,

and λ has a change range in which the optimization equations can give the convergent solution. So we may choose the different λ values for the different requirements of the filter bank, and therefore the different optimal pole sets will be obtained.

2.3.4 Applications of the optimal poles to the design of the filter banks

In order to check the optimization results, the optimal poles approach is applied to calculate the corresponding optimal *Kalman* gain coefficients according to (2.13). Then the frequency responses of the filters can be computed by (2.10) or (2.31).

A third-octave filter bank, with $N = 33$ and $\lambda = 0.8$, has been designed by determining the optimal poles and the corresponding optimal gain coefficients. The frequency responses of the last several filters in high band of the bank are plotted in Fig.2.8, where the continuous curves are the frequency responses with using the general poles defined in (2.14a) and the broken line curves are the responses using the optimal poles. It can be seen that the peaks of the response curves do move to the center frequency points and the sidelobe behaviour improves.

We designed another filter bank, a twelfth-octave filter bank with $N = 85$. Because the 85 center frequencies cover whole *Nyquist* frequency band and the last zero and pole are on the negative real axis of the z-plane, we have some difficulties to use the optimal pole angles in the range $(0, \pi)$ to calculate the optimal Kalman gain coefficients K_j. This is because, due to the pole and zero structure, there always is a term very near zero in the denominator in (2.31). Therefore, we have to optimize the poles in the range $(0, 2\pi)$. This means that much more computation is needed.

The method of *Steepest Descent* has been used to solve the large optimization equation set. The optimal poles and the corresponding Kalman gain coefficients have been calculated. Fig.2.9 shows the Log-magnitude frequency response of the whole twelfth-

octave filter bank with the application of the optimal poles.

2.4 Sensitivities and Finite-Word-Length Effects of FIFB Filter Banks[98]

When filter banks are implemented on a computer or with special purpose DSP processors (typical as TMS320 & Motorola DSP), the errors and constraints due to finite-word-length are unavoidable. The main sources of finite-register-length effects are errors due to **A/D** conversion of the input signals, errors due to roundoff in the arithmetic, constraints on signal levels imposed by the need to prevent overflow, and quantization of the filter bank coefficients.

In this section, the coefficient quantization and computational roundoff effects in frequency interpolation filter banks are studied. Filter sensitivities with respect to different parameters are derived and discussed. The effects of parameter quantization on filter frequency responses and pole positions are evaluated. The white noise models are applied to analyze the effects of filter bank arithmetic roundoff, and the noise powers at filter outputs are calculated by numerical integration techniques. Finally we will give a brief discussion about the constraints on the input to prevent overflow and zero input limited cycles of FIFB filter banks.

2.4.1 Sensitivity properties of FIFB filter banks

An important characteristics of the frequency interpolation filter bank is the sensitivity of the filter functions to the Kalman gain coefficient changes, or zero and pole positions[96]. In this subsection, single parameter sensitivity is derived in the z-domain.

The sensitivity of $H(z)$ with respect to x is defined as a partial derivative as

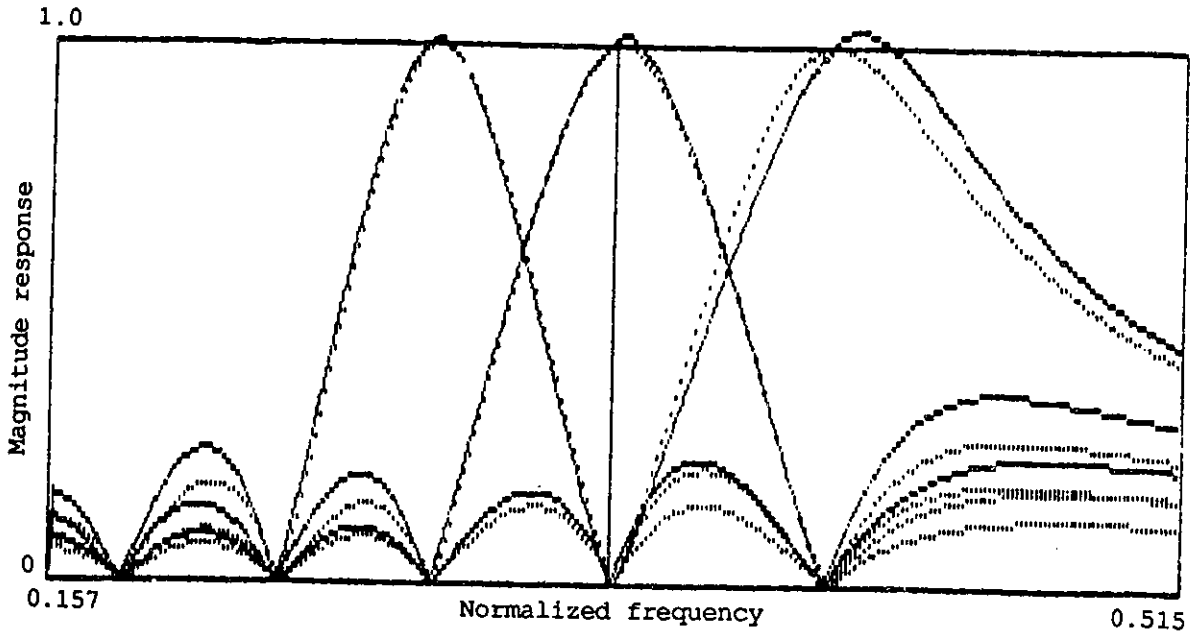

Figure 2.8 Frequency responses with general and optimal poles(N=33).
Dotted curves: Responses with general poles.
Solid curves: Responses with optimal poles.

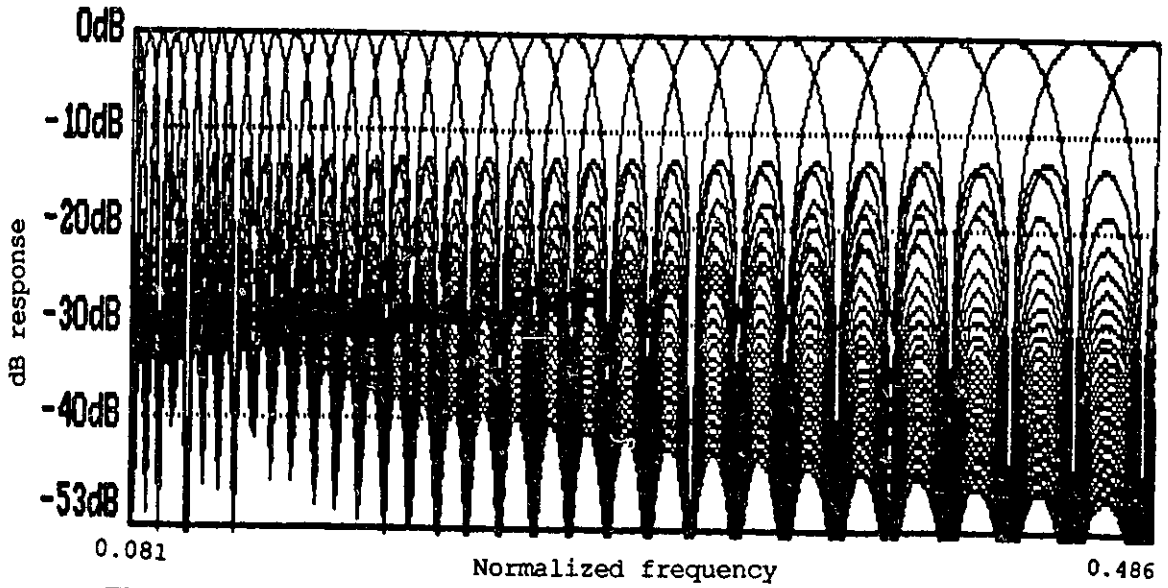

Figure 2.9 Log-magnitude frequency response of a twelfth-octave filter bank.

$$\frac{\partial H(z)}{\partial x} = S_x^{H(z)}, \tag{2.50}$$

where the changes in filter transfer function $\partial H(z)$ is related to the variations in parameter x. The operator, s, is dropped for brevity, e.g.,$H(z)$ to H. Consider the z-form transfer function of i^{th} filter in (2.11) rewritten as

$$H_i(z) = \frac{N_i(z)}{D(z)} = \frac{N_i(z)}{1 + \sum_{j=1}^{N} N_j(z)}. \tag{2.51}$$

The coefficient K_i or K_j and zero z_i or z_j sensitivity formulas for the i^{th} filter are derived and shown as follows:

$$S_{z_i}^{H_i(z)} = \frac{\partial}{\partial z_i} H_i(z) = \frac{1}{K_i} H_i^2(z)[1 + \sum_{k=1,k\neq i}^{N} N_k(z)\,] \tag{2.52}$$

$$S_{z_j}^{H_i(z)} = \frac{\partial}{\partial z_j} H_i(z) = \frac{-K_i}{K_j} \frac{1}{z - z_i} H_j^2(z) \tag{2.53}$$

$$\begin{aligned} S_{K_i}^{H_i(z)} = \frac{\partial}{\partial K_i} H_i(z) &= \frac{1}{K_i} H_i(z) \frac{1 + \sum_{k=1,k\neq i}^{N} N_k(z)}{1 + \sum_{k=1}^{N} N_k(z)} \\ &= \frac{1}{K_i} H_i(z)[1 - H_i(z)\,] \end{aligned} \tag{2.54}$$

$$S_{K_j}^{H_i(z)} = \frac{\partial}{\partial K_j} H_i(z) = \frac{-1}{K_j} H_j(z) H_i(z) \tag{2.55}$$

Because of the interpolating properties of the filter bank, i.e., $H_i(z_i) = 1$, and $H_i(z_j) = 0$ if $j \neq i$, from (2.54) and (2.55) it follows that in the vicinity of any zero z_m, $(m = 1, 2, ..., N)$ of the filters, the sensitivity with respect to any Kalman gain coefficient K_n $(n = 1, 2, ..., N)$ will be small concerning both the magnitude and phase and it will be zero if $z = z_i$, $(i = 1, 2, ..., N)$. The equations (2.52) and (2.53) can be easily changed to the following forms:

$$\begin{aligned} S_{z_i}^{H_i(z)} = &\frac{1}{K_i} H_i(z) \frac{N_i(z)}{(z - z_j) + K_j + \sum_{k=1,k\neq j}^{N} (z - z_j) N_k(z)} \\ &[\,(z - z_j) + K_j + \sum_{k=1,k\neq i,j}^{N} (z - z_j) N_k(z)\,] \end{aligned} \tag{2.56}$$

$$S_{z_j}^{H_i(z)} = \frac{-K_i}{K_j} H_j(z) \frac{N_j(z)}{(z - z_i) + K_i + \sum_{k=1,k\neq i}^{N} (z - z_i) N_k(z)} \tag{2.57}$$

where j is any number except i among $1, 2, ..., N$. From (2.52) and (2.56), and (2.53) and (2.57), it can be seen that the sensitivity with respect to any zero z_j, except at zero z_i and its vicinity, is the same case as the sensitivity with respect to K_i above. In Table II.1, we list some special sensitivity values with respect to Kalman gain coefficient K_i and zero z_i for the different frequency points.

Table II.1: Some special sensitivity values.

$S_{K_j}^{H_i(z_k)}$		$S_{z_j}^{H_i(z_k)}$	
j = i k = i	0	j = i k = i	$\frac{1}{K_i}(1 + \sum_{k=0,k\neq i}^{N-1} N_k(z_i))$
j = i k ≠ i	0	j = i k ≠ i	0
j ≠ i k = i	0	j ≠ i k ≠ i i = k	0
j ≠ i k ≠ i	0	j ≠ i k ≠ i i ≠ k	0

The general formula of the sensitivity of the i^{th} filter transfer function with respect to the j^{th} pole of the bank is given by (the long derivation is omitted)

$$S_{p_j}^{H_i(z_k)} = \frac{z_i - z_k}{(z_k - p_j)(z_i - p_j)} \tag{2.58}$$

where z_k is the k^{th} zero, p_j is the j^{th} pole, and i, j and k take any integer number between 1 and N. The equation (2.58) shows that the i^{th} filter transfer function sensitivity with

respect to the i^{th} pole, or with respect to the j^{th} pole ($j \neq i$) have zero values at the i^{th} zero. Numerical analysis of coefficient quantization effects on the filter bank performance is studied next.

2.4.2 Effects of the coefficient quantization

The design procedures of FIFB filter banks generally lead to filter coefficients K_i and parameters z_i with arbitrary accuracy and the implementation of the filter banks then requires that the K_i and z_i be modified to fit the available register length. Even if these filter banks have good sensitivity in their configurations, when realized on the hardware processors, the performance of the filter banks will be affected by the finite-word-length of registers and this will perhaps lead to a problem of stability since our filters are IIR filters. To evaluate the numerical effects, simulation programs for parameter quantization distortions on filter frequency responses have been developed. Different lengths of number of bits have been calculated for different kinds of filter banks (uniform-band spacing, third-octave and twelfth-octave). The results, in general, are in accordance with the sensitivity expression derived above. Meanwhile they show that the lower the frequency at which the filter is located in the bank, the stronger the quantization effects on the filter for nonuniform-band spacing banks, and thus uniform band filter banks suffer somewhat less than nonuniform-band banks. In Fig.2.10, distortion curves on filter magnitude frequency responses are plotted with number of bits $(B+1)$=10, 12, and 16, for a typical filter(seventh filter) in a 16-filter third-octave bank. We may see that when the registers are longer than 12 bits, the quantization distortions are small enough to be negligible. Since it is hard to obtain a mathematical relation between the i^{th} pole and quantized parameter K_j and z_k, the numerical *Newton's* method[97] is used to find the poles. Table II.2 lists poles before and after 12 bit parameter-quantization for the third-octave filter bank, and Fig.2.11 shows the pole changes caused by quantization. The

calculation results, once again show that if the filter banks are not very large(16-filter or 20-filter banks) and if the number of bits is larger than 12, the quantization effects on the pole positions may be ignored and filter banks have no problem of stability. Thus, with the application of general DSP processors, such as TMS320C25 and Motorola 56000 (both are with 16 bit registers), these FIFB filter-bank implementations are almost not affected by parameter quantization. However, when the number of the filters in the banks increases, specially for logarithmically spaced filter-banks, more poles of filters will be located at the positions closer to $z = 1.0$ in the z-plane, and thus they are more sensitive to parameter quantization[29].

2.4.3 Roundoff noise with fixed-point arithmetic

A convenient and reasonable means for analyzing the effects of roundoff errors is to represent the error statistically[29]. For the case of fixed-point arithmetic, roundoff is introduced after the multiplication and the approach is to model the effect of the rounding at each multiplier by a white-noise source uniformly distributed in amplitude between plus and minus $(1/2)2^{-B}$, where $(B+1)$ is the length of registers (including sign bit). Each of the noise source is assumed to be linearly independent of each other and of the input signal. Experimentally, these assumptions have been justified for a broad class of inputs including random signals, speech, etc. If the impulse response from the i^{th} noise source of the system to the output is $h_i(n)$ then the steady-state output-noise-variance due to the i^{th} noise source is

$$\sigma_i^2 = \sigma_\epsilon^2 \sum_{n=0}^{\infty} h_i^2(n), \tag{2.59}$$

where σ_ϵ^2 is the signal source noise variance and

$$\sigma_\epsilon^2 = \frac{1}{12} 2^{-2B}. \tag{2.60}$$

Since all the N noise sources are assumed to be uncorrelated, the total output noise is

$$\sigma_o^2 = \sigma_\epsilon^2 \sum_{i=1}^{N} \sum_{n=0}^{\infty} h_i^2(n). \tag{2.61}$$

An N filter FIFB filter bank has N resonator branches. Each of the branches, in fact, is a first order complex IIR filter and has two multipliers. The structure block-diagram of a FIFB filter bank is drawn in Fig.2.12. The signal flow graph of the filter bank with the linear rounding noise model is illustrated in Fig.2.13, where the error noise e_i for i^{th} branch is the combination of the two multiplication rounding error sources. Since we are dealing with complex multiplications, these elemental noise sources are complex. Defining the complex variance σ_B^2 as the expected squared magnitude of such a noise source, we have

$$\sigma_B^2 = 2\frac{2^{-2B}}{3} \tag{2.62}$$

where it is assumed that each of the four real-multiplications used to perform the complex multiplication is rounded separately. All N rounding noise sources in the bank contribute to each filter output-noise-power. Instead of using the impulse responses from the noise source inputs to the filter outputs in time domain, the corresponding frequency responses are applied to calculate the noise powers. It can be shown if $|H_{ij}(e^{j\omega})|$ is the frequency response in magnitude from i^{th} noise source to j^{th} output of the bank, then the power spectrum element of the j^{th} output noise caused by i^{th} source noise $e_i = e_B$ is

$$P_{ij}(\omega) = \sigma_B^2 |H_{ij}(e^{j\omega})|^2. \tag{2.63}$$

The total power spectrum of the j^{th} output noise caused by all the noise source inputs is

$$P_j(\omega) = \sum_{i=1}^{N} P_{ij}(\omega) = \sigma_B^2 \sum_{i=1}^{N} |H_{ij}(e^{j\omega})|^2. \tag{2.64}$$

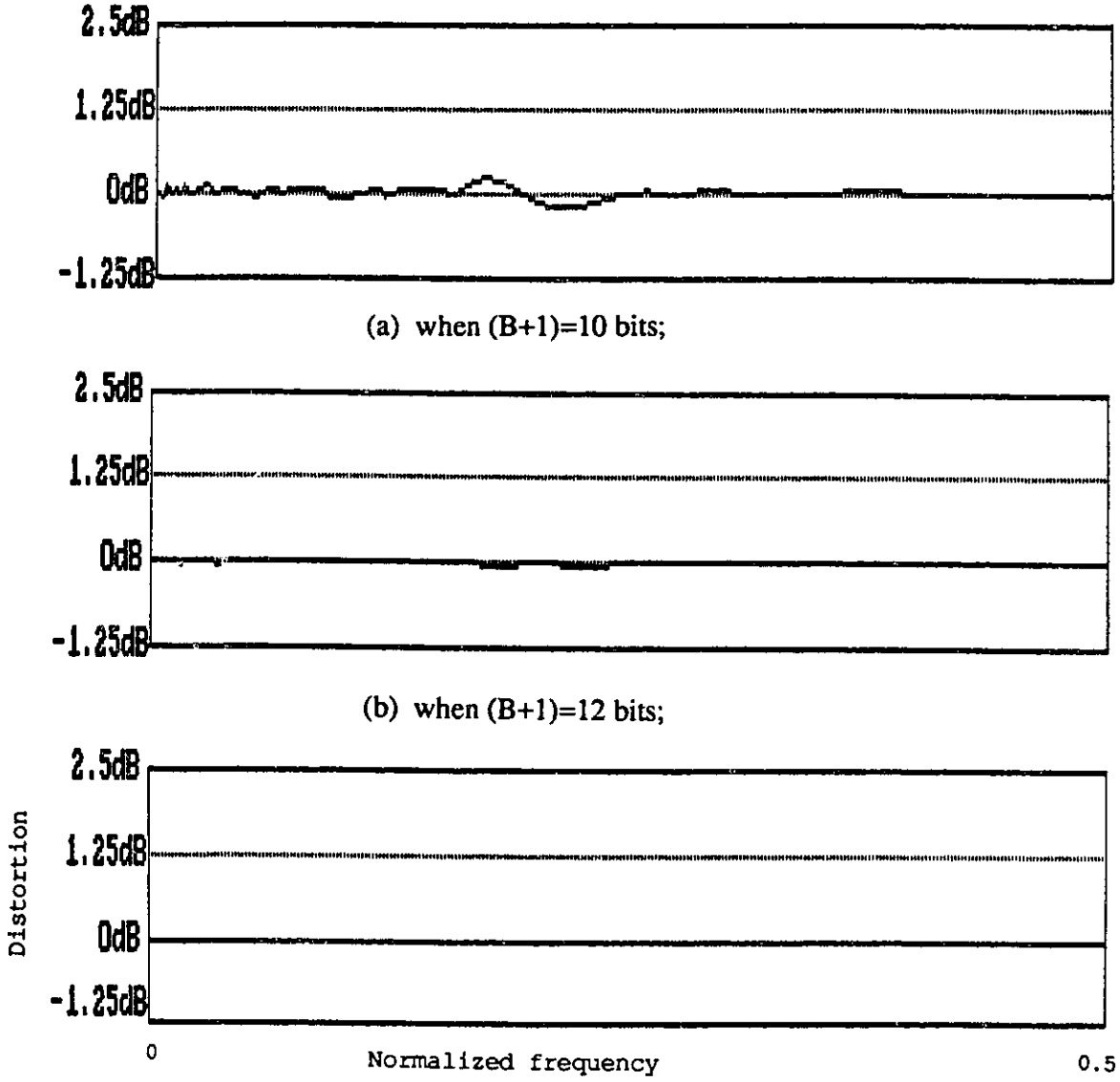

Figure 2.10 Seventh filter frequency response distortions in a 16-filter third-octave bank by parameter quantization.

Table II.2: Pole modulus of third-octave filter bank with N=16 and (B+1)=12.

Filter	Before Q(.)	After Q(.)
1	0.98910640	0.98925812
2	0.98595891	0.98620681
3	0.98221774	0.98234266
4	0.97734496	0.97653006
5	0.97104295	0.97199576
6	0.96293141	0.96327307
7	0.95252180	0.95214825
8	0.93920081	0.93967267
9	0.92221549	0.92321266
10	0.90066890	0.90018159
11	0.87354333	0.87354724
12	0.83978564	0.84013819
13	0.79852634	0.79773919
14	0.74959998	0.74955809
15	0.69477035	0.69468012
16	0.62860795	0.62851262

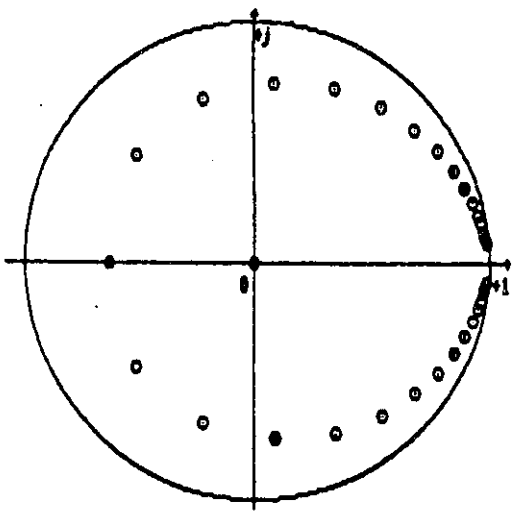

Figure 2.11 Pole change plot with pramater-quantization for the third-octave filter bank.
Circles: Ideal poles; Dots: Poles after quantization.

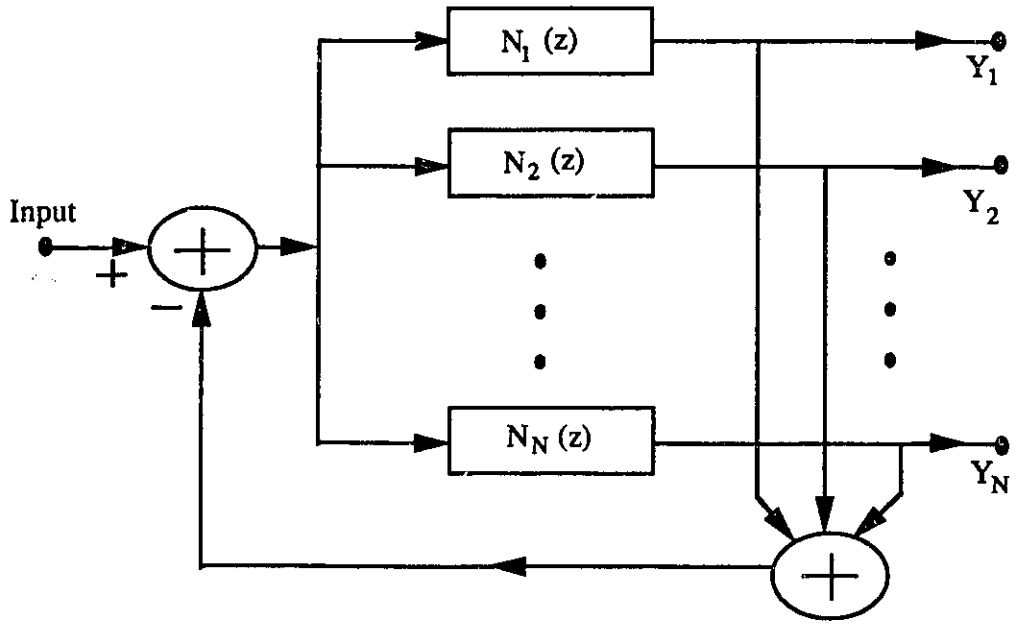

Figure 2.12 The block digram of the structure of a FIFB filter bank.

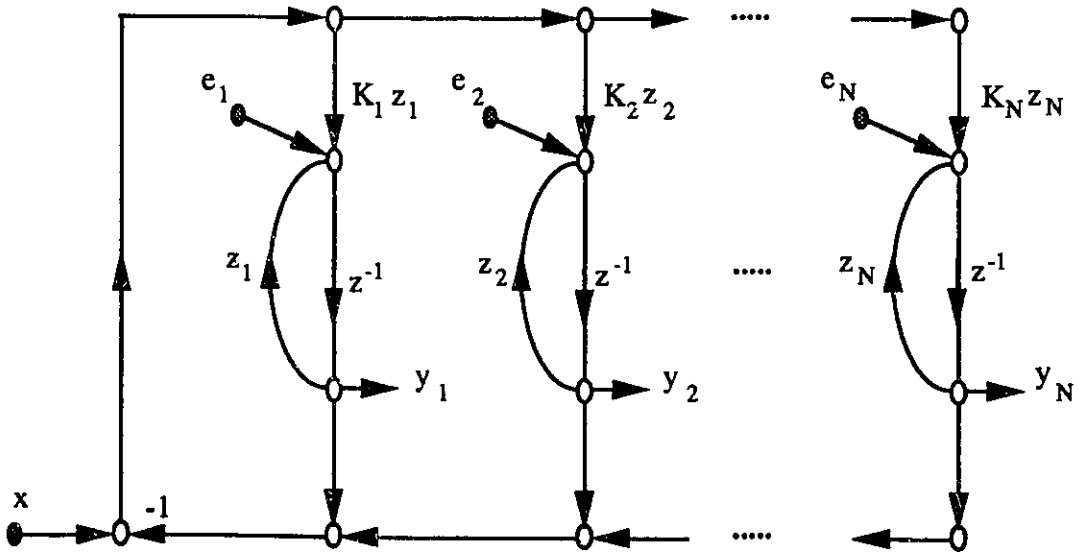

Figure 2.13 Signal flow graph of the FIFB filter bank with combined linear noise models.

Thus, the variance of the output noise in the j^{th} filter is

$$\sigma_j^2 = \sigma_B^2 \frac{1}{2\pi} \int_{-\pi}^{\pi} \sum_{i=1}^{N} |H_{ij}(e^{j\omega})|^2 d\omega. \tag{2.65}$$

From Fig.2.13, the transfer functions $H_{ij}(z)$ are not hard to derive, and then the frequency responses can be expressed as

$$H_{ij}(e^{j\omega}) = \frac{\frac{1}{e^{j\omega}-e^{j\omega_i}} G_j(e^{j\omega})}{1+\sum_{r=1}^{N} \frac{K_r e^{j\omega_r}}{e^{j\omega}-e^{j\omega_r}}} \tag{2.66}$$

and

$$G_j(e^{j\omega}) = \begin{cases} 1, & \text{if j=i;} \\ \frac{K_j e^{j\omega_j}}{e^{j\omega}-e^{j\omega_j}}, & \text{otherwise.} \end{cases} \tag{2.67}$$

However, since the outputs of the filters from $(N/2+1)$ to N(N always is a even number in the case) are complex conjugate of the outputs of the filters from 1 to $N/2$, the whole filter bank thus is realized by implementing only first $N/2$ filters. The feedback in Fig.2.12 should, of course, be two times the summation of the real parts of the filter outputs. Consequently, only $N/2$ roundoff-noise-sources need to be considered, and the noise power, which is reduced, may be calculated in

$$\sigma_j^2 = \frac{2^{-2B}}{3\pi} \int_{-\pi}^{\pi} \sum_{i=1}^{N/2} |H_{ij}(e^{j\omega})|^2 d\omega\,. \tag{2.68}$$

Note that when the input is a real signal, the noise powers of filter outputs are reduced by three-fourths, since the eight real multiplications in each resonator branch of Fig.2.12 are reduced to six.

The calculations of filter output noise powers of the banks are accomplished by *Gaussian Quadratures*[97] integration techniques. The numerical results for the two filter banks, one 16-filter third-octave bank and another 20-filter uniform-band bank, are listed in Table II.3. It can be seen that the output noise power depends on the frequency bandwidth of the filter. For example, the noise gain (the integration part in equation

(2.68)) of the last filter (with the widest bandwidth) in the third-octave bank is about 41.5 times of first one (with the narrowest bandwidth). However, when $(B+1) = 16$, the output powers(-75dB) are still very small and good in practical applications of these FIFB filter banks. The filter output-noise-gains are approximately directly proportional to the filter bandwidths. For example, for the 16-filter third-octave filter bank, we have an approximate relation:

$$\frac{[Bandwidth]}{[NoiseGain]} \approx 2.7 * 10^{-4}. \tag{2.69}$$

2.4.4 Dynamic range considerations for fixed-point implementation of FIFB filter banks

The possibility of overflow must be considered in the implementation of FIFB filter banks with fixed-point arithmetic. With the convention that each fixed-point register represents a signed fraction, each node in the filter bank structure must be constrained to maintain a magnitude less than unity in order to avoid overflow. As we have defined $x(n)$ as the filter bank input, and letting $y_k(n)$ and $h_k(n)$ denote the output and impulse response for the k^{th} node in the filter bank, then

$$y_k(n) = \sum_{r=0}^{\infty} h_k(r)\, x(n-r). \tag{2.70}$$

If x_{max} denotes the maximum of the absolute value of the input then

$$|y_k(n)| \leq x_{max} \sum_{r=0}^{\infty} |h_k(r)|. \tag{2.71}$$

Thus , since we require that $|y_k(n)| < 1$, (2.71) requires that

$$x_{max} < \frac{1}{\sum_{r=0}^{\infty} |h_k(r)|}, \qquad for\ all\ k. \tag{2.72}$$

Equation (2.72) thus provides an upper bound on the maximum value of the input to insure that no overflow occurs in the k^{th} node. For a general input (2.72) in fact provides

a least upper bound, i.e., if the maximum value of the input exceeds the bound, overflow can occur. The condition in (2.72) would be satisfied by applying attenuation to the signal at filter bank input. This result can be used in any kinds of IIR filters or IIR filter banks.

In practical case, a scaling of the input on the basis of (2.72) can be considered to be somewhat pessimistic since the probability of equality being attained in (2.72) is extremely small. Furthermore, it is difficult to compute the sum in (2.72). For the FIFB filter banks, as we mentioned before, the whole N filters in a FIFB bank will be realized in N/2 filters, where the feedback is two times the sum of the real parts of first N/2 filter outputs. To reduce the computations and avoid possible overflow, scaling by 2 in the feedback is removed and is completed together with $K_i z_i$ multipliers. Thus, the implementation structure diagram of the filter bank is as Fig.2.14, where we have noted that the outputs get 6 dB gain because of the position of scaling by 2. Considering the worst and special case, i.e., when the input is real cosine signal as $cos(n\omega_i)$, the feedback gets the same signal as the input since now all the outputs except i^{th} one, have the zero output, the i^{th} filter output $cos(n\omega_i)$. The error signal is zero and the filter bank has no overflow. In general, if magnitudes of the input are smaller than unity the error is not equal to zero but still very small since the feedback signal closes to the value of the input. All the nodes of filter bank have the signal magnitude not larger than unity. This has been verified by analogue computer experiments. Thus, the maximum magnitude of the input of the FIFB filter banks, x_{max}, is unity. This means that there is no overflow problem with fixed-point arithmetic. Based on the analysis above, we have known that the maximum magnitude of the filter output is unity also and consequently so is the maximum filter output power. Therefore the dB values listed in Table II.3, in fact, are the maximum noise-to-signal ratio.

Table II.3: Filter normalized bandwidths and output noise powers(in -dB) of two filter banks with (B+1)=16 and a real input signal.

20-filter uniform-bandbank with filter Nor.bandwidth as 0.02	All the filters have the same output noise power as 85					
16-filter third-octave filter bank	No.	Nor.bandwidth	Noise power	No.	Nor.bandwidth	Noise power
	1	0.002872	91.20	9	0.018234	83.03
	2	0.003618	90.08	10	0.022974	82.02
	3	0.004559	89.07	11	0.028945	80.94
	4	0.005744	88.06	12	0.036469	79.90
	5	0.007236	87.06	13	0.045948	78.78
	6	0.009117	86.06	14	0.057891	77.84
	7	0.011487	85.05	15	0.072938	76.54
	8	0.014473	84.05	16	0.091896	75.02

Note that the experiments of the filter bank implementation shows that these filter banks sustain small zero-input limit cycles. This is not surprising since they are IIR filter banks with two layers feedback loops, i.e., the inside feedback loops of each branch and the outside feedback loop of the whole filter bank. The effect of the small zero-input limit cycles due to roundoff is not serious with the 16-bit wordlength implementation, and therefore we will not attempt to treat this complex and difficult topic in any mathematical sense. However, it is helpful to note that the limit cycles in the bank system (see Fig. 2.12) vary from filter to filter, and even though the system input is zero, the branch inputs do not vanish because of the outside feedback loop. Thus, the limit cycles in the outputs of filters are not constant in the amplitude.

2.5 Summary

In this chapter, the frequency interpolation filter bank was first introduced from the point of view of an equivalent adaptive filtering structure, the approximation of the Kalman gain coefficients, the design procedure and the implementation strategy of the filter banks. Then, the design of maximally flat FIFB filter banks is considered. A procedure is proposed to find the optimal poles: use the same way to keep the radius of the poles for a more constant-Q for the filters as for the general FIFB banks, but adjust the phase angles of the poles to make the peaks of the frequency responses occur at the center frequencies and to make the values of the peaks be unity. The nonlinear optimal pole equations are derived, and the optimal poles of some particular filter banks and the filter gain coefficients with the optimal poles have been calculated to design the banks. The results show that the maximally flat filter banks are achieved, and more symmetrical passband property and better sidelobe behaviour are obtained due to the optimal poles. Finally, the sensitivity formulas of the filter transfer functions to the coefficient, and pole and zero positions are derived and discussed. The results of analysis and numerical cal-

culations show that frequency interpolation filter banks have good parameter sensitivity, and when they have the size with 16-filters or 20-filters and are implemented with general 16-bit word length DSP processors, such as TMS320C25 or Motorola 56000, the effects of coefficient quantization and arithmetic roundoff errors may be negligible.

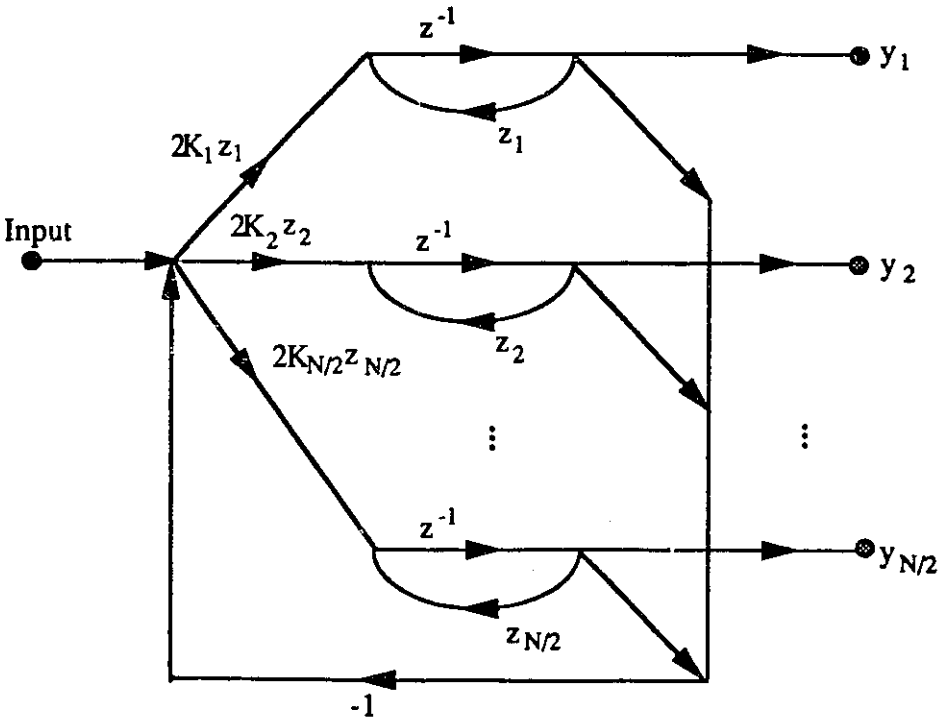

Figure 2.14 The signal flow graph of the FIFB filter banks implemented.

III RESONATOR-BASED LOGARITHMIC FILTER BANKS

3.1 Introduction

In the last chapter, we described the frequency interpolation filter banks based on an adaptive filtering structure. Besides allowing for the arbitrary spacing of the filter center-frequencies, the FIFB filter bank is very efficient in computation and implementation. However, the frequency responses could be improved for more applications because the frequency responses have appreciable sidelobes and non-constant-Q filters, or non-constant crossover gain of the filter banks. In this chapter, we will present a new approach to the design and analysis of the filter banks. The digital resonator with purely imaginary transfer function on the unit circle is treated as the basic element of the filter bank. Since the frequency interpolation structure is applied, the filter bank designed by this technique still retains the properties similar to FIFB banks. But the new approach makes the bank behaviour much better and clearer.

First, the general theory of resonator filters is presented, concentrating on the *Foster* property of the resonators. Then, the approximation problem for logarithmic filter banks, the sensitivity properties, a numerical example of an 85-filter bank, and the design theory for an infinite filterbank are studied. Finally the connection to normalized LMS adaptive filtering is made.

3.2 Resonator Filters

The essential element of the filter banks in question is a set of resonators with resonant frequency ω_i. These resonators have the transfer function

$$\frac{p_i}{(z - p_i)}, \tag{3.1}$$

where a pole p_i of a resonator is on the unit circle with $p_i = e^{j\omega_i}$. The analysis of these structures is based on continual use of the identity

$$\frac{p_i}{(z-p_i)} = -\frac{1}{2} + \frac{1}{2}\frac{(z+p_i)}{(z-p_i)}. \tag{3.2}$$

On the unit circle, this is a decomposition of $\frac{p_i}{(z-p_i)}$ into its real and imaginary parts. However, this mixture of real and imaginary parts makes a connection with classical filter theory difficult, since that theory deals with elements that are either purely real (resistors), purely imaginary (the imaginary resistor) or purely reactive (the capacitor, the inductor, the shunt resonator–open circuit at resonance and the series resonator–short circuit at resonance). Consequently we are proposing that the basic element of this theory be the element

$$Z_i(z) = K_i\frac{(z+p_i)}{(z-p_i)}, \tag{3.3}$$

with the real and positive number K_i the resonator gain (or Kalman gain like that in the last chapter), and p_i the unity magnitude resonator pole is characteristic of the real resonator frequency ω_i $(-\pi < \omega_i \leq \pi)$, and

$$p_i = e^{j\omega_i}. \tag{3.4}$$

This unit-resonator has a zero at $-p_i$, and $Z_i(z)$ is purely imaginary on the unit circle.

The resonator transfer function is a reactance function: $Z_i(z)$ is purely imaginary on the unit circle, has a real part that is negative inside the unit circle, and a real part that is positive outside the unit circle. As well, the slope of the resonator imaginary part is positive on the unit circle and thus obeys the *Foster* reactance property.

The modification of a reactance function by the addition of an imaginary constant is usually of no theoretical consequence, and this permits a variety of normalizations, forcing a zero at an appropriate location on the unit circle. For example, it might be

useful, for theoretical reasons, to force all reactance functions to have a zero at 1, or -1; this is possible as long as they do not have a pole at the same point! That is why it is very important to note that a resonator is described by its pole at p_i and not by the zero at $-p_i$.

A general *Foster* function on the unit circle is thus described by the N poles p_i, the N corresponding real gain constants K_i and a constant jB, representing the constant reactance. Consequently, the resonator may be considered as the bilinear transformation of the s-domain resonator $\frac{1}{(sL-jX)}$.

Because of the positive slope property of reactance, the usual results[99] for reactance may be stated: if $Z_i(z)$ is a reactance function, so is $\frac{1}{Z_i(z)}$, and $CZ_i(z)$ where C is real and positive. The sum of two reactance functions is a reactance function, and we thus have the fundamental result that if the number of poles of a reactance function is finite, the poles are simple, the function has the same number of zeros as that of the poles, and the poles and zeros are interlaced. Finally, if $Z = \sum_j Z_j(z)$ is a reactance function, then the zeros of $[1 + Z(z)]$ are inside the unit circle. This follows simply because the real part of $Z(z)$ is positive outside the unit circle, and thus $[1 + Z(z)]$ cannot vanish there.

It is clear that a theory of digital prototype filters based on passive networks is possible, and they will be expected to have the same desirable properties as passive filters. In the present context, however, we are only interested in one such configuration (see the block diagram in Fig.3.1), which corresponds to a transfer function given by

$$H_i(z) \;=\; \frac{Z_i(z)}{[\,1 + Z(z)\,]} \;=\; \frac{Z_i(z)}{D(z)}, \tag{3.5}$$

or specifically

$$H_i(z) = \frac{Z_i(z)}{[\,1 + \sum_{j=1}^{N} Z_j(z)\,]} = \frac{K_i \frac{(z+p_i)}{(z-p_i)}}{1 \;+\; \sum_{j=1}^{N} K_j \frac{(z+p_j)}{(z-p_j)}}. \tag{3.6}$$

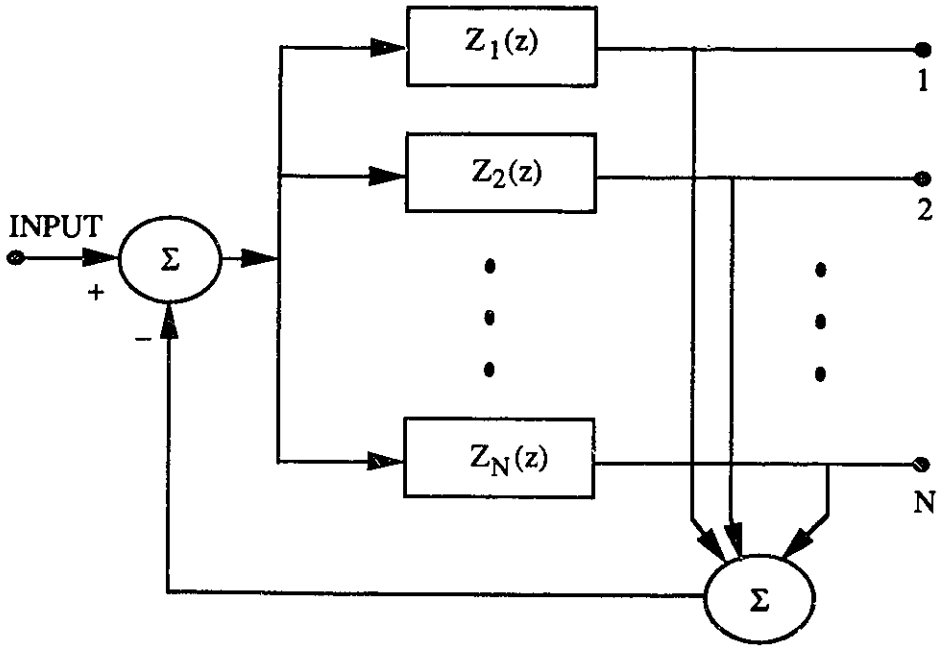

Figure 3.1 The block diagram of RFB filter bank.

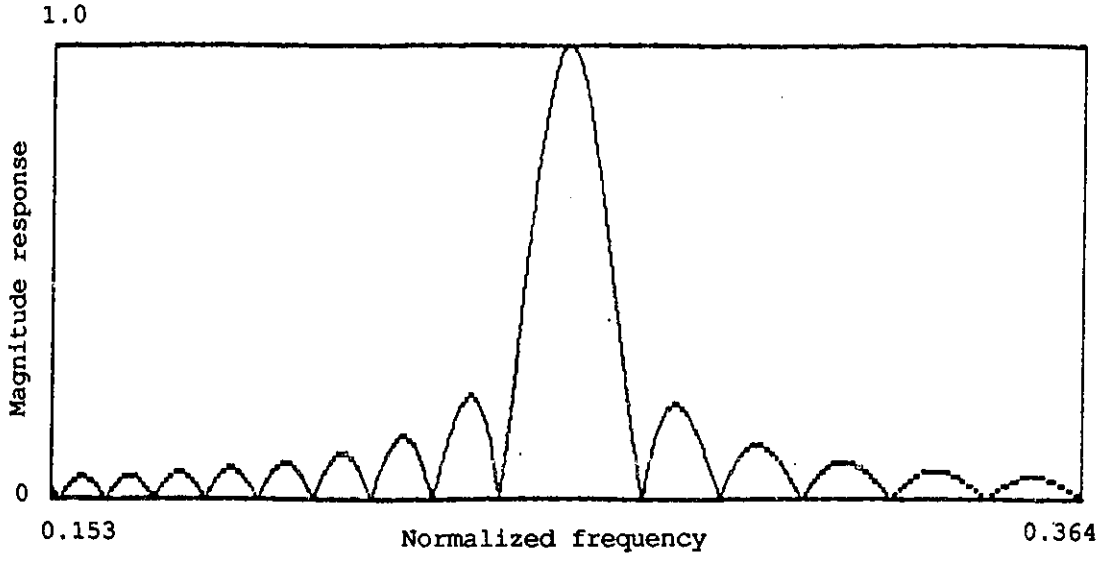

Figure 3.2 Frequency response of a typical filter in the RFB filter banks.

As a matter of fact, the same FIFB structure is applied(see Fig.2.12) but the basic element of the system is the resonators with the purely imaginary magnitudes on the unit circle. $H_i(z)$ in (3.6) is called a resonator-based frequency interpolating filter because its response satisfies

$$H_i(e^{j\omega_j}) = \delta(i-j), \qquad 1 \leq j, i \leq N \tag{3.7}$$

that is, it is unity at the frequency ω_i and zero at the other frequencies $\omega_j, j \neq i$. Another fundamental property of this filter class is that the magnitude of $\frac{1}{[1+Z(z)]}$ is always less than unity on the unit circle. This follows because $Z(z)$ is purely imaginary on the unit circle. Consequently the magnitude of $H_i(z)$ on the unit circle is always less than that of $Z_i(z)$. In addition, this kind of filter banks(Fig.3.1), described by $H_i(z)$, $1 \leq i \leq N$, have the maximally flat frequency responses since it can be shown that $\frac{\partial}{\partial \omega} H_i(e^{j\omega}) \mid_{\omega=\omega_i} = 0$.

The frequency behaviour of this function $H_i(z)$ is rather difficult to evaluate aside from the pole locations p_i but one other set of frequencies is useful to consider, the zeros q_j of $Z(z)$, $1 \leq j \leq N$. We know that the zeros q_j interlace the poles p_j, and at these zeros the responses of $H_i(z)$ and $Z(z)$ match, that is

$$H_i(q_j) = Z_i(q_j), \qquad 1 \leq i, j \leq N. \tag{3.8}$$

In particular, the real part of $H_i(z)$ is zero at a zero q_j; $H_i(z)$ is purely imaginary at these frequencies. The frequency response will thus have the general shape of Fig.3.2.

Finally note that based on the basic element of the FIFB banks, i.e., the first-order complex filter $N(z)$ in (2.11), we have

$$\begin{aligned} K_i \frac{z_i z^{-1}}{1 - z_i z^{-1}} + K_i^* \frac{z_i^* z^{-1}}{1 - z_i^* z^{-1}} \\ = \frac{2z^{-1}[Re(K_i z_i) - z^{-1} Re(K_i)]}{1 - 2Re(z_i) z^{-1} + z^{-2}}, \end{aligned} \tag{3.9a}$$

and based on the basic element of the RFB banks, i.e., the purely imaginary magnitude resonator $Z_i(z)$, we have

$$\begin{aligned} K_i\frac{(z+p_i)}{(z-p_i)} + K_i\frac{(z+p_i^*)}{(z-p_i^*)} & \\ &= 2K_i\frac{(z-1)(z+1)}{(z-p_i)(z-p_i^*)} \\ &= \frac{2K_i(z^{-2}-1)}{1-2Re(p_i)z^{-1}+z^{-2}}, \end{aligned} \tag{3.9b}$$

where $Re(x)$ denotes taking the real-part of a complex number x, and K_i^*, z_i^*, and p_i^* are the complex conjugates of K_i, z_i, and p_i, respectively. If one is dealing only with real signals, these would be more natural definitions for the resonators, since all the coefficients are real. However, we usually require the complex filter for most applications.

3.3 Approximation for Filter Banks

In this section, three approaches are described for the approximation of the RFB filter banks, i.e., for the calculation of the filter coefficients K_i, $1 \leq i \leq N$.

(1) To calculate K_i from assigned p_i and q_i: In general, the poles p_i are specified in advance, and a "desirable" frequency response known. The denominator $D(z)$ in equation (3.5) is common for all the filters $H_i(z)$. If the zeros q_j of $Z(z)$ are also specified, then the overall denominator is

$$1 + G\,\frac{Q(z)}{P(z)}, \tag{3.10}$$

where

$$Q(z) = \prod_{j=1}^{N}(z-q_j) \tag{3.11}$$

$$P(z) = \prod_{j=1}^{N}(z-p_j), \tag{3.12}$$

and the G is a gain adjustable for better frequency property. Generally, the gain G is a complex number, but for the filter bank structures considered in following sections, G is a real number(see the proof in Appendix-B). The poles p_i and the zeros q_i must interlace. With a logarithmic spacing for the frequencies ω_i, it would be natural to choose the zeros q_i as the harmonic mean or geometric mean of the adjacent poles p_i and p_{i+1} along the unit circle. For deriving the remaining gain coefficients K_i, if the zeros of $Q(z)$ are determined after p_i, then from equations (3.6), (3.10), (3.11) and (3.12), the following relation can be obtained

$$\sum_{j=1}^{N} \frac{K_j(z+p_j)}{(z-p_j)} = G \frac{\prod_{j=1}^{N}(z-q_j)}{\prod_{j=1}^{N}(z-p_j)}. \tag{3.13}$$

Thus it is easy to derive the i^{th} gain K_i as

$$K_i = \frac{G}{2p_i} \frac{\prod_{j=1}^{N}(p_i-q_j)}{\prod_{j=1,j\neq i}^{N}(p_i-p_j)}. \tag{3.14}$$

(2) To determine q_i from assigned p_i and K_i: Another way is that the coefficients K_i may be simply specified, then q_i is determined by (3.13). In many cases the sum of the K_i is unity, (resulting in a pole at the origin), so assigning to K_i the fraction of the unit circle near the pole p_i is logical.

(3) More generally, if the zeros of the denominator polynomial $D = P+Q$ are specified in advance, for example all at the origin, then the values of p_i, q_i and K_i may be determined by considering the partial polynomials as $(D+D_*)/2$ and $(D-D_*)/2$. where D_* means to take complex conjugate of the coefficients of D and to reverse their order in the polynomial.

3.4 Logarithmic Filter Banks (Numerical Example)

In this section, the design of a twelfth-octave filterbank with 7 octaves is considered, which is useful to analyze music. This results in 7 * 12 + 1 = 85 frequencies ω_i, or,

since negative frequencies must be included, 170 frequencies. This specifies the poles p_i. The zeros of $Z(z)$, q_i, will be chosen so that the imaginary part of their logarithm is the harmonic mean or geometric mean of the adjacent frequencies ω_i and ω_{i+1}. This specifies all of the zeros of $Z(z)$.

The harmonic mean has the property that the frequency difference between the zero below and the zero above a pole is equal, and therefore, promises that the filters in the banks will have better symmetric passband property. The geometric mean gives a slightly different mean value from the harmonic mean.

Based on whether the number of the poles or zeros of $Z(z)$ is even or odd, and whether $z = 1$ and $z = -1$ are a zero or a pole of $Z(z)$, there exist four different pole-zero structures:

(1) Even number of poles with zeros at $z = \pm 1$ (see Fig.3.3 (1)).

(2) Even number of poles with poles at $z = \pm 1$ (see Fig.3.3 (2)).

(3) Odd number of poles with a pole at $z = 1$ and a zero at $z = -1$ (see Fig.3.3 (3)).

(4) Odd number of poles with a zero at $z = 1$ and a pole at $z = -1$ (see Fig.3.3 (4)).

Now let's consider the case (2), where a pole of $Z(z)$ is placed at unity, and another at $z = -1$. Since the zeros correspond to musical quartertones, make the largest zero correspond to musical semitone as well; this fixes the sampling frequency. Thus choose the pole frequencies–the center frequencies of the filter bank as:

$$f_r = 0.5e^{[-(r-1)\frac{ln2}{12}]}, \qquad (r = 1, 2, ..., 85) \tag{3.15}$$

$$f_{86} = 0.0, \tag{3.16}$$

$$f_{86+r} = -f_{86-r}, \qquad (r = 1, 2, ..., 85) \tag{3.17}$$

and

$$\omega_r = 2\pi f_r, \tag{3.18}$$

$$p_r = e^{(j\omega_r)}, \qquad (r = 1, 2, ..., 170) \tag{3.19}$$

Similarly, according to the harmonic mean the zero frequencies are chosen as

$$\nu_r = (0.5e^{[-(r-1)\frac{ln2}{12}]})/(1 + e^{(\frac{ln2}{12})}), \qquad (r = 1, 2, ..., 85) \tag{3.20}$$

$$\nu_{r+85} = -\nu_{86-r}, \qquad (r = 1, 2, ..., 85) \tag{3.21}$$

and

$$\phi_r = 2\pi\nu_r \tag{3.22}$$

$$q_r = e^{(j\phi_r)}, \qquad (r = 1, 2, ..., 170) \tag{3.23}$$

The gain coefficients K_r have been calculated, and when computing the coefficient to frequency ratios $\frac{K_r}{f_r}$ we find the ratios are almost constant, which is to be expected since the gain will be approximately the same at the frequencies ν_r.

The calculations for the four different pole-zero structures described above have been done with the zeros of $Z(z)$, q_r, being chosen according to both harmonic mean and geometric mean. For harmonic mean zeros, even though for all cases the K_r are almost proportional to the frequency f_r, but K_r changes with f_r somewhat and there are different frequency responses. The increasing ratios $\frac{K_r}{f_r}$, with frequency in the structures (2) and (3) give more reasonable frequency responses than the structures (1) and (4), where $\frac{K_r}{f_r}$ decreases with frequency(see Fig.3.4). It is also interesting that in the pole-zero structures (2) and (3), the geometric mean zero structure leads constant ratio $\frac{K_r}{f_r}$ except near the end (zero center frequency), and an approximate constant crossover gain of the logarithmically spaced frequency filter bank(see Fig.3.5). The significant fact is that the scalar G thus may be used helpfully to improve the passband as well as to control the crossover gain of the filters. The G can be determined by following equation (see Appendix-C)

$$G = |\frac{1}{K_I}\frac{q_I - p_I}{q_I + p_I}|10^{-\frac{M}{20}}, \tag{3.24}$$

where M is the crossover gain in dB value and I is a typical number between 1 and order N, but the experiments show that I should be from 2 to $Round(\frac{1}{6}N)$ for harmonic mean, and from 2 to $Round(\frac{4N}{5})$ for geometric mean. Note that the K_I is calculated according to equation (3.14) with unity G. Fig.3.6 shows the Log-magnitude frequency responses of the filters with the geometric mean zeros and the pole-zero structure (3). The scalar G is determined as 1.08 for -3dB crossover gain in the filter bank.

For further exploration, note that the gross behaviour in the stop band is determined by the factor $Z_i(z)$ which is the product of the real number K_i and the "universal" function $\frac{(z+p_i)}{(z-p_i)}$. At the zeros of $Z(z)$, the response of $H_i(z)$ is linear in K_i (we are neglecting the complicated relationship between the zeros q_i and the coefficients K_i). In order to gain control of the passband behaviour, let us assume that the zeros occur at harmonic means, and calculate the frequency response neglecting the denominator. In particular at the first zero above and below a pole the response is

$$-jK_i cot[\ 0.5 * \omega_i\ tanh(\frac{ln2}{24})\ ], \tag{3.25}$$

which is approximately

$$\frac{-jK_i}{(\omega_i\ \frac{ln2}{48})} = \frac{-jK_i}{(\frac{\omega_i}{2\pi} * 0.0907)} \tag{3.26}$$

since $ln(2)$ is 0.69314. A 3-dB loss at this frequency will require

$$K_i = 0.707 * \omega_i * 0.0144 = 0.06412 * \frac{\omega_i}{(2\pi)}. \tag{3.27}$$

Thus we have a simple rule to obtain the gain coefficients.

3.5 Filter Bank with an Infinite Number of Filters

The previous section has shown that the filter responses that result when a finite structure is used is basically uniform except near the ends. In this section we consider a filter bank with infinite number of filters from the theoretical point of view.

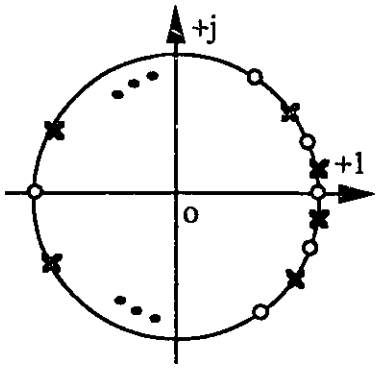

(1) Even number of poles

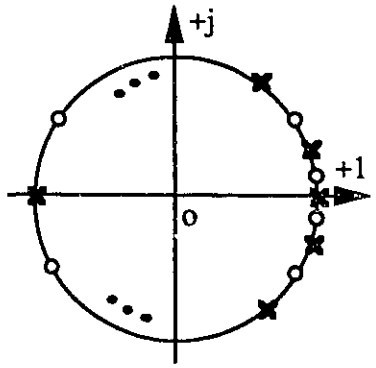

(2) Even number of poles

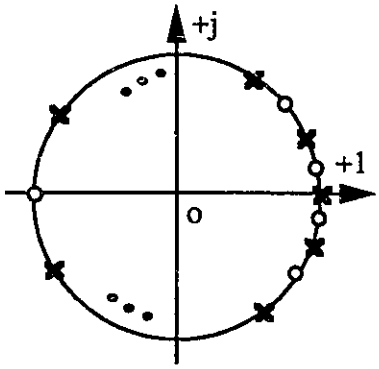

(3) Odd number of poles

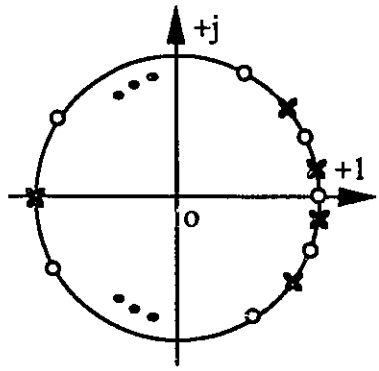

(4) Odd number of ploes

Figure 3.3 The pole and zero structures of Z(z).

✖ -- pole, o -- zero.

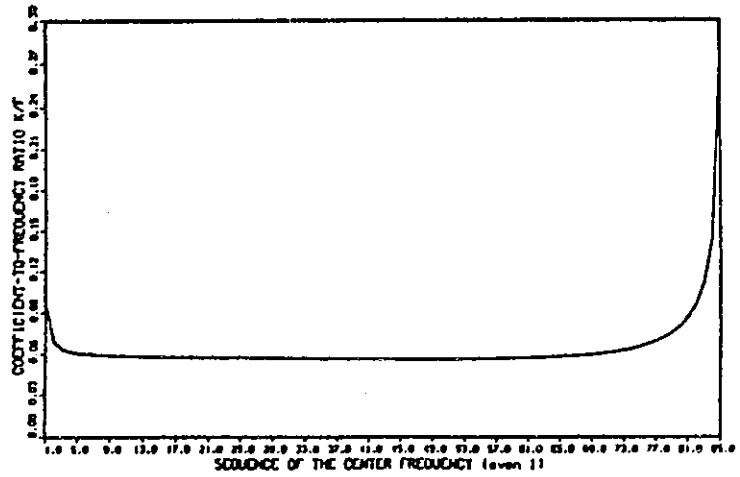

(a) Pole-zero structure (1)

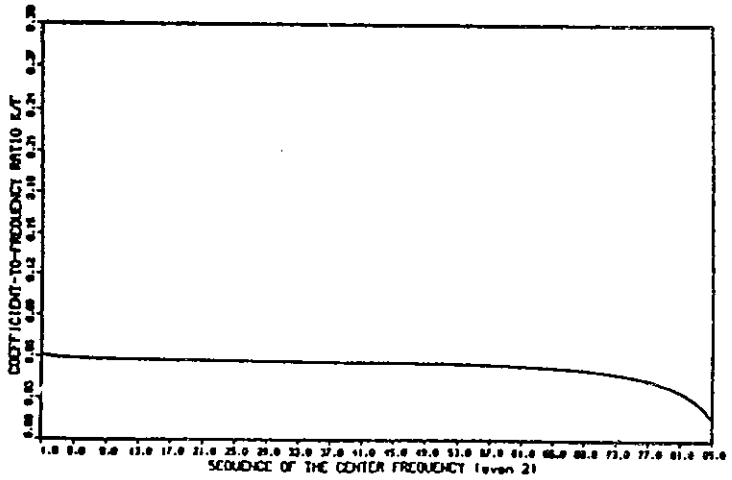

(b) Pole-zero structure (2)

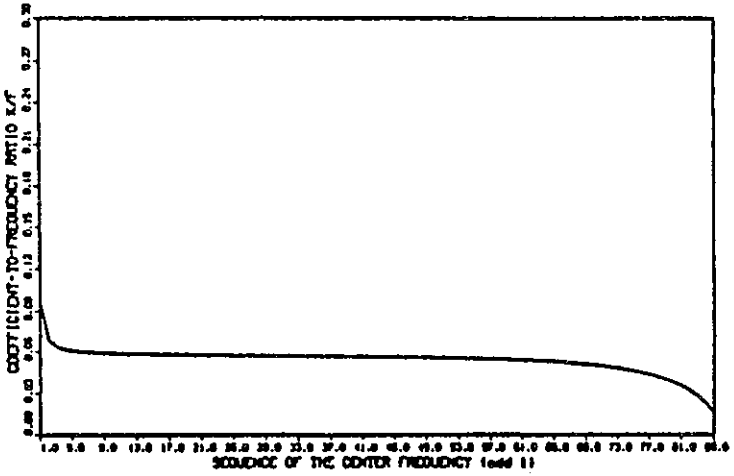

(c) Pole-zero structure (3)

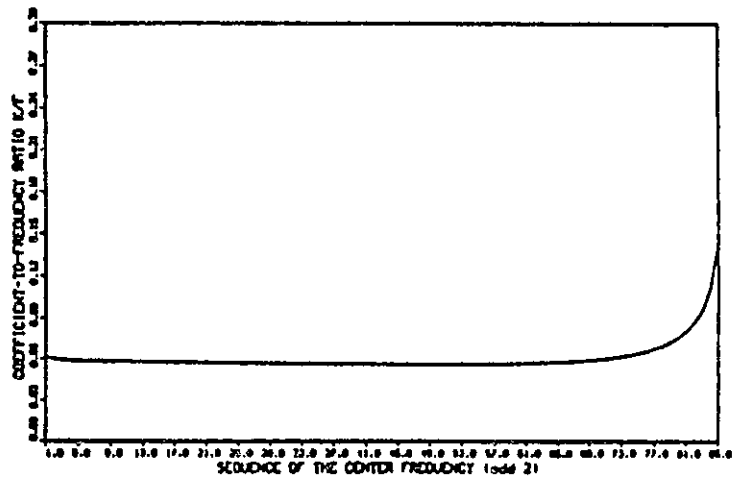

(d) Pole-zero structure (4)

Figure 3.4 The ratio Kr/fr curves.

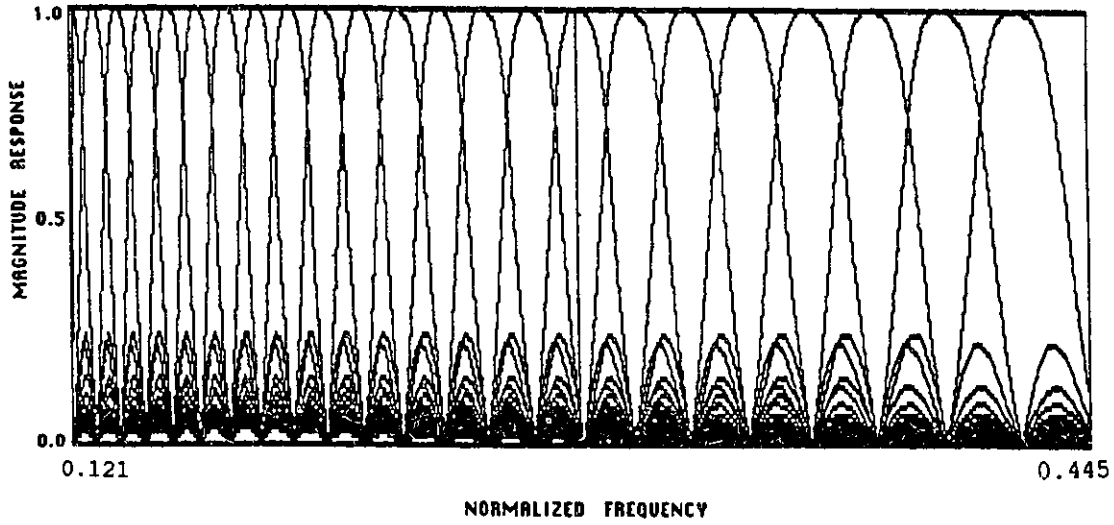

Figure 3.5 Frequency response of the filter bank with geometric mean zero structure.

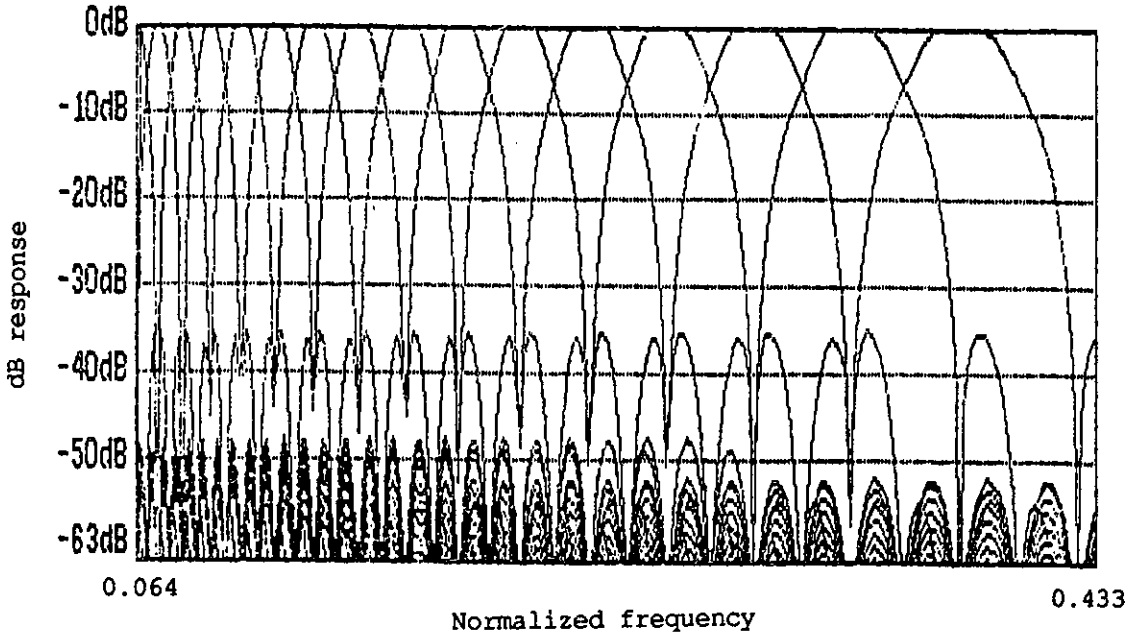

Figure 3.6 Log frequency response of a sixth-octave filter bank.

Since the frequencies ω_i are related geometrically, the sum of the frequencies is finite. Furthermore, if the gain coefficients K_i are proportional to frequency as recommended in the last section, the sum of the K_i is also finite. It is advantageous in many cases to have the sum of the gains equal to unity; if under this precondition and

$$K_i = \eta|\omega_i|, \tag{3.28}$$

where η is a small real constant. Then we have

$$1 = \sum_j K_r = \eta \sum_r |\omega_r|, \tag{3.29}$$

or

$$K_i = \frac{|\omega_i|}{\sum_r |\omega_r|}, \tag{3.30}$$

so if (geometric mean)

$$|\omega_r| = \pi e^{-(r-1)\frac{Ln2}{12}}, \qquad (r = 1, 2, ..., N) \tag{3.31}$$

we have

$$\begin{aligned} K_r &= (e^{-r\frac{Ln2}{12}})(1 - e^{-\frac{Ln2}{12}}) \\ &\simeq \frac{Ln2}{12} e^{-r\frac{Ln2}{12}}. \end{aligned} \tag{3.32}$$

If the sum of the gains K_i is unity, then other possibilities arise. For example,

$$1 = \frac{1 + \sum_{r=1}^{N} K_r \frac{z+p_r}{z-p_r}}{1 + \sum_{r=1}^{N} K_r \frac{z+p_r}{z-p_r}} = \frac{\sum_{r=1}^{N} K_r \frac{2z}{z-p_r}}{1 + \sum_{r=1}^{N} K_r \frac{z+p_r}{z-p_r}} \tag{3.33}$$

give a perfect reconstruction. Similarly, $[Z(z) - 1]/[1 + Z(z)]$ is all pass. Therefore

$$\frac{\sum_{r=1}^{N} K_r \frac{z+p_r}{z-p_r} - 1}{1 + \sum_{r=1}^{N} K_r \frac{z+p_r}{z-p_r}} = \frac{\sum_{r=1}^{N} \frac{2p_r K_r}{z-p_r}}{1 + \sum_{r=1}^{N} K_r \frac{z+p_r}{z-p_r}} \tag{3.34}$$

is all pass with increasing phase.

Also, by calculating equation (3.14), with increasing order N and unity G value, to see the tendency of the ratio $\frac{K_r}{f_r}$, we find that with increasing N the horizontal part of the curves extends, the nonlinear piece near the end shortens (see Fig.3.7), and the constant ratio value keeps the same value (0.05776). Thus we may suppose that an infinite filter bank will result in an over all constant ratio: $\frac{K_r}{f_r} = 0.05776$. In comparison with the approximate ratios obtained in equations (3.27) and (3.32), they are very close. This provides an important theoretical basis for the design of this class of filter banks.

3.6 Sensitivity Properties and Implementation of RFB Banks

Similar to FIFB filter banks, RFB banks have good sensitivity. The filter transfer function sensitivity formulas with respect to the gain coefficients and the poles of $Z(z)$ have been derived and given as follows:

$$\begin{aligned} S_{p_i}^{H_i(z)} &= \frac{\partial}{\partial p_i} H_i(z) \\ &= \frac{1}{K_i} H_i^2(z) \frac{2z}{(z+p_i)^2} [1 + \sum_{r=1, r\neq i}^{N} Z_j(z)\,]. \end{aligned} \tag{3.35}$$

$$\begin{aligned} S_{p_j}^{H_i(z)} &= \frac{\partial}{\partial p_j} H_i(z) \\ &= \frac{-2zK_i}{K_j} \frac{(z+p_i)}{(z-p_i)(z+p_j)^2} H_j^2(z). \end{aligned} \tag{3.36}$$

$$\begin{aligned} S_{K_i}^{H_i(z)} &= \frac{\partial}{\partial K_i} H_i(z) \\ &= \frac{1}{K_i^2} H_i^2(z) \frac{(z-p_i)}{(z+p_i)} [1 + \sum_{r=1, r\neq i}^{N} Z_r(z)\,] \\ &= \frac{1}{K_i} H_i(z)[1 - H_i(z)\,]. \end{aligned} \tag{6.37}$$

$$S_{K_j}^{H_i(z)} = \frac{\partial}{\partial K_j} H_i(z) = \frac{-1}{K_j} H_j(z) H_i(z). \tag{3.38}$$

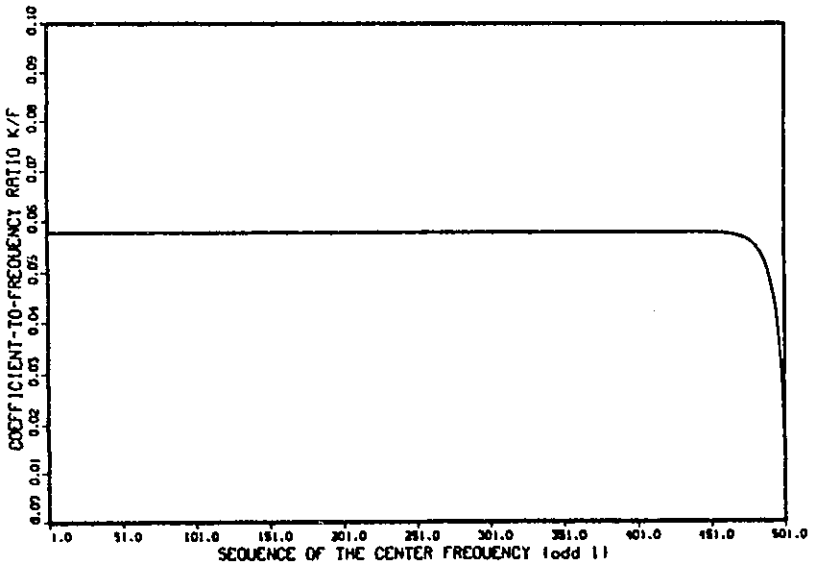

(a) When N=501 and with pole-zero structure (3);

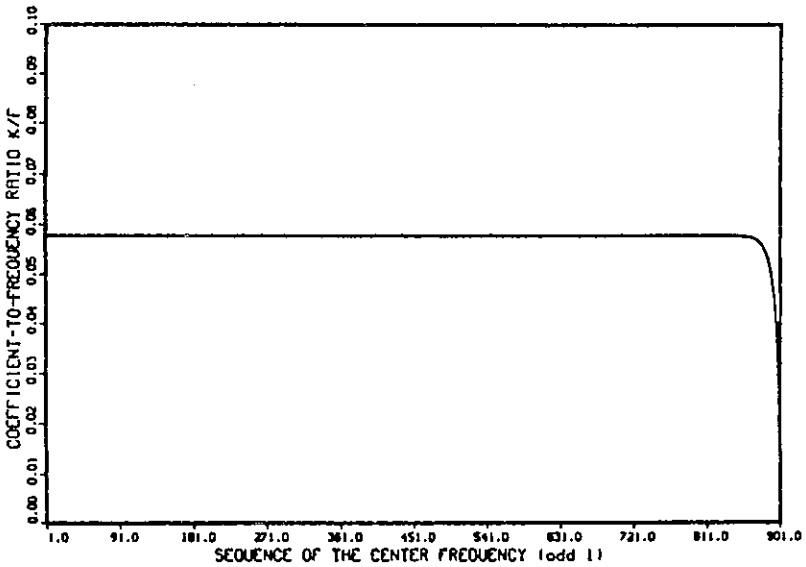

(b) When N=901 and with pole-zero structure (3);

Figure 3.7 The radio Kr/fr cuvers with very large size banks.

Note that in equations (3.36) and (3.38), $j \neq i$. The same as FIFB filter banks in the last chapter, because of the interpolating properties of the filter bank, i.e., $H_i(p_i) = 1$, and $H_i(p_j) = 0$ if $j \neq i$, from (3.37) and (3.38) it follows that in the vicinity of any zero p_i, $(i = 1, 2, ..., N)$ of the filters, the sensitivity with respect to any gain coefficient K_r $(r = 1, 2, ..., N)$ will be small concerning both the magnitude and phase and it will be zero if $z = p_i$, $(i = 1, 2, ..., N)$. Equations (3.35) and (3.36) can be easily changed to the following forms:

$$S_{p_i}^{H_i(z)} = H_i(z)\frac{2z}{(z^2 - p_i^2)} \frac{(z - p_j) + K_j(z + p_j) + \sum_{r=1, r\neq i,j}^{N}(z - p_j)Z_r(z)}{(z - p_j) + K_j(z + p_j) + \sum_{r=1, r\neq j}^{N}(z - p_j)Z_r(z)}, \tag{3.39}$$

$$S_{p_j}^{H_i(z)} = \frac{-2K_i z(z + p_i)}{(z^2 - p_j^2)} \frac{H_j(z)Z_j(z)}{(z - p_i) + K_i(z + p_i) + \sum_{r=1, r\neq i}^{N}(z - p_i)Z_r(z)}, \tag{3.40}$$

where j is any number except i among $1, 2, ..., N$. From (3.35) and (3.39), and (3.36) and (3.40), it can be seen that the sensitivity with respect to any zero p_j, except at zero p_i and its vicinity, is the same case as the sensitivity with respect to K_i above.

Considering the realization structure of the filter banks discussed above in this chapter, we find that when the system is implemented **directly according to** equation (3.6) the signal flow graph of the bank system has a delay-free loop and therefore noncomputable. This can be seen clearly in Fig.3.8. However, the resonator-based filter bank is realizable since the form of function (3.6) may be changed to correspond to a computable signal flow graph, where all the loops are with one unit delay element. The derivation is given here as follows: If the sum of all the coefficients K_j is unity, i.e., if $\sum_{j=1}^{N} K_j = 1$, the

denominator $D(z)$ in (3.5) is as

$$D(z) = 1 + \sum_{j=1}^{N} K_j \frac{z - p_j + 2p_j}{z - p_j} = 2\ (\ 1 + \sum_{j=1}^{N} \frac{k_j p_j}{z - p_j}\ ), \tag{3.41}$$

and meanwhile we have

$$Z_m = K_m \frac{z + p_m}{z - p_m} = K_m + 2\frac{K_m p_m}{z - p_m}. \tag{3.42}$$

Thus the new form of the filter function is obtained as

$$H_m(z) = \frac{K_m + 2\frac{K_m p_m}{z - p_m}}{2(1 + \sum_{j=1}^{N} \frac{K_j p_j}{z - p_j})} = \frac{\frac{K_m}{2} + \frac{K_m p_m z^{-1}}{1 - p_m z^{-1}}}{1 + \sum_{j=1}^{N} \frac{K_j p_j z^{-1}}{1 - p_j z^{-1}}}. \tag{3.43}$$

From equation (3.43), the computable signal flow graph is achieved and shown in Fig.3.9.

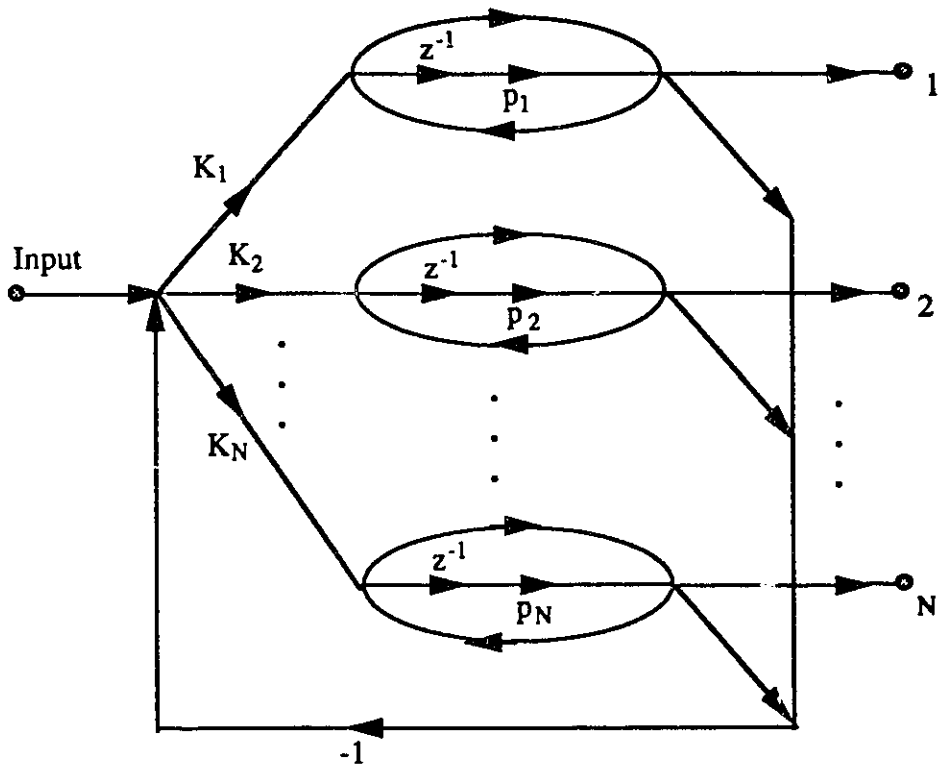

Figure 3.8 Siginal flow graph of the filter bank when the transfer function (3.6) is implemented directly.

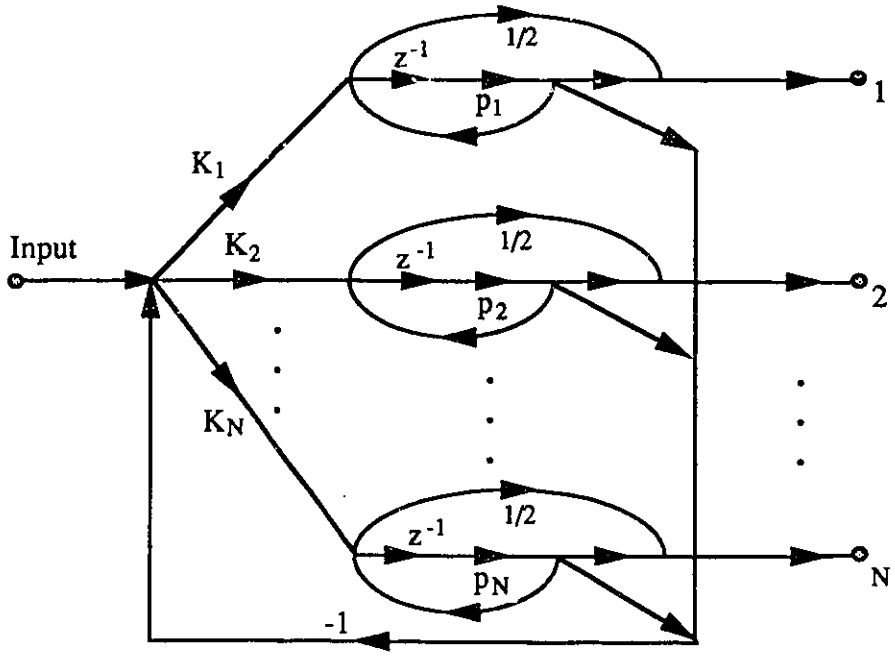

Figure 3.9 SFG of the filter bank when the sum of the filter coefficients is unity.

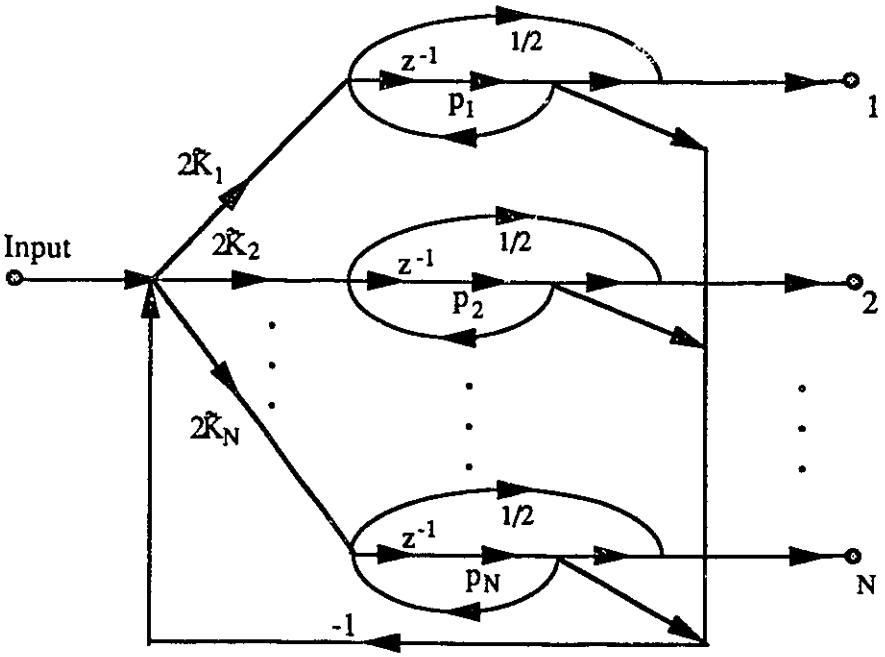

Figure 3.10 SFG of the filter bank when the sum of the coefficients is not unity.

More generally, if $\sum_{j=1}^{N} K_j = A$, then

$$D(z) = 1 + \sum_{j=1}^{N} K_j + \sum_{j=1}^{N} \frac{2K_j p_j}{z - p_j} = B + \sum_{j=1}^{N} \frac{2k_j p_j}{z - p_j}, \tag{3.44}$$

where $B = 1 + A$. Since the Z_m is the same as (3.42), the m^{th} filter can be expressed as

$$H_m(z) = \frac{K_m + 2\frac{K_m p_m}{z - p_m}}{B + \sum_{j=1}^{N} \frac{2K_j p_j}{z - p_j}} = \frac{\tilde{K}_m + \frac{2\tilde{K}_m p_m z^{-1}}{1 - p_m z^{-1}}}{1 + \sum_{j=1}^{N} \frac{2\tilde{K}_j p_j z^{-1}}{1 - p_j z^{-1}}}, \tag{3.45}$$

where $\tilde{K}_m = \frac{K_m}{B}$. The computable signal flow graph of the system is drawn in Fig.3.10 from (3.45), which is realizable.

The effects of the finite-word-length on the filter-bank performance are similar to those in FIFB filter banks, and because of equation (3.43) and (3.45), there is no possibility of system instability due to parameter quantization.

3.7 Relationship to Adaptive Algorithm

In the last chapter, the FIFB filter bank was derived based on the adaptive filtering structure. In this chapter, the similar resonator-based filter bank is derived from the lossless-resonator-units, so there should be some links between the RFB filter bank and the adaptive algorithm. The relationship will be studied in this section and we will show that if the normalized LMS algorithm is used where the updating weights vary from frequency to frequency, the same structure as the resonator-based frequency interpolation filter bank is obtained.

The normalized LMS algorithm is based on projection[95]. In essence, like that in section 2.2, an input d_n sampled at time n is matched to a weighted sum, in our case, a weighted sum of oscillators. The weight coefficients are $C_{n,i}$, the i^{th} weight at sample time n. The oscillator outputs are $X_{n,i} = e^{j\omega_i n}$. Two errors arise in the theory of adaptive

equalizers, the a posteriori error and the a priori error defined by **(a posteriori)**

$$\varepsilon_n = d_n - \sum_{i=1}^{N} C_{n,i}\ X_{n,i}, \tag{3.46}$$

and **(a priori)**

$$\alpha_n = d_n - \sum_{i=1}^{N} C_{n-1,i}\ X_{n,i}. \tag{3.47}$$

The a priori error represents the difference between the input d_n and the estimate. The a posteriori error is minimized. Classical normalized LMS forces ε_n to be zero while the change in the weights is minimized. Thus, subject to $\varepsilon_n = 0$, minimize

$$\sum_{i=1}^{N} \frac{|C_{n,i} - C_{n-1,i}|^2}{\rho_i}. \tag{3.48}$$

Ordinarily the quantity ρ_i is independent of i; making it i-dependent is crucial to our argument. The solution to this problem may be solved using the technique of *Lagrange* multipliers and results in the following equations

$$C_{n,i} = C_{n-1,i} + \alpha_n\ X^*_{n,i}\ \rho'_i, \tag{3.49}$$

where

$$\rho'_i = \frac{\rho_i}{\sum_{j=1}^{N} \rho_j}. \tag{3.50}$$

(Note that the sum of the primed ρ's is unity.) Define the quantity

$$H_{n,i} = C_{n,i}\ e^{j\omega_i(n+1)}. \tag{3.51}$$

Then $H_{n,i}$ satisfies the equations

$$H_{n,i} = p_i H_{n-1,i} + \alpha_n\ p_i\ \rho'_i, \tag{3.52}$$

and the error α_n is then

$$\alpha_n = d_n - \sum_{i=1}^{N} H_{n-1,i}. \tag{3.53}$$

Now, if d_n is a sinusoid then the LMS algorithm may be analyzed using z-transforms and the result is

$$H_i(z) = \frac{\rho'_i \frac{p_i z}{(z-p_i)}}{1 + \sum_{j=1}^{N} \frac{\rho'_j p_j}{(z-p_j)}}. \tag{3.54}$$

Using the relation in equation (3.3), the denominator may be rewritten as

$$\begin{aligned} 1 - \frac{1}{2}\sum_{j=1}^{N} \rho'_j + \sum_{j=1}^{N} \frac{\rho'_j}{2} \frac{(z+p_j)}{(z-p_j)} \\ = \frac{1}{2}[1 + \sum_{j=1}^{N} \rho'_j \frac{(z+p_j)}{(z-p_j)}], \end{aligned} \tag{3.55}$$

and the numerator may be written as

$$z\frac{\rho'_i}{2}\frac{(p_i - z) + (z + p_i)}{(z - p_i)} = z\frac{\rho'_i}{2}[\frac{(z+p_i)}{(z-p_i)} - 1]. \tag{3.56}$$

Thus we conclude that the same filter structure results when using a weighted sum of oscillators to approximate a signal using the LMS algorithm with weighted coefficient change minimization. This gives an alternate way to view the filter banks. The realization of the filter response is made in a slightly different manner, by noting that

$$\begin{aligned} 1 + \sum_{i=1}^{N} K_i \frac{(z+p_i)}{(z-p_i)} \\ = 1 + \sum_{i=1}^{N} K_i \frac{(z - p_i + 2p_i)}{(z-p_i)} \\ = 1 + \sum_{i=1}^{N} K_i + \sum_{i=1}^{N} 2K_i p_i \frac{z^{-1}}{(1 - p_i z^{-1})}. \end{aligned} \tag{3.57}$$

If the condition $\sum_{i=1}^{N} K_i = 1$ is satisfied, then $(1 + Z(z))$ has a zero at the origin. Furthermore, the value of the numerator at $z = \infty$ is, under this constraint, 2.

The normalized LMS algorithm has the sum of the gains ρ'_i unity, and this is because of the requirement that ε_n is identically zero. The argument may be easily generalized by

considering the problem of minimizing

$$\sum_{i=1}^{N} \frac{|C_{n,i} - C_{n-1,i}|^2}{\rho_n} + \mu|\varepsilon_n|^2. \tag{3.58}$$

3.8 Summary

In this chapter, a new technique has been proposed to design bandpass filter banks where the center frequencies are spaced logarithmically. The filter bank is derived from a lossless resonators based structure. The approximation techniques for the filter gain coefficients have been presented and a variety of pole-zero structures have been studied. Calculations show that the pole-zero structure(2) and (3) (Fig.3.3) give better frequency property for the harmonic and geometric mean zeros, and the geometric mean zero structure results in good control ability of crossover gain. Much better filter bank behaviours are achieved comparing with the FIFB design method. The design procedure of the filter bank is summarized as follows: (a) determine the center frequencies in a way similar to that in section 3.5; (b) determine the zeros of resonators according to the harmonic or geometric means of adjacent poles; (c) calculate the filter gain coefficients K_i from equation (3.14) with unity G; (d) find the required factor G. Then calculate the frequency responses and adjust gain K_i.

IV WINDOWING TECHNIQUES FOR THE PERFORMANCE IMPROVEMENT OF THE FILTER BANKS

4.1 Introduction

In chapter II, the frequency interpolation filter bank (FIFB) has been introduced based on adaptive filtering structure[93], and in chapter III, digital resonator-based filter bank(RFB) has been proposed based on the elementary lossless digital resonator (LDR)[88,89]. The filter banks designed using these two techniques have the properties: (1) All the filters in the bank have the same poles, unit response at the filter center frequency and zero response at all the other center frequencies. (2) The center frequencies of the filter banks may be spaced arbitrarily, in other words, the filter bandwidths may be constant, linear, nonlinear function of frequency and so on. This greatly widens the area where the filter banks may be applied. (3) These filter banks have low round off noise and good sensitivity. (4) The filter banks are very efficient in the computation and the implementation. However, the elementary filters alone, in the banks designed by both approaches above, have poor passband behaviour and appreciable sidelobes(see Fig.3.6, the highest sidelobe only about -13 dB down).

In this chapter, we apply the "windowing" techniques to suppress the sidelobes and to improve the passband performance. What windowing is and why the windows work are discussed first in the next section. Then, the mathematical models for window optimization are derived based on the RFB filter banks, and linear programming techniques are used to search out the optimal weight coefficients. Following this, examples of the filter banks with the application of optimal windows are given. Finally this chapter has discussions of the trade-offs among the window widths, the passband and stopband per-

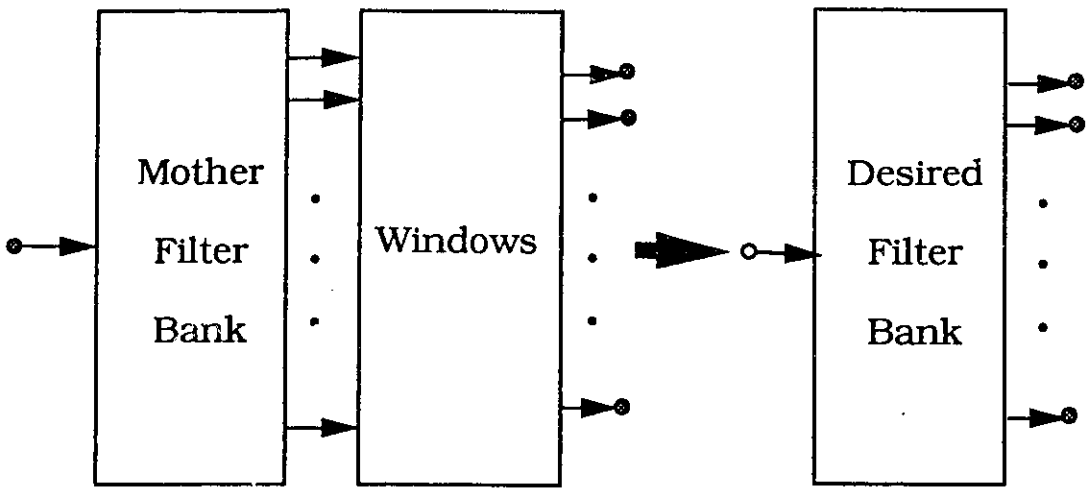

Figure 4.1 Block diagram of equivalent filter bank with window processing.

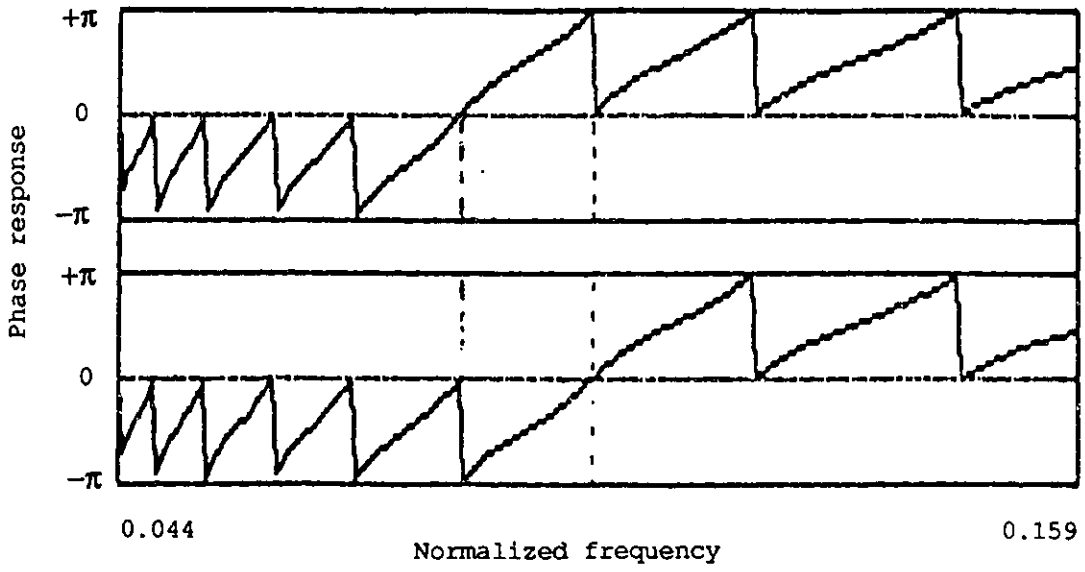

Figure 4.2 The phase responses of two adjacent filters in a bank.

formance of filters, crossover gain of the banks and the computation complexity.

4.2 What is Windowing and Why Windowing

The tentative idea to suppress the sidelobes has been given in [49] by adding together appropriately weighted elementary filter outputs, where the "mother" filter banks were designed by the approach in chapter II. By analogy to the effect of windows (Hamming, Hanning, etc.) on DFT(discrete fourier transform) computation [100], we call this process "windowing". In [101,102], we have more systematically studied the windowing technique in the design of logarithmic FIFB filter banks and concentrated on the filter bank stopband optimization with windowing processing. From the block diagram of the equivalent filter banks shown in Fig.4.1, we can see that windowing is a DSP procedure to produce a final-desired filter bank from a mother filter bank. The windowing procedure consists of a set of "windows" and each of the windows is a summation of some weighted filter outputs of the mother filter bank(see Fig.4.3). This summation is the output a desired-filter of the final bank and the weighting coefficients are called the weights of the windows. Sometimes this procedure is called equivalent frequency domain windowing. This is because with the DFT, instead of the time windowing before the transform for the reduction of spectrum leakage, the equivalent function may be performed in frequency domain by taking the DFT first and then operating the windowing similar to that above [49,97].

The answer to the question why the windows work may be found when the phase responses of these filter banks are examined. Fig.4.2 gives the phase responses of 8^{th} and 9^{th} filters in a third octave filter bank. An interesting property is the phase difference that exists between adjacent filters. As the notation used before, the phase difference between i^{th} and $(i+1)^{th}$ filters is approximately π for $\omega_i < \omega < \omega_{i+1}$ and zero elsewhere. Here the ω_i is the phase angle of the i^{th} zero on the unit circle, i.e., the center frequency of the

i^{th} filter in the bank. This suggests that the window with alternate signs associated with each adjacent filter weight will suppress the sidelobes.

The width of the window, or the number of the weights in a window, is a very important parameter of the windows. Generally speaking, the wider the window, the better it works. Later in this chapter, we will find this is not only in the sense of the property of stopband, but also in the sense of the passband property. Because the filter banks under consideration are either real filter banks or complex filter banks, the windows may be with real coefficients or complex coefficients. However, resonator-based filter banks simplify the reasoning, because for them the purely imaginary resonators make the complex weighting coefficients of no advantage compared to the real ones (see Appendix-D). Another issue about windowing is that the windows can be symmetrical or asymmetrical around the center frequency of the final filter. If the filter bank with uniform bandwidths is designed, the symmetrical windows are usually applied. But asymmetrical windows are preferred in the design of nonlinearly-spaced-center-frequency filter banks.

4.3 Windowing Optimization

4.3.1 Theory background

The design of the logarithmic frequency RFB bank with the application of windows consists of deciding the specification of a mother filter bank according to desired filter bank requirement, choosing the type of windows, and finding the optimal weighting coefficients. From the block diagram of the equivalent filter banks in Fig.4.1, we can see that the function of the windows is to improve upon the frequency responses of the mother bank (mainly to suppress the appreciable sidelobes and flatten the passband). Since the center frequencies of the filters are nonlinearly spaced, the responses of the filters in the bank are nonuniformly distributed in frequency. Thus, there must be a set of optimal weighting

coefficients for each output filter, which can be found by defining a linear approximation problem and by solving it in the linear programming technique. We present this in this subsection and the following two subsections.

In the lossless digital resonator-based filter bank, the transfer function of i^{th} filter in frequency-domain is

$$H_i(\omega) = \frac{N_i(\omega)}{D(\omega)} = \frac{K_i \frac{1+e^{j(\omega_i-\omega)}}{1-e^{j(\omega_i-\omega)}}}{1+\sum_{j=1}^{N} K_j \frac{1+e^{j(\omega_j-\omega)}}{1-e^{j(\omega_j-\omega)}}} \tag{4.1}$$

where ω_j and K_j, $j = 1, 2, ..., N$, are the center frequencies of the filters and the corresponding real gain coefficients, respectively. Because of the lossless elementary resonators, the numerators $N_i(\omega)$ are purely imaginary at any frequency ω since the term $[1 + e^{j(\omega_i-\omega)}]/\ [1 - e^{j(\omega_i-\omega)}]$ is purely imaginary number and K_i is real. "Windowing" means to combine several weighted filters in the mother bank to give a resulting filter in desired bank, and thus a window may be described as

$$\hat{F}(\omega) = \sum_{r=M1}^{M2} (-1)^{(r-M1)} W_{r+1-M1} H_r(\omega), \tag{4.2}$$

where W_j, $j = 1, 2, ..., M$, are the weighting coefficients to be found, M, equal to $(M2 - M1 + 1)$, is the number of the windowing coefficients to express the width of the window, and the alternate signs of the weights has been applied . $\hat{F}(\omega)$ is the transfer function of the resulting filter obtained from M filters $H_j(\omega)$ $(j = 1, 2, ..., M)$ in the mother bank. Because of the purely imaginary numerators $N_i(\omega)$ and the same denominator $D(\omega)$ for all the mother filters $H_j(\omega)$ the optimal weights $\{W_i\}$ should be a set of **real** coefficients, i.e., a set of complex weighting coefficients contributes nothing more than the real coefficients for the improvement of the magnitude responses of the resultant filters. Furthermore, the signs $(-1)^{(r-M1)}$ in equation (4.2) guarantee that there exists a set of **positive and real** weighting coefficients $\{W_i\}$, which will be able to work for the stopband as well as for the

passband. If we let $F(\omega)$ be the desired magnitude characteristic of the filter, then the approximation problem is to find a set of weighting coefficients $\{W_i\}$ such that

$$| \,|\hat{F}(\omega)| - F(\omega)\, | \leq \varepsilon(\omega), \tag{4.3}$$

or

$$-\varepsilon(\omega) \leq |\hat{F}(\omega)| - F(\omega) \leq \varepsilon(\omega), \tag{4.4}$$

where $\varepsilon(\omega)$ is a tolerance function on the error which allows for unequal weighting of errors as a function of frequency. Since $F(\omega)$ and $\varepsilon(\omega)$ are generally specified functions of frequency, equation (4.4) can be expressed as a set of linear inequalities in the $W_i's$. For example, in the stopband, i.e., when $\omega \leq \omega_{M1-1}$ and $\omega \geq \omega_{M2+1}$, all the M filters applied have the same phase. Therefore we may define

$$\begin{aligned} |\hat{F}(\omega)| = &+ W_1|H_{M1}(\omega)| - W_2|H_{M1+1}(\omega)| \\ &+ W_3|H_{M1+2}(\omega)| - \ldots + W_M|H_{M2}(\omega)|, \\ &\omega_{M1-1} \geq \omega \geq \omega_{M2+1} \end{aligned} \tag{4.5}$$

or

$$|\hat{F}(\omega)| = \frac{|S(\omega)|}{|D(\omega)|} \tag{4.6}$$

with definition

$$|S(\omega)| = \sum_{r=M1}^{M2} (-1)^{(r-M1)} W_{r+1-M1}|N_r(\omega)|. \tag{4.7}$$

Thus, the linear inequalities, or the constraints on the stopband may be written in the form

$$-|S(\omega)| + |D(\omega)|[F(\omega) + \varepsilon(\omega)] \geq 0, \quad \omega_{M1-1} \geq \omega \geq \omega_{M2+1} \tag{4.8}$$

$$+|S(\omega)| - |D(\omega)|[F(\omega) - \varepsilon(\omega)] \geq 0, \quad \omega_{M1-1} \geq \omega \geq \omega_{M2+1}. \tag{4.9}$$

With the additional linear inequalities

$$W_i \geq 0, \qquad i = 1, 2, ..., M \tag{4.10}$$

we completely define the approximation problem if only the constraints on the stopband are considered. Notice that $W_i \geq 0$ is necessary to avoid passband deterioration based on the sign strategy in equation (4.5) or (4.7). Given the precondition that some center weights are fixed to unity, the approximation problem above will be solved to give reasonable results which are generally consistent with the case when both the stopband and the passband are considered. Thus we may think of this as a simple but rough way to find the weighting coefficients.

If the approximation is extended to the passband, due to the opposite phases between adjacent filters, the signs in equation (4.7) will become irregular for the passband frequency range. For example, when $M = 3$, based on the $|N_r(\omega)|$, and using $|P_1(\omega)|$ for first half part of the passband and $|P_2(\omega)|$ for second half part of the passband instead of $|S(\omega)|$ in (4.6), the equations similar to (4.7) may be expressed as

$$\begin{aligned} |P_1(\omega)| &= +W_1|N_{M1}(\omega)| + W_2|N_{M1+1}(\omega)| - W_3|N_{M2}(\omega)| \\ & \omega_{M1} \leq \omega \leq \omega_{M1+1} \end{aligned} \tag{4.11}$$

$$\begin{aligned} |P_2(\omega)| &= -W_1|N_{M1}(\omega)| + W_2|N_{M1+1}(\omega)| + W_3|N_{M2}(\omega)| \\ & \omega_{M1+1} \leq \omega \leq \omega_{M2} \end{aligned} \tag{4.12}$$

The corresponding linear inequalities are adjusted to be

$$-|P_1(\omega)| + |D(\omega)|[F(\omega) + \varepsilon(\omega)] \geq 0 \quad \omega_{M1} \leq \omega \leq \omega_{M1+1} \tag{4.13}$$

$$+|P_1(\omega)| - |D(\omega)|[F(\omega) - \varepsilon(\omega)] \geq 0 \quad \omega_{M1} \leq \omega \leq \omega_{M1+1} \tag{4.14}$$

$$-|P_2(\omega)| + |D(\omega)|[F(\omega) + \varepsilon(\omega)] \geq 0 \quad \omega_{M1+1} \leq \omega \leq \omega_{M2} \tag{4.15}$$

$$+|P_2(\omega)| - |D(\omega)|[F(\omega) - \varepsilon(\omega)] \geq 0 \quad \omega_{M1+1} \leq \omega \leq \omega_{M2} \tag{4.16}$$

Thus, the question of whether or not there exists a digital filter in desired bank with magnitude response $F(\omega)$ and tolerance function $\varepsilon(\omega)$ is equivalent to the question of whether or not there exists a set of weights satisfying the system of constraints defined by (4.8)-(4.10) and (4.13)-(4.16). The question can be answered by using the linear programming technique[97] which has been applied to design different types of filters[103-105]. In fact, by adding an auxiliary variable v to the right side of equations (4.8)-(4.9) and (4.13)-(4.16), the linear programming problem may be stated to find $\{W_i\}$, $i = 1, 2, ..., M$, subject to the constraints

$$W_i \geq 0, \qquad i = 1, 2, ..., M \tag{4.17}$$

$$v \geq 0 \tag{4.18}$$

$$-|S(\omega)| + |D(\omega)|[F(\omega) + \varepsilon(\omega)] + v \geq 0 \tag{4.19}$$

$$+|S(\omega)| - |D(\omega)|[F(\omega) - \varepsilon(\omega)] + v \geq 0 \tag{4.20}$$

$$-|P_k(\omega)| + |D(\omega)|[F(\omega) + \varepsilon(\omega)] + v \geq 0 \tag{4.21}$$

$$+|P_k(\omega)| - |D(\omega)|[F(\omega) - \varepsilon(\omega)] + v \geq 0 \tag{4.22}$$

such that v is minimized. Note that k is from 1 to $M-1$ where M is the width of the window. In equations (4.19)-(4.20) the frequency range is $\omega \geq \omega_{M2+1}$ and $\omega \leq \omega_{M1-1}$, and in equations (4.21)-(4.22), $\omega \geq \omega_{M1+k-1}$ and $\omega \leq \omega_{M1+k}$. Clearly, a solution to constraints (4.8)-(4.10) and (4.13)-(4.16) exists if and only if the minimum value of v under constraints (4.17)-(4.22) is zero. In other words, if the minimum value of v is zero, a set of weights may be obtained directly as the output of linear programming

routine. If v is not equal to zero, then, either $F(\omega)$, or $\varepsilon(\omega)$, or both must be modified to obtain a solution. In the following parts of the section we illustrate the above procedure by considering the specific design examples and report the results of different windows optimized under the constraints on the stopband, and on both the stopband and the passband.

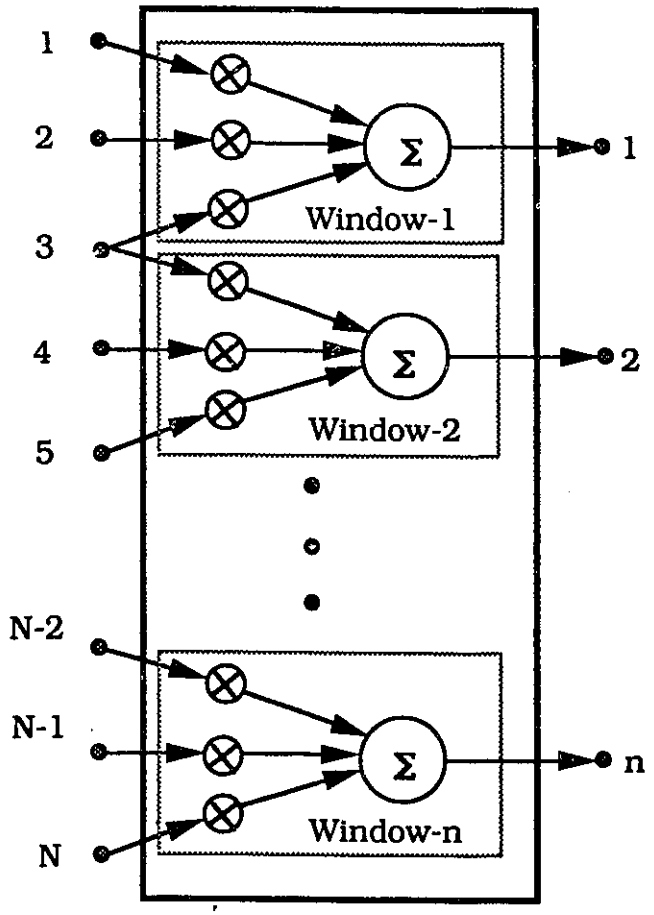

Figure 4.3 The detailed structure of a 3-weight window processing.

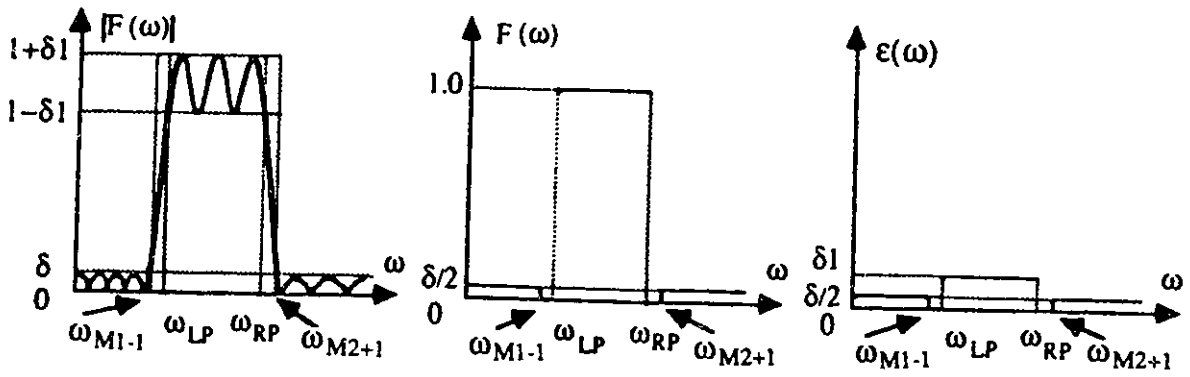

Figure 4.4 (a) Bounds of the approximation; (b) Desired magnitude function; (c) Tolerance function.

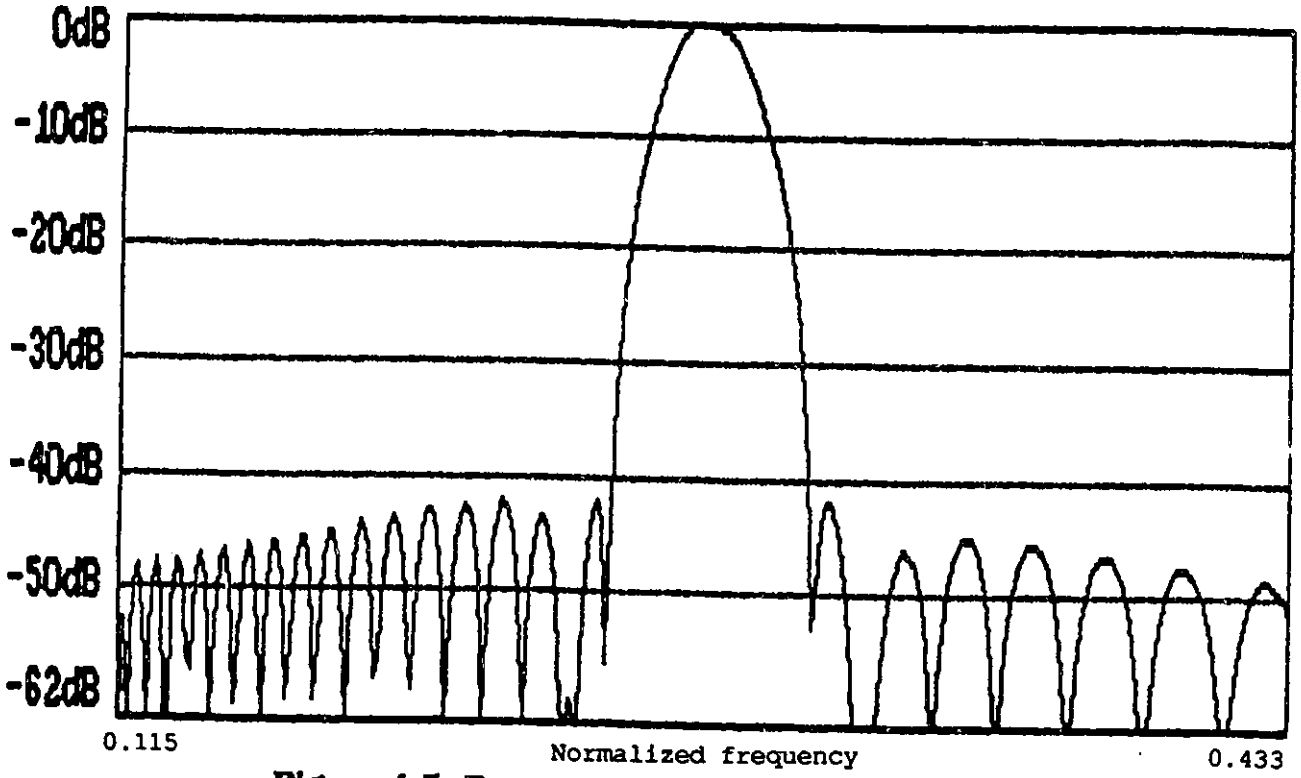

Figure 4.5 Frequency response of the filter obtained by 3-weight window processing.

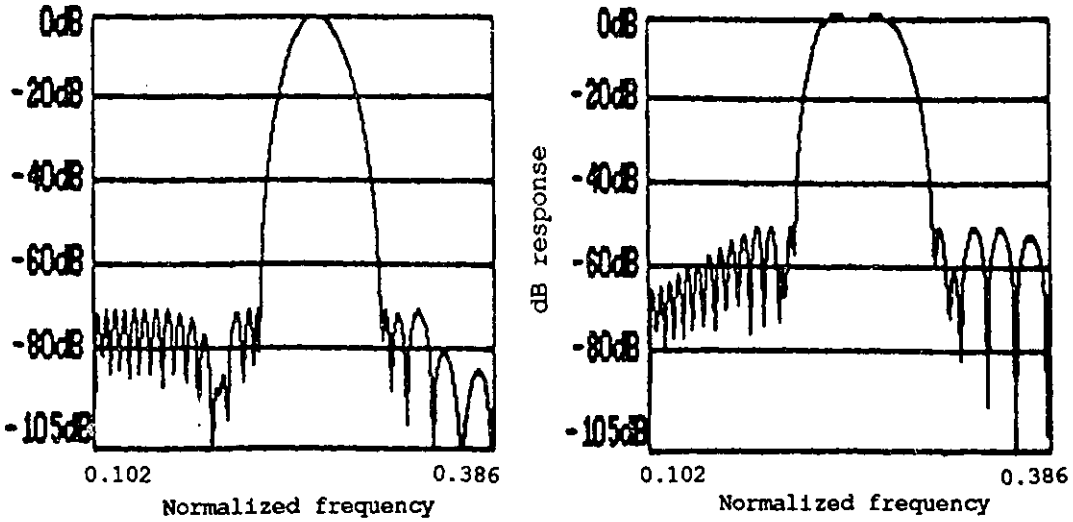

(a) Using window 4; **(b) Using window 6;**

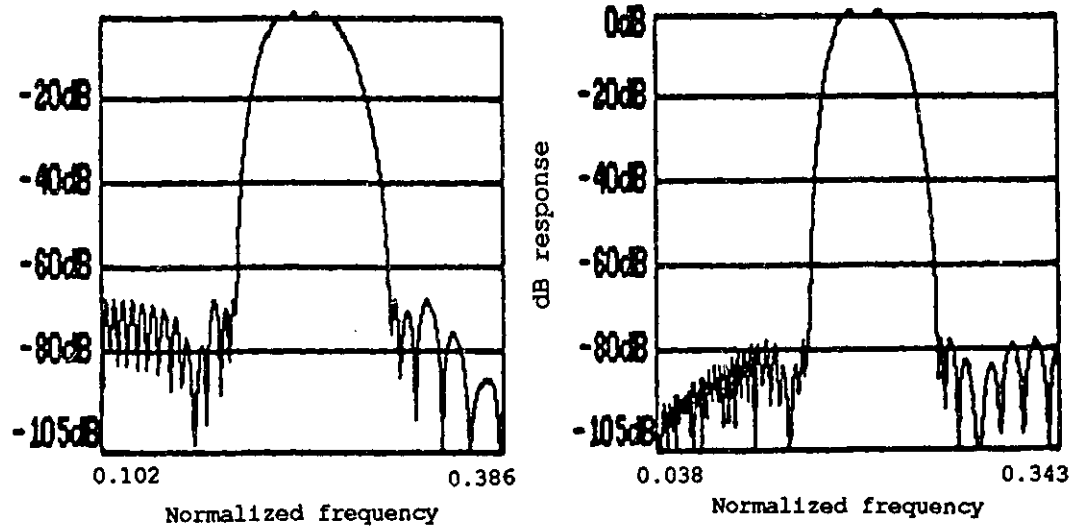

(c) Using window 8; **(d) Using window 10;**

Figure 4.6 Frequency responses of the filters obtained using different windows in Table IV.1.

TABLE IV.1. Optimal windows with constraints on the stopband:

No.	M	L	Minimax Sidelobe (-dB)	Weighting Coefficients
1.	3	1	42.11	w1=0.4246, w2=1.0, w3=0.4397
2.	4	2	52.70	w1=0.2591, w2=w3=1.0, w4=0.2590
3.	5	3	42.82	w1=0.3985, w2=w3=w4=1.0, w5=0.4160
4.	5	1	70.28	w1=0.0931, w2=0.5825, w3=1.0, w4=0.5970, w5=0.0970
5.	6	4	49.59	w1=0.3055, w2=w3=w4=w5=1.0, w6=0.3054
6.	6	2	81.81	w1=0.0455, w2=0.3987, w3=w4=1.0, w5=0.3985, w6=0.0453
7.	7	5	41.38	w1=0.3950, w2=w3=w4=w5=w6=1.0, w7=0.4139
8.	7	3	67.43	w1=0.1045, w2=0.5950, w3=w4=w5=1.0, w6=0.6091, w7=0.1111
9.	8	6	48.31	w1=0.3242, w2=w3=...=w7=1.0, w8=0.3239
10.	8	4	77.41	w1=0.0632, w2=0.4743, w3=w4=w5=w6=1.0, w7=0.4744, w8=0.0633

M: Number of the weights in windows.
L: Number of the center-unity weights in windows.

4.3.2 Constraining the stopband

For the window with three weights which weights and adds three filters in a mother bank to obtain a resultant filter in the windowed bank(see the details of the window structure in Fig.4.3), if we let δ be the peak approximation error in the stopband, or the minimum highest sidelobe value, it is easy to define the function $F(\omega)$ and $\varepsilon(\omega)$(see Fig.4.4). Since we ignore the passband, simply letting $F(\omega)$ equal to zero and $\varepsilon(\omega)$ equal to δ in the stopband results in a pair of weights which will suppress the highest sidelobe to a value of $20Log_{10}(\delta)$, if the v, which is the variable to be minimized in linear programming problem, is minimized to zero. In turn, if the highest sidelobe V dB is desired, $F(\omega)$ and $\varepsilon(\omega)$ may be chosen as zero and $10^{\frac{V}{20}}$, respectively. Two programs have been made to implement the above procedure. One is designed following the general simplex algorithm given in [97] with PASCAL running on IBM-PC. Another is based on the subroutine ZX3LP(FORTRAN)[106] on the CMS main frame, which applies the revised simplex algorithm to the dual linear programming problem, since in our case the number of constraints(the number of discrete frequency samples in considered band) (more than 400) is much larger than the number of weighting coefficients(several). Fig.4.5 shows the frequency response of a resulting filter obtained by the window with three weights. The weighting coefficients are $W_1 = 0.4246, W_2 = 1.0$, and $W_3 = 0.4397$, which are optimized using the linear programming routine with $F(\omega) = 0$ and $\varepsilon(\omega) = \delta$, and one center unity weight. The smallest δ is obtained in an iterative way and the highest sidelobe is suppressed to minimum value -42.1 dB from original -13 dB(see Fig.4.6).

We have extended the procedure to different widths of windows with different number of center unity weights. TABLE IV.1 lists a part of the results, where type of windows, the corresponding weighting coefficients and minimax sidelobe (dB) values are given. Four typical filter responses are plotted in Fig.4.6, where windows 4, 5, 8, and 10 in TABLE

IV.1 are applied. From the results above, we may see that the wider the window, the better the filter performance. Moreover a wider window has more flexibility to control the resulting filter properties than a narrower one. Thus a trade-off exists between the filter property and the computational complexity when implemented. For the M-point window, there is the second trade-off when we consider the highest sidelobe and the transition bandwidth. More center unity weights will shorten the transition band, but make the stopband performance get worse. The same will happen when the passband constraints are applied, and more discussion will be given in the next subsection.

4.3.3 Constraining both the stopband and the passband

The results in the previous part show us that even though only the stopband constraints are considered, the windows obtained produce the reasonable passbands as well as improved stopband. The ripples in the passband generally are less than 1 dB in Fig.4.6. This is because of the original characteristics of the mother filter bank and the alternate signs with the weights. However, the passband performance is not under exact control without the constraints on the passband. Furthermore, in order to approximate the desired crossover gain of the banks and reduce the transition bandwidth, it is necessary to extend constraints to the passband. For this, we need, naturally, to adjust the magnitude characteristic function $F(\omega)$ and the tolerance function $\varepsilon(\omega)$. As before, with δ expressing the peak approximation error in the stopband, and δ_1 in the passband, the function $F(\omega)$ and $\varepsilon(\omega)$, based on the corresponding magnitude response of the filter $|\hat{F}(\omega)|$, are defined by equations (4.23)-(4.24) and drawn in Fig.4.4.

$$\begin{aligned} F(\omega) &= 1.0, && \omega_{LP} \le \omega \le \omega_{RP} \\ &= 0, (or\ \delta/2) && \omega_{M2+1} \le \omega \le \omega_{M1-1} \end{aligned} \tag{4.23}$$

$$\begin{aligned} \varepsilon(\omega) = \ & \delta_1, && \omega_{LP} \leq \omega \leq \omega_{RP} \\ = \ & \delta, (or\ \delta/2) && \omega_{M2+1} \leq \omega \leq \omega_{M1-1} \end{aligned} \tag{4.24}$$

where ω_{LP} and ω_{RP} are the left side and right side passband cutoff frequencies. It is obvious that $|\hat{F}(\omega)|$ in Fig.4.4 (a) is less than or equal to $F(\omega) + \varepsilon(\omega)$ and greater than or equal to $F(\omega) - \varepsilon(\omega)$.

Generally speaking, the passband ripple δ_1 may be taken as β times of the stopband ripple δ, i.e., $\delta_1 = \beta * \delta$ (β is a constant), and thus we may use an iterative procedure to find the smallest δ. In practice, however, we are interested in improving the stopband performance as much as possible with the satisfaction of the passband requirement(fixed δ_1). This is equivalent to searching for the smallest δ such that the approximation problem has a solution. Thus, an iterative procedure must be used, because δ enters into the design constraints in a nonlinear manner. However, one simple way is to let $\varepsilon(\omega)$ equal to zero in the stopband and to choose the required δ_1, since we are interested in improving the stopband performance as much as possible with the satisfication of the passband. This does not mean we will get a zero stopband filter, but it is a way to transfer the approximation error, or the minimum highest sidelobe value of the desired filter, from δ to v, the variable of linear programming problem. Of course, now that v equals to zero is no longer the criterion for whether or not there is a solution to the problem, since in this case the convergence of the optimization algorithm and the optimality of the resulting filter in the given case are guaranteed. The results in this part are calculated according to the second criterion.

TABLE IV.2 lists the optimal windows with three weights obtained under the constraints of different passband widths(given by the number of discrete samples in the passband). δ_1 is chosen as 0.085 so that selected passband ripples are less than 0.8 dB. Frequency responses of the filters using windows 3, 4, 6 and 8 in TABLE IV.2, are plotted

in Fig.4.7. It can be seen that there is a trade-off between the passband property and the highest sidelobe. Better passband performance and shorter transition bandwidth are achieved at the cost of higher minimax sidelobe.

TABLE IV.2. Optimal 3-weight windows with various passband widths:

No.	Passband Widths*	Minimax Sidelobe (-dB)	W1	W3
1.	8	42.10	0.4246	0.4397
2.	10	42.10	0.4246	0.4397
3.	12	42.10	0.4246	0.4397
4.	14	30.71	0.4957	0.5084
5.	16	25.53	0.5607	0.5797
6.	18	22.58	0.6191	0.6433
7.	20	20.62	0.6709	0.6991
8.	22	19.20	0.7166	0.7482
9.	24	18.53	0.7634	0.7642

* Number of discrete frequency samples in passbands.

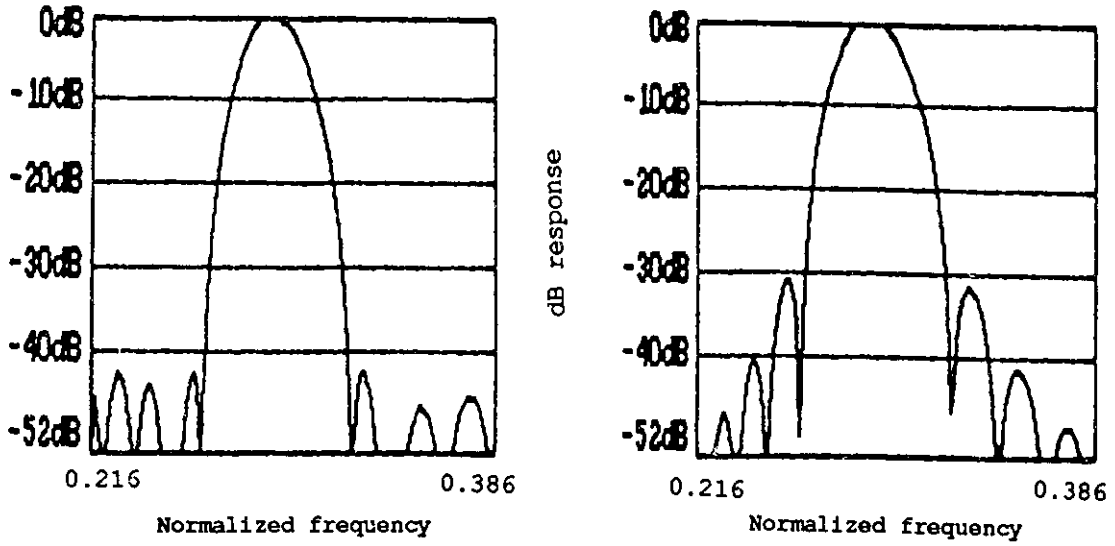

(a) Using window 3; **(b) Using window 4;**

(c) Using window 5; **(d) Using window 8;**

Figure 4.7 Frequency responses of the filters obtained using different 3-weght windows in Table IV.2.

The extension of the above procedure to other types of windows (different widths) is straightforward and will not be discussed here. In the next section we will present several examples of filter banks which were designed based on a twelfth-octave mother bank, and using different optimal windows.

4.4 Final Filter Bank Examples

In the preceding section we have shown that the linear programming method does give reasonable solution for the resulting filters, and does optimize the window coefficients which produce much better filters based on the filters in the mother bank. Also we have found the trade-offs between the type of windows and the performance of resulting filters. In this section we present examples to show the selection and application of windows for design of logarithmic RFB filter banks.

Given the specifications of a filter bank, the design procedure with the window processing, basically, consists of the following four steps:

1. Choose the type of windows;
2. Decide the specifications of mother filter bank;
3. Design the mother bank and calculate the bank frequency responses;
4. Optimize the weights of windows based on the mother filter bank;
5. Check the frequency response of the final filter bank.

There is a lot of flexibility in the selection of the weights of the windows between a mother bank and a desired bank. Widening the window, i.e., increasing the number of the filters in the window, will increase the window's power to suppress the sidelobe and improve the passband performance. In addition, a wider window, i.e., a window with more weights has more adjustability than a narrower one. Increasing the number of the

center unity weights, or the number of discrete samples in the passband, will result in shorter transition bandwidth and higher crossover gain. And the number of mother filters which the window shares with the previous one(or with the next one), strongly affects the crossover gain too. Thus a comprehensive design must be made.

EXAMPLE I: Design a third-octave filter bank based on the twelfth-octave mother filter bank, with as much sidelobe suppression as possible and 6 dB crossover gain. In order to obtain a third-octave bank from a twelfth-octave bank, the number of the filters which are applied in the window but not applied in the previous one is equal to $12/3 = 4$(12 from twelfth and 3 from third). This means the windows have, at least, five weights.

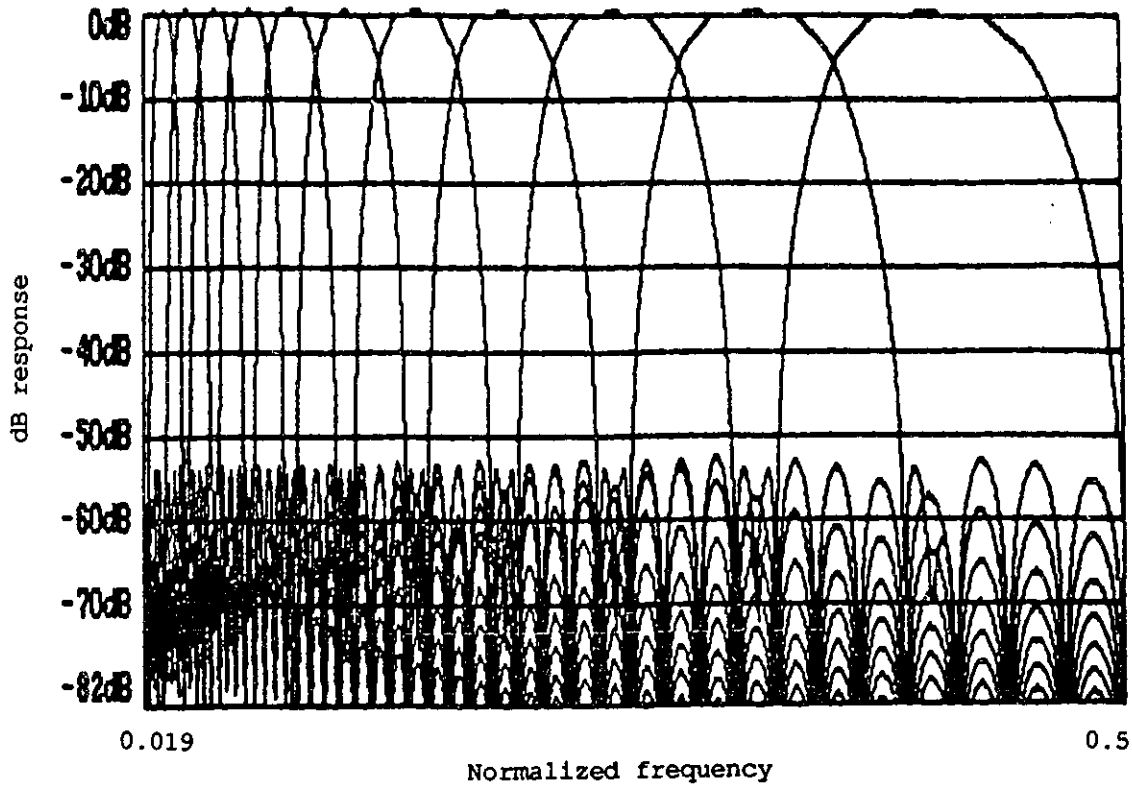

Figure 4.8 Frequency response of a third-octave filter bank using 6-weight windows on a twelfth-octave mother bank.

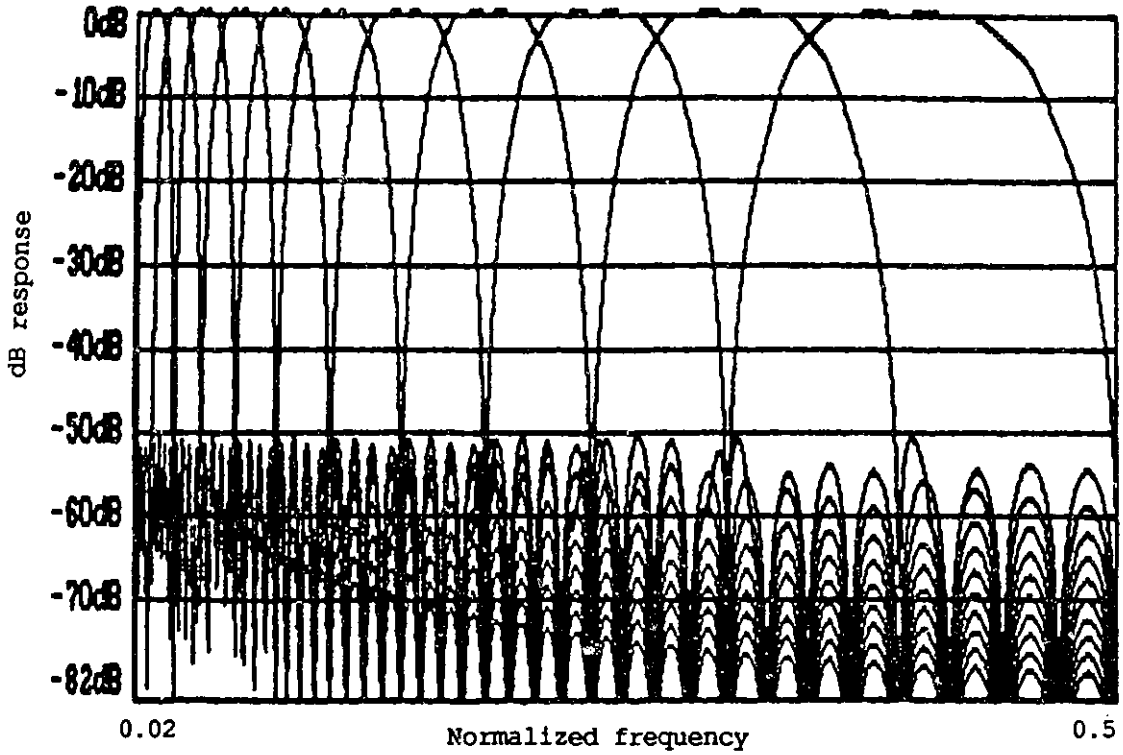

Figure 4.9 Frequency response of a third-octave filter bank using 7-weight windows on the twelfth-octave mother bank.

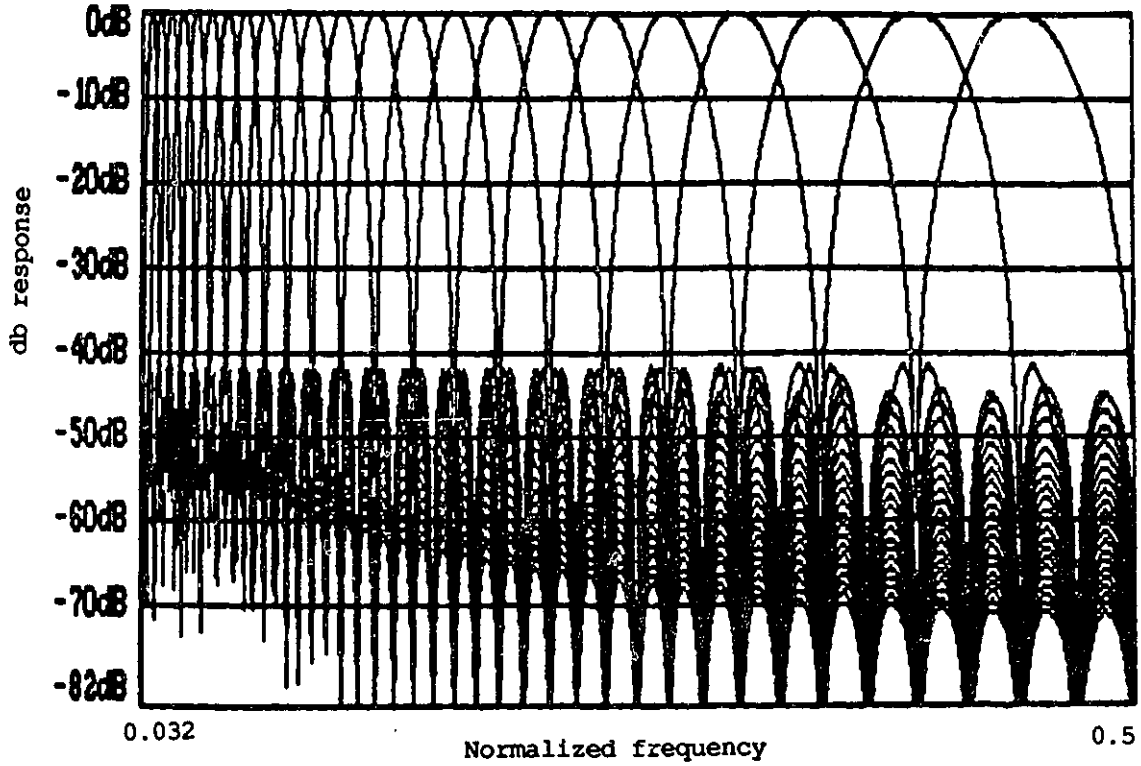

Figure 4.10 Frequency response of a sixth-octave filter bank using 3-weight windows on the twelfth-octave mother bank.

We first choose the windows with six weights considering the 6 dB crossover gain and the implementation load. Then the windows are optimized to approximate crossover gain. The dB requirement is met by adjusting the passband constraints. The desired third-octave bank is produced and its frequency response is plotted in Fig.4.8, where we can see the highest sidelobes are reduced to -53 dB from -13 dB of the mother bank, and the relative transition bands of the filters are smaller relative to those in the mother bank.

EXAMPLE II: Design the same filter bank as example I but for 3 dB crossover gain. The windows with seven weights are used and optimized to give reasonable desired filter bank. Fig.4.9 shows the frequency response of the bank. It can be seen that because of required 3 dB crossover gain the optimal wider(seven weights) windows make only 37 dB improvement in the stopband (from -13 dB to -50 dB).

EXAMPLE III: Design a sixth-octave bank based on the same twelfth-octave mother filter bank. The windows must have $12/6 = 2$ new mother filters which are not used in the previous window. The narrowest windows, i.e., the windows with three weights, are applied and the frequency response of the resulting bank is plotted in Fig.4.10, where only the stopband performance is under consideration and the highest sidelobe is supressed to 41.5 dB of the desired filter bank from 13 dB of the mother filter bank.

4.5 Summary

In this chapter, the optimal windowing technique for improving performance of logarithmic octave filter banks is presented. The technique based on the mother banks, sets up a linear programming problem which is solved using a simplex algorithm to produce the optimal weighting coefficients for desired filter bank specifications. The linear programming problem is formulated in two ways: constraining only the stopband and both the stopband and the passband. Examples of optimal windows and bank designs were

given and some trade-offs among the selection of windows, the computational complexity, and the performances of the stopband and passband of filter banks are discussed. The results show that the filter banks with much better frequency responses are obtained at the cost of windowing processing.

V FIFB FILTER BANK-BASED ALLPASS ANALYSIS/SYNTHESIS SYSTEMS

5.1 Introduction

In chapter I, we reviewed the digital filter bank and the filter bank-based analysis/synthesis system. In chapter II to chapter III, the frequency interpolation digital filter banks based on the adaptive filter structure or based on the complex unit resonator, have been derived and frequency-domain windowing techniques are proposed to improve the filter responses in chapter IV. In this chapter, we will study the logarithmically-spaced FIFB filter bank-based analysis/synthesis systems[107].

The block diagram of an analysis/synthesis system is shown in Fig.5.1, where the input signal is analyzed into its frequency constituents with an analysis bank, processed, and then a new signal is resynthezied from these processed elements. It is useful in such cases that the analysis/synthesis combination not seriously affect the signal. Sometimes it is required that the analysis and synthesis be perfect, i.e., the combination produces an output signal that is unchanged from the input signal except perhaps for some processing delay.

As we discussed in chapter I, many researchers have made their contributions to the design of uniform-bandwidth filter banks and corresponding analysis/synthesis systems, and there have been many successful approaches. For example, the QMF filter banks were introduced in sub-band coding system and have advantages for analysis and synthesis, in that the aliasing distortion of decimation and interpolation operation is completely compensated.

In this chapter, we are considering the similar problem, but without involving deci-

mation and interpolation. In other words, we will design an allpass system consisting of an analysis filter bank and a synthesis filter bank, where the analysis filter bank is a FIFB bank. Then a synthesis filter bank will be derived for the perfect reconstruction property. However, the filter banks in the allpass analysis/synthesis systems we consider may have an arbitrary spacing of the frequencies and bandwidths. They are useful for some acoustic signal processing systems such as speech enhancement and noise cancellation[108].

5.2 The FIFB Filter Bank Analysis/Synthesis System

5.2.1 The analysis filter banks

The analysis filter bank in Fig. 5.1 is chosen as a FIFB filter bank. Fig.5.2 shows the structure of the FIFB filter bank, which consists of first order complex matched filters for a sinusoid at the center frequencies ω_i of various filters, and overall feedback is applied to stabilize the frequency response. The i^{th} filter in the bank, from the input to the i^{th} output, has the transfer function

$$H_i(z) = \frac{K_i \frac{z_i z^{-1}}{1-z_i z^{-1}}}{1 + \sum_{j=1}^{N} K_j \frac{z_j z^{-1}}{1-z_j z^{-1}}} = \frac{N_{H_i}(z)}{D(z)}, \tag{5.1}$$

where

$$N_{H_i}(z) = K_i \frac{z_i z^{-1}}{1 - z_i z^{-1}}, \tag{5.2}$$

and $z_i = e^{j\omega_i} = e^{j2\pi f_i}$, is i^{th} pole of $N_{H_i}(z)$ which corresponds the center frequency ω_i of the i^{th} filter in the bank. The K_i's are the filter coefficients, and may be determined in different ways (see Chapter II and Chapter III). However, in this chapter, the calculation of the K_i plays an important role in the design of an allpass system, which will be discussed in following sections. From above equations it can be seen that all the filters in the bank have the same poles since all $H_i(z)$, $1 \leq i \leq N$, have the same denominator $D(z)$. The frequency interpolation property is described as that the i^{th} filter has unity response at

ω_i, and zero responses at other frequencies ω_j for $j \neq i$. Notice that these filter banks may be implemented in different adaptive filtering structures(see chapter II).

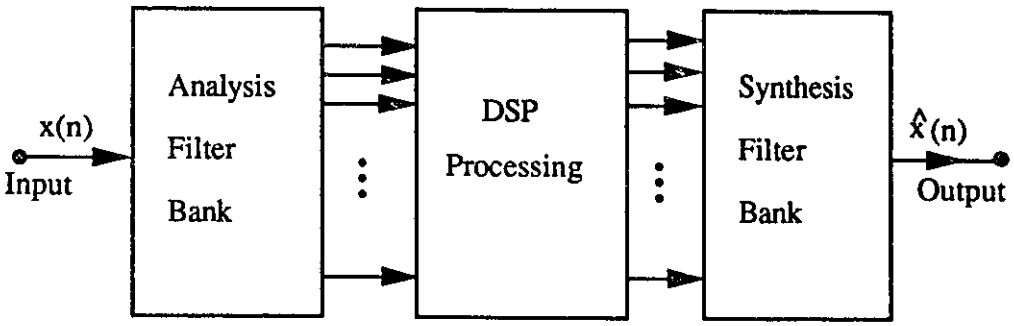

Figure 5.1 The block diagram of a bank-based analysis/synthesis system.

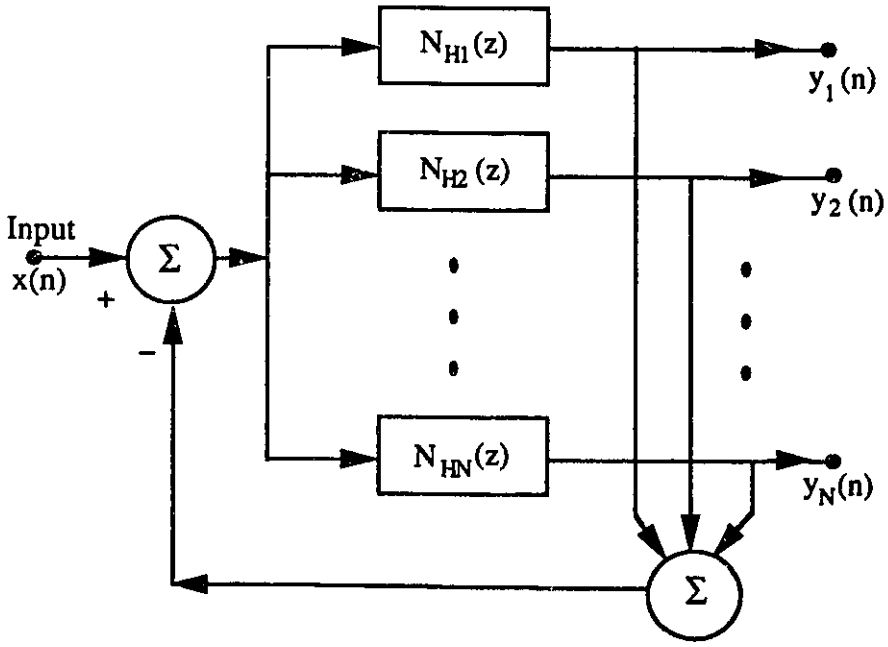

Figure 5.2 The block diagram of a FIFB analysis filter bank.

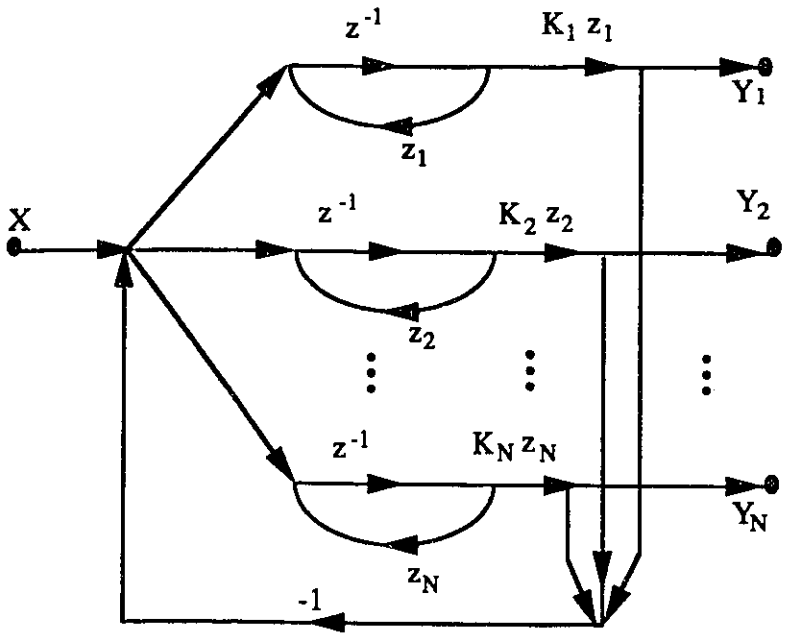

Figure 5.3 The signal flow graph of the FIFB bank in Fig.5.2.

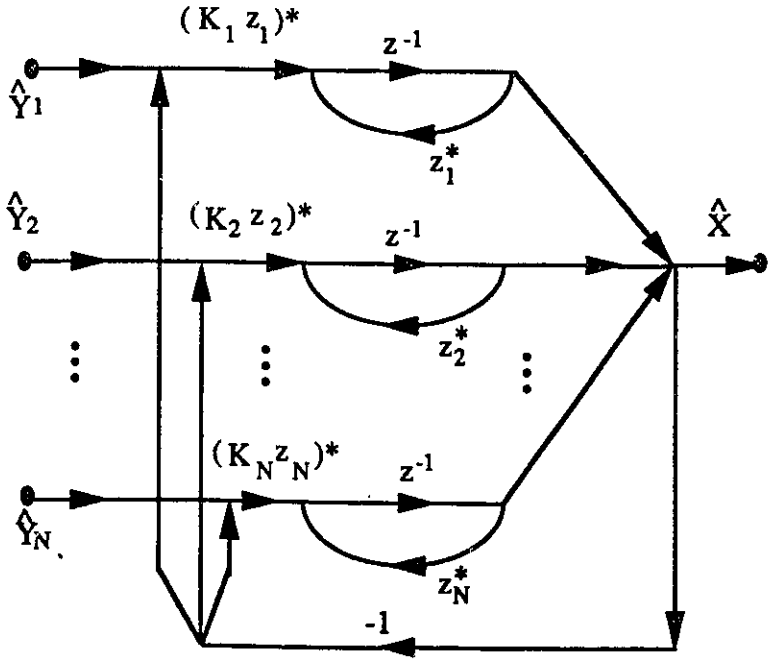

Figure 5.4 The complex conjugate transposed form of the SFG in Fig.5.3.

5.2.2 The structure of the synthesis filter bank

There are two important factors for the design of the synthesis filter banks. One is which kind of the structure to be applied to realize the synthesis bank. Another is how to calculate the filter coefficients K_i's to obtain an allpass analysis/synthesis system.

It is natural that the structure of the synthesis filter bank be the dual structure of the analysis bank structure. The signal flow graph (SFG) of the analysis bank is plotted in Fig.5.3 based on Fig.5.2 and equation (5.1). To determine this dual structure, we first study the complex conjugate transposed form of the SFG of the analysis filter bank. The complex conjugate transposition of a SFG is accomplished by reversing the directions of all branches in the network while changing each branch transmittance (except for delay branches) into its complex conjugate form and reversing the roles of the input and the output so that source nodes become sink nodes and vice versa.

The SFG of the synthesis filter bank, the complex conjugate transposed SFG of the analysis bank is derived and plotted in Fig.5.4, where a single-input/N-output system becomes an N-input/single-output system. Notice that the input and the output nodes are interchanged and the notation $\hat{y}_i$ and $\hat{x}$ in Fig.5.4 are applied to differ from x_i and y in the analysis bank. The i^{th} filter, i.e., the filter from the i^{th} input $\hat{y}_i$ to the output $\hat{x}$ in the stnthesis bank, has the transfer function as

$$G_i(z) = \frac{\frac{K_i^* z_i^* z^{-1}}{1-z_i^* z^{-1}}}{1 + \sum_{j=1}^{N} \frac{K_j^* z_i^* z^{-1}}{1-z_i^* z^{-1}}} = \frac{N_{G_i}(z)}{[D(z)]}, \tag{5.3}$$

where

$$N_{G_i}(z) = \frac{K_i^* z_i^* z^{-1}}{1 - z_i^* z^{-1}}, \tag{5.4}$$

and note that because of the structure of FIFB filter banks, $G_i(z)$ has the same denominator as $H_i(z)$.

If $T(z)$ denotes the overall transfer function of the system, from the input x of the analysis filter bank to the output $\hat{x}$ of the synthesis filter bank, then we have

$$T(z) = \frac{N(z)}{D(z)^2}, \tag{5.5}$$

and

$$N(z) = \sum_{i=1}^{N} \frac{|K_i|^2 z^{-2}}{(1 - z_i z^{-1})(1 - z_i^* z^{-1})} = \sum_{i=1}^{N} \frac{|K_i|^2 z^{-2}}{1 - 2z^{-1} Re(z_i) + z^{-2}}, \tag{5.6}$$

where $Re(x)$ means taking the real part of x.

This complex conjugate transposition structure is a good form to realize the synthesis filter bank. However, based on this structure, it is difficult to find the coefficient K_i's to meet the allpass requirement. The problem is to separate $N(z)$ into two factors, with one factor having the zeros inside the unit circle the same as the zeros of $D(z)$, and with another having the zeros outside the unit circle and having the same magnitude as that of $D(z)$.

5.2.3 The allpass systems

By taking the complex conjugate transposition to the SFG of the analysis filter bank, the structure of the synthesis filter bank has been obtained as shown in Fig.5.4, and the overall analysis/synthesis system transfer function $T(z)$ has been derived as equation (5.5). But the synthesis filter bank must be designed to obtain an allpass analysis/synthesis system. In other words, we have to find some synthesis filter bank with the satisfaction of the allpass requirement of $T(z)$.

If the denominator of $G_i(z)$ is chosen as the same as that of $H_i(z)$ but the numerator of $G_i(z)$ as

$$N_{G_i}(z) = \frac{K_i^*}{1 - z_i z^{-1}}, \tag{5.7}$$

then the transfer function of the i^{th} filter in the synthesis bank is

$$G_i(z) = \frac{K_i^* \frac{z}{z-z_i}}{1 + \sum_{j=1}^{N} K_j \frac{z_j}{z-z_j}} = \frac{N_{G_i}(z)}{D(z)}, \tag{5.8}$$

and consequently, the overall system has the transfer function as

$$T(z) = \sum_{j=1}^{N} \frac{|K_j|^2 \frac{z_j z}{(z-z_j)^2}}{D(z)\ D(z)} = \frac{N(z)}{D(z)^2}, \tag{5.9}$$

where

$$N(z) = \sum_{i=1}^{N} N_{H_i}(z)\ N_{G_i}(z) = \sum_{i=1}^{N} \frac{|K_i|^2 z_i z}{(z-z_i)^2}. \tag{5.10}$$

The question whether or not the system will be of the perfect reconstruction property is equivalent to the question if the magnitude of $T(z)$ will be unity. Now let's study if this structure can be made as an allpass network. This means to analyze the possibility of unity $|T(z)|$. We start this from examining the zeros of the numerator of $T(z)$. Assuming that z_o is a zero of the $N(z)$, that is

$$N(z_o) = \sum_{i=1}^{N} \frac{|K_i|^2 z_i z_o}{(z_o - z_i)^2} = 0, \tag{5.11}$$

then we have

$$\left(\sum_{i=1}^{N} \frac{|K_i|^2 z_i z_o}{(z_o - z_i)^2} \right)^* = 0. \tag{5.12}$$

However we can show that

$$\begin{aligned} [N(z_o)]^* &= \sum_{i=1}^{N} \frac{|K_i|^2 z_i^* z_o^*}{(z_o^* - z_i^*)^2} \\ &= \sum_{i=1}^{N} \frac{|K_i|^2 z_i \frac{1}{z_o^*}}{(\frac{1}{z_o^*} - z_i)^2} \\ &= N(\frac{1}{z_o^*}). \end{aligned} \tag{5.13}$$

Note that we have multiplied the numerator and denominator of the summation by $(z_i)^2$ firstly and by $\frac{1}{(z_o^*)^2}$ secondly, and the relation $z_i^* z_i = 1$ has been used.

Equations (5.11-13) show that the numerator $N(z)$ has the property that if z_o is a zero of $N(z)$, then there is a matching zero at the reciprocal conjugate position, i.e., at $\frac{1}{z_o^*}$. Furthermore, from the simulation results we find that if all the z_i's are chosen on the unit circle and the magnitude of the coefficient $|K_i|$ is directly proportional to the bandwidth of i^{th} filter, then $N(z)$ has no zeros on the unit circle. Thus if z_0 is inside the unit circle, the pairing zero $\frac{1}{z_0^*}$ is outside the unit circle, and consequently we summarize that $N(z)$ has totally 2N zeros, and N zeros are inside the unit circle and N zeros outside the unit circle. Apparently there is a zero at $z = 0$ and another at infinite position since every term of the summation has zero at $z = 0$ and at infinite position for $N(z)$.

We classify the zeros of $N(z)$ into two groups: Group 1 is all the zeros inside the unit circle, i.e., $\hat{z}_{ok}$, $1 \leq k \leq N$, and Group 2 is all the zeros outside the unit circle, i.e., $\check{z}_{ok}$, $1 \leq k \leq N$, and we have the relation $\hat{z}_{ok} = \frac{1}{\check{z}_{ok}^*}$. If $\bar{N}_I(z)$ and $\bar{N}_O(z)$ express the partial factors of the numerators of $N(z)$, with including all the first group of zeros and all the second group of zeros, respectively, we have

$$N(z) = \frac{\bar{N}_I(z)\,\bar{N}_O(z)}{D_N(z)}, \tag{5.14}$$

with

$$\bar{N}_I(z) = \prod_{k=1}^{N}(z - \hat{z}_{ok}), \tag{5.15}$$

and

$$\bar{N}_O(z) = \prod_{k=1}^{N}(z - \check{z}_{ok}), \tag{5.16}$$

where $D_N(z)$ is the denominator of $N(z)$ in equation (5.10), and $\hat{z}_{ok}$ and $\check{z}_{ok}$ are k^{th} pair zeros, one inside of the unit circle and another outside of the unit circle. To find the strategy for the cancellation of the zeros between $D(z)^2$ and $N(z)$, we determine $\bar{N}_I(z)$ and $\bar{N}_O(z)$ by reviewing and applying the following definition[95].

For a general complex polynomial $F(z)$,

$$F(z) = a_0 + a_1 z + a_2 z^2 + ... + a_N z^N, \tag{5.17}$$

we have

$$[\ F(z)\ ]_* = z^N\ [\ F(\frac{1}{z^*})\ ]^*, \tag{5.18}$$

or

$$[\ F(z)\ ]_* = a_0^*\ z^N + a_1^*\ z^{N-1} + ... + a_{N-1}^*\ z + a_N^*. \tag{5.19}$$

According to the definition, thus we have

$$\begin{aligned} [\ \bar{N}_I(z)\ ]_* &= z^N\ [\bar{N}_I(\frac{1}{z^*})\ ]^* \\ &= z^N \prod_{k=1}^{N}(\frac{1}{z^*} - \hat{z}_{ok})^* \\ &= z^N \prod_{k=1}^{N}(\frac{1}{z} - \hat{z}_{ok}^*) \\ &= \prod_{k=1}^{N}(1 - z\ \hat{z}_{ok}^*). \end{aligned} \tag{5.20}$$

From the last line of (5.20), we see $[\bar{N}_I(z)]_*$ has N zeros at $\frac{1}{\hat{z}_{ok}^*}$, $1 \le k \le N$, which are just the zeros of $[\bar{N}_O(z)]$. Thus, $\prod_{k=1}^{N} \hat{z}_{ok}^* \prod_{k=1}^{N}(\frac{1}{\hat{z}_{ok}^*} - z) = \prod_{k=1}^{N} \hat{z}_{ok}^*(-1)^N \bar{N}_O(z)$. Therefore

$$\bar{N}_O(z) = \frac{(-1)^N}{\prod_{k=1}^{N}\ \hat{z}_{ko}^*}\ [\ \bar{N}_I(z)\ ]_*. \tag{5.21}$$

Thus we may conclude that $N(z)$ can be factorized into $\bar{N}_I(z)$ and $[\bar{N}_I(z)]_*$, i.e.,

$$\begin{aligned} N(z) &= \frac{(-1)^N}{\prod_{k=1}^{N}\ \hat{z}_{ok}^*}\ \frac{\bar{N}_I(z)\ [\ \bar{N}_I(z)\ ]_*}{D_N(z)} \\ &= \frac{\bar{N}_I(z)\ [\ \bar{N}_I(z)\ ]_*}{\bar{D}_N(z)}, \end{aligned} \tag{5.22}$$

where, clearly, $\bar{D}_N(z) = D_N(z) \prod_{k=1}^{N}\ (-\hat{z}_{ok}^*)$.

Substituting equation (5.22) in (5.9), $T(z)$ may therefore be expressed as

$$T(z) = \frac{\frac{\tilde{N}_I(z)[\tilde{N}_I(z)]_*}{\tilde{D}_N(z)}}{D(z)^2}. \tag{5.23}$$

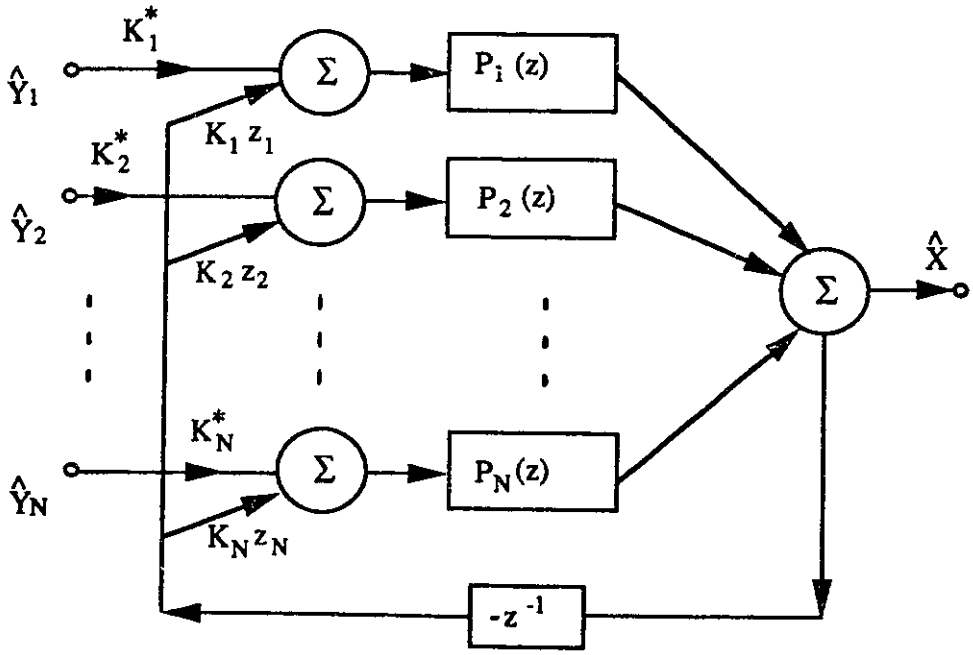

Figure 5.5 The block diagram of the synthesis filter bank, where Pi (z) = z / (z - zi) .

If it is assumed that first

$$D(z)^2 = \frac{N_D(z)^2}{D_D(z)}, \tag{5.24}$$

secondly

$$D_D(z) = G\,\tilde{D}_N(z) = \tilde{G}\prod_{i=1}^{N}(z - z_i)^2, \tag{5.25}$$

(this is reasonable) with G and $\tilde{G}$ being two complex constants, and then finally let $N_D(z)$

have the same zeros as the zeros of $\bar{N}_I(z)$, we will obtain the $T(z)$ expression from (5.23)

$$T(z) = \frac{[N_D(z)]_*}{N_D(z)}. \tag{5.26}$$

It is obvious that $T(z)$ is an allpass transfer function[29] since $[N_D(z)]_*$ and $N_D(z)$ have the same magnitude on the unit circle.

Frequency responses of the synthesis filters now are

$$G_i(e^{j\omega}) = \frac{K_i^* \frac{e^{j\omega}}{e^{j\omega}-z_i}}{1 + \sum_{j=1}^{N} K_j \frac{z_j}{e^{j\omega}-z_j}}. \tag{5.27}$$

It is not hard to show that the magnitude response of the i^{th} filter in the synthesis bank, $|G_i(e^{j\omega})|$, is just the same as that of the i^{th} filter in the analysis bank, i.e., $|[\ H_i(e^{j\omega})\ ]|$. The synthesis filter bank is realizable and stable (since it has the same poles as the analysis filter bank). The structure shown in Fig 5.5 may be applied to implement the synthesis bank, where

$$P(z) = \frac{1}{(1 - z_i z^{-1})}. \tag{5.28}$$

The overall analysis/synthesis system is a stable system since all the poles of $T(z)$ are inside the unit circle. But it is not a minimum phase system because all of the zeros are outside the unit circle. It is a maximum phase system!

5.2.4 The design of the analysis and synthesis filter banks

The design technique for a single analysis filter bank has been presented in chapter II and chapter III. The poles of the filter transfer function are chosen for good frequency response, and then the filter coefficients K_i's are calculated based on the pole selection. In chapter II, the poles of the FIFB filter bank were set at the position with the same phase angle as the corresponding zeros but closer to the unit circle for lower frequencies. The formula for K_i's is equation (2.13).

To obtain the perfect reconstruction analysis/synthesis system, the analysis and synthesis filter banks have to be designed to meet the requirements in the assumptions given in the previous section. It was supposed that all the zeros inside of the unit circle, of the numerator of the overall system function $N(z)$, should be the same as the zeros of the denominator of the transfer function of the analysis filter. Thus, the zeros inside the unit circle of $N(z)$ have to be found first. For this, we see from equation (5.13) that one set of the magnitudes of the filter coefficients should be initialized.

The design procedure, consequently, is listed below:

(1). Given z_i, choose $|K_i^I|$ $1 \leq i \leq N$, and calculate $N(z)$.

(2). Find the partial factor $\bar{N}_I(z)$ which has all the zeros inside the unit circle of $N(z)$, in fact, that is $D(z)$.

(3). Calculate the filter coefficients K_i's from a partial fraction expansion of $D(z)$ (in fact, by assigning the zeros calculated in (2) as the zeros of $D(z)$).

(4). Chech if the ratio $\frac{|K_i|}{|K_i^I|}$ is a constant for all i. If so, we have obtained the K_i for an all-pass analysis/synthesis system. Otherwise, repeat the procedure with the paramater adjustment.

The formula for calculating K_i's is the same as equation (2.13). However, in (2.13), the pole function $\Gamma(\phi_i)$ is taken by N zeros obtained in step (2). It is because the zeros of $\bar{N}_I(z)$ are used to calculate K_i in step (3) that the ratio of $|K_i|$ and $|K_i^I|$ should be a constant for i=1, 2, ..., N. So we may say that the design procedure is to find the proper phase angles of the filter coefficients to ensure that the analysis filter bank has all the poles just to cancel all the first Group of zeros of the whole analysis/synthesis system, i.e., the zeros inside of the unit circle of $N(z)$.

5.3 The Design Examples

In this section, we illustrate the design procedure by presenting four different analysis/synthesis reconstruction systems.

Example I: Design an uniform-bandwidth analysis/synthesis system. 20 filters are uniformly spaced from 0.1 to 0.5 normalized frequency band and the center frequencies are

$$f_{20} = 0.49, \tag{5.29}$$

$$f_i = f_{i+1} - 0.02, \qquad for\ i = 1, 2, ..., 19 \tag{5.30}$$

The initial values of the filter coefficients $|K_i^I|$ are chosen as a constant and the calculation results show this is necessary since the bandwidths of all the filters are a constant. The step two is very important, where we don't care the zeros outside the unit circle but try to find all the zeros of $N(z)$ which are inside the unit circle. *Maehly's* method[109] is applied to accomplish this.

If the $P(x)$ is a N^{th} order x polynomial, and $P(x)$ has N zeros x_i for i=1,2,...,N, then one step of *Maehly's* procedure[109] which recursively calculates an estimate of the zeros of $P(x)$, taking an estimate x_i^k into a new estimate x_i^{k+1} of the i^{th} zero of $P(x)$, can be written as

$$\begin{aligned} x_i^{k+1} &= x_i^k - \frac{P(x_i^k)}{P'(x_i^k) - P(x_i^k) \sum_{j=1}^{i-1}(x_i^k - x_j)^{-1}} \\ &= x_i^k - \frac{1}{\frac{P'(x_i^k)}{P(x_i^k)} - \sum_{j=1}^{i-1}(x_i^k - x_j)^{-1}}. \end{aligned} \tag{5.31}$$

Now we have the objective function as equation (5.10) and therefore

$$N'(z) = \frac{d\,N(z)}{d\,z} = -\sum_{i=1}^{N} \frac{z_i\,|K_i|^2\,(z + z_i)}{(z - z_i)^3}. \tag{5.32}$$

If the r^{th} zero of $N(z)$ in the k^{th} guess is z_{or}^k, then the $(k+1)^{th}$ guess z_{or}^{k+1} may be calculated by

$$z_{or}^{k+1} = z_{or}^k + \frac{1}{\sum_{j=1}^{r-1} \frac{1}{(z_{or}^k - z_{oj})} - \frac{N'(z_{or}^k)}{N(z_{or}^k)}}, \tag{5.33}$$

where z_{oj} is j^{th} final zero of $N(z)$ which has been found already before k^{th} trying, i.e., in above equation, we always have

$$j \leq r - 1. \tag{5.34}$$

It is very important to select the initial guess of the zeros properly. Otherwise the routine will either diverge, or converge but with some zeros of the final zero set outside the unit circle. Of course when it is convergent the speed of convergence is strongly related to the initial guess also. For the uniform system, besides one zero at $z = 0$, all other N-1 zeros are initially near the unit circle at the phases which are the arithmetic average of the phases of the two adjacent center frequencies.

The solutions for the zeros inside the unit circle and the final filter coefficients K_i's are shown in Table V.1 and Table V.2, where we can see that the magnitudes of K_i's are constant and the phases of K_i's are inversely proportional to the center frequencies of the filter banks. The magnitude frequency responses of the analysis or synthesis filter bank are plotted in Fig.5.6. The phase and magnitude responses of the overall analysis/synthesis system are plotted in Fig.5.7.

Example II: Design a third-octave bandwidth analysis/synthesis system with the number of the subbands N=16. Because the center frequencies of the filter banks are logarithmically spaced as

$$f_i = 0.5\, e^{-\frac{ln2}{3}(i-0.5)} \qquad for\ i = 1, 2, ..., N \tag{5.35}$$

and the constant-Q filters are desired, the initial magnitudes of K_i's are taken proportionally to the filter bandwidths. The initial guess of the zeros of $N(z)$ are chosen in the similar way above but the phase angles of the zeros are strongly deviated to the phase of lower one of the two adjacent center frequencies. The calculation results of the zeros and the gain coefficients are printed in Table V.3 and Table V.4, and the response curves are plotted in Fig.5.8 ans Fig.5.9.

Table V.1 The zeros of N(z) for 20-filter uniform band bank.

Magnitude	Angle
0.8714891875	179.9999999991
0.0000000000	0.0000000000
0.8715651423	172.7890347110
0.8717942336	165.5779964107
0.8721788713	158.3668068740
0.8727234122	151.1553905535
0.8734342593	143.9436477061
0.8743202135	136.7314731217
0.8753927606	129.5187337709
0.8766671538	122.3052683866
0.8781631839	115.0908680343
0.8799065972	107.8752526410
0.8819317384	100.6580346331
0.8842850099	93.4386638105
0.8870309339	86.2163104966
0.8902630643	78.9896530551
0.8941237903	71.7564400090
0.8988462989	64.5124516880
0.9048542562	57.2486697071
0.9130543293	49.9415048913
0.9260861916	42.5016379989

Table V.2 The filter coefficients of 20-filter uniform band bank.

Magnitude	Phase
0.0302627735	0.7681354529
0.0302627895	2.3110886325
0.0302627936	3.8742586971
0.0302627880	5.4719110978
0.0302627863	7.1196524601
0.0302627835	8.8350903452
0.0302627883	10.6386752178
0.0302627978	12.5549056306
0.0302627981	14.6138468418
0.0302627960	16.8534502551
0.0302627974	19.3230354346
0.0302627920	22.0885195638
0.0302627888	25.2410216669
0.0302627924	28.9115795062
0.0302627939	33.2977853772
0.0302627941	38.7167380415
0.0302627945	45.7225548542
0.0302627947	55.4142461402
0.0302627948	70.4912058355
0.0302627950	101.5543685800

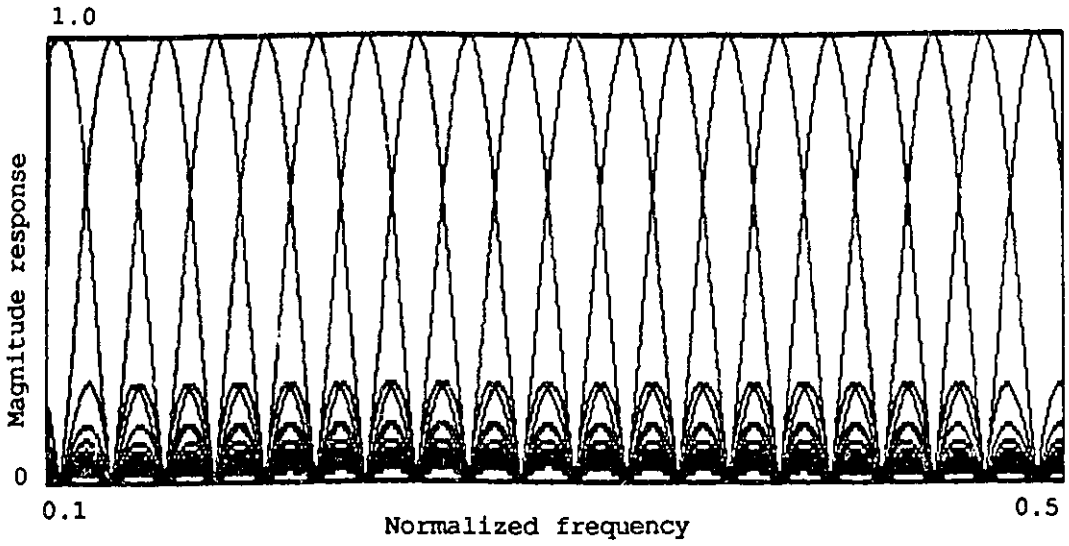

Figure 5.6 Frequency response of 20-filter uniform band bank (analysis filter bank or synthesis filter bank).

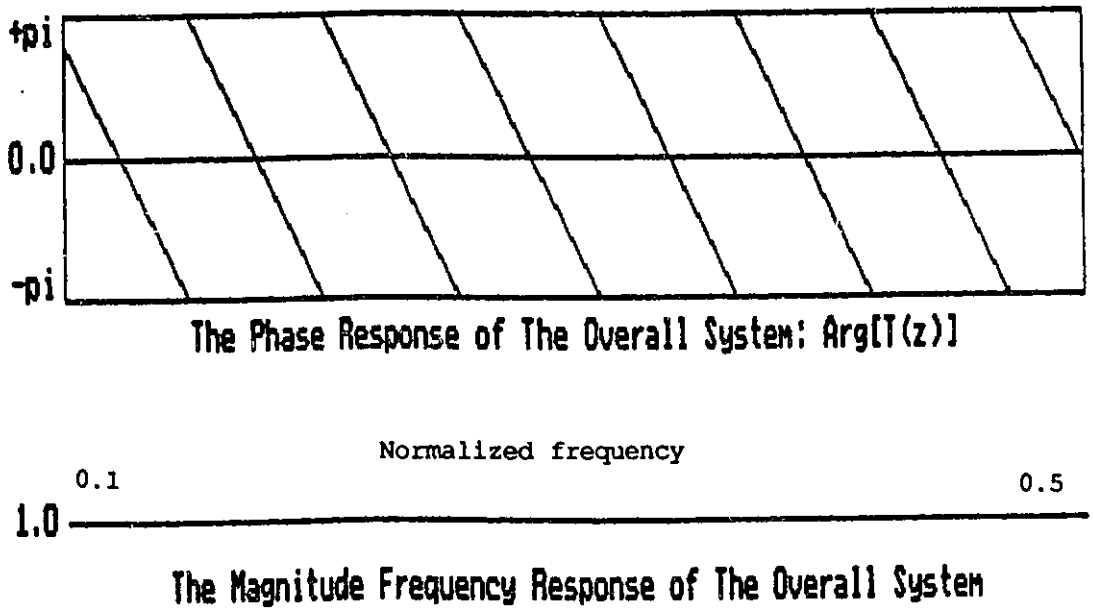

Figure 5.7 Phase and magnitude responses of uniform band filter bank-based allpass system.

Table V.3 The zeros of N(z) for 16-filter third-octave bank.

Magnitude	Angle
0.6286079520	180.0000000005
0.0000000000	0.0000000000
0.6947703526	136.8324063303
0.7495999863	106.7307348452
0.7985263443	83.7768785252
0.8397856355	65.9710785446
0.8735433277	52.0538929000
0.9006689017	41.1288383141
0.9222154969	32.5286507433
0.9392008085	25.7456503824
0.9525218002	20.3886454382
0.9629314086	16.1537898647
0.9710429495	12.8038900934
0.9773449572	10.1533447949
0.9822177397	8.0574314808
0.9859589108	6.4070546475
0.9891064072	5.1376974405

Table V.4 The filter coefficients of 16-filter third-octave bank.

Magnitude	Phase
0.1070072981	-2.2462456663
0.0849317489	-1.3538606305
0.0674103732	-0.5714146279
0.0535036488	0.2398064859
0.0424658746	1.1561234536
0.0337051870	2.2391405808
0.0267518250	3.5537920835
0.0212329388	5.1773584521
0.0168525938	7.2078579132
0.0133759118	9.7756796106
0.0106164683	13.0634603226
0.0084262964	17.3447907370
0.0066879559	23.0707825948
0.0053082342	31.0998870082
0.0042131483	43.4976325219
0.0033439780	68.3671614248

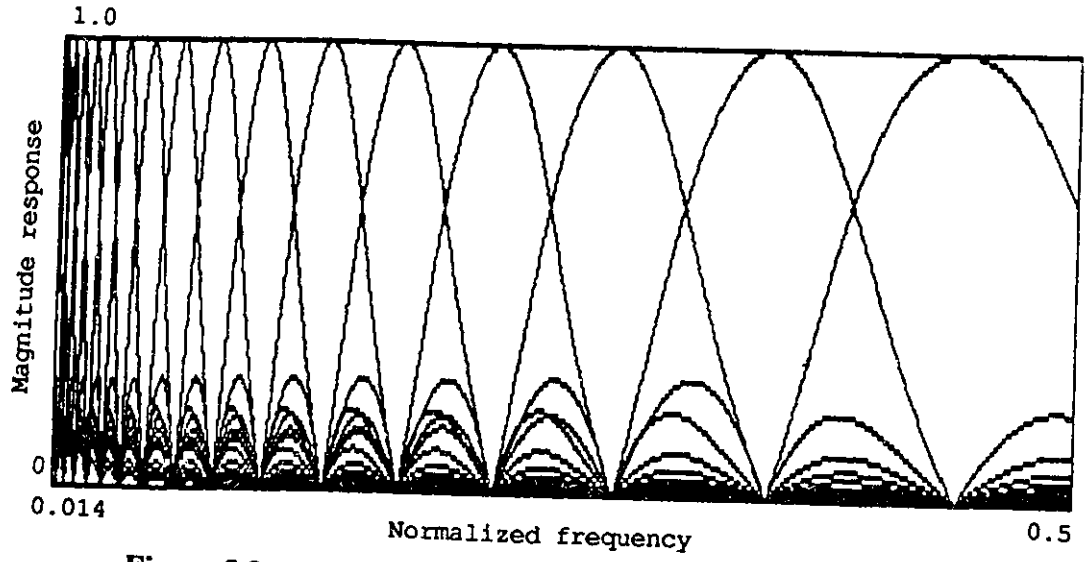

Figure 5.8 Frequency response of 16-filter third-octave bank (analysis filter bank or synthesis filter bank).

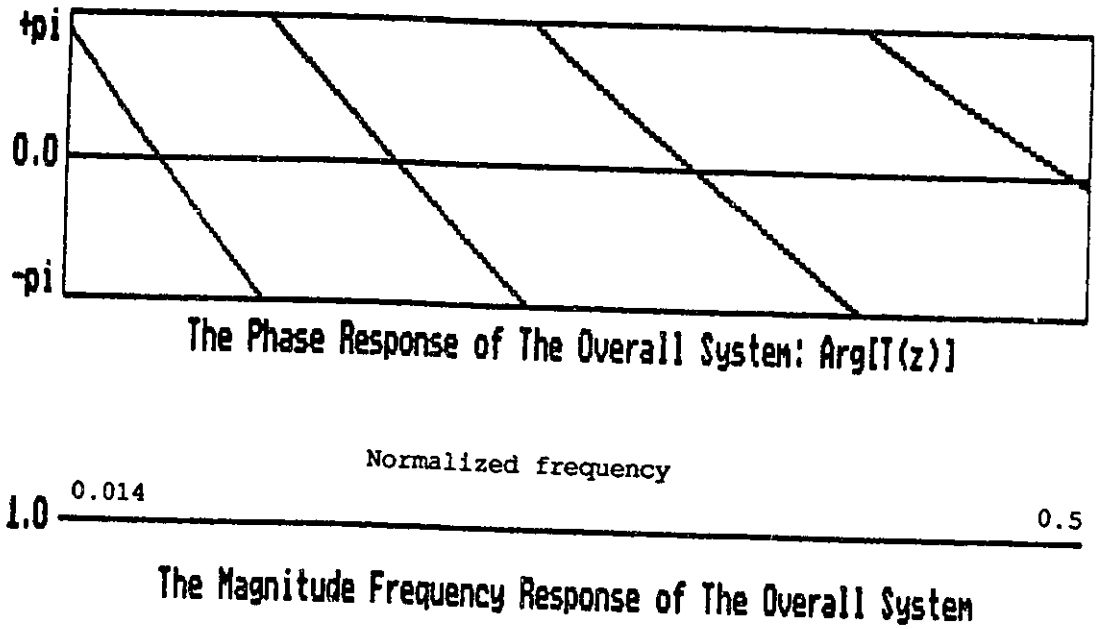

Figure 5.9 Phase and magnitude responses of third-octave filter bank-based allpass system.

Other two examples are a sixth-octave bandwidth system and a twelfth-octave bandwidth system. The results are shown in Table V.5-V.8 and Fig.5.10-5.13. It is shown that because of the nonlinearly spacing center frequencies and the bandwidths of the filters the phase responses are not linear even though the perfect reconstructions in magnitude are obtained.

All the zero plots of $N(z)$ in z-plan for four different examples above are shown in Fig.5.14, where we can see that the higher the frequencies to which the zeros correspond, the farther away from the unit circle the zeros, and the lower the frequencies the closer to the unit circle. The changes of the radii of the zeros along the angles are depended on the spacing of the frequencies. For example, for uniform filter bank, the change is not obvious in high frequency, but for third-octave filter bank, the change is very large, from 0.6286 of the zero at the highest frequency to 0.9891 of the zero at the lowest frequency.

5.4 Discussions

First since the same FIFB filter bank structures are applied for the analysis/synthesis system, the good sensitivity property is still retained for the analysis filter bank and for the synthesis filter bank. The efficient adaptive realization structure may be used to implement the analysis filter bank. Secondly, since the i^{th} filter in the analysis bank has the same magnitude response as the i^{th} filter in the synthesis bank, we may have

$$\sum_{i=1}^{N} \mid H_i \mid^2 \; = \; 1, \tag{5.36}$$

and therefore

$$Max\{\mid H_i \mid\} \; = \; 1, \qquad for\ i = 1, 2, ..., N. \tag{5.37}$$

This means these filter banks are maximum flat, i.e., all the filters obtain their responses with the maximum unity value at their center frequencies. Thus these filter banks form a useful basis for the windowing procedures described in previous chapter.

Table V.5 The zeros of N(z) for 35-filter sixth-octave bank.

Magnitude	Angle
0.7746684101	179.9999999987
0.0000000000	0.0000000000
0.7943231371	158.1545580404
0.8104544562	140.0170781108
0.8274793403	124.1948916858
0.8441990558	110.2628432005
0.8600361895	97.9517826419
0.8747359096	87.0527316776
0.8882063322	77.3922228681
0.9004427646	68.8222656582
0.9114883823	61.2148840933
0.9214121671	54.4585535724
0.9302958710	48.4556101285
0.9382260849	43.1202406928
0.9452893791	38.3768611429
0.9515693604	34.1587737097
0.9571449620	30.4070368160
0.9620895353	27.0695024746
0.9664704645	24.0999893918
0.9703491190	21.4575680968
0.9737810196	19.1059398676
0.9768161328	17.0128950618
0.9794992386	15.1498392352
0.9818703270	13.4913776035
0.9839650042	12.0149499428
0.9858148814	10.7005094981
0.9874479386	9.5302405634
0.9888888451	8.4883105363
0.9901592226	7.5606537433
0.9912778187	6.7347867916
0.9922605389	5.9996609625
0.9931202335	5.3455746820
0.9938662127	4.7642314085
0.9945053242	4.2492889294
0.9950704552	3.7986784112
0.9958787920	3.4149438852

Table V.6 The filter coefficients of 35-filter sixth-octave bank.

Real part	Imaginary part
0.0562245705	-0.0011068207
0.0500959244	-0.0006474948
0.0446329322	-0.0003261358
0.0397643996	-0.0000819720
0.0354259521	0.0001116327
0.0315599489	0.0002686181
0.0281149233	0.0003977281
0.0250449646	0.0005049983
0.0223091336	0.0005948310
0.0198709314	0.0006705517
0.0176978192	0.0007347340
0.0157607891	0.0007894056
0.0140339791	0.0008361868
0.0124943293	0.0008763870
0.0111212751	0.0009110750
0.0098964721	0.0009411314
0.0088035511	0.0009672884
0.0078278983	0.0009901602
0.0069564576	0.0010102681
0.0061775540	0.0010280595
0.0054807322	0.0010439249
0.0048566101	0.0010582111
0.0042967428	0.0010712334
0.0037934933	0.0010832869
0.0033399048	0.0010946559
0.0029295674	0.0011056240
0.0025564661	0.0011164821
0.0022147882	0.0011275334
0.0018986466	0.0011390902
0.0016016262	0.0011514423
0.0013159338	0.0011647435
0.0010305592	0.0011786180
0.0007265299	0.0011906583
0.0003610894	0.0011890202
-0.0002164958	0.0010856914

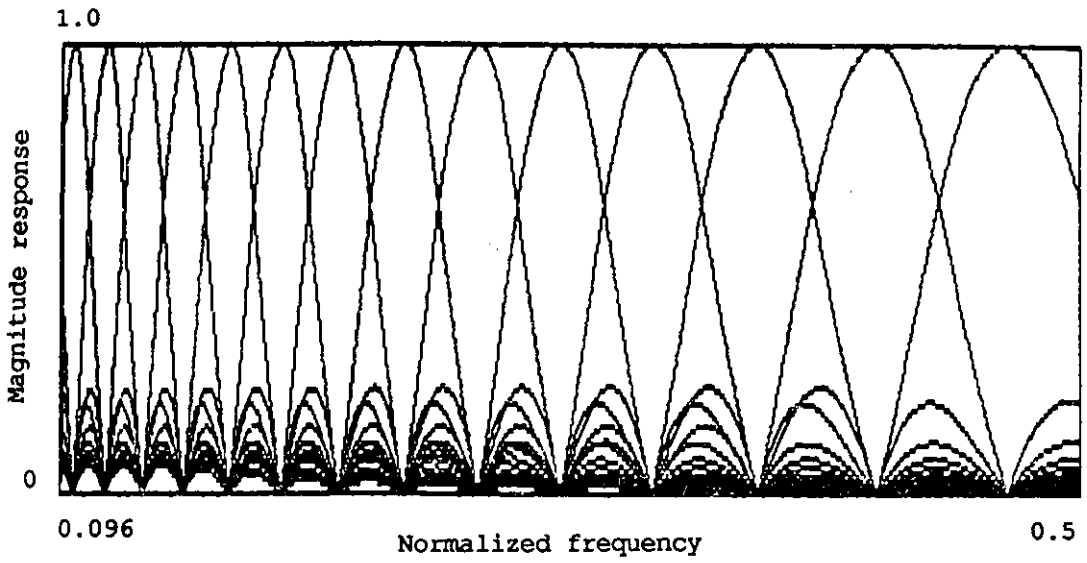

Figure 5.10 Frequency response of 35-filter sixth-octave bank (analysis filter bank or synthesis filter bank).

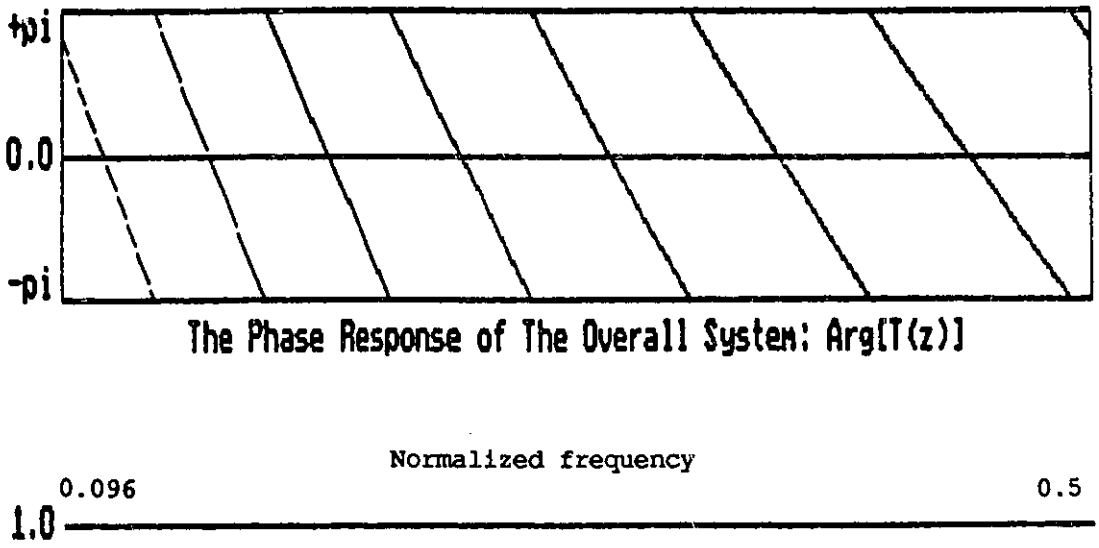

Figure 5.11 Phase and magnitude responses of sixth-octave filter bank-based allpass system.

Table V.7 The zeros of N(z) for 60-filter twelfth-octave bank.

Magnitude	Angle	Magnitude	Angle
0.8685292054	180.0000000005	0.9745350363	31.1300560332
0.0000000000	0.0000000000	0.9760386108	29.3771080040
0.8739468912	169.1047126564	0.9774540916	27.7231386171
0.8775543531	159.2621979236	0.9787863842	26.1625322257
0.8820268674	150.0934017081	0.9800401562	24.6899951974
0.8869477620	141.4945126457	0.9812198403	23.3005371443
0.8920572173	133.4116444381	0.9823296418	21.9894532131
0.8972060799	125.8057344855	0.9833735427	20.7523075236
0.9023043342	118.6443436192	0.9843553100	19.5849175925
0.9072952855	111.8989076560	0.9852785012	18.4833397397
0.9121372283	105.5435389197	0.9861464723	17.4438553724
0.9168161597	99.5543365399	0.9869623828	16.4629581470
0.9213146225	93.9093539306	0.9877292026	15.5373419257
0.9256248752	88.5881043518	0.9884497156	14.6638895397
0.9297435382	83.5714656657	0.9891265238	13.8396623550
0.9336703625	78.8415510396	0.9897620482	13.0618905890
0.9374073619	74.3816036128	0.9903585263	12.3279645398
0.9409581834	70.1759073924	0.9909180064	11.6354267797
0.9443276448	66.2097099426	0.9914423336	10.9819656010
0.9475213870	62.4691539365	0.9919331270	10.3654102764
0.9505456119	58.9412157892	0.9923917418	9.7837291399
0.9534068817	55.6136500030	0.9928192094	9.2350327742
0.9561119662	52.4749384051	0.9932161545	8.7175871686
0.9586677232	49.5142434716	0.9935827115	8.2298482549
0.9610810095	46.7213653303	0.9939186070	7.7705459681
0.9633586102	44.0867019825	0.9942242760	7.3388880571
0.9655071871	41.6012122975	0.9945073231	6.9350257565
0.9675332384	39.2563817328	0.9948125688	6.5606222683
0.9694430702	37.0441902816	0.9953019554	6.2159766151
0.9712427757	34.9570826823	0.9962441939	5.8881952270
0.9729382211	32.9879404939		

Table V.8 The filter coefficients of 60-filter twelfth-octave bank.

Real part	Imaginary part	Real part	Imaginary part
0.0299652696	-0.0002428394	0.0051571950	0.0012100963
0.0282843446	-0.0000464124	0.0048497257	0.0012164152
0.0266966921	0.0001114880	0.0045583161	0.0012222041
0.0251973875	0.0002442895	0.0042819779	0.0012275130
0.0237815665	0.0003585049	0.0040197693	0.0012323867
0.0224445138	0.0004578127	0.0037707918	0.0012368644
0.0211817663	0.0005446027	0.0035341856	0.0012409804
0.0199892913	0.0006205159	0.0033091261	0.0012447644
0.0188637428	0.0006869423	0.0030948196	0.0012482411
0.0178016724	0.0007462496	0.0028904986	0.0012514304
0.0167985087	0.0007992311	0.0026954171	0.0012543468
0.0158511218	0.0008463959	0.0025088451	0.0012569990
0.0149564586	0.0008884627	0.0023300621	0.0012593882
0.0141115746	0.0009260593	0.0021583502	0.0012615072
0.0133136718	0.0009597231	0.0019929842	0.0012633372
0.0125601011	0.0009899164	0.0018332210	0.0012648445
0.0118483571	0.0010170390	0.0016782845	0.0012659749
0.0111760716	0.0010414389	0.0015273466	0.0012666451
0.0105410061	0.0010634193	0.0013795005	0.0012667301
0.0099410449	0.0010832463	0.0012337241	0.0012660433
0.0093741885	0.0011011534	0.0010888264	0.0012643034
0.0088385465	0.0011173464	0.0009433675	0.0012610810
0.0083323321	0.0011320072	0.0007955340	0.0012557041
0.0078538555	0.0011452963	0.0006429368	0.0012470854
0.0074015187	0.0011573563	0.0004822629	0.0012333841
0.0069738100	0.0011683137	0.0003086370	0.0012112859
0.0065692990	0.0011782810	0.0001143458	0.0011742776
0.0061866314	0.0011873584	-0.0001140016	0.0011077620
0.0058245247	0.0011956351	-0.0004026515	0.0009709301
0.0054817634	0.0012031907	-0.0008044838	0.0005806007

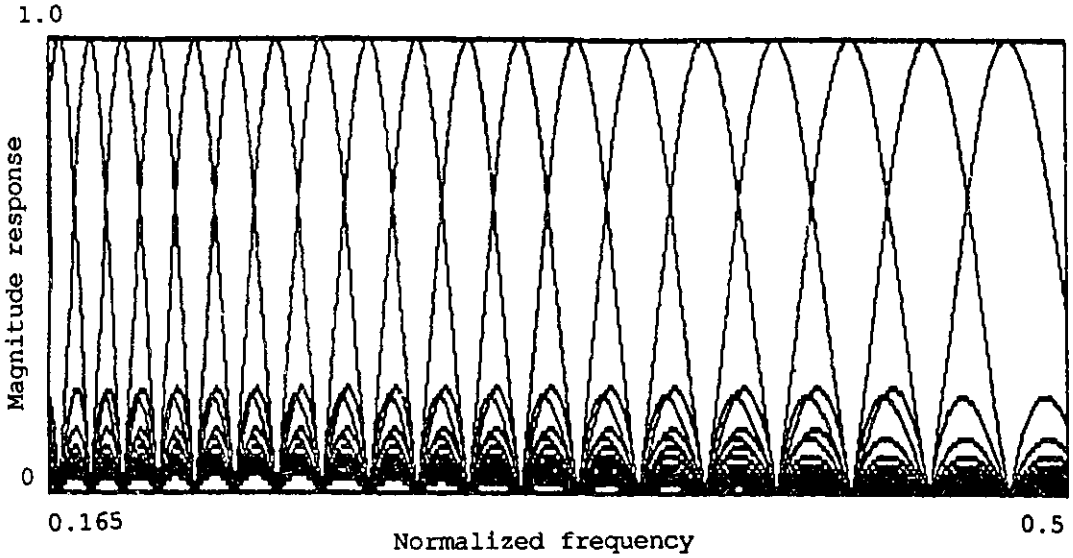

Figure 5.12 Frequency response of 60-filter twelfth-octave bank (analysis filter bank or synthesis filter bank).

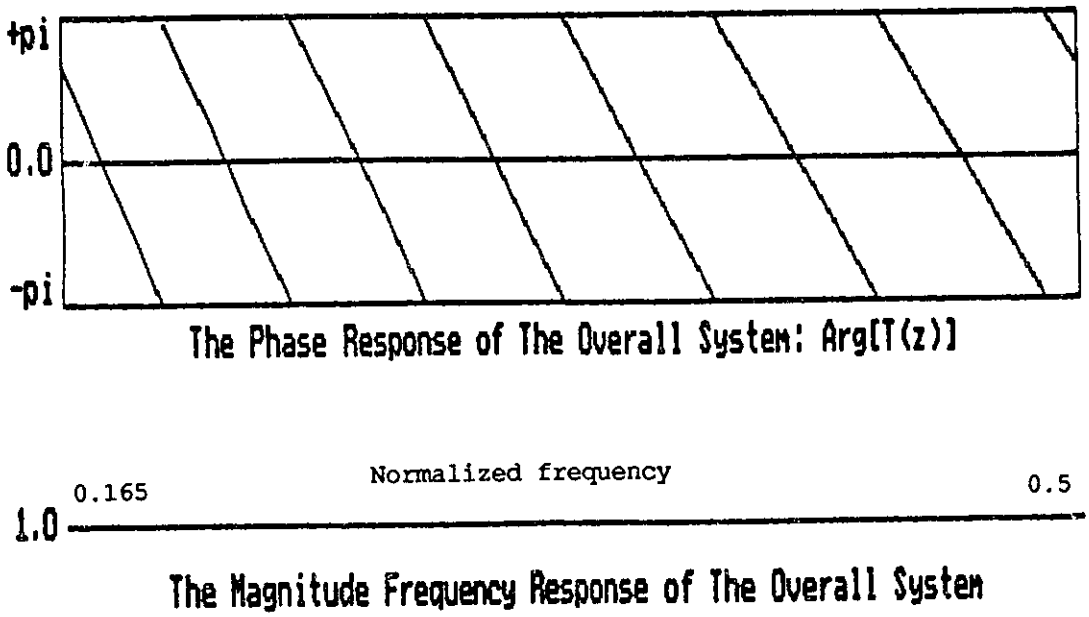

Figure 5.13 Phase and magnitude responses of twelfth-octave filter bank-based allpass system.

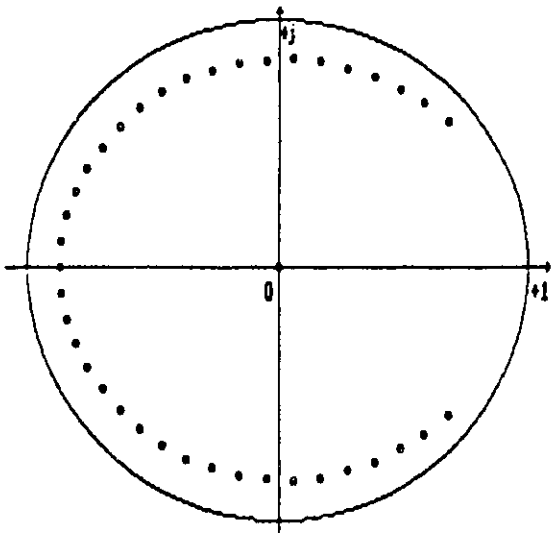

(a) 20-filter uniform band bank-based system;

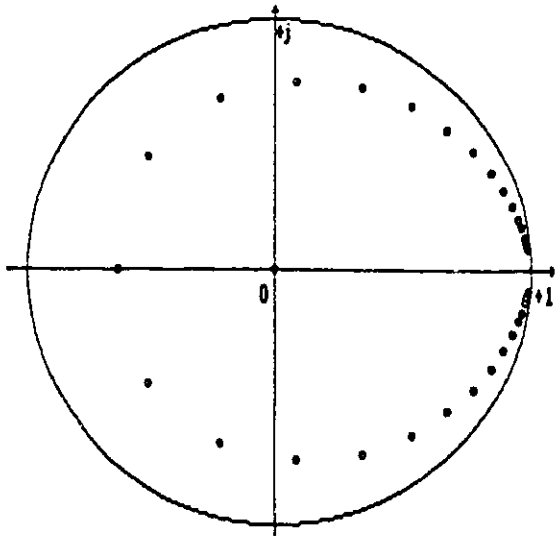

(b) 16-filter third-octave bank-based system;

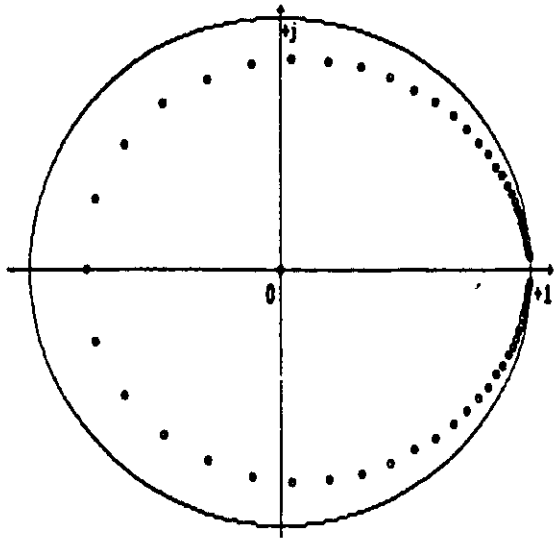

(c) 35-filter sixth-octave bank-based system;

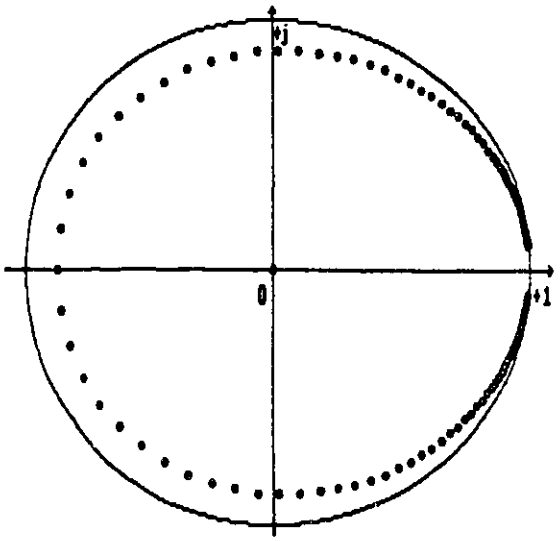

(d) 60-twelfth-octave bank-based system;

Figure 5.14 The plots of the zeros of N(z) for four different filter bank-based allpass systems.

Finally,because there is a zero for $D(z)$ at $z = 0$ (since $N(z)$ has a zero at $z = 0$), we have

$$[1 + \sum_{i=1}^{N} \frac{K_i \; z_i z^{-1}}{(1 - z_i z^{-1})}]|_{z=0} \; = \; 0, \tag{5.38}$$

thus

$$\sum_{i=1}^{N} K_i \; = \; 1, \tag{5.39}$$

i.e., the summation of all the filter coefficients is unity. Consequently, we may derive the relation

$$1 + \sum_{i=1}^{N} \frac{K_i \; z_i z^{-1}}{(1 - z_i z^{-1})} \; = \; \sum_{i=1}^{N} \frac{K_i}{(1 - z_i z^{-1})}. \tag{5.40}$$

This means

$$\frac{\sum_{i=1}^{N} \frac{K_i}{(1 - z_i z^{-1})}}{1 + \sum_{i=1}^{N} \frac{K_i \; z_i z^{-1}}{(1 - z_i z^{-1})}} \; = \; 1. \tag{5.41}$$

Thus we may see that the filter bank with its i^{th} transfer function as

$$\hat{H}_i(z) \; = \; \frac{\frac{K_i}{(1 - z_i z^{-1})}}{1 + \sum_{i=1}^{N} \frac{K_i \; z_i z^{-1}}{(1 - z_i z^{-1})}} \tag{5.42}$$

has the same magnitude frequency response as that with $H_i(z)$ and is an allpass filter bank. This will be useful in some DSP processing systems.

5.5 Calculation of Imaging Rejection

In previous sections we have succeeded in designing the analysis and synthesis filter banks to consist of an allpass system without changing sampling rate. In order to extend the application of this system to the subband coding area, it is necessary to insert in decimation and interpolation procedures between the analysis and synthesis filter banks. This will distort the allpass property of the system. This section will evaluate the aliasing and imaging distortion caused by downsampling and upsampling.

The block diagram of the analysis/synthesis system with decimation and interpolation is illustrated in figure 5.15, where R, an integer and smaller than or equal to N, is the downsampling or upsampling rate. In the i^{th} channel, the pure decimation and interpolation procedures are described in frequency domain as

$$X_i''(e^{j\omega}) = \frac{1}{R}\sum_{k=0}^{R-1} X_i'(e^{j(\omega-\frac{2\pi k}{R})}), \tag{5.43}$$

and then

$$\hat{X}_i(e^{j\omega}) = \frac{1}{R}G_i(e^{j\omega})\ \sum_{k=0}^{R-1} X(e^{j(\omega-\frac{2\pi k}{R})})\ H_i(e^{j(\omega-\frac{2\pi k}{R})}). \tag{5.44}$$

Equation (5.43) is derived in chapter VI (see (6.7)). Thus the system frequency response $T(e^{j\omega})$, which in fact is the system output $\hat{X}(e^{j\omega})$ with an impulse input, may be expressed as

$$\begin{aligned} T(e^{j\omega}) &= \frac{1}{R}\sum_{i=1}^{N} G_i(e^{j\omega})\ \sum_{k=0}^{R-1} H_i(e^{j(\omega-\frac{2\pi k}{R})}) \\ &= \frac{1}{R}\sum_{i=1}^{N} G_i(e^{j\omega})\ H_i(e^{j\omega}) \\ &+ \frac{1}{R}\sum_{i=1}^{N} G_i(e^{j\omega})\ \sum_{k=1}^{R-1} H_i(e^{j(\omega-\frac{2\pi k}{R})}) \\ &= A(e^{j\omega}) + B(e^{j\omega}). \end{aligned} \tag{5.45}$$

where

$$A(e^{j\omega}) = \frac{1}{R}\sum_{i=1}^{N} G_i(e^{j\omega})\ H_i(e^{j\omega}) \tag{5.46}$$

is the ideal response of the allpass system, and

$$B(e^{j\omega}) = \frac{1}{R}\sum_{i=1}^{N} G_i(e^{j\omega})\ \sum_{k=1}^{R-1} H_i(e^{j(\omega-\frac{2\pi k}{R})}) \tag{5.47}$$

presents the aliasing and imaging distortions coursed by decimation and interpolation. Usually $B(e^{j\omega})$ is called "imaging rejection".

In Figure 5.16 the magnitude imaging rejections with sampling rate change as 2, 3, 4, and N(=16) for the third-octave filter bank in example 2 of section 5.3, are drawn. We can see that the peak values of the distortions increase as the decimation rate R increases. The smallest one for $R = 2$ is about 0.05244 or 25.6dB, and when $R = N$, the system suffers the maximum of distortion as 0.10897 or 19.3dB. In comparison with the sidelobes of the filters in the banks, these are small enough. However, for applications of the systems, they still need to be reduced. This may be possible if the allpass system is designed under the consideration of the circular windowing procedures between the two filter banks and the decimation/interpolation step.

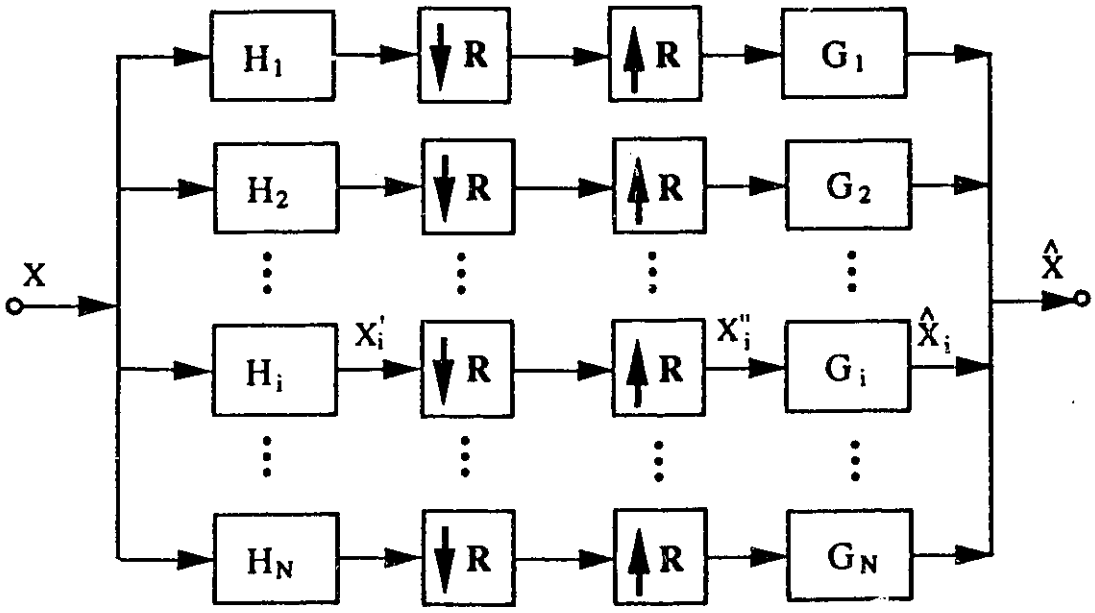

Figure 5.15 The block diagram of analysis/synthesis system with decimation and interpolation procedures.

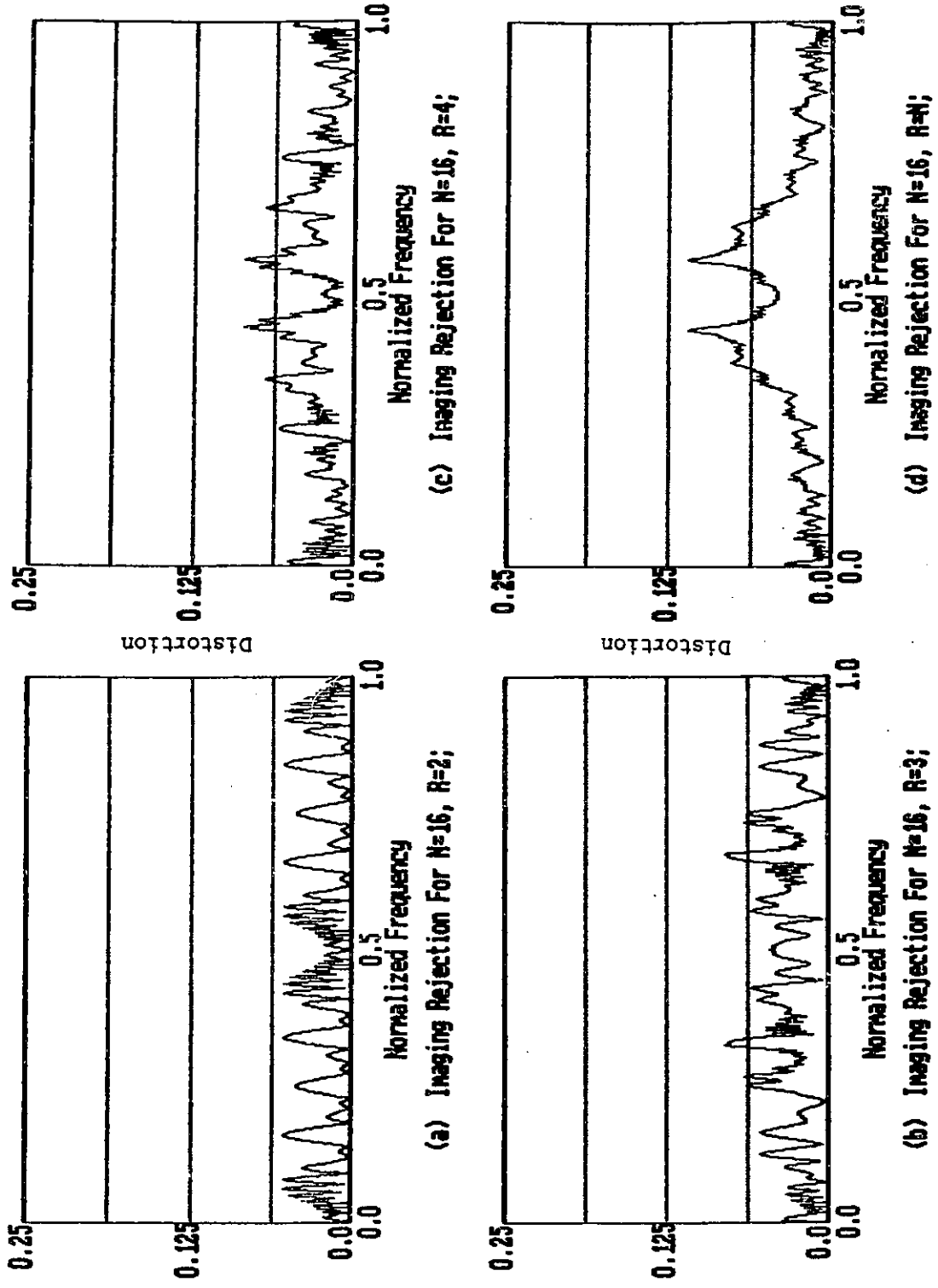

Figure 5.16 The imaging rejections of the third-octave filter bank-based allpass system.

5.6 Summary

In this chapter, we propose the techniques for the design of the FIFB filter bank-based analysis/synthesis system. The perfect reconstruction systems are achieved by the design procedure, which depends on the overall structure built by a general FIFB analysis filter bank and a special synthesis filter bank. By evaluating and calculating the imaging rejection, we find that when the decimation and interpolation procedures are performed after the analysis filter bank, the allpass system will suffer significant distortion because of high sidelobes in the filter frequency responses of the filter banks. However the windowing techniques may be applied to improve the system quality. Meanwhile these filter banks form a useful basis for the windowing processing for the better quality filter banks, and the useful single allpass filter bank results from the derivations.

VI PERFECT RECONSTRUCTION ANALYSIS/SYNTHESIS SYSTEMS BASED ON THE FIFB FILTER BANKS

6.1 Introduction

Analysis/synthesis systems are the systems that divide an input signal into frequency bands in an analysis stage, and later create an output signal by merging the bands in a synthesis stage. Systems of this type have been studied and used in many application areas, including time-scale modification, speech enhancement, speech coding, and imaging processing. Analysis/synthesis systems are of particular interest in the speech coding area because the properties of aural perception are most appropriately exploited in the frequency domain. In speech coding applications, the primary objective is to reduce the bit rate while maintaining the perceived quality of the coding system. Since in frequency domain coders, the bit rate is directly related to the number of frequency domain samples per unit time, it is important to represent the output of each channel with the minimum number of samples. Thus, the N subband signals after the analysis filter bank (N analysis filters) are, first downsampled (or subsampled) by a factor R, and then the decoded signals at receiver are upsampled by the same factor before going the synthesis filters. The whole system structure is shown in Fig.6.1. This kind of filter bank-based systems is usually refered to as multirate filter bank systems.

In the last chapter, the design of FIFB filter banks for allpass analysis/synthesis systems were studied without involving the sampling rate changing by decimation and interpolation. The results show that the exact reconstruction of the magnitude frequency response are obtained by the analysis and synthesis filter banks which have the similar structures and magnitude responses. However these allpass analysis/synthesis systems are largely limited in their applications due to the high sampling rate in all channels. In this

chapter, we will put the effort into trying to extend the FIFB filter bank techniques to the multirate FIFB filter bank analysis/synthesis systems. In other words, the systems with the structure in Fig.6.1 where the filter banks are the FIFB filter banks, are explored.

We start out the discussion in section 6.2 with some introductions to the basic notions and operations about multirate filter bank systems. Section 6.3 briefly reviews the matrix theory of multirate filter banks or analysis/synthesis systems developed by Smith and Barnwell[110] and Vetterli[78] at the same time. This matrix theory gives out the general direction for finding the synthesis filter bank which corresponds to the analysis filter bank and makes the whole system able to be an aliasing-free or perfect reconstruction system. Section 6.4 derives in theory the synthesis filter banks based on the FIFB analysis filter banks, where the matrix formulations are applied to produce more general forms of the synthesis filter banks. The interesting results are achieved and the final synthesis filter banks are FIR filter banks with zeros closely related to the poles and zeros of the analysis filter banks. Section 6.5 simulates the synthesis filter banks. The examples with uniformly and logarithmically spaced channels and the computation results are discussed. Finally section 6.6 summarizes the work described in this chapter. Note that in this chapter the investigation of the multirate FIFB filter bank systems are based on the structure in the speech subband coding application.

6.2 The Basic Notions and Operations of the Multirate Filter Banks

The two fundamental operations in multirate filter bank systems are downsampling and upsampling, which are realized by the decimator and the interpolator shown in Fig.6.2 (a) and (b). We will only consider integer sampling rate changes in following, since rational ones can be obtained by cascading integer ones[28]. A R-fold decimator takes an input sequence $x(n)$ and retains only samples that occur at times which are multiples of R. The

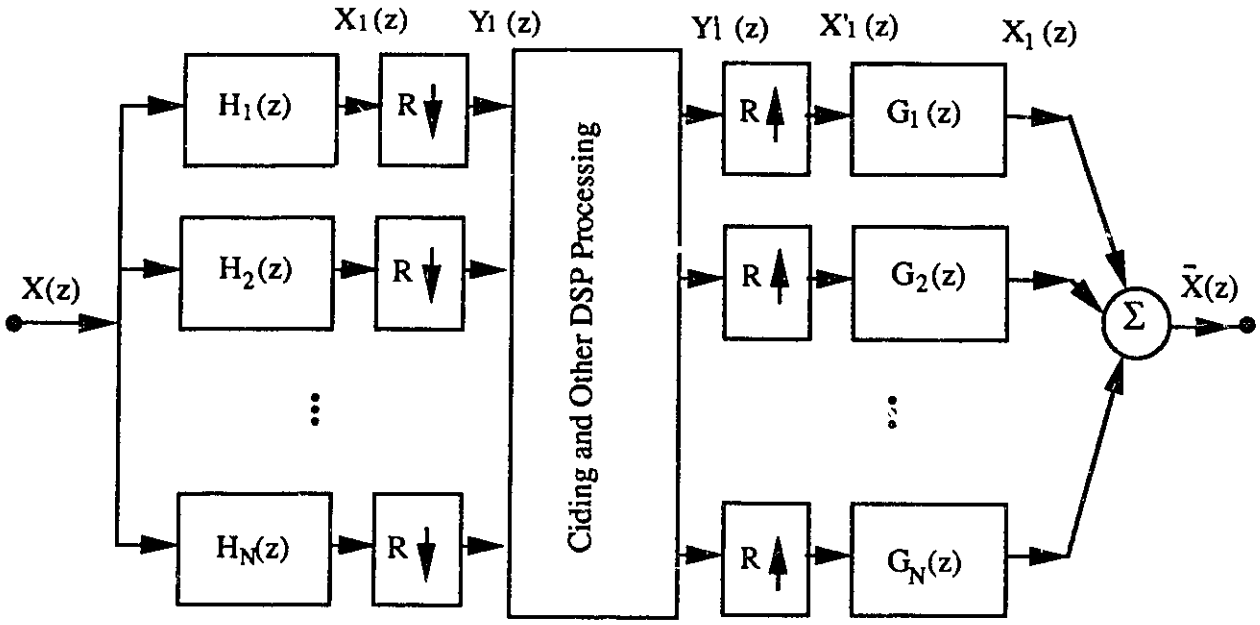

Figure 6.1 The structure of the analysis/synthesis filter bank-based system.

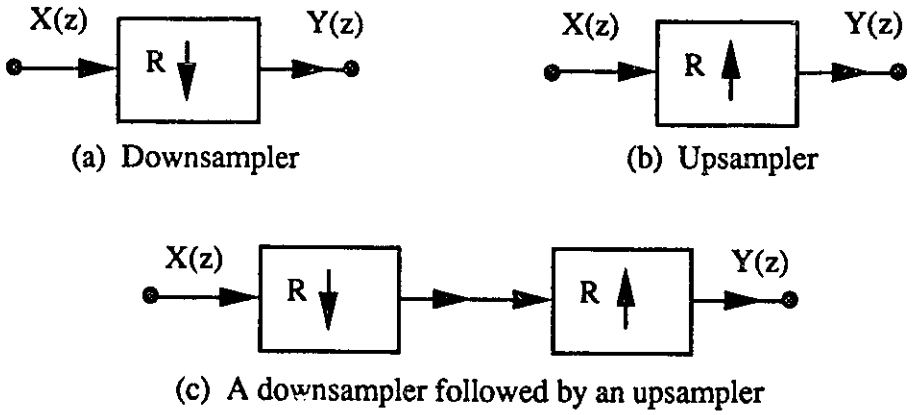

Figure 6.2 The basic operations in multirate filter banks.

input-output relation is therefore

$$y(n) = x(Rn). \tag{6.1}$$

As shown in [27,33], the z transform relation is

$$Y(z) = \frac{1}{R}\sum_{k=0}^{R-1} X(W^k z^{\frac{1}{R}}) \tag{6.2}$$

where $W = e^{\frac{-j2\pi}{R}}$. For frequency spectral interpretations, (6.2) may become with $z = e^{j\omega}$ as

$$Y(e^{j\omega}) = \frac{1}{R}\sum_{k=0}^{R-1} X(e^{\frac{j(\omega-2\pi k)}{R}}) \tag{6.3}$$

which shows that $Y(e^{j\omega})$ is a sum of R uniformly shifted versions of an R-fold stretched version of $X(e^{j\omega})$. Fig.6.3(b) depicts this idea for $R = 2$. The original signal frequency spectrum is plotted in Fig.6.3(a).

If the sampling rate is increased by an integer factor R as shown in Fig.6.2(b), the input signal of the interpolator $x(n)$ is filled in with $R-1$ zero-valued samples between each sample of $x(n)$, giving the signal

$$y(n) = \begin{cases} x(\frac{n}{R}), & \text{if n=multiple of R;} \\ 0, & \text{otherwise.} \end{cases} \tag{6.4}$$

In the transform domain this is equivalent to

$$\begin{aligned} Y(z) &= X(z^R) \\ Y(e^{j\omega}) &= X(e^{j\omega R}). \end{aligned} \tag{6.5}$$

As illustrated by the spectral interpretation in Fig.6.3(c), $Y(e^{j\omega})$ is merely a compressed version of $X(e^{j\omega})$ but with the period $\frac{2\pi}{R}$.

If a decimator is followed by an interpolator as in Fig.6.2(c), the input-output relationship as well as the transformed forms are

$$y(n) = \begin{cases} x(n), & \text{n=multiple of R;} \\ 0, & \text{otherwise.} \end{cases} \tag{6.6}$$

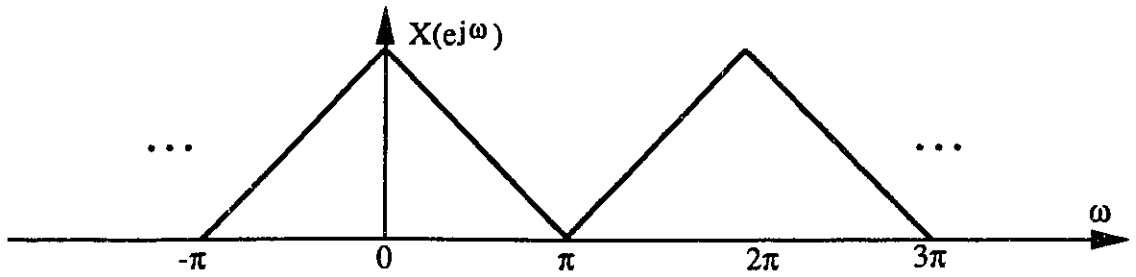

(a) The original frequency spectrum

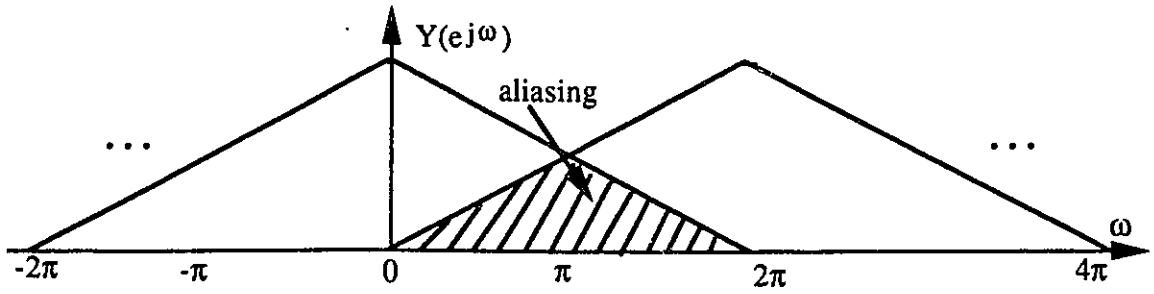

(b) Effect of downsampler by 2

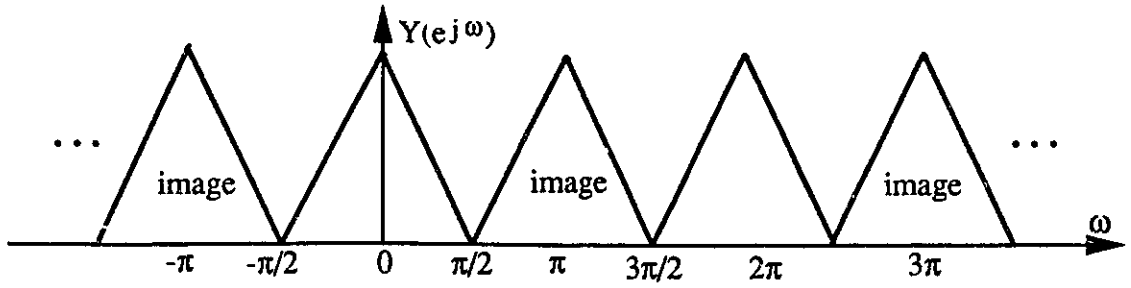

(c) Effect of upsampler by 2

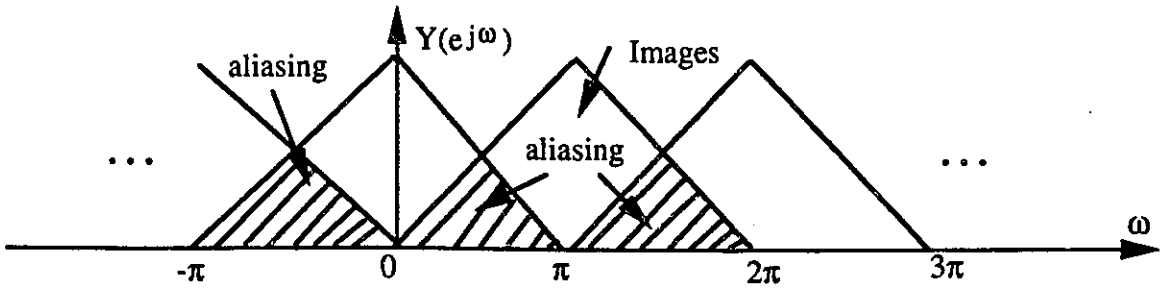

(d) Effect of downsampler followed by upsampler

Figure 6.3 Frequency-domain illustration of the sampling rate change, where $X(e^{j\omega})$ is the spectrum of the input singal x(n) for all the three cases: (b) a decimator(R=2); (c) an interpolator(R=2); (d) a decimator(R=2) followed by an interpolator(R=2). Note that ω is the radian frequency.

and

$$Y(z) = \frac{1}{R}\sum_{k=0}^{R-1} X(W^k z)$$
$$Y(e^{j\omega}) = \frac{1}{R}\sum_{k=0}^{R-1} X(e^{j(\omega-\frac{2\pi k}{R})}). \tag{6.7}$$

And the overall effect is as illustrated in Fig.6.3(d), where we can see that there are multiple copies of the input spectrum $X(e^{j\omega})$, and successive copies can possibly overlap to produce the aliasing distortions.

If filtering is placed between the decimator and the interpolator as shown in Fig.6.2(d), the time domain input-output relation will be

$$y(n) = \begin{cases} \sum_{k=-\infty}^{\infty} x(k)h(\frac{n}{R}-k), & \text{n=multiple of R;} \\ 0, & \text{otherwise.} \end{cases} \tag{6.8}$$

which is not easy to interpret, but the transformed forms(see below equation (6.9)) are obvious that the filter appears simply as a multiplicative factor with R^{th} power of z.

$$Y(z) = \frac{1}{R}H(z^R)\sum_{k=0}^{R-1} X(W^k z)$$
$$Y(e^{j\omega}) = \frac{1}{R}H(e^{j\omega R})\sum_{k=0}^{R-1} X(e^{j(\omega-\frac{2\pi k}{R})}). \tag{6.9}$$

In all practical systems based on multirate filter bank analysis/synthesis techniques, there are two types of distortion[110]. One type of distortion is processing distortion which is introduced by processing performed on the analysis filter outputs and caused by the finite-word-length effects. Processing distortion is usually related to such characteristics as the number and center frequencies of the filter bank channels, the quality of the frequency resolution, the system processing delay, and the system complexity. The second type of distortion is intrinsic distortion, including all those distortions which would be

present in the absence of any processing of the analysis output and any finite-wordlength-effects. The intrinsic distortions may be divided three different types of distortion[110]: interband aliasing distortion; short-time frequency (magnitude) distortion; and short-time phase distortion. In speech coding, interband aliasing is relatively easy to perceive, while moderate amounts of phase distortion and small amounts of magnitude distortion may be virtually imperceivable. The interband aliasing distortions are produced by the decimators and the interpolator, however the proper design of the analysis and synthesis filter banks may help to reduce the distortions, to cancel the aliasing distortions, and even completely to cancel all intrinsic distortions. This is the topic of this chapter but based on the FIFB filter bank techniques.

There are numerous methods [61,26,24,69,62], which have been proposed to attempt to design the analysis/synthesis systems to represent the input signal by a finite number of minimally-sampled frequency channels and minimize the distortion between the input and the output signals. Studying all different design methods and techniques, Smith and Barnwell[110] and Vetterli[78], almost at the same time, have derived similar unifying matrix theories for the design and analysis of multirate filter bank systems. In the next section the general matrix framework will be reviewed briefly.

6.3 The Matrix Formulation of Multirate Filter Bank Systems

The matrix theories founded by Smith and Barnwell and Vertteli individually are basically the same. However, Vertteli developed a more general matrix formulation for the application to speech coding as well as transmultiplexing with the inclusion of the polyphase and modulation representation of periodically time-varying linear systems (note that downsampling units are linear time-varying elements). Smith and Barnwell mainly focus on the application of speech coding, and simply introduced the matrix concepts and

then derived a general theory The core of the matrix theory is a matrix in transform domain, which expresses the input signal and frequency shifted versions of the input signal after the analysis filter bank. Smith and Barnwell call this matrix as aliasing component matrix or AC-matrix, while Vertteli calls his matrix, a transition form of AC-matrix, modulated filter matrix, since all the elements except for first line are the modulated version of the analysis filters. In following parts of this section, we introduce the AC-matrix and the matrix formulations with using Smith and Barnwell's notions and notations. This is a preparation for the development of FIFB perfect reconstruction analysis/synthesis systems in the rest of this chapter.

For the general multirate filter bank system shown in Fig.6.1, if the coding and transmission are ideal, the output $\hat{X}(z)$ may be expressed as

$$\hat{X}(z) = \frac{1}{R} \sum_{r=0}^{R-1} \sum_{k=1}^{N} H_k(W^r z)\, X(W^r z)\, G_k(z) \tag{6.10}$$

where $W = e^{\frac{-j2\pi}{R}}$. If an input vector $\mathbf{x}$, and a synthesis filter vector $\mathbf{g}$ are defined as

$$\mathbf{x} = [\, X(z),\ X(Wz),\ X(W^2 z),\ \ldots, X(W^{R-1} z)\,]^T \tag{6.11}$$

and

$$\mathbf{g} = [\, G_1(z),\ G_2(z),\ G_3(z),\ \ldots, G_N(z)\,]^T, \tag{6.12}$$

then the system equation (6.10) may be written as a matrix form

$$\hat{X}(z) = \frac{1}{R}\, \mathbf{g}^T\, \mathbf{M}^T\, \mathbf{x}. \tag{6.13}$$

The matrix $\mathbf{M}$ is the R-by-N AC-matrix defined as

$$\mathbf{M} = \begin{pmatrix} H_1(z) & H_2(z) & \cdots & H_N(z) \\ H_1(Wz) & H_2(Wz) & \cdots & H_N(Wz) \\ \vdots & \vdots & \ddots & \vdots \\ H_1(W^{R-1}z) & H_2(W^{R-1}z) & \cdots & H_N(W^{R-1}z) \end{pmatrix} \tag{6.14}$$

The basic question to be explored is: Given an analysis filter bank, how should one choose the synthesis filter bank $\mathbf{g}$ to result in a system that meets the requirements for system performance. Since aliasing degrades performance, it is desirable to explicitly remove its presence from the output. The first row of AC-matrix represents the transfer functions of the analysis filters, while the elements in the other rows correspond to the aliasing terms in the reconstruction equation (6.13). Thus, it is easy to see the system properties if equation (6.13) is rewritten as

$$\hat{X}(z) \;=\; \frac{1}{R}\,\mathbf{b}^T\,\mathbf{x} \tag{6.15}$$

of course, with the vector $\mathbf{b}$ as

$$\mathbf{b} \;=\; \mathbf{M}\,\mathbf{g} \;=[\mathbf{b_1},\ \mathbf{b_2}]^T, \tag{6.16}$$

where $\mathbf{b_1}$ and $\mathbf{b_2}$ are 1 by 1 and $(R-1)$ by 1 vectors, respectively. The vector $\mathbf{b}$ is called distortion vector since all the elements of $\mathbf{b_2}$ express the aliasing components of the system. Note that if without any DSP processing between the decimation and interpolation, the effect of $\mathbf{b_2}$ on the system is just the imaging rejection which is expressed by $B(e^{j\omega})$ in the last chapter (see (5.47)). Now the fundamental properties of the analysis reconstruction system may be easily stated using above relation (6.15).

i) Aliasing-free output is achieved if

$$\mathbf{b} \;=\; [\ R\,F(z),\ 0,\ 0,\ \ldots\ ,0\ ]^T \tag{6.17}$$

where $F(z)$ is an arbitrary transmission filter of the whole system.

ii) Perfect reconstruction is obtained if

$$\mathbf{b} \;=\; [\ R\,z^{-k},\ 0,\ 0,\ \ldots\ ,0\ ]^T \tag{6.18}$$

where z^{-k} is an arbitrary delay of the whole system with integer k.

From the point view of number of the equations R (or the rate ratio) and the number of unknowns N (or the number of filters in the analysis bank), there are two different classes of realizable systems. Firstly, when R is less then N, the system generates more frequency domain samples than time domain samples and therefore is inefficient in terms of its representation. However we have more freedom to find the desirable synthesis filters from the known analysis filters. Secondly, when R is equal to N, the system is called a maximally decimated system since the number of the samples in the frequency-domain is exactly equal to the number of samples in the time-domain input. This type of system is efficient, and therefore attractive. In this case, the AC-matrix is square and thus, when given the analysis filters, the synthesis filter bank is solely determined by following equation:

$$\mathbf{g} = \mathbf{M}^{-1}\,\mathbf{b}. \tag{6.19}$$

Since the bottom $(N-1)$ elements of $\mathbf{b}$ are zero for both aliasing-free and perfect reconstruction cases, the synthesis filter bank solutions for aliasing-free or perfect reconstruction, are easily obtained by first, multiplying the first column of the adjoint matrix of $\mathbf{M}$ and the gain N by the $F(z)$ or z^{-k}, and then dividing the product by the determinant of $\mathbf{M}$†. However, we must remember the stability of the synthesis filter bank is not guaranteed by the general procedure above, since the determinant of $\mathbf{M}$ may introduce poles outside the unit circle. For the FIFB analysis filter banks given, the question whether or not there exist a corresponding stable synthesis filter bank for aliasing-free or perfect reconstruction, will be studied in the next two sections.

6.4 Derivation of Perfect Reconstruction FIFB Multirate Filter Banks

† For the case in which N is greater than R, and thus the matrix $\mathbf{M}$ is not a square matrix, the singular-value decomposition technique may be applied to obtain its generalized inverse matrix $\mathbf{M}^{\#}$.

For a general FIFB analysis filter bank, the i^{th} filter has the transfer function:

$$H_i(z) = \frac{\frac{K_i z_i z^{-1}}{1-z^{-1}z_i}}{1 + \sum_{j=1}^{N} \frac{K_j z_j z^{-1}}{1-z^{-1}z_j}} = \frac{N_i(z)}{D(z)}, \tag{6.20}$$

where $z_i = e^{j\omega_i} = e^{j2\pi f_i}$, and f_i is the center frequency of i^{th} filter in the bank.

The AC-matrix $\mathbf{M}$ here for the minimized sampling rate case, i.e., $N = R$, is

$$\mathbf{M} = \begin{pmatrix} \frac{\frac{K_1 z_1 z^{-1}}{1-z^{-1}z_1}}{D(z)} & \frac{\frac{K_2 z_2 z^{-1}}{1-z^{-1}z_2}}{D(z)} & \cdots & \frac{\frac{K_N z_N z^{-1}}{1-z^{-1}z_N}}{D(z)} \\ \frac{\frac{K_1 z_1 z^{-1} W^{-1}}{1-z^{-1}z_1 W^{-1}}}{D(zW)} & \frac{\frac{K_2 z_2 z^{-1} W^{-1}}{1-z^{-1}z_2 W^{-1}}}{D(zW)} & \cdots & \frac{\frac{K_N z_N z^{-1} W^{-1}}{1-z^{-1}z_N W^{-1}}}{D(zW)} \\ \vdots & \vdots & \ddots & \vdots \\ \frac{\frac{K_1 z_1 z^{-1} W^{-N+1}}{1-z^{-1}z_1 W^{-N+1}}}{D(zW^{N-1})} & \frac{\frac{K_2 z_2 z^{-1} W^{-N+1}}{1-z^{-1}z_2 W^{-N+1}}}{D(zW^{N-1})} & \cdots & \frac{\frac{K_N z_N z^{-1} W^{-N+1}}{1-z^{-1}z_N W^{-N+1}}}{D(zW^{N-1})} \end{pmatrix} \tag{6.21}$$

The key procedure to obtain the desired synthesis filter bank $\mathbf{g}$ is to find the inverse of the AC-matrix. It is because of the frequency interpolation structure of FIFB filter bank that the AC-matrix $\mathbf{M}$ in (6.21) displays many regularities. The AC-matrix thus may easily factored into the product of three matrices as

$$\mathbf{M} = \mathbf{D}(z)\ \mathbf{C}(z)\ \mathbf{K} \tag{6.22}$$

with

$$\mathbf{D}(z) = \begin{pmatrix} \frac{z^{-1}}{D(z)} & 0 & \cdots & 0 \\ 0 & \frac{z^{-1}W^{-1}}{D(zW)} & \cdots & 0 \\ \vdots & \vdots & \ddots & \vdots \\ 0 & 0 & \cdots & \frac{z^{-1}W^{-N+1}}{D(zW^{N-1})} \end{pmatrix} \tag{6.22a}$$

$$\mathbf{C}(z) = \begin{pmatrix} \frac{1}{1-z^{-1}z_1} & \frac{1}{1-z^{-1}z_2} & \cdots & \frac{1}{1-z^{-1}z_N} \\ \frac{1}{1-z^{-1}z_1 W^{-1}} & \frac{1}{1-z^{-1}z_2 W^{-1}} & \cdots & \frac{1}{1-z^{-1}z_N W^{-1}} \\ \vdots & \vdots & \ddots & \vdots \\ \frac{1}{1-z^{-1}z_1 W^{-N+1}} & \frac{1}{1-z^{-1}z_2 W^{-N+1}} & \cdots & \frac{1}{1-z^{-1}z_N W^{-N+1}} \end{pmatrix} \tag{6.22b}$$

and

$$\mathbf{K} = \begin{pmatrix} K_1 z_1 & 0 & \cdots & 0 \\ 0 & K_2 z_2 & \cdots & 0 \\ \vdots & \vdots & \ddots & \vdots \\ 0 & 0 & \cdots & K_N z_N \end{pmatrix} \tag{6.22c}$$

We can see that the matrices $\mathbf{D}(z)$ and $\mathbf{K}$ are diagonal matrices whose inverses are immediate. For the inverse of $\mathbf{M}$ matrix, we have the relation

$$\mathbf{M}^{-1} = \mathbf{K}^{-1}\,\mathbf{C}^{-1}(z)\,\mathbf{D}^{-1}(z) \tag{6.23}$$

and thus, whether or not the inverse of the AC-matrix exists is equivalent to whether or not the inverse of the $\mathbf{C}(z)$ exists.

Examining the $\mathbf{C}(z)$ matrix, we may find that: **1**) The elements in first row are the first order IIR filters with the poles z_i, the same as corresponding zeros in the analysis filter bank; **2**) The element in all other rows are frequency-shifted version of the filters in the same column of the first row, shifted by normalized frequency $\frac{(i-1)}{N}$ (i means i^{th} row); **3**) All the elements have the similar form of $\frac{1}{(1-a)}$ with a general complex $a = z_j W^{-(i-1)} z^{-1}$.

Since the sum of first N terms of the complex series a^r (for r=1, 2, ...) with $a \neq 1$ is

$$\sum_{r=0}^{N-1} a^r = \frac{1-a^N}{1-a} \tag{6.24}$$

we have the relation

$$\frac{1}{1-a} = \frac{\sum_{r=0}^{N-1} a^r}{1-a^N}. \tag{6.25}$$

Considering the complex $a = z_j W^{-(i-1)} z^{-1}$ in equation (6.25) and applying $W^{N(i-1)} = 1$, we have

$$\frac{1}{1 - z_j W^{-(i-1)} z^{-1}} = \frac{1 + (z_j W^{-(i-1)} z^{-1}) + (z_j W^{-(i-1)} z^{-1})^2 + \ \ldots\ + (z_j W^{-(i-1)} z^{-1})^{N-1}}{1 - z_j^N z^{-N}} \tag{6.26}$$

Thus, the matrix $\mathbf{C}(z)$ in (6.22) may be divided into the product of four new N-by-N submatrices as

$$\mathbf{C}(z) = \mathbf{W}^*\ \mathbf{C}_z(z)\ \mathbf{C}_v\ \mathbf{C}_d(z) \tag{6.27}$$

where $*$ means complex conjugation and the four submatrices are

$$\mathbf{W} = \begin{pmatrix} 1 & 1 & 1 & \dots & 1 \\ 1 & W^{-1} & W^{-2} & \dots & W^{1-N} \\ 1 & W^{-2} & W^{-4} & \dots & W^{2(1-N)} \\ \vdots & \vdots & \vdots & \ddots & \vdots \\ 1 & W^{1-N} & W^{2(1-N)} & \dots & W^{-(N-1)^2} \end{pmatrix}, \tag{6.28}$$

$$\mathbf{C_z}(z) = \begin{pmatrix} 1 & 0 & \dots & 0 \\ 0 & z^{-1} & \dots & 0 \\ \vdots & \vdots & \ddots & \vdots \\ 0 & 0 & \dots & z^{1-N} \end{pmatrix}, \tag{6.29}$$

$$\mathbf{C_v} = \begin{pmatrix} z_1^0 & z_2^0 & \dots & z_N^0 \\ z_1^1 & z_2^1 & \dots & z_N^1 \\ \vdots & \vdots & \ddots & \vdots \\ z_1^{N-1} & z_2^{N-1} & \dots & z_N^{N-1} \end{pmatrix} = \begin{pmatrix} Z_{11} & Z_{12} & \dots & Z_{1N} \\ Z_{21} & Z_{22} & \dots & Z_{2N} \\ \vdots & \vdots & \ddots & \vdots \\ Z_{N1} & Z_{N2} & \dots & Z_{NN} \end{pmatrix}, \tag{6.30}$$

and

$$\mathbf{C_d}(z) = \begin{pmatrix} \frac{1}{1-z^{-N}z_1^N} & 0 & \dots & 0 \\ 0 & \frac{1}{1-z^{-N}z_2^N} & \dots & 0 \\ \vdots & \vdots & \ddots & \vdots \\ 0 & 0 & \dots & \frac{1}{1-z^{-N}z_N^N} \end{pmatrix}, \tag{6.31}$$

respectively. The matrices $\mathbf{C_z}(z)$ and $\mathbf{C_d}(z)$ are simple diagonal matrices and so their inverses are easy to find. The matrix $\mathbf{W}$ is the DFT matrix. The matrix $\mathbf{C_v}$ consists of different powers of the zeros of the analysis filter bank, in fact, a very famous matrix, a *Vandermonde* matrix. The inverse of the matrix $\mathbf{W}^*$ is the complex conjugate of the inverse of the DFT matrix. Thus

$$\begin{aligned} \mathbf{W}^{*-1} = \mathbf{W}^{-1*} &= \frac{1}{N} \begin{pmatrix} 1 & 1 & 1 & \dots & 1 \\ 1 & W^{+1} & W^{+2} & \dots & W^{N-1} \\ 1 & W^{+2} & W^{+4} & \dots & W^{2(N-1)} \\ \vdots & \vdots & \vdots & \ddots & \vdots \\ 1 & W^{N-1} & W^{2(N-1)} & \dots & W^{(N-1)^2} \end{pmatrix} \\ &= \frac{1}{N}\mathbf{W}. \end{aligned} \tag{6.32}$$

Based on the knowledge about the *Vandermonde* matrix[109], if the z_i are not the same for $i = 1, 2, ..., N$ (this is true for our analysis filter bank), the inverse of the $\mathbf{C_v}$ exists

and is

$$\mathbf{C_v}^{-1} = \frac{1}{|\mathbf{C_v}|} \begin{pmatrix} \overline{Z}_{11} & \overline{Z}_{21} & \dots & \overline{Z}_{N1} \\ \overline{Z}_{12} & \overline{Z}_{22} & \dots & \overline{Z}_{N2} \\ \vdots & \vdots & \ddots & \vdots \\ \overline{Z}_{1N} & \overline{Z}_{2N} & \dots & \overline{Z}_{NN} \end{pmatrix} \tag{6.33}$$

where $\overline{Z}_{ji}$ is the cofactor of the element Z_{ij} of the matrix $\mathbf{C_v}$, $|\mathbf{C_v}|$ is the determinant of the $\mathbf{C_v}$, and

$$|\mathbf{C_v}| = \prod_{1 \le j < i \le N} (z_i - z_j) \tag{6.34}$$

for all pair of number (i, j) $(1 \le j < i \le N)$.

Now examine the inverse of the matrix $\mathbf{M}(z)$. Substituting equation (6.27) in (6.23) and considering the submatrices (6.28-6.31), the inverse of $\mathbf{M}(z)$ may be written as

$$\mathbf{M}^{-1} = \mathbf{K}^{-1} \ \mathbf{C_d}^{-1}(z) \ \mathbf{C_v}^{-1} \ \mathbf{C_z}^{-1}(z) \ \mathbf{W}^{*-1} \ \mathbf{D}^{-1}(z) \tag{6.35}$$

Focusing on equation (6.19) and applying $\mathbf{b}$ as equation (6.18) for perfect reconstruction with $R = N$ in the case, some manipulation will lead to

$$\begin{pmatrix} G_1(z) \\ G_2(z) \\ \vdots \\ G_N(z) \end{pmatrix} = \begin{pmatrix} \frac{z^{-k+1}(1-z_1^N z^{-N})\ D(z)}{g_1\ K_1 z_1} \prod_{i=2}^{N}(z - z_i) \\ \frac{z^{-k+1}(1-z_2^N z^{-N})\ D(z)}{g_2\ K_2 z_2} \prod_{i=1, i\neq 2}^{N}(z - z_i) \\ \vdots \\ \frac{z^{-k+1}(1-z_N^N z^{-N})\ D(z)}{g_N\ K_N z_N} \prod_{i=1}^{N-1}(z - z_i) \end{pmatrix} \tag{6.36}$$

where the coefficients g_i's are

$$g_j = \prod_{i=1, i\neq j}^{N} (z_j - z_i), \qquad for\ j = 1, 2, ..., N \tag{6.37}$$

$D(z)$ is the denominator of the filter transfer function of FIFB banks (see equation (6.20)), z_j's are the zeros of the analysis filter bank, and K_j's are the analysis filter coefficients. Equation (6.36) is the final synthesis filter bank for the perfect reconstruction. Changing the factor z^{-k} into $F(z)$ in all the elements of the right side of (6.36) will give the synthesis filter bank for aliasing-free analysis reconstruction system.

In (6.36), if the number k of the delay samples is N and after more manipulations, the j^{th} synthesis filter is changed as

$$\begin{aligned} G_j(z) &= \frac{1}{g_j K_j z_j}(1 - z_j^N z^{-N})\ D(z) \prod_{i=1, i\neq j}^{N} (1 - z_i z^{-1}) \\ &= \left(\frac{1}{g_j K_j z_j}\frac{(1 - z_j^N z^{-N})}{(1 - z_j z^{-1})}\right) \left[\left(\prod_{i=1}^{N}(1 - z_i z^{-1})\right)\left(1 + \sum_{r=1}^{N}\frac{K_r z_r z^{-1}}{1 - z_r z^{-1}}\right)\right] \\ &= Q_j(z)\ P_N(z) \end{aligned} \tag{6.38}$$

where the first factor

$$\begin{aligned} Q_j(z) &= \frac{1}{g_j K_j z_j}\frac{(1 - z_j^N z^{-N})}{(1 - z_j z^{-1})} \\ &= \frac{1}{g_j K_j z_j}(1 + z_j z^{-1} + z_j^2 z^{-2} + \ \ldots\ + z_j^{N-1} z^{-(N-1)}) \end{aligned} \tag{6.39}$$

which is a $(N-1)^{th}$ order polynomial of z^{-1} and consequently is a FIR filter with $(N-1)$ zeros on the unit circle. The second factor in (6.38) is

$$\begin{aligned} P_N(z) &= \left(\prod_{i=1}^{N}(1 - z_i z^{-1})\right)\left(1 + \sum_{r=1}^{N}\frac{K_r z_r z^{-1}}{1 - z_r z^{-1}}\right) \\ &= \prod_{i=1}^{N}(1 - z_i z^{-1}) + K_1 z_1 \prod_{i=2}^{N}(1 - z_i z^{-1}) + \ldots + K_N z_N \prod_{i=1}^{N-1}(1 - z_i z^{-1}) \\ &= z^{-N}\prod_{i=1}^{N}(z - P_i) \end{aligned} \tag{6.40}$$

where the P_i for $i = 1, 2, ..., N$ are all the poles of the analysis filter bank, since $P_N(z)$ is just the numerator of the denominator of the filter transfer function in the analysis filter bank. $P_N(z)$ is obviously a FIR filter too, and is a common factor for all the channels in the synthesis bank. This makes sense for reducing the computation when implemented. From the filtering structure point of view, $P_N(z)$ may be thought as a post-filter following a pre-synthesis bank with filters $Q_j(z)$ for $j = 1, 2, \ \ldots\ , N$, and the realization structure is shown in Fig.6.4.

In conclusion to this section, perfect reconstruction FIFB analysis/synthesis systems are derived according to AC-matrix theory. The theory shows that for given any FIFB analysis filter bank (uniformly or logarithmically spaced), there exist a corresponding synthesis filter bank for perfect reconstruction system. These synthesis filter banks are FIR filter banks with $(2N-1)^{th}$ order FIR filters for a N channel system. The delay of the whole system is N sample periods. The special feature of this perfect reconstruction filter bank system, consisting of (6.20) and (6.38), is that both analysis bank and synthesis bank are computationally efficient to implement and are given by closed forms.

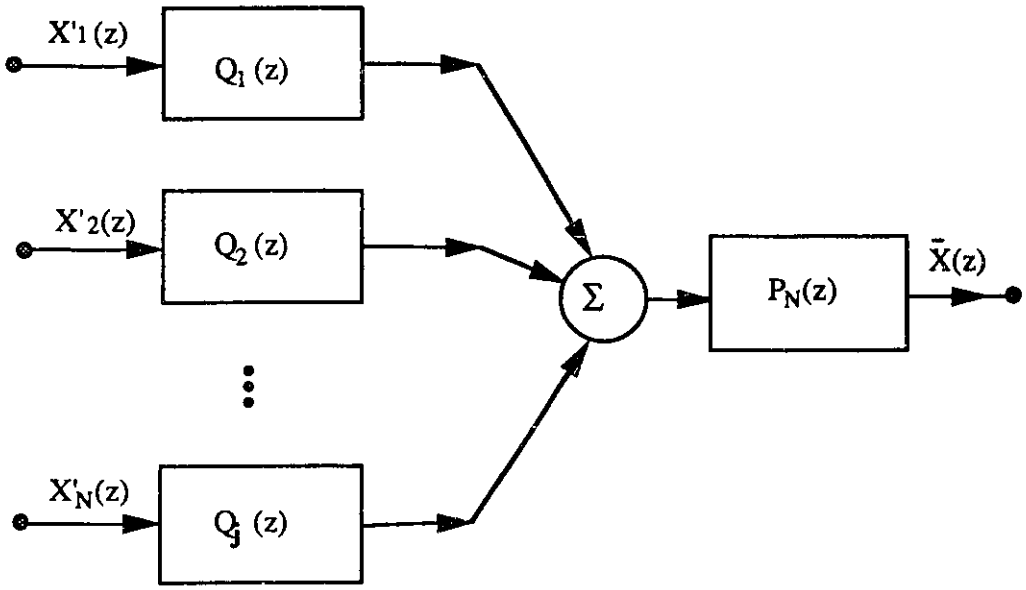

Figure 6.4 The structure of the FIR synthesis filter bank.

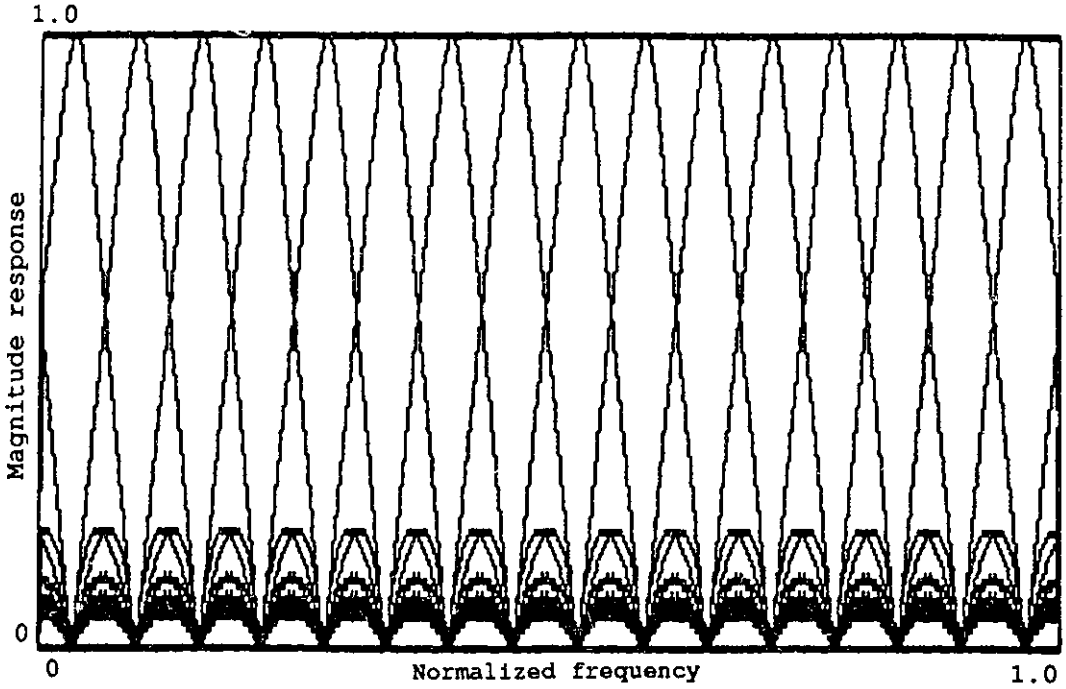

(a) when λ =0.85;

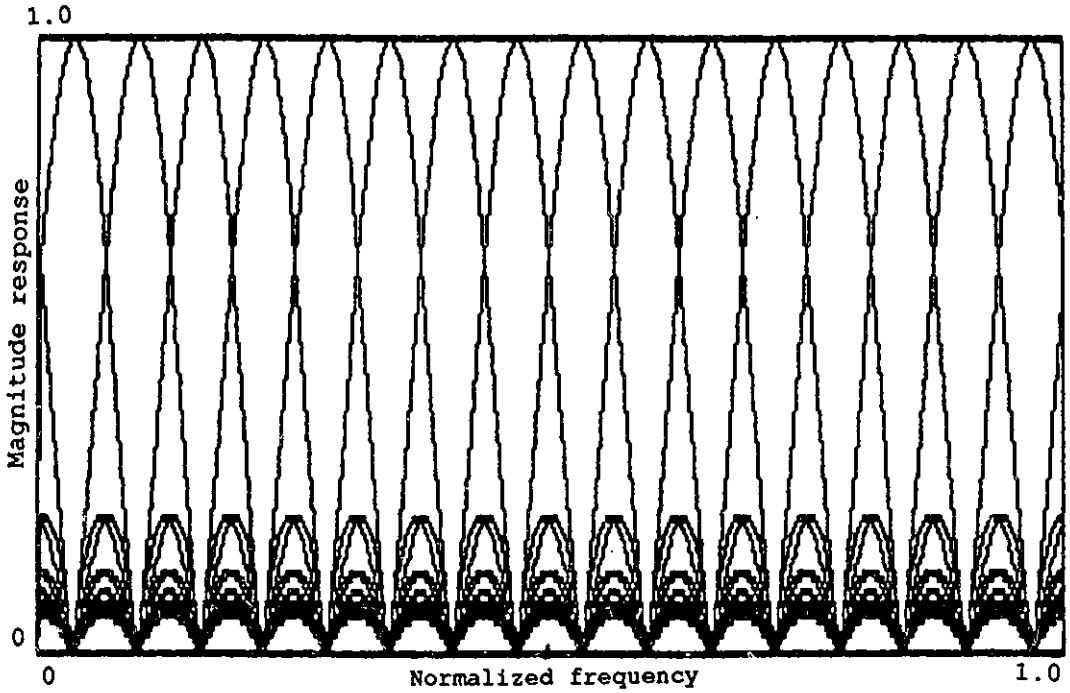

(b) when λ =0.75;

Figure 6.5 Frequency responses of a 16-filter uniform band analysis bank.

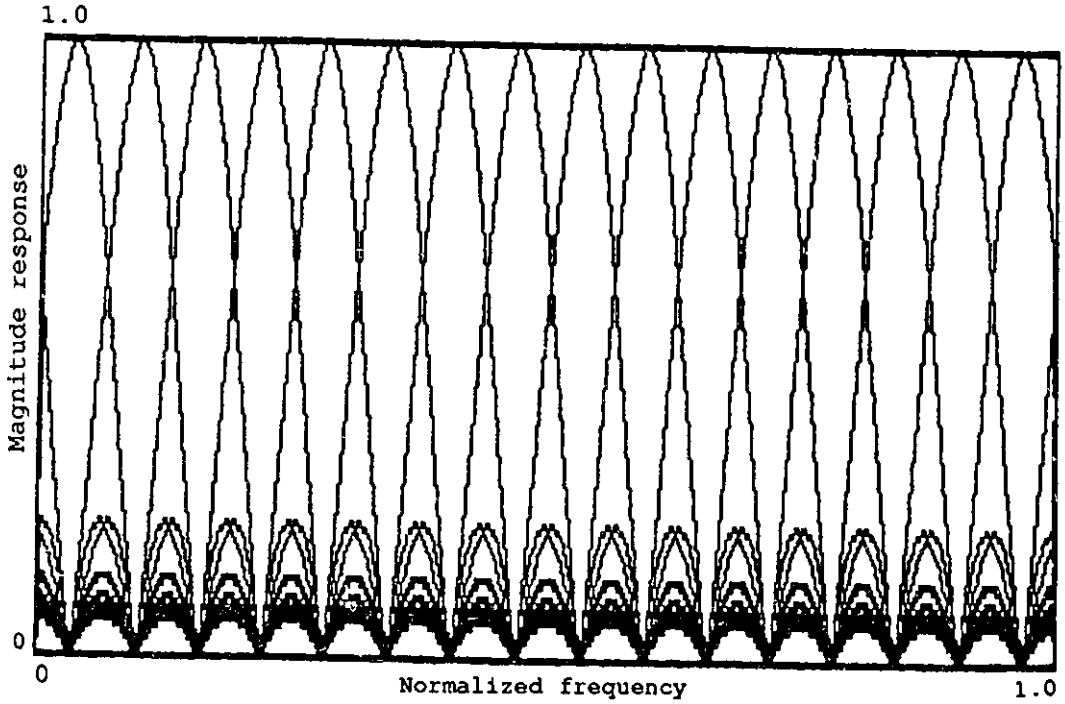

(a) Response of sub-filter bank Q(z), λ =0.85;

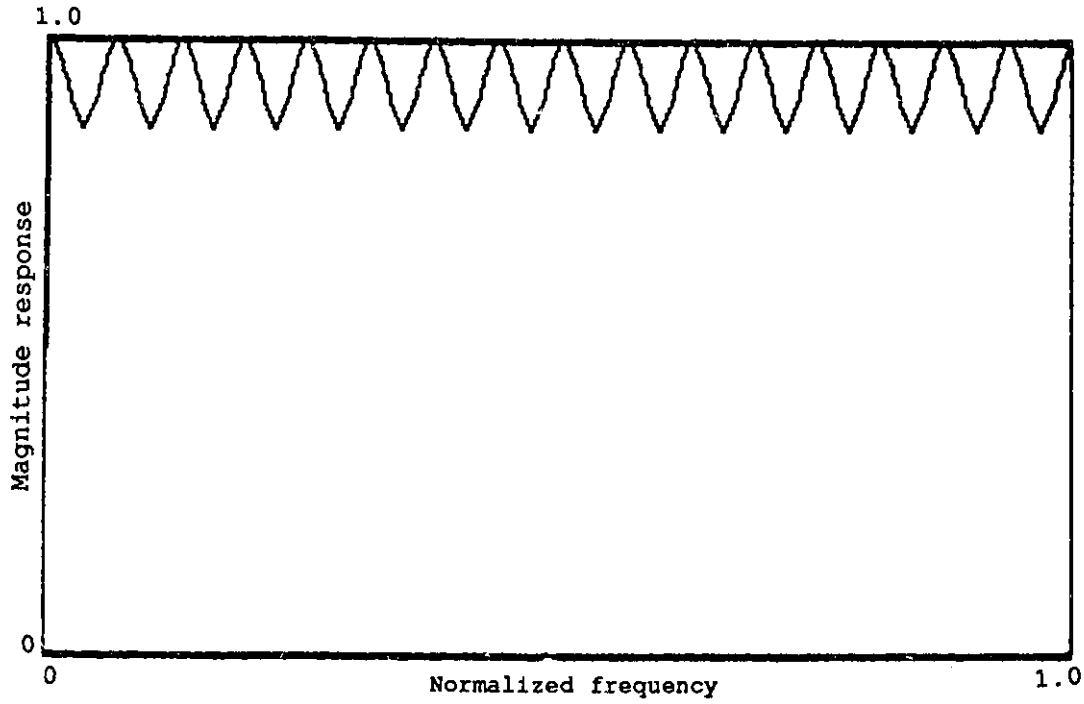

(b) Response of post-filter $P_N(z)$, λ =0.85;

Figure 6.6 Frequency responses of sub-filter banks and past-filters in the uniform band filter banks.

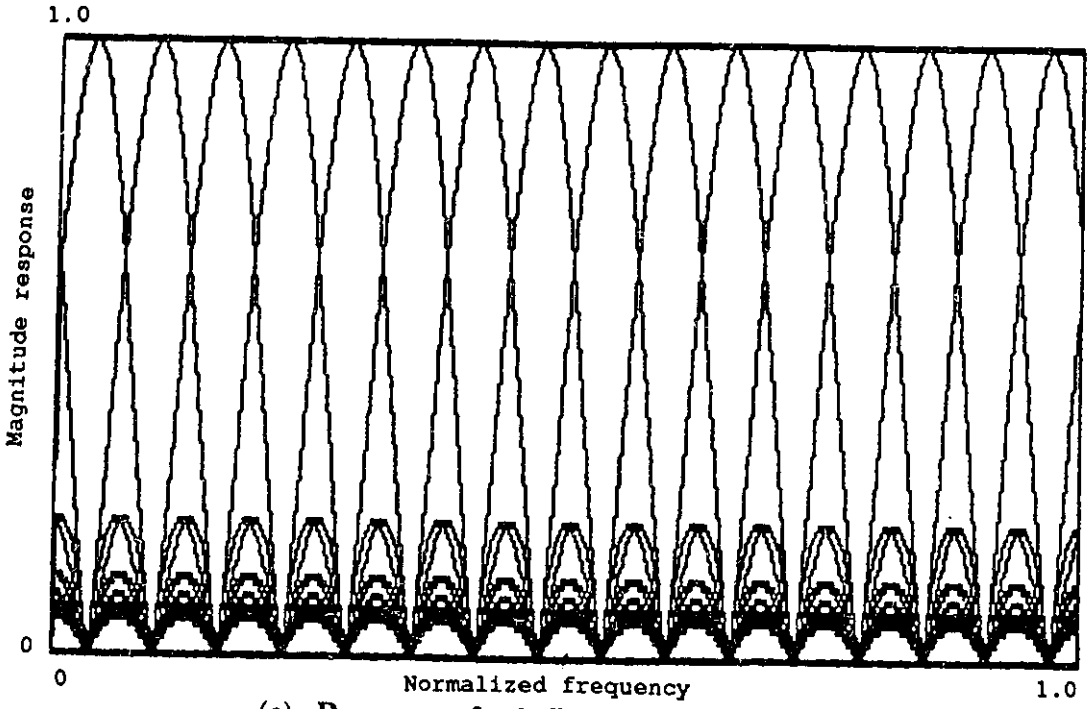

(c) Response of sub-filter bank Q(z), λ=0.75;

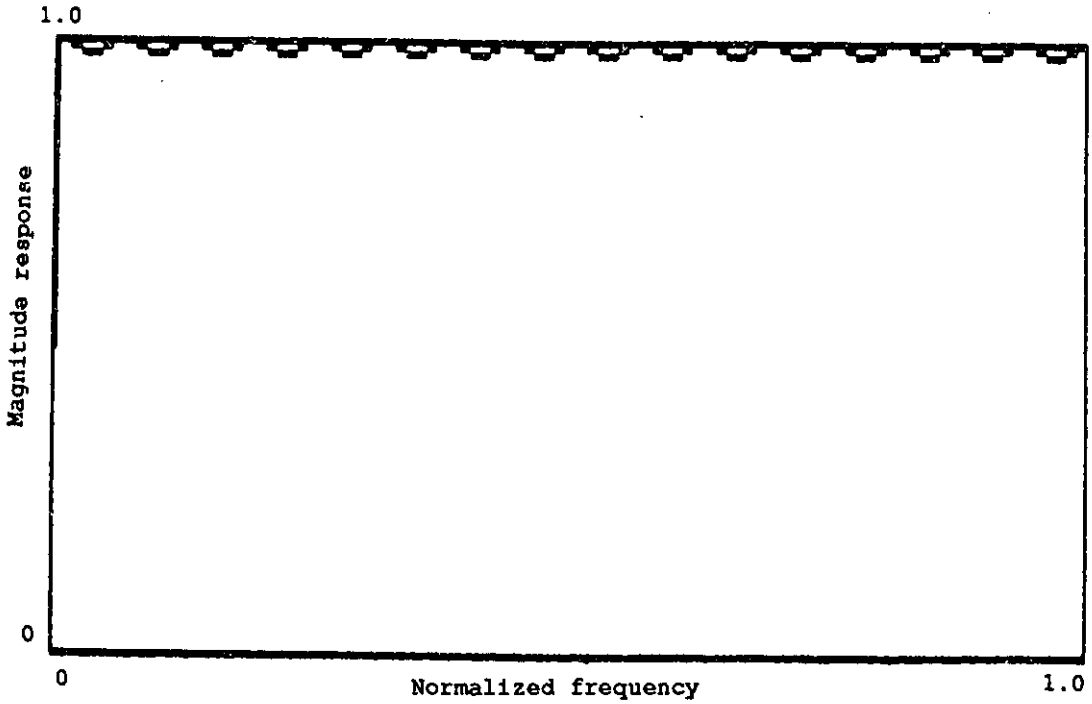

(d) Response of post-filter $P_N(z)$, λ=0.75;

Figure 6.6 Frequency responses of sub-filter banks and past-filters in the uniform band filter banks.

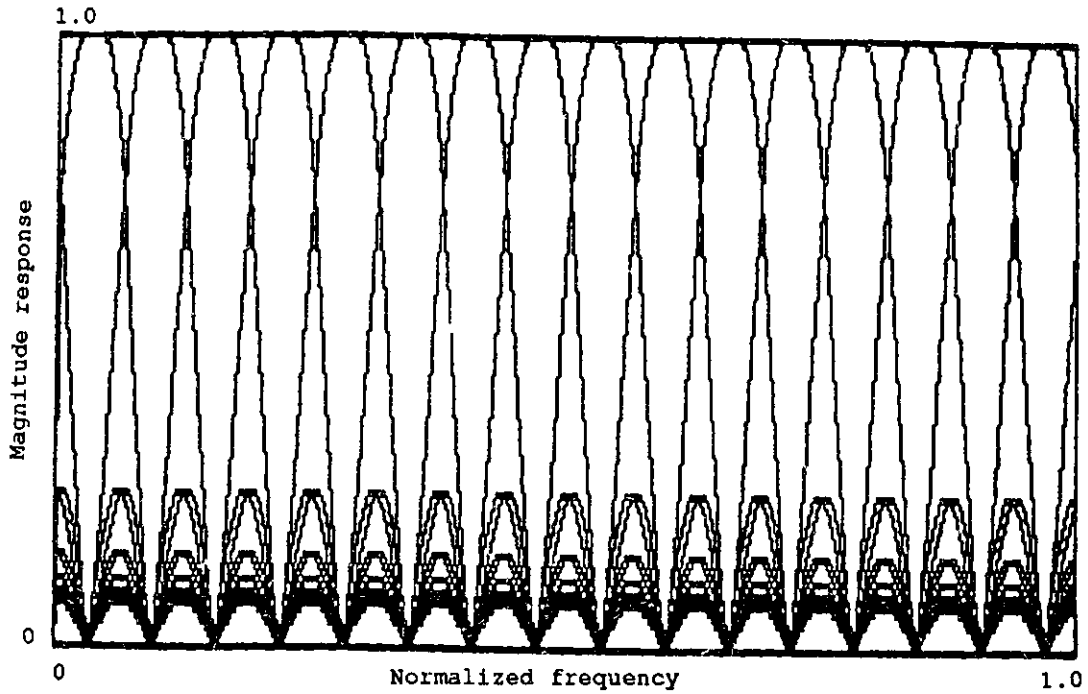

(a) when λ=0.85;

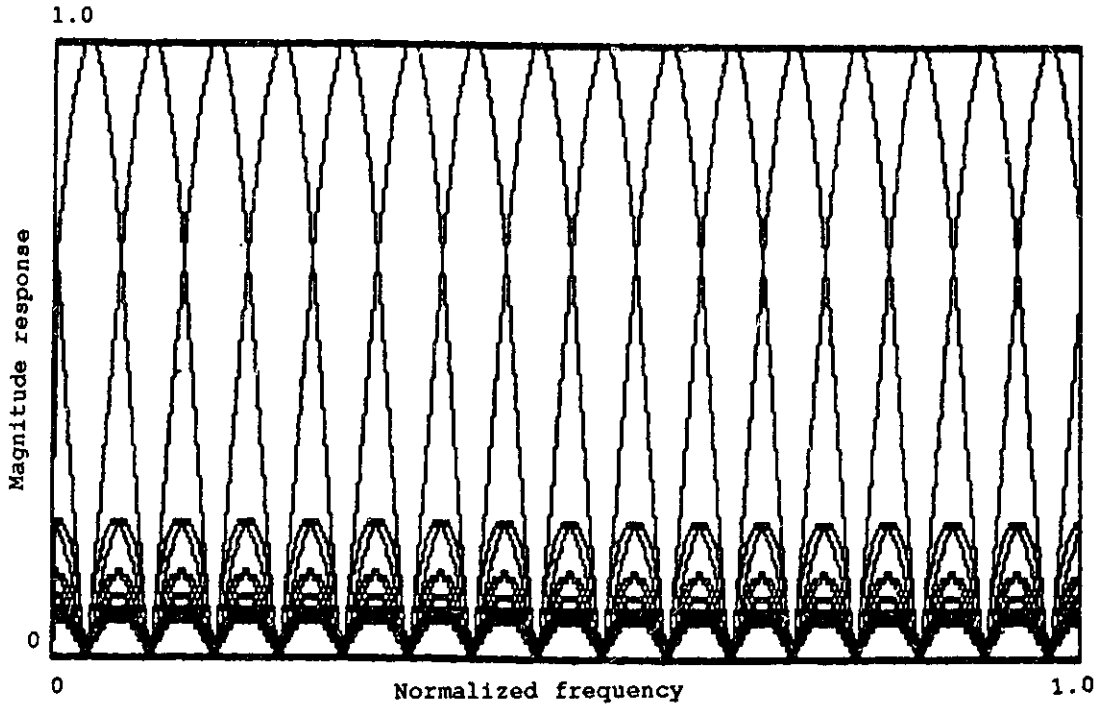

(b) when λ=0.75;

Figure 6.7 Frequency responses of the final FIR synthesis filter bank.

6.5 Calculation Results

We will illustrate the calculation results of perfect reconstruction analysis/synthesis systems proposed in the previous sections, by several linear and non-linear spacing frequency multirate filter banks in this section. The design of the FIFB analysis filter banks is the same as that given in chapter II. Filter coefficients K_i are decided by specifying all the poles of the filter bank, where the pole optimization for maximally flat filter banks may be considered.

Example I: Design an uniform-band analysis/synthesis system with perfect reconstruction property, where the number of the channels are 16. The K_i (see Table VI.1) are calculated according to (2.13) and the pole angles are optimized by (2.42) with different forgetting factors ($\lambda = 0.85$ *or* 0.75). The magnitude frequency responses for the analysis filter banks are plotted in Fig.6.5. For the synthesis filter banks, the FIR sub-filter $Q_j(z)$ and $P_N(z)$ are separately simulated based on the zero z_i, the pole P_i, and the coefficient K_i, and the response curves are given in Fig.6.6, respectively. The responses of final FIR filters $G_j(z)$ in synthesis banks are shown in Fig.6.7. The results shows that the synthesis filter banks have similar frequency responses to the analysis filter banks, but the different λ leads to the different tradeoffs between the filter passband and stopband. It is clear that better passband of the synthesis bank is obtained at the cost of poor passband of the analysis bank.

Example II: Design the same uniform-band perfect reconstruction system with the forgetting factor $\lambda = 0.0$, i.e., all the poles of the analysis filter bank are forced to be at the origin. This structure implies that first, the system is FIR system, since both the analysis and synthesis banks are FIR filter banks. Secondly, the common postfilter $P_N(z)$ is disappeared from the synthesis filter bank and thus we get a pare of STFT (short time fourier transform) and ISTFT (inverse of STFT). The 16-filter magnitude responses of

this kind of analysis and synthesis filter banks are shown in Fig.6.8, where both banks are the same each other from the response point of view.

Example III: Design a third-octave band perfect reconstruction system with the 16 channels. The center frequencies of the analysis bank are chosen according to (5.35) and the pole function is the same as that in chapter II (see equation (2.25)). The difference between this system from the systems in the examples above is not only in aspect of the nonuniform-band spacing, but also here all the filters in the banks do not cover the whole half band. Consequently this multirate filter bank is not minimally sampled frequency case, even though we have $R = N$. The simulation results are shown in Fig.6.9 and fig.6.10. Fig.6.9 illustrates the magnitude responses of the analysis filter bank. But for clarity, the filter responses of the synthesis bank are separately plotted in Fig.6.10 one by one. These synthesis filter responses make us disappointed due to the poor filtering quality. Thus even though the perfect reconstruction, the short system delay, and stable FIR synthesis filter banks are obtained, we don't think this is a good way for the design of the nonuniform-band analysis reconstruction systems.

6.6 Summary

In this chapter, we present the perfect reconstruction analysis/synthesis systems based on the FIFB filter bank techniques. Some notion and basic operations of the multirate filter banks are reviewed first, and then based on the introduction of the AC-matrix theory in transform domain for perfect or aliasing-free reconstruction, the design techniques for perfect reconstruction FIFB systems are derived. General speaking, from the FIFB analysis bank with N FIFB IIR filters, the N FIR filters, constructing the synthesis bank, are easily achieved. The design procedure of a whole perfect reconstruction system is: 1) Decide the channel specification, i.e., the center frequencies of the filters. This

defines the zeros of the analysis filter bank, z_i. 2) Choose the poles of the analysis filter bank, P_i, and optimize pole position for maximally flat frequency response. 3) Calculate the filter coefficients K_i to realize the analysis filter bank (see equation (6.20) and Fig.6.1). 4) Determine g_i and then FIR filter coefficients to implement the synthesis filter bank (see equation (6.39)-(6.40) and Fig.6.4). Several examples are designed and the simulation results show that this technique works for uniform-band systems but not good for nonuniform-band case.

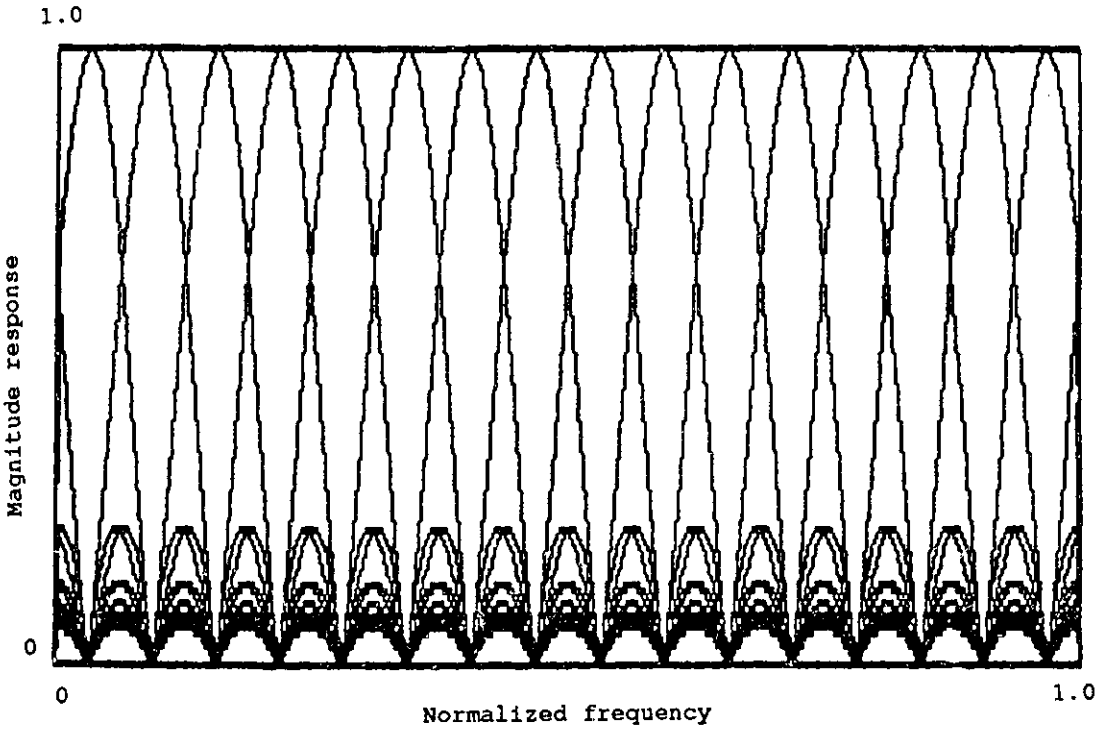

(a) FIR analysis filter bank;

Figure 6.8 Frequency responses of perfect reconstruction analysis/synthesis filter banks with all-poles at the origin.

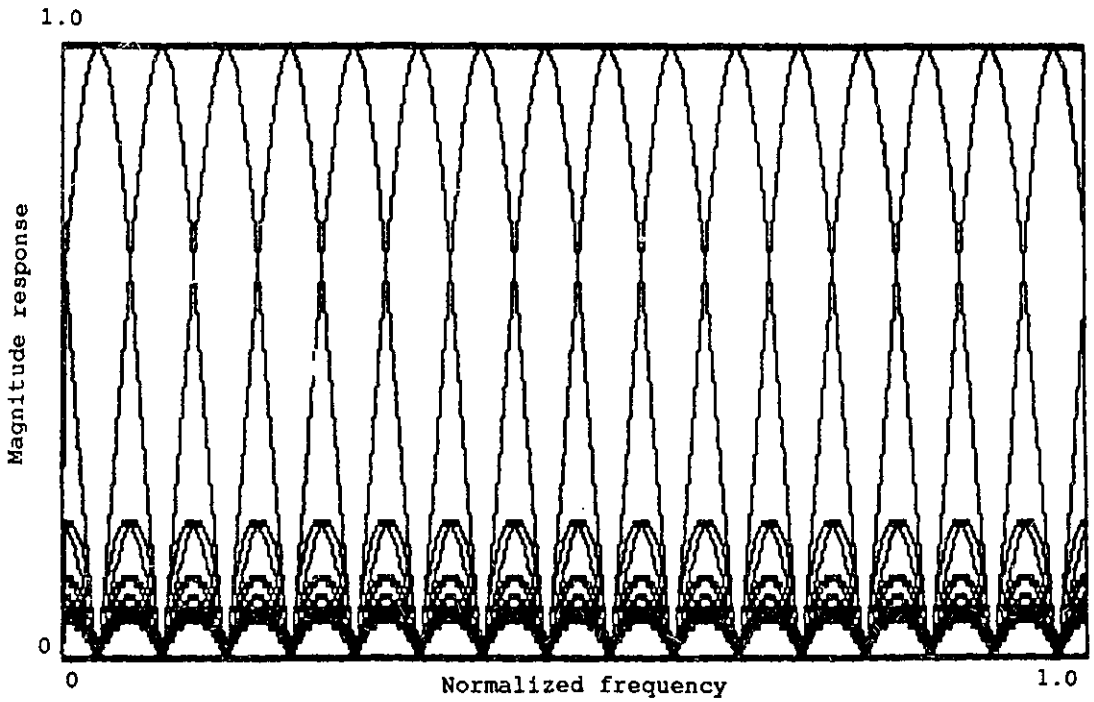

(b) FIR synthesis filter bank;

Figure 6.8 Frequency responses of perfect reconstruction analysis/synthesis filter banks with all-poles at the origin.

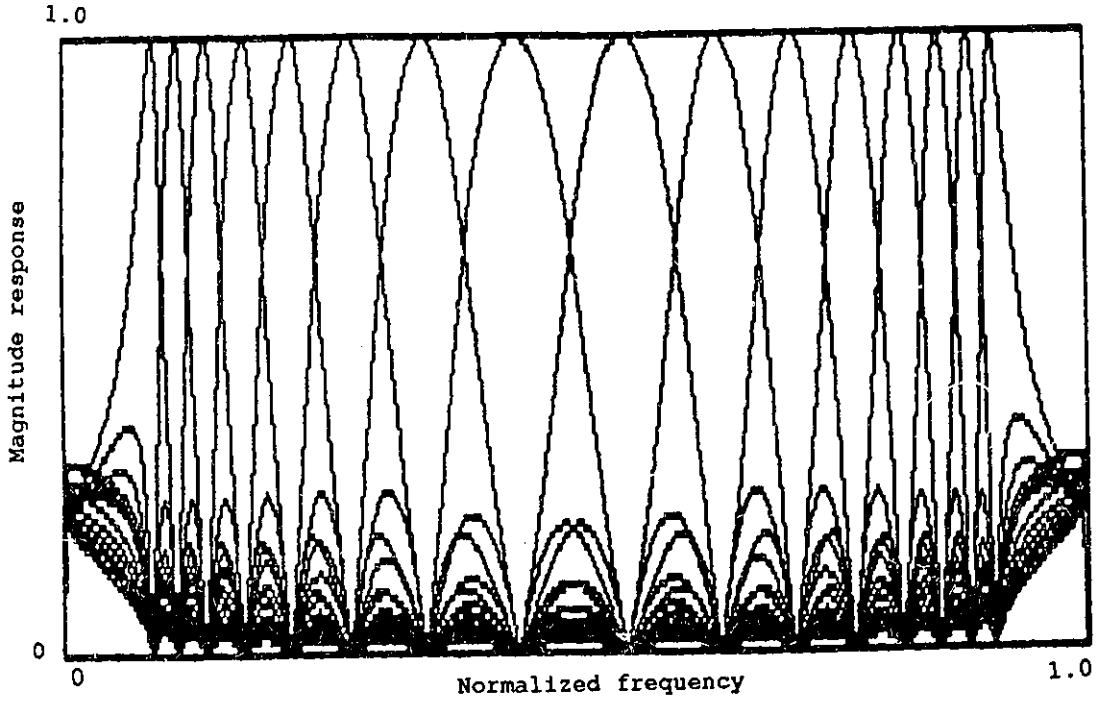

Figure 6.9 Frequency responses of the analysis filter bank in a third-octave analysis/synthesis perfect reconstruction system.

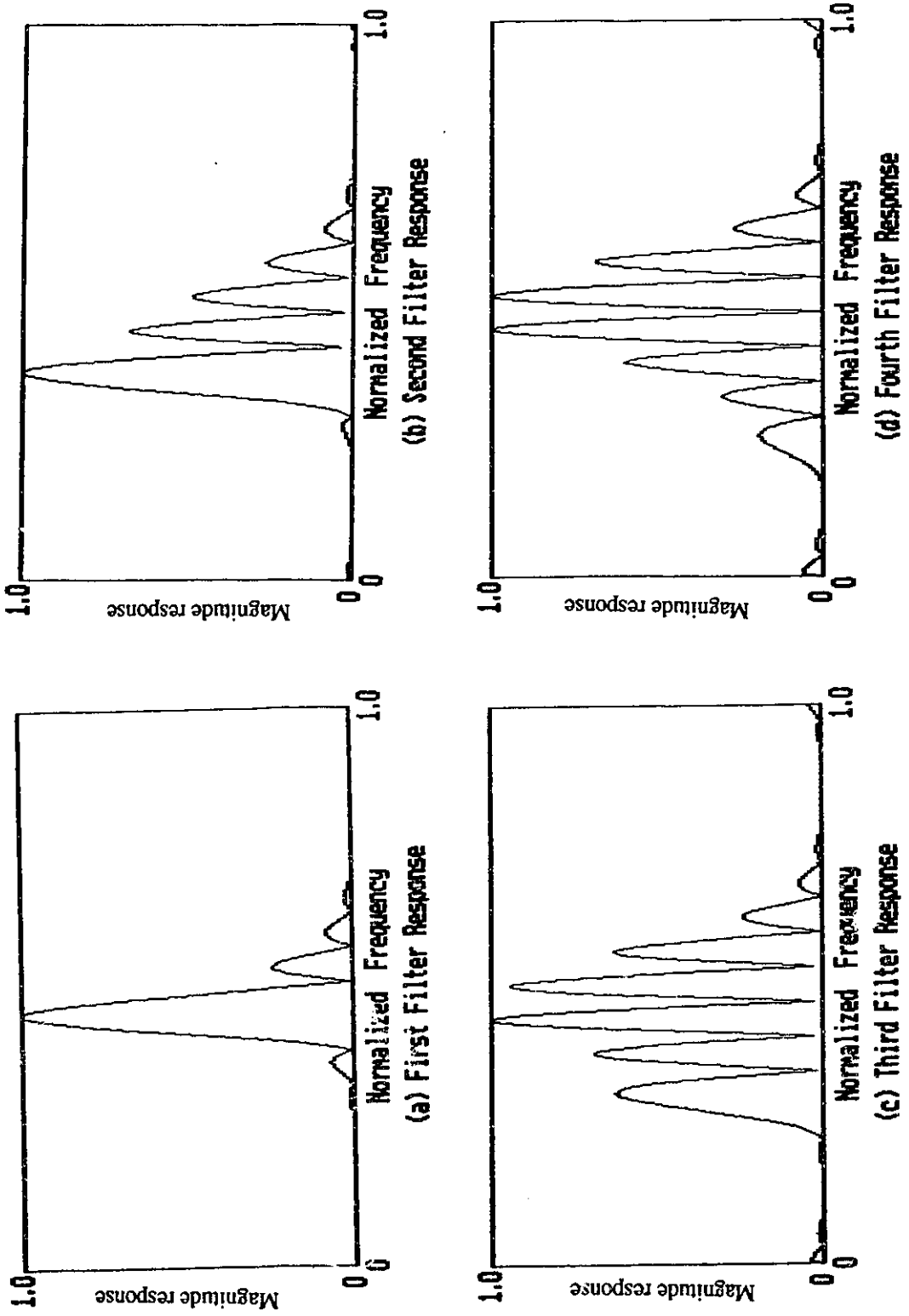

Figure 6.10 Filter responses of the synthesis filter bank in the third-octave analysis/synthesis perfect reconstruction system.

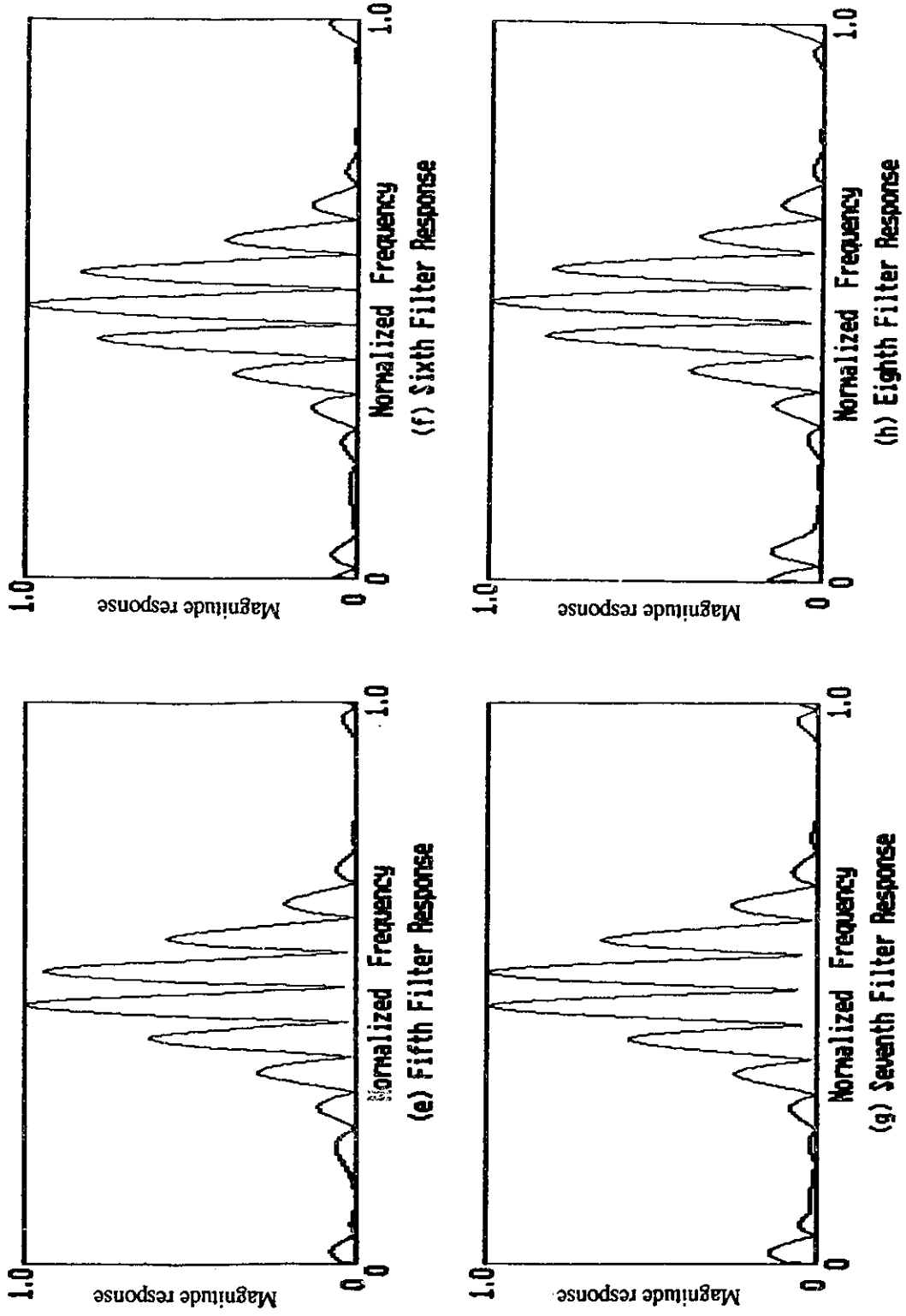

Figure 6.10 Filter responses of the synthesis filter bank in the third-octave analysis/synthesis perfect reconstruction system.

VII CONCLUSIONS AND SUGGESTIONS FOR FUTURE RESEARCH

7.1 Conclusions

In this thesis, we presented the design, performance analysis, and implementation of the digital filter banks, in which the filter center-frequencies may be arbitrarily spaced and the filter bandwidths may selected nonuniformly. The frequency interpolation filter bank(FIFB) was introduced at first based on the adaptive filtering structure. Then the digital resonator-based filter bank(RBF) has been proposed based on the purely-imaginary elemental resonator on the unit circle. These filter banks are efficient in computation and implementation, and have good frequency responses with the arbitrary center-frequency spacing. Equivalent frequency-domain windowing techniques have been studied for the improvement of filter bank stopband and passband performance. Finally, the FIFB filter bank techniques proposed in this thesis are successfully extended to the field of allpass and perfect reconstruction analysis/synthesis systems. This widens the area of the FIFB filter bank applications.

In chapter II, the frequency interpolation filter banks have been introduced. Different adaptive algorithms, such as, LMS, normalized LMS, and RLS, are applied to the design of the filter banks. A good approach found is to put the poles with the same angles to the corresponding zeros but closer to the unit circle for lower frequencies for more constant-Q filters and the design procedure and examples were shown. Different possibilities for the implementation of the filter banks are considered and the H-formulation implementation obtains the highest operation speed (a 16-filter third-octave filter bank can be realized on TMS320C25 under the real-time processing with the maximum sampling frequency as

12.8kHz). The filter function sensitivity of the FIFB filter banks are derived and finite-word-length effects are studied. The numerical results show that coefficient quantization effects and filter bank output noise powers caused by fixed-point arithmetic rounding may be readily predicted when implemented with general finite-word-length DSP processors. In order to overcome the non-flat peak of the filter bank frequency responses, maximally-flat FIFB filter banks are studied and new design procedure is presented with the application of the pole optimization.

A new frequency interpolation filter bank has been proposed in chapter III based on the digital lossless resonators as the basic units of the filter bank structure. The RFB filter bank retains the characteristics as the FIFB bank, such as good sensitivity and high efficiency in commutation and implementation, but the frequency response is improved. With these new techniques, our attention has focused on the study of the design of logarithmic filter banks, i.e., filter banks with center frequencies spaced logarithmically. The design procedure is derived and a variety of zero-pole structures are examined. The results show that better frequency responses are achieved with the zero-pole structure (2) and (3) in figure 3.3. The filter banks with very high orders are explored and the exact constant-Q filter bank would be obtained with the constant ratio: $K_r/f_r = 0.057776$ if the bank has an infinite number of filters. Even though the infinite filter bank is impossible in practice, but because the serious changes in filter Q value only occur near one end of frequency band for the filter bank with finite filters, good crossover gain filter banks may still designed (see the typical frequency responses).

Windowing techniques are presented to suppress the appreciable sidelobes and to improve the passband performance of the filter banks in chapter IV. Considering the purely imaginary resonators on the unit circle of the z-plane in the RFB filter banks, the symmetrical real windows with different widths are studied. The linear programming

problem is formulated in two ways: constraining only the stopband, and constraining both the stopband and the passband. This permits the direct application of the simplex algorithm. The calculated results show that the performance of RFB filter banks is improved significantly by the optimal windows. The three-weight windows may reduce the highest sidelobe of the banks from -13.5 dB to -42.3 dB, the five-weight windows may reduce the highest sidelobes to -53 dB and the eight-weight windows can produce the final filter bank with highest sidelobes low to -80 dB, i.e., 66 dB improvement is achieved. With the reduction of the highest sidelobes, the relative transition bandwidths are reduced and the passband performance is improved. The interesting thing is that the selection of the windows may be used to control the crossover gains of the filter banks. For example, we may obtain a 3 dB bandwidth bank or a 6 dB bandwidth bank from the same mother filter bank by using different windows and different window arrangements.

Another contribution of this thesis research is that the FIFB filter bank techniques are applied to design and realize single-rate filter bank-based allpass analysis/synthesis systems or multirate perfect reconstruction filter bank systems. This extends the FIFB filter bank technique itself and widens the application area of these filter banks. The allpass system is considered in chapter V, which consists of an analysis filter bank and a synthesis filter bank. The analysis bank is a general FIFB bank with an arbitrary spacing of the filter frequencies and bandwidths, and the synthesis filter bank is derived based on the allpass requirement. The key in the system design is to find all the poles of the analysis filter bank, which just cancel all the zeros outside the unit circle of $N(z)$, the numerator of the transfer function of the system. The calculation examples have successfully shown the following design procedure: (1) Given z_i, initialize $|K_i^I|$ for i=1,2,...N, and calculate $N(z)$. (2) Find the partial factor $\bar{N}_I(z)$ which has all the zeros inside the unit circle of $N(z)$, in fact, that is $D(z)$, the denominator of filter banks. (3) Calculate the filter coefficients K_i from a partial fraction expansion of $D(z)$. By evaluating and calculating the imaging

rejection, we find that when the decimation and interpolation procedures are performed after the analysis filter bank, the allpass system will suffer some distortions because of high sidelobes in the filter frequency responses. However the windowing techniques may be applied to improve the system quality.

The multirate FIFB filter bank-based perfect reconstruction analysis/synthesis systems are presented in chapter VI. Based on the introduction of the AC-matrix theory in transform domain for perfect or aliasing-free reconstruction, the design techniques for perfect reconstruction FIFB systems are derived. General speaking, from the FIFB analysis bank with N FIFB IIR filters, the N $(2N-1)^{th}$ order FIR filters, constructing the synthesis bank, are easily achieved for perfect reconstruction. Both the analysis bank and synthesis bank are computationally efficient to implement and are given by closed forms. The design procedure of a whole perfect reconstruction system is: (1) Decide the channel specification, i.e., the center frequencies of the filters. This defines the zeros of the analysis filter bank, z_i. (2) Choose the poles of the analysis filter bank, P_i, and optimize pole position for maximally-flat frequency response. (3) Calculate the filter coefficients K_i to realize the analysis filter bank. (4) Determine g_i and then FIR filter coefficients to implement the synthesis filter bank. Calculation results show that this technique works well for uniform-band system but not well for the nonuniform-band case.

7.2 Suggestions for Future Research

The non-uniform band digital filter banks are still attracting the attention of many researchers in the world. The research work done for this thesis has produced unsolved problems and research directions. Some of them are:

1. In chapter VI, even though maximally decimated perfect reconstruction analysis/synthesis multirate bank-based systems are achieved, the filter responses in the syn-

thesis banks, with logarithmically spacing center frequencies, is too bad for the systems to be useful. This is because of nonuniform filter bandwidths but the equal integer sampling changing rate R in filter banks. It would be interesting to study the unequal integer rate R for different bandwidth filters and to study the case of the fractional sampling changing rates for the FIFB multirate filter banks.

2. In chapter V, the FIFB bank-based allpass analysis/synthesis systems are obtained without sampling rate changing. The significant imaging rejections result if decimation and interpolation are included. There may be a practical way to design multirate FIFB filter bank-based analysis/synthesis systems using the design techniques in chapter V using the windowing procedures.

3. To extend one-dimensional FIFB filter bank techniques to two-dimensional case, to relate the FIFB filter banks to the wavelet theory, to explore the relationship between the filter banks considered in the thesis to the analog *Cauer* filters, and to study the application of the FIFB filter banks presented to different practical systems, are all interesting and worthwhile for future research.

APPENDIX-A:

SOME OPTIMAL POLE CALCULATION RESULTS

Optimal poles when N=2:

```
**********************************************************************************************************************
 FILTER BANK (ORDER=2)
LAMBDA:=   0.95000
CIGAMA:=0.00000001
 I     ORIGINAL POLE POSITIONS: PHIBAI          OPTIMAL POLE POSITIONS: PHII          THE RADII OF THE FILTERS: TEMPO[I]/2
 1      2.000000000001 37E-0001                  2.0001626482250 3E-0001               9.7963009573262 2E-0001
 2      2.200000000009093E-0001                  2.1 99837350392 5E-0001               9.7768535746345 4E-0001
**********************************************************************************************************************
```

```
**********************************************************************************************************************
 FILTER BANK (ORDER=2)
LAMBDA:=   0.90000
CIGAMA:=0.00000001
 I     ORIGINAL POLE POSITIONS: PHIBAI          OPTIMAL POLE POSITIONS: PHII          THE RADII OF THE FILTERS: TEMPO[I]/2
 1      2.000000000001 37E-0001                  2.0025385977193 2E-0001               9.5852082714412 9E-0001
 2      2.200000000009093E-0001                  2.1974913913977 3E-0001               9.5474998145522E-0001
**********************************************************************************************************************
```

Oprimal poles when N=3:

```
**********************************************************************************************************************
 FILTER BANK (ORDER=3)
LAMBDA:=   0.95000
CIGAMA:=0.00000001
 I     ORIGINAL POLE POSITIONS: PHIBAI          OPTIMAL POLE POSITIONS: PHII          THE RADII OF THE FILTERS: TEMPO[I]/2
 1      2.00000000000137E-0001                   2.000191352931 8E-0001               9.796839011891 4E-0001
 2      2.20000000000093E-0001                   2.2000869101801 5E-0001              9.776830332202 4E-0001
 3      2.40000000000048E-0001                   2.3997389428261 1E-0001              9.756824567603 0E-0001
**********************************************************************************************************************
```

```
**********************************************************************************************************************
 FILTER BANK (ORDER=3)
LAMBDA:=   0.90000
CIGAMA:=0.00000001
 I     ORIGINAL POLE POSITIONS: PHIBAI          OPTIMAL POLE POSITIONS: PHII          THE RADII OF THE FILTERS: TEMPO[I]/2
 1      2.00000000000137E-0001                   2.00311930283744E-0001               9.586684879823 2E-0001
 2      2.20000000000093E-0001                   2.20098087859950E-0001               9.546797872435 3E-0001
 3      2.40000000000048E-0001                   2.39889919511335E-0001               9.507666356166 4E-0001
**********************************************************************************************************************
```

Optimal poles when N=4:

```
**********************************************************************************************************************
 FILTER BANK (ORDER=4)
LAMBDA:=   0.95000
CIGAMA:=0.00000001
 I     ORIGINAL POLE POSITIONS: PHIBAI          OPTIMAL POLE POSITIONS: PHII          THE RADII OF THE FILTERS: TEMPO[I]/2
 1      2.00000000000137E-0001                   2.00020503298872E-0001               9.796889887533 4E-0001
 2      2.20000000000093E-0001                   2.20012650712178E-0001               9.776824574955 5E-0001
 3      2.40000000000048E-0001                   2.40023807243935E-0001               9.756766344034 4E-0001
 4      2.56250000000103E-0001                   2.56187009155025E-0001               9.740609375215 9E-0001
**********************************************************************************************************************
```

```
**********************************************************************************************************************
 FILTER BANK (ORDER=4)
LAMBDA:=   0.90000
CIGAMA:=0.00000001
 I     ORIGINAL POLE POSITIONS: PHIBAI          OPTIMAL POLE POSITIONS: PHII          THE RADII OF THE FILTERS: TEMPO[I]/2
 1      2.00000000000137E-0001                   2.00346773796276E-0001               9.586614614130 3E-0001
 2      2.20000000000093E-0001                   2.20215964033154E-0001               9.546560745420 2E-0001
 3      2.40000000000048E-0001                   2.40363626894905E-0001               9.506104369638 1E-0001
 4      2.56250000000103E-0001                   2.55317628599360E-0001               9.476206534533 9E-0001
**********************************************************************************************************************
```

Optimal poles when N=33:

FILTER BANK (ORDER=33)
LAMBDA:= 0.99000
SIGAMA:=0.00000001

I	ORIGINAL POLE POSITIONS: PHIBAI	OPTIMAL POLE POSITIONS: PHII	THE RADII OF THE FILTERS: TEMPO(I)/2
1	6.87500000000203E-0003	6.87500043928471E-0003	9.99861817421333E-0001
2	7.81249999999630E-0003	7.81250031869183E-0003	9.99842975826141E-0001
3	8.74999999999875E-0003	8.74999988552818E-0003	9.99824134591108E-0001
4	9.99999999999539E-0003	1.00000003497858E-0002	9.99799013477059E-0001
5	1.12499999999932E-0002	1.12500004864816E-0002	9.99773892999656E-0001
6	1.25000000000086E-0002	1.25000002140766E-0002	9.99748773162537E-0001
7	1.38749999999928E-0002	1.38743997424273E-0002	9.99721142073213E-0001
8	1.56249999999926E-0002	1.56250003041859E-0002	9.99685976314140E-0001
9	1.74999999999975E-0002	1.75000000570835E-0002	9.99648300105036E-0001
10	1.96875000000062E-0002	1.96875001546722E-0002	9.99604346314300E-0001
11	2.21874999993826E-0002	2.21875002729460E-0002	9.99554115776846E-0001
12	2.50000000000171E-0002	2.50000005947245E-0002	9.99497609436730E-0001
13	2.79999999999960E-0002	2.80000005751986E-0002	9.99437339533870E-0001
14	3.12499999999852E-0002	3.12500001420217E-0002	9.99372051248429E-0001
15	3.49999999999950E-0002	3.50000000901022E-0002	9.99296723903171E-0001
16	3.93750000000125E-0002	3.93750004768209E-0002	9.99206849167189E-0001
17	4.42499999999782E-0002	4.42500001466829E-0002	9.99110940721948E-0001
18	5.00000000000342E-0002	5.00000014885766E-0002	9.98993847126278BE-0001
19	5.59374999999985E-0002	5.59375009452921E-0002	9.98876250538160E-0001
20	6.24999999999704E-0002	6.25000010552745E-0002	9.98744496802829E-0001
21	6.96875000000223E-0002	6.96874999985025E-0002	9.98600215054466E-0001
22	7.81250000000173E-0002	7.81250007938294E-0002	9.98430367385650E-0001
23	8.75000000000599E-0002	8.74999983522193E-0002	9.98242737055079E-0001
24	1.00000000000065E-0001	1.00000003245666E-0001	9.97931951559033E-0001
25	1.12499999999932E-0001	1.12500004535474E-0001	9.97741229215535E-0001
26	1.24999999999941E-0001	1.25000000603116E-0001	9.97490563921865E-0001
27	1.39375000000045E-0001	1.39374999799999E-0001	9.97203389510676E-0001
28	1.56250000000035E-0001	1.56250001397022E-0001	9.96864136951719E-0001
29	1.75000000000120E-0001	1.74999996404226E-0001	3.96488562088416E-0001
30	2.00000000000137E-0001	2.00000005875852E-0001	9.95987832468293E-0001
31	2.24999999999864E-0001	2.25000007732367E-0001	9.95467563502625E-0001
32	2.49999999999852E-0001	2.49999973260435E-0001	9.94967437157761E-0001
33	2.78750000000089E-0001	2.78749976069634E-0001	9.94413636096375E-0001

Optimal poles when N=33 (cont.):

FILTER BANK (ORDER=33)
LAMBDA:= 0.90000
SIGAMA:=0.00000001

I	ORIGINAL POLE POSITIONS: PHIBAI	OPTIMAL POLE POSITIONS: PHII	THE RADII OF THE FILTERS: TEMPOII)/2
1	6.875000000002895E-0003	6.880502333601006-0003	9.985511340131955-0001
2	7.812499999996306-0003	7.816585743365366-0003	9.983542367554086-0001
3	8.749999999993756-0003	8.749462451585296-0003	9.981520028324976-0001
4	9.999999999995936-0003	1.000452016755176-0002	9.978340578339466-0001
5	1.124999999999326-0002	1.125601724589146-0002	9.976309311553826-0001
6	1.250000000000866-0002	1.250290318596756-0002	9.973688429618056-0001
7	1.387499999999286-0002	1.387284335482396-0002	9.970809688575176-0001
8	1.562499999999266-0002	1.562857087044476-0002	9.967121483259696-0001
9	1.749999999999756-0002	1.750118710503846-0002	9.963189236768816-0001
10	1.968750000000626-0002	1.968980837359906-0002	9.958595387597606-0001
11	2.218749999998266-0002	2.219140579432106-0002	9.953347205154396-0001
12	2.500000000001716-0002	2.500759708371776-0002	9.947442335378586-0001
13	2.799999999999606-0002	2.800736171484276-0002	9.941156409822726-0001
14	3.124999999999526-0002	3.125263786507736-0002	9.934360494462456-0001
15	3.499999999999506-0002	3.500197955320016-0002	9.926514802264146-0001
16	3.937500000001256-0002	3.938120552045366-0002	9.917356689160826-0001
17	4.424999999997826-0002	4.425350010042546-0002	9.907182012266286-0001
18	5.000000000003426-0002	5.001824335499686-0002	9.895154543610266-0001
19	5.593749999999856-0002	5.595051224286326-0002	9.882792796097426-0001
20	6.249999999997046-0002	6.251336979196036-0002	9.869135010740146-0001
21	6.96875000002236-0002	6.968347509357086-0002	9.854222513730606-0001
22	7.812500000001736-0002	7.813403824455226-0002	9.836703138416856-0001
23	8.750000000005996-0002	8.748462578240926-0002	9.817340320623776-0001
24	1.000000000000686-0001	1.000396816425066-0001	9.791401749707806-0001
25	1.124999999999326-0001	1.125544128813476-0001	9.765614696152626-0001
26	1.249999999999416-0001	1.250115517621686-0001	9.740013757309506-0001
27	1.393750000000456-0001	1.393750418057486-0001	9.710578328667916-0001
28	1.562500000000356-0001	1.562636570179816-0001	9.676091465440806-0001
29	1.750000000001206-0001	1.749627851419566-0001	9.638030228342776-0001
30	2.000000000001376-0001	2.000663347274366-0001	9.587181144397626-0001
31	2.249999999999646-0001	2.250802365584416-0001	9.536780487959746-0001
32	2.499999999995826-0001	2.499537835974816-0001	9.486925359983516-0001
33	2.787500000000896-0001	2.786664372699436-0001	9.430056764554046-0001

APPENDIX-B:

THE PROOF OF PURELY REAL NUMBER G

From equations (3.5) and (3.10) or (3.13), and noting that on the unit circle

$$Z(z) = \sum_{r=1}^{N} Z_r(z) = \sum_{r=1}^{N} \frac{K_r(z+p_r)}{(z-p_r)} \qquad (B-1)$$

is a purely imaginary number, we know that the term

$$G\,\frac{\prod_{r=1}^{N}(z-q_r)}{\prod_{r=1}^{N}(z-p_r)} \qquad (B-2)$$

is purely imaginary too. However, since

$$\begin{aligned}\sqrt{\frac{z}{q_r}} - \sqrt{\frac{q_r}{z}} &= e^{j\frac{(\omega-\phi_r)}{2}} - e^{j\frac{(\phi_r-\omega)}{2}} \\ &= 2j\ sin(\frac{\omega-\phi_r}{2})\end{aligned} \qquad (B-3)$$

and

$$\begin{aligned}\sqrt{\frac{z}{p_r}} - \sqrt{\frac{p_r}{z}} &= e^{j\frac{(\omega-\omega_r)}{2}} - e^{j\frac{(\omega_r-\omega)}{2}} \\ &= 2j\ sin(\frac{\omega-\omega_r}{2}),\end{aligned} \qquad (B-4)$$

we have

$$\begin{aligned}G\,\frac{\prod_{r=1}^{N}(z-q_r)}{\prod_{r=1}^{N}(z-p_r)} &= G\,\frac{\prod_{r=1}^{N}\sqrt{zq_r}(\sqrt{\frac{z}{q_r}} - \sqrt{\frac{q_r}{z}})}{\prod_{r=1}^{N}\sqrt{zp_r}(\sqrt{\frac{z}{p_r}} - \sqrt{\frac{p_r}{z}})} \\ &= G\,\frac{\prod_{r=1}^{N} sin(\frac{\omega-\phi_r}{2})}{\prod_{r=1}^{N} sin(\frac{\omega-\omega_r}{2})}\ \prod_{r=1}^{N} e^{j(\phi_r-\omega_r)}.\end{aligned} \qquad (B-5)$$

Since the middle factor in the final expression of (B-5) is purely real and the last factor is a complex, thus the parameter G must be a complex for the purely imaginary product. But for all the four different pole-zero structures discussed in the chapter III, the last factor is a purely imaginary number, and therefore G is real.

APPENDIX-C:

THE DERIVATION OF EQUATION (3.24)

From (3.6) and (3.13), we have

$$H_i(z) = \frac{K_i\frac{(z+p_i)}{(z-p_i)}}{1 + \sum_{j=1}^{N} K_j\frac{(z+p_j)}{(z-p_j)}} = \frac{\frac{K_i(z+p_i)}{(z-p_i)}}{1 + G\frac{\prod_{j=1}^{N}(z-q_j)}{\prod_{j=1}^{N}(z-p_j)}}, \qquad (C-1)$$

and when $z = q_i$,

$$|H_i(z)| = |K_i\frac{q_i + p_i}{q_i - p_i}|. \qquad (C-2)$$

If we assume that firstly

$$K_i = K_I G, \qquad (C-3)$$

where K_I is calculated at $G = 1$, and secondly

$$-20Log|H_i(z)| = M. \qquad (C-3)$$

Thus at $z = q_i$ and $i = I$,

$$20Log|K_I G\frac{q_I + p_I}{q_I - p_I}| = -M. \qquad (C-4)$$

Since G is real and positive, we can easily obtain

$$G = |\frac{1}{K_I}\frac{q_I - p_I}{q_I + p_I}|10^{-\frac{M}{20}}. \qquad (C-5)$$

We have supposed that q_I is the frequency at I^{th} crosspoint of filter bank frequency responses. This is true for big size RFB filter banks.

APPENDIX-D:

THE PURELY IMAGINARY RESONATORS MAKE THE COMPLEX WINDOWS OF NO VALUE COMPARED TO THE REAL ONES

From equation (3.3) in chapter III we know that on the unit circle the i^{th} resonator or the numerator of the i^{th} filter in the mother filter bank is

$$Z_i(e^{j\omega}) = K_i \frac{e^{j\omega} + e^{j\omega}}{e^{j\omega} - e^{j\omega}}. \qquad (D-1)$$

It is easy to show $Z_i(e^{j\omega})$ is purely imaginary with the real and positive $Kalman$ gains K_i. Expressing $e^{j\omega}$ as $(cos\omega + jsin\omega)$, we have

$$\frac{e^{j\omega} + e^{j\omega}}{e^{j\omega} - e^{j\omega}} = \frac{(cos\omega_i + cos\omega) + j(sin\omega_i + sin\omega)}{(cos\omega_i - cos\omega) + j(sin\omega_i - sin\omega)}. \qquad (D-2)$$

Transferring the denominator of the equation (D-2) into real by multiplying the denominator and numerator by $(cos\omega_i - cos\omega) - j(sin\omega_i - sin\omega)$ leads to the real part of (D-2) as

$$\frac{(cos^2\omega_i - cos^2\omega + sin^2\omega_i - sin^2\omega)}{(cos\omega_i - cos\omega)^2 + (sin\omega_i - sin\omega)^2} \qquad (D-3)$$

which is zero because of the relation $(cos^2\omega + sin^2\omega) = 1$. Since all the mother filter $H_m(z)$ for $m = 1, 2, ..., N$ have the same denominator and all their numerators are purely imaginary, thus weighting is just on the numerators of $H_m(z)$, and therefore there is no difference between the real weights and the complex ones from the suppressing sidelobe point of view. In other words, if a_i is real, then to minimize $|\sum W_i a_i|$, it is sufficient to consider W_i real. Consequently, in a window, the complex weighting coefficients contribute no thing more than the real coefficients for the improvement of the magnitude response of the result filter. This simplifies the window design and optimization.

References

[1] R. W. Schafer and L. R. Rabiner, "Design of digital filter banks for speech analysis," Bell Syst. Tech. J., vol. 50, No.10, pp.3097-3115, Dec. 1971.

[2] S. L. Freeny, R. B. Kieburtz, K. V. Mina, and S. K. Tewksbury, "Design of digital filters for an all digital frequency division multiplex-time division multiplex translator," IEEE Trans. Circuit Theory, Vol. CT-18. pp.702-711, Nov. 1971.

[3] S. L. Freeny, R. B. Kieburtz, K. V. Mina, and S. K. Tewksbury, "System analysis of a TDM-FDM translator/digital a-type channel bank," IEEE Trans. Commun, Vol. COM-19, pp.1050-1059, Dec. 1971.

[4] R. W. Schafer and L. R. Rabiner, "Design and simulation of a speech analysis-synthesis system based on short-time Fourier analysis," IEEE Trans. Audio Elec.,Vol. AU-21, No.3, pp.165-174, June. 1973.

[5] R. W. Schafer, L. R. Rabiner and O. Herrmann, "FIR digital filter banks for speech analysis," Bell Syst. Tech. J., vol. 54, No.3, pp.531-544, March 1975.

[6] M. Bellanger and J. L. Daguet, "TDM-FDM transmultiplexer: digital polyphase and FFT," IEEE Trans. Commun, Vol. COM-22, pp.1199-1205, Sep. 1974.

[7] M. Bellanger, G. Bonnerot, and M. Coudreuse, "Digital filtering by polyphase network: application to sample rate alternation and filter banks," IEEE Trans. Acoust. Speech Signal Process., Vol.ASSP-24, No.2, pp.109-114, April 1976.

[8] M. R. Portnoff, "Implementation of the digital phase vocoder using the fast Fourier transform," IEEE Trans. Acoust. Speech Signal Process., Vol.ASSP-24, No.2, pp.243-248, June 1976.

[9] J. B. Allen, "Short-time spectral analysis, synthesis and modification by discrete Fourier transform," IEEE Trans. Acoust. Speech Signal Process., Vol.ASSP-25, pp.1558-1564, Nov. 1977.

[10] J. B. Allen and L. R. Rabiner, "A unified approach to short-time Fourier analysis and synthesis," Proc. IEEE Vol.65, pp.1558-1564, Nov. 1977.

[11] R. E. Crochiere, S. A. Webber, and J. L. Flanagan, "Digital coding of speech in sub-bands," Bell Syst. Tech. J., vol. 55, pp.1669-1085, Oct. 1976.

[12] D. Esteban and C. Galand, "Application of quadrature mirror filters to split band voice coding schemes," Proc.1977 IEEE Int. Conf. Acoust Speech Signal Process., Hartford, Conn., pp.191-195, May 1977.

[13] J. M. Tribolet and R. E. Crochiere, "Frequency domain coding of speech," IEEE Trans. Acoust. Speech Signal Process., Vol.ASSP-27, No.5 pp.512-530, Oct. 1979.

[14] M. J. Narasimha and A. M. Pererson, "Design and application of uniform digital bandpass filter banks," Proc.1978 IEEE Int. Conf. Acoust Speech Signal Process., Tulsa, Okla, pp.499-503, April 1978.

[15] T. A. Classen and W. F. Mecklenbrauker, "A generalized scheme for an translator," IEEE Trans. Circuit Syst., Vol. CAS-25, No.5, pp.252-259, May 1978.

[16] P. Vary, "On the design of digital filter banks based a modified principle of polyphase," Arch. Elekt. Ubertrag. (AEU), Vol.33, pp. 293-300, 1979.

[17] G. A. Nelson, L. L. Pfeifer, and R. C. Wood, "High speed octave band digital filtering," IEEE Trans. Audio Elec.,Vol. AU-20, No.1, pp.8-65, March 1972.

[18] L. R. Rabiner and R. W. Schafer, *Digital Processing of Speech Signals*, Englewood Cliffs, N.J.: Prentice-Hull, 1978.

[19] P. Vary and U. Heute, "A short-time spectrum analyzer with polyphase network and DFT," Signal Processing, Vol. 2 , pp.55-65, Jan. 1980.

[20] M. Smith and T. Barnwell, "A procedure for designing exact reconstruction filter banks for tree-structured subband coders," Proc.1984 IEEE Int. Conf. Acoust Speech Signal Process., pp.27.1.1-27.1.4, March 1984.

[21] M.Vetterli and D.Le Call, "Perfect reconstruction FIR filter banks: some properties and factorizations," IEEE Trans. Acoust. Speech Signal Process., Vol.ASSP-37, pp.1057-1071, July 1989.

[22] E. Viscito and J. Allebach, "The design of tree structured M-channel filter banks using perfect reconstruction filter blocks," Proc.1988 IEEE Int. Conf. Acoust Speech Signal Process., New York, pp.1475-1478, April 1988.

[23] T. Nguyen and P. P. Vaidyanathan, "Two channel perfect reconstruction FIR QMF structures which yield linear phase FIR analysis and synthesis filters," IEEE Trans. Acoust. Speech Signal Process., Vol.ASSP-37, pp.676-690, May 1989.

[24] P. P. Vaidyanathan, "Perfect reconstruction QMF banks for two dimensional applications," IEEE Trans. Circuit Syst., Vol. CAS-34, pp.976-978, Aug.1987.

[25] P. P. Vaidyanathan, "Theory and design of M-channel maximally decimated quadrature mirror filters with arbitrary M, Having the perfect reconstruction property," IEEE Trans. Acoust. Speech Signal Process., Vol.ASSP-35, No.4, pp.476-492, april 1987.

[26] M. Smith and T. Barnwell, "Exact reconstruction techniques for the tree-structured subband coders," IEEE Trans. Acoust. Speech Signal Process., Vol.ASSP-34, pp.437-441, June 1986.

[27] P. P. Vaidyanathan and P. Q. Hoang, "Lattice structures for optimal design and robust implementation of two-channel perfect reconstruction QMF banks," IEEE Trans. Acoust. Speech Signal Process., Vol.ASSP-36, pp.81-94, Jan. 1988.

[28] R. E. Crochiere and L. R. Rabiner, *Multirate Digital Signal Processing*, Englewood Cliffs, N.J.: Prentice-Hull, 1983.

[29] A. V.Oppenheim and R. W. Schafer, *Digital Signal Processing*, Englewood Cliffs, N.J.: Prentice-Hull, 1975.

[30] P.P. Vaidyanathan, "Multirate digital filters, filter banks, polyphase networks, and applications: a tutorial," Proc. IEEE, vol.78, pp.56-93, Jan. 1990.

[31] J. D. Johnston, "A filter family designed for use in quadrature mirror filter banks," Proc.1980 IEEE Int. Conf. Acoust Speech Signal Process., pp.291-294, April 1980.

[32] B. Widrow, P. Baudrenghien, M. Vetterli and P. F. Tichener, "Fundamental relations between the LMS algorithm and the DFT," IEEE Trans. Circuit and Systems, Vol.CAS-34, pp.814-819, July 1987.

[33] W. F. McGee, "Computationally efficient digital bandpass filter banks with arbitrary center frequencies," Tech. Report, Dept. of Elec. Engg., Univ. of Ottawa, 1988.

[34] M. Padmanabhan and K. Martin, "Resonator-based filter-banks for frequency-domain applications," IEEE Trans. Circuit and Systems, Vol.CAS-38, pp.1145-1159, Oct. 1991.

[35] M. J. Narasimha and A. M. Peterson, " Design and applications of uniform digital filter banks," Proc.1978 IEEE Int. Conf. Acoust Speech Signal Process., pp.499-503, April 1978.

[36] M. J. Narasimha and A. M. Peterson, "Design and applications of uniform digital bandpass filter banks," Proc.1978 IEEE Int. Conf. Acoust Speech Signal Process., pp.499-503, April 1978.

[37] T. Aoyama, F. Mano, K. Wakabayashi, R. Maruta and A. Tomozawa, "120-channel transmultiplexer design and performance," IEEE Trans. Commun. Technol., Vol. COM-28, pp.1709-1717, Sept. 1980.

[38] R. Maruta and A. Tomozawa, " An improved method for digital SSB-FDM modulation and demodulation," IEEE Trans. Commun. Technol., Vol. COM-26, pp.720-725, May 1978.

[39] G. Bonnerot, M. Coudreuse, and M. G. Bellanger, " Digital processing techniques in the 60 channel transmultiplexer," IEEE Trans. Commun. Technol., Vol. COM-26, pp.698-706, May 1978.

[40] K. Wong and V. K. Aatre, "Commutativity and applications of digital interpolation filters and modulators," IEEE Trans. Commun. Technol., Vol. COM-28, pp.244-249, May 1980.

[41] S. L. Freeny, R. Kieburtz, K. V. Mina and S. Tewksbury, "Systems analysis of a TDM-FDM translator/digital A-type channel bank," IEEE Trans. Commun. Technol., Vol. COM-19, pp.1050-1059, Dec. 1971.

[42] C. Kurth, "SSB/FDM utilizing TDM digital filters," IEEE Trans. Commun. Technol., Vol. COM-19, pp.61-71, Feb. 1971.

[43] R. E. Crochiere, "On the design of sub-band coders for lowbit rate speech communication," Bell Syst. Tech. J., pp.747-771, May-Jane 1977.

[44] C. Galand and D. Esteban, " 16 Kbps real-time QMF sub-band coding implementation," Proc.1980 IEEE Int. Conf. Acoust Speech Signal Process., pp.332-335, April 1980.

[45] R. Cox D. Bock, K. Bauer, J. D. Johnston and J. Snyder, "The analog voice privacy system," AT&T Tech. J., Vol.66, pp.119-131, Jan-Feb. 1978.

[46] D. O'Shaughnessy, *Speech Communication : Human and machine*, Addison-Wesley Publishing Company, 1987.

[47] T. Parsons, *Voice and Speech Processing*, McGraw-Hill Book Company, 1986.

[48] W. F. McGee and P. Merkley, "Realtime logarithmic-frequency phase vocoder," Computer Music Journal, Vol.15, pp.20-27, March 1991.

[49] G. Zhang and W. F. McGee, "Efficient realization of third-octave filter banks using DSP," CCECE/89, pp.632-635, Sept. 1989, Montreal.

[50] B. A. Doutrich, L. R. Rabiner, and T. B. Martin, "On the effects of varying filter bank parameters on isolated word recognition," IEEE Trans. Acoust. Speech Signal Process., Vol.ASSP-31, pp.793-807, Aug. 1983.

[51] J. H. McClellan, T. W. Parks, and L. R. Rabiner, "A computer programm for designing optimum FIR linear phase digital filters," IEEE Trans. Audio Elec.,Vol. AU-21, pp.506-526, Dec. 1973.

[52] D. C. Farden and L. L. Scharf. "Statistical design of non-recursive digital filters," IEEE Trans. Acoust. Speech Signal Process., Vol.ASSP-22, pp.188-196, June 1974.

[53] A. Dembo and D. Malah, "The design of optimal uniform filter banks with specified composite response," IEEE Trans. Acoust. Speech Signal Process., Vol.ASSP-35, pp.807-817, June 1987.

[54] A. Dembo and D. Malah, "WMMSE design of digital filter banks with specified composite response," IEEE Trans. Acoust. Speech Signal Process., Vol.ASSP-34, pp.1529-1542, Dec. 1986.

[55] R. E. Crochiere, "A weighted overlap add method of Fourier analysis/synthesis," IEEE Trans. Acoust. Speech Signal Process., Vol.ASSP-28, pp.99-102, Feb. 1980.

[56] C. Braccini and A. V. Oppenheim, "Unequal bandwidth spectral analysis using digital frequency warping," IEEE Trans. Acoust. Speech Signal Process., Vol.ASSP-22, pp.236-244, Aug. 1974.

[57] D. M. Bell and J. N. Gowdy, "Power spectral estimation via nonlinear frequency warping," IEEE Trans. Acoust. Speech Signal Process., Vol.ASSP-26, pp.436-441, Aug. 1978.

[58] R. Sudhaker, R. C. Agarwal and S. C. Dutta Roy, " Fast computation of Fourier transform at arbitrary frequencies," IEEE Trans. Acoust. Speech Signal Process., Vol.ASSP-28, pp.972-980, Aug. 1981.

[59] R. E. Crochiere, S. A. Webber, and J. L. Flanagan, "Digital coding of speech in sub-bands," Bell Syst. Tech. J., vol. 55, pp.1669-1085, Oct. 1976.

[60] M. Bellanger, G. Bonnerot and M. Coudreuse, "Digital filtering by polyphase network: application to simple rate alteration filter banks," IEEE Trans. Acoust. Speech Signal Process., Vol.ASSP-24, pp.109-114, April 1976.

[61] A. Croisier, D. Esteban, and C. Galand, "Perfect channel splitting by use of interpolation/decimation tree decomposition techniques," Int. Conf. Inf. Sci. Sys., Patras, Aug. 1976.

[62] T.A. Ramstad and O. Foss, "Sub-band coder design using recursive quadrature mirror filters," EUSPICO-80, 1980.

[63] T. Barnwell, "An experimental study of sub-band coder design incorporating recursive quadrature filters and optimum APDCM," Proc.1981 IEEE Int. Conf. Acoust Speech Signal Process., pp.808-811, April 1981.

[64] D. Esteban and C. Galand, "HOMF: Halfband quadrature mirror filters," Proc.1981 IEEE Int. Conf. Acoust Speech Signal Process., pp.220-223, April 1981.

[65] V. K.Jain and R. E. Crochiere, "A noval approach to the design of analysis/synthesis filter banks," Proc.1983 IEEE Int. Conf. Acoust Speech Signal Process., April 1983.

[66] J. H. Rothweiler, "Polyphase quadrature filters, a new sub-band coding technique," Proc.1983 IEEE Int. Conf. Acoust Speech Signal Process., April 1983.

[67] R. Crochiere, R. Cox and J. Johnston, "Real-time speech coding," IEEE Trans. Commun., Vol. COM-30, pp.621-634, April 1982.

[68] P. Chu, "Quadrature mirror filter design for arbitrary number of equal bandwidth channels," IEEE Trans. Acoust. Speech Signal Process., Vol.ASSP-33, pp.203-218, Feb. 1985.

[69] T. Barnwell, "Sub-band coder design incorporating recursive quadrature filters and optimum ADPCM coders," IEEE Trans. Acoust. Speech Signal Process., Vol.ASSP-30, pp.751-765, Oct. 1982.

[70] T.A.Ramstad and O. Foss, "Sub-band coder design using recursive quadrature mirror filters," Signal Processing: Theories and Applications, pp.745-752, 1980.

[71] H. Gockler, "Design of recursive polyphase networks with optimum magnitude and minimum phase," Signal Processing 3, 1981, North-Holland Publishing Company, pp.365-376.

[72] P. P. Vaidyanathan, S. K. Mitra, and Y. Neuvo, "A new approach to the realization of low-sensitivity IIR digital filters," IEEE Trans. Acoust. Speech Signal Process., Vol.ASSP-34, pp.350-361, Feb. 1986.

[73] P. P. Vaidyanathan, P. Regalia, and S. K. Mitra, "Design of doubly complementary IIR digital filter using single complex allpass filter, with multirate application," IEEE Trans. Circuit and Systems, Vol.CAS-34, pp.378-389, April 1987.

[74] F. Mintzer, "Filters for distortion free two-band multirate filter banks," IEEE Trans. Acoust. Speech Signal Process., Vol.ASSP-33, pp.626-630, June 1985.

[75] H. S. Malvar and D. H. Staelin, "Reduction of blocking effects in image coding with a lapped orthogonal transform," Proc.1988 IEEE Int. Conf. Acoust Speech Signal Process., pp.781-784, April 1988.

[76] H. Malvar, "The LOT: A link between block transform coding and multirate filter banks," Proc.1988 IEEE Int. Sym. Circuit and Systems, pp.835-838, June 1988.

[77] J. Princen and A. Bradley, "Analysis/synthesis filter bank design based on time domain aliasing cancellation," IEEE Trans. Acoust. Sp ech Signal Process., Vol.ASSP-34, pp.1153-1161, Oct. 1986.

[78] M.Vetterli, "A theory of multirate filter banks," IEEE Trans. Acoust. Speech Signal Process., Vol.ASSP-35, pp.356-372, March 1987.

[79] M. Smith and T. Barnwell, "A unifying framework for maximally decimated analysis/synthesis systems," Proc.1985 IEEE Int. Conf. Acoust Speech Signal Process., pp.521-524, March 1985.

[80] P. A. Regalia, S. K. Mitra, P. P. Vaidyanatan, M. Renfors, and Y. Neuvo, "Tree-structured complementary filter banks using all-pass sections," IEEE Trans. Acoust. Speech Signal Process., Vol.ASSP-35, pp.1470-1484, Dec. 1987.

[81] P. Mock, "Add DTMF generation and decoding to DSP-uP designs," in Digital Signal Processing Applications with the TMS320 Family, Vol.1, Prentice Hall 1987.

[82] J. R. Glover, " Adaptive noise cancelling applied to sinuoidal interferences," IEEE Trans. Acoust. Speech Signal Process., Vol.ASSP-25, pp.484-491, Dec. 1977.

[83] J. B. Allen, "Cochlear Modeling," IEEE ASSP Magazine, pp.3-29, 1985.

[84] R. F. Lyon, "A computational model of filtering, detection and compression in the cochlear," Proc.1982 IEEE Int. Conf. Acoust Speech Signal Process., pp.1282-1285, March 1982.

[85] T. Hirahara and T. Komakine, " A computational cochlear nonlinear processing model with adaptive Q circuits," Proc.1989 IEEE Int. Conf. Acoust Speech Signal Process., pp.496-499, April 1989.

[86] B. Mondere and A. A. Lazar, "Speech signal detection at output of a cochlear model," Proc.1988 IEEE Int. Conf. Acoust Speech Signal Process., pp.63-66, April 1988.

[87] T. Barnwell and M. Smith, "Filter banks for analysis reconstruction systems: a tutorial," Proc.1990 IEEE Int. Sym. Circuits and Systems, pp.1999-2003, May 1990.

[88] W. F. McGee and G. Z. Zhang, "Logarithmic filter banks," Proc.1990 IEEE Int. Sym. Circuits and Systems, pp.661-664, New Orleans, USA, May 1990.

[89] G. Zhang and W. F. McGee, "Resonator-based logarithmic filter banks," IEE Proc.-I, Communications, Speech and Vision, vol.139, pp.36-44, Feb. 1992.

[90] G. Peceli, "Resonator-based digital filters," IEEE Trans. Circuit and Systems, vol. CAS-36, pp.156-159, Jan. 1989.

[91] G. Peceli, "Structurelly passive resonator-based digital filters," in Proc. Int. Symp. Circuit and Systems, pp.1563-1566, 1988.

[92] G. Peceli, "Sensitivity properties of resonator-based digital filters," IEEE Trans. Circuit and Systems, vol. CAS-35, pp.1195-1197, Sept. 1988.

[93] W. F. McGee, "Frequency interpolation filter banks," ISCAS/89, in Proc. Int. Symp. Circuit and Systems, pp.1563-1566, May 1989, Portland Oregon.

[94] G. H. Hostetter, "Recursive discrete Fourier transformation," IEEE Trans. Acoust. Speech Signal Process., Vol.ASSP-28, pp.184-190, Apr. 1980.

[95] Simon Haykin, *Adaptive Filter Theory*, Prentice-Hall, New Jersey, 1986.

[96] G. Zhang and W. F. McGee, "Design of maximally flat frequency interpolation filter banks," Proc.1990 IEEE Int. Conf. Signal and Processing, pp.761-764, Nov. 1990.

[97] Gilbert Strang, *Introduction to Applied Mathematics*, Wellesley Cambridge Press, 1986.

[98] G. Zhang and W. F. McGee, "On coefficient quantization and computational roundoff effects in frequency interpolation filter banks," in the Proc.1991/CCECE, Vol. II, pp.70.4.1-70.4.4, Sept. 1991.

[99] V. Belevitch, *Classical Network Theory*, Holden-Day Inc., San Francisco, 1968.

[100] F. J. Harris, "On the use of windows for harmonic analysis with the discrete Fourier transform," Proc. IEEE, vol. 66, Jan. 1978.

[101] G. Zhang and W. F. McGee, "Improved stopband performance of frequency interpolation filter banks," Proc. of CCECE/90, pp.61.1.1-61.1.4, Sept. 1990, Ottawa.

[102] G. Zhang and W. F. McGee,"Windowing techniques in design of resonator-based logarithmic filter banks," in the Proc.1991 IEEE Int. Conf. Acoust Speech Signal Process., Vol. III, pp.1821-1824, May 1991.

[103] L. R. Rabiner, "Linear program design of finite impulse response digital filters," IEEE Trans. Audio Electroacoust., vol. AU-20, Oct. 1972.

[104] D. W. Burlage and R. C. Houts, "The use of linear programming to design digital filters from impulse-response specifications," in Proc. 10th Ann. IEEE Region Conv., April 1972.

[105] L. R. Rabiner, N. Y. Graham and H. D. Helms, "Linear programming design of IIR digital filters with arbitrary magnitude function," IEEE Trans. on ASSP, vol. ASSP-22, No. 2, April 1974.

[106] The IMSL Libraries: Program-solving software systems for numerical FORTRAN programming, 1986.

[107] W. F. McGee and G. Zhang, " Allpass analysis-synthesis frequency interpolation filter banks," in the Proc.1991 IEEE Int. Conf. Acoust Speech Signal Process., Vol. III, pp.1829-1832, May 1991.

[108] L. Gagnon and W. F. McGee,"Speech enhancement using resonator filter banks," in the Proc.1991 IEEE Int. Conf. Acoust Speech Signal Process., Vol. II, pp.981-984, May 1991.

[109] W. H. Press, B. P. Flannery, S. A. Teukolsky and W. T. Vetterling, *Numerical Recipes*: The art of scientific computing, Cambridge University Press, 1986.

[110] M. Smith and T. Barnwell, "A new filter bank theory for time-frequency representation," IEEE Trans. Acoust. Speech Signal Process., Vol.ASSP-35, pp.314-327, March 1987.